2014

Local calibration of the MEPDG prediction models for pavement rehabilitation and evaluation of top-down cracking for Oregon Roadways

Md Shaidur Rahman
Iowa State University

Local calibration of the MEPDG prediction models for pavement rehabilitation and evaluation of top-down cracking for Oregon Roadways

by

Md Shaidur Rahman

A dissertation submitted to the graduate faculty

in partial fulfillment of the requirements for the degree of

DOCTOR OF PHILOSOPHY

Major: Civil Engineering (Civil Engineering Materials)

Program of Study Committee:
R. Christopher Williams, Major Professor
Kejin Wang
Jeramy C. Ashlock
W. Robert Stephenson
Thomas J. Rudolphi

Iowa State University
Ames, Iowa
2014

TABLE OF CONTENTS

Page

LIST OF FIGURES

LIST OF TABLES

Page

ACKNOWLEDGEMENTS

I would like to thank almighty God for his numerous blessings and gifts given to human being. I would like to dedicate this work to the soul of my father who was an inspiration and mentor before being a parent. Also, my deepest gratitude goes to my mother and brothers who always encouraged me during the course of my graduate studies.

I would like to express my deepest gratitude to my major professor, Dr. R. C. Williams, for his invaluable guidance, motivation, and constant encouragement throughout this research work. He always provided me with technical guidance and professional mentorship during my stay at Iowa State University (ISU). Without his support and thoughtfulness this dissertation could not have taken shape. I would like to convey my special thanks to Dr. Kejin Wang, Dr. Jeramy C. Ashlock, W. Robert Stephenson, and Dr. Thomas J. Rudolphi for making time out of their busy schedules to serve on my committee.

I acknowledge the Oregon Department of Transportation (ODOT) and the Federal Highway Administration (FHWA) for funding this research project. I would also like to gratefully acknowledge Oregon State University (OSU) and ODOT engineers for all the technical assistance and data provided. I would like to extend my gratitude toward Mr. Jon Lazarus, Mr. Justin G. Moderie, and Mr. Norris Shippen from ODOT and Dr. Todd Scholz from OSU for their cooperation and assistance provided throughout this research. Finally, I would like to thank all my friends and colleagues in the asphalt materials research group from ISU who supported and assisted me during my research and lab work, Andy Cascione, Ka Lai, Dr. Ashley Buss, Dr. Joana Peralta, Dr. Sheng Tang, Jianhua Yu, Can Chen, Joseph Podolsky, and Paul Ledtje.

ABSTRACT

The Oregon Department of Transportation (ODOT) is in the process of implementing the recently introduced AASHTO Mechanistic-Empirical Pavement Design Guide (MEPDG) for new pavement sections. However, the vast majority of pavement work conducted by ODOT involves rehabilitation of existing pavements. Hot mix asphalt (HMA) overlays are the preferred rehabilitation treatment for both flexible and rigid pavements in Oregon. However, like new work sections, HMA overlays are also susceptible to fatigue cracking (alligator cracking and longitudinal cracking), rutting, and thermal cracking. Additional work was therefore needed to calibrate the design process for rehabilitation of existing pavement structures. 38 pavement sections throughout Oregon were included in this calibration study. A detailed comparison of predictive and measured distresses was made using the MEPDG released software Darwin M-E (Version 1.1). It was found that Darwin M-E predictive distresses did not accurately reflect measured distresses, calling for a local calibration of performance prediction models was warranted. Four distress prediction models (rutting, alligator cracking, longitudinal cracking, and thermal cracking) of the HMA overlays were calibrated for Oregon conditions. A comparison was made between the results before and after the calibration to assess the improvement in accuracy of the distress prediction models provided by the local calibration. While the thermal cracking model could not be calibrated, the locally calibrated models of rutting, alligator cracking, and longitudinal cracking provided better predictions with lower bias and standard error than the nationally (default) calibrated models. However, there was a high degree of variability between the predicted and measured distresses, especially for longitudinal cracking, even after the calibration. It is believed that there is a significant lack-of-fit modeling error for the occurrence of thermal cracks. The Darwin M-E calibrated models of rutting and alligator cracking can be implemented, however, it is recommended that additional sites, which would contain more detailed inputs (mostly Level 1), be established and be included in the future calibration efforts and thus, further improve the accuracy of the prediction models.

Recently, the Oregon Department of Transportation (ODOT) has identified hot mix asphalt concrete (HMAC) pavements that have displayed top-down cracking within three years of construction. The objective of the study was to evaluate the top-down cracked pavement sections and compare the results with the non-cracked pavement sections. Research involved evaluating

six surface cracked pavements and four non-cracked pavement sections. The research included extensive field and laboratory investigations of the 10 pavement sections by conducting distress surveys, falling weight deflectometer (FWD) testing, dynamic cone penetrometer (DCP) testing, and coring from the cracked and non-cracked pavement sections. Cores were then subjected to a full laboratory-testing program to evaluate the HMAC mixtures and binder rheology. The laboratory investigation included dynamic modulus, indirect tensile (IDT) strength, and specific gravity testing on the HMAC cores, binder rheological tests on asphalt binder and aggregate gradation analysis. The FWD and DCP tests indicated that top-down cracked pavement sections were structurally sound, even some of the sections with top-down cracking showed better structural capacity compared to non-cracked sections. The study also found that top-down cracking initiation and propagation were independent of pavement cross-section or the HMAC thickness. The dynamic modulus testing indicated that cores from all the top-down cracked pavement sections except one section (OR 140) possessed stiffer mixtures than that of non-cracked pavement sections. All four non-cracked pavement areas were found to be exhibiting fairly high IDT strength, and low variability in IDT strength and HMAC density when compared to top-down cracked sections as indicated by the IDT strength tests and air void analysis. Asphalt binder rheological test result indicated that asphalt binders from all the top-down cracked sections except OR140 showed higher complex shear modulus (stiffer binder) compared to non-cracked pavement sections. The study concluded that top-down cracking could be caused by a number of contributors such as stiffer HMAC mixtures, mixture segregation, binder aging, low HMAC tensile strength, and high variability in tensile strength or by combination of any.

CHAPTER 1 - INTRODUCTION

Background

The new Mechanistic-Empirical Pavement Design Guide (MEPDG) and software were developed through the National Cooperative Highway Research Program (NCHRP) 1-37A project in recognition of the limitations of the current American Association of State Highway and Transportation Officials (AASHTO) Design Guide (NCHRP, 2004). It represents a transitioning of the empirically-based pavement design to a mechanistic-empirical procedure that combines the strengths of advanced analytical modeling and observed field performance. The pavement performance prediction models in the MEPDG were calibrated primarily using design inputs and performance data largely from the national Long-Term Pavement Performance (LTPP) database. However, these performance prediction models warrant detailed validation and calibration because of potential differences between national and local conditons. Therefore, it is necessary to calibrate these performance prediction models for implementation in local conditions by taking into account local material properties, traffic patterns, environmental conditions, construction, and maintenance activities.

The importance of local calibration of performance prediction models contained in MEPDG is well-documented by different transportation agencies throughout the United States. Hall (Hall et al., 2011) conducted a local calibration of performance prediction models in MEPDG for Arkansas. Rutting and alligator (bottom-up) cracking models were successfully calibrated, however, longitudinal (top-down) cracking and thermal (transverse) cracking models were not calibrated due to the nature of data. Souliman (Souliman et al., 2010) calibrated distress models for alligator cracking, longitudinal cracking, rutting, and roughness for hot mix asphalt (HMA) pavements for Arizona using 39 LTPP pavement sections. It was found that national calibrated MEPDG under predicted alligator cracking and AC rutting while the longitudinal cracking and the subgrade rutting were over predicted. Significant improvement of performance prediction for alligator cracking and AC rutting resulted after calibration; however, only marginal improvement was realized for longitudinal cracking and roughness models. Hoegh (Hoegh et al., 2010) conducted a local calibration of the rutting model for MnROAD test sections. They concluded that the locally calibrated model greatly improved the MEPDG rutting prediction for various pavement designs in MnROAD conditions. A study by Von Quintus (Von Quintus, 2008) found that the measurement error of the performance data had the greatest effect on the precision of MEPDG performance models. MEPDG performance models were verified for Iowa using Pavement Management Information System (PMIS) data (Kim et al., 2010). Systematic differences were observed for rutting and cracking models. Muthadi and Kim (Muthadi and Kim, 2008) performed the MEPDG calibration for HMA pavements located in North Caorlina (NC) using version 1.0 of the MEPDG software. Two distress models, rutting and alligator cracking, were used for this effort. This study concluded that the standard error for the rutting model and the alligator cracking model was significantly lower after the calibration.

The properly calibrated MEPDG will enable more economical designs as well as potentially linking pavement design with actual material characteristics-, and construction processes. Further, as newer technologies and materials are developed, characterization of their material properties will expedite their use in the MEPDG. Several examples exist including the use of warm mix asphalt, post consumer asphalt roofing shingles in asphalt mixtures, and the evaluation of other technologies such as additives and modifiers.

It is imperative that performace prediction models contained in MEPDG be properly calibrated to local conditions prior to adopting and using them for design purposes (ARA, 2007). The local calibration process involves three important steps: verification, calibration, and validation. The term verification refers to assessing the accuracy of the nationally (default) calibrated prediction models for local conditions. The term calibration refers to the mathematical process through which the total error or difference between observed and predicted values of performance is minimized. The term validation refers to the process to confirm that the locally calibrated performance prediction models can produce robust and accurate predictions for cases other than those used for model calibration.

For over a century, highways have been paved using asphalt concrete mixes in State of Oregon as well as across the United States. However, a major problem still exists involving premature pavement failures caused by cracking, rutting, potholes etc. Recently Oregon Department of Transportation (ODOT) has constructed hot mix asphalt concrete (HMAC) pavements that have displayed premature cracking within three years of construction. Early cracking allows moisture to penetrate the pavement structure reducing the pavement section’s design life and significantly increasing the life cycle cost. Also within the last several years, design and material changes occurred that may or may not have contributed to the early cracking. The changes include an increase in the quantity of recycled asphalt pavement (RAP) allowed in the wearing surface; the use of binder modifications including acid and polymers; and a shift in mix gyration levels. Construction factors like properties of the produced mix (volumetrics) and placement also play a part of the pavement performance.

It has been well recognized that cracking of hot-mix asphalt concrete (HMAC) pavements is a major mode of premature failure. Currently, four major mode of failure associated with HMAC cracking are identified: (Birgisson et al.,2002, Von Quintus and Moulthrop, 2007) 1) fatigue cracking, also known as bottom-up cracking, which starts at the bottom of the HMAC pavement and propagates upward to the surface of the pavement, 2) top-down cracking, also known as longitudinal cracking, initiating at the top of the asphalt pavement layer in a direction along the wheel path and propagating down-ward, 3) thermal cracking, and 4) reflective cracking, in which existing cracks or joints cause stress concentrations that result in crack propagation through an HMAC overlay. Notional investigations into cracking have identified areas where the cracking is top-down versus bottom-up. While both are serious, bottom-up cracking typically indicates the pavement structure was underdesigned indicating a need to change structural design practices. Top-down cracking, however, may indicate that material selection process can be fine-tuned. The only means to differentiate between top-down versus bottom-up cracking is through coring.

Traditionally, most flexible pavement design methods consider fatigue cracking initiating at the bottom of the HMA layer and propagating upward as the most critical criteria for the fatigue failure of HMA pavements. However, recent research has suggested that premature pavement fatigue failure initiates at the surface of HMA pavement and propagates downward, which is known as top-down cracking (shown in Figure 1-1). The only way to differentiate top-down cracking from bottom-up cracking is to take cores and trench sections. For years pavement engineers within the Washington State Department of Transportation (WSDOT) have observed that asphalt concrete pavements in the State of Washington have displayed longitudinal and fatigue cracks (multi-connected) that appear to crack from the top of the pavement and propagate downward. Often, the cracks stop at the interface between the wearing course and the underlying bituminous layers (a depth of about 50 mm).The top-down cracking was observed in thicker sections with thinner sections cracking full depth. Top-down cracking generally started within three to eight years of paving for pavement sections that were structurally adequate and were designed for adequate ESALs (Uhlmeyer et al., 2000).

Figure 1-1 Pictures showing the development of top-down cracking

Objectives

The Oregon Department of Transportation (ODOT) is in the process of implementing the new Mechanistic-Empirical pavement design guide (MEPDG) for new pavement sections. Internally, ODOT has been evaluating the MEPDG for new sections for both hot mix asphalt and Portland cement concrete interstate pavement sections. Work is also currently being conducted at Oregon State University to develop design inputs and evaluate the three principal pavement performance models (e.g., fatigue cracking, rutting, and thermal cracking models) that are integral to the design process of new work sections for asphalt concrete (AC) pavement structures. However, the vast majority of pavement work conducted by ODOT involves rehabilitation of existing pavements. Additional work is therefore needed to calibrate the design process for rehabilitation of existing pavement structures. Asphalt mix overlays are the preferred rehabilitation treatment for both hot mix asphalt (HMA) and Portland cement concrete (PCC) pavements in Oregon. However, like new work sections, overlays are also susceptible to fatigue cracking (both alligator and longitudinal cracking), rutting, and thermal cracking (transverse cracking) - thus, the need to include these forms of distress in the calibration process.

Secondly, the objectives of the research are to determine the causes of early cracking on the State of Oregon highways system. The results of the study will be used to modify the pavement design process including modifications to the Pavement Design Guide and Mix Design Guidelines. By doing so, the ODOT will be able to design pavements that are long lasting, resulting in significant benefits to the department by reducing the life cycle cost needed to maintain the state highway system.

Organization of Dissertation

This dissertation is divided into seven chapters and follows a journal paper format including three papers published or submitted to journals and conferences for peer review. The first chapter covers a brief introduction to the necessity of the Mechanistic-Empirical Pavement Design Guide (MEPDG) calibration and top-down cracking evaluation, and outlines study objectives and dissertation chapters. Chapter 2 summarizes literature review with regard to implementing the MEPDG and local calibration at national and local research levels. It also discusses the local calibration methodology employed in this study. Chapter 2 also summarizes literature review with regard to top-down cracking in asphalt concrete pavement Chapter 3 discusses the development of a calibration plan and pavement sections to be included in the top-down cracking evaluation study

Chapter 4 and 5 describes the input parameters needed for Darwin M-E, the design software that was developed for use of the MEPDG models. While chapter 4 presents the findings of the verification-calibration-validation studies of the fatigue prediction models within MEPDG, chapter 5 discusses the outcomes of the calibration studies including rutting model. Chapter 6 describes the field and laboratory testing procedures employed for top-down cracking study. The results of field and laboratory tests are also summarized and discussed in Chapter 6. Finally, Chapter 7 provides a summary, conclusions and recommendations for future research.

CHAPTER 2 - LITERATURE REVIEW

Local Calibration of the MEPDG Prediction Models

The national calibration-validation process was successfully completed for Mechanistic-Empirical Pavement Design Guide (MEPDG) in 2004 (NCHRP, 2004). Although this effort was comprehensive, a further validation study is highly recommended as a prudent step in implementing a new design procedure that is so different from current procedures. The objective of this task is to review available existing literature with regard to implementing the MEPDG and local calibration at national and local research levels. A comprehensive literature review was undertaken specifically to identify the following information:

- Identify local calibration steps detailed in National Cooperative Highway Research Program (NCHRP) projects for local calibration.
- Examine how State agencies apply the NCHRP projects' local calibration procedures in their pavement systems.
- Summarize MEPDG pavement performance models' local calibration coefficients reported in literature.

Summary of NCHRP Projects for MEPDG Local Calibration

At the request of the American Association of State Highway and Transportation Officials (AASHTO) Joint Task Force on Pavements (JTFP), the NCHRP initiated the project, 1-40 "*Facilitating the Implementation of the Guide for the Design of New and Rehabilitated Pavement Structures*" following NCHRP 1- 37A (NCHRP, 2004) for implementation and adoption of the recommended MEPDG (TRB 2009). A key component of the NCHRP 1-40 is an independent, third-party review to test the design guide's underlying assumptions, evaluate its engineering reasonableness and design reliability, and to identify opportunities for its implementation in day-to-day design production work. Beyond this immediate requirement, NCHRP 1-40 includes a coordinated effort to acquaint state DOT pavement designers with the principles and concepts employed in the recommended guide, assist them with the interpretation and use of the guide and its software and technical documentation. NCHRP 1-40 also includes step-by-step procedures to help State DOT engineers calibrate distress models on the basis of local and regional conditions for use in the recommended guide, and perform other activities to facilitate its acceptance and adoption.

There are two NCHRP research projects that are closely related to local calibration of MEPDG performance predictions. They are:

1. NCHRP 9-30 project (NCHRP 2003a, NCHRP 2003b), "*Experimental Plan for Calibration and Validation of Hot Mix Asphalt Performance Models for Mix and Structural Design"*, and
2. NCHRP 1-40B (Von Quintus et al. 2005, NCHRP 2007, Von Quintus et al. 2009a, Von Quintus et al. 2009b, NCHRP 2009, TRB, 2010), "*User Manual and Local Calibration Guide for the Mechanistic-Empirical Pavement Design Guide and Software*".

Under the NCHRP 9-30 project, pre-implementation studies involving verification and recalibration have been conducted in order to quantify the bias and residual error of the flexible pavement distress models included in the MEPDG (Muthadi, 2007). Based on the findings from the NCHRP 9-30 study, the NCHRP 1-40B project has focused on preparing (i) a user manual for the MEPDG and software and (ii) detailed, practical guide for highway agencies for local or regional calibration of the distress models in the MEPDG and software. The manual and guide have been presented in the form of a draft AASHTO recommended practices; the guide shall contain two or more examples or case studies illustrating the step-by-step procedures. It was also noted that the longitudinal cracking model be dropped from the local calibration guide development in NCHRP 1-40B study due to lack of accuracy in the predictions (Muthadi 2007, Von Quintus and Moulthrop 2007). NCHRP 1-40 B was completed in 2009 and the draft of report was transferred to the AASHTO Joint Technical Committee on Pavements for review and future action (TRB, 2010).

NCHRP 1-40B study (NCHRP, 2007) initially provided three primary steps for calibrating the MEPDG to local conditions and materials as follows:

Step. 1. *Verification of MEPDG performance models with national calibration factors*: Run the current version of the MEPDG software for new field sections using the best available materials and performance data. The accuracy of the prediction models was evaluated using the bias (defined as average over or under prediction) and the residual error (defined as the predicted minus observed distress) as illustrated in Figure 2-1. If there is a significant bias and residual error, it is recommended to calibrate the models to local conditions leading to the second step.

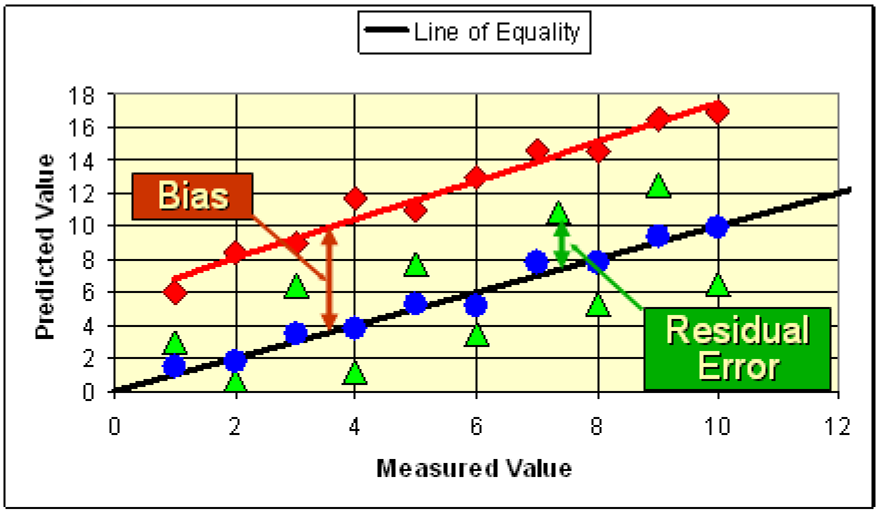

Figure 2-1 The bias and the residual error (Von Quintus 2008a)

Step. 2. *Calibration of the model coefficients*: eliminate the bias and minimize the standard error between the predicted and measured distresses.

Step. 3. *Validation of MEPDG performance models with local calibration factors*: Once the bias is eliminated and the standard error is within the agency's acceptable level after the calibration, validation is performed on the models to check for the reasonableness of the performance predictions.

NCHRP 1-40B study (NCHRP, 2009) continued on the work from the 2007 study and detailed the initial three steps into 11 steps for local calibration of the MEPDG. These 11 steps are depicted in Figure 2-2 and Figure 2-3 below and each of the 11 steps are summarized in the following subsections. Please note that the Accelerated Pavement Testing (APT) has been cross-hatched to reflect this is not viable as APT facilities do not exist in Oregon.

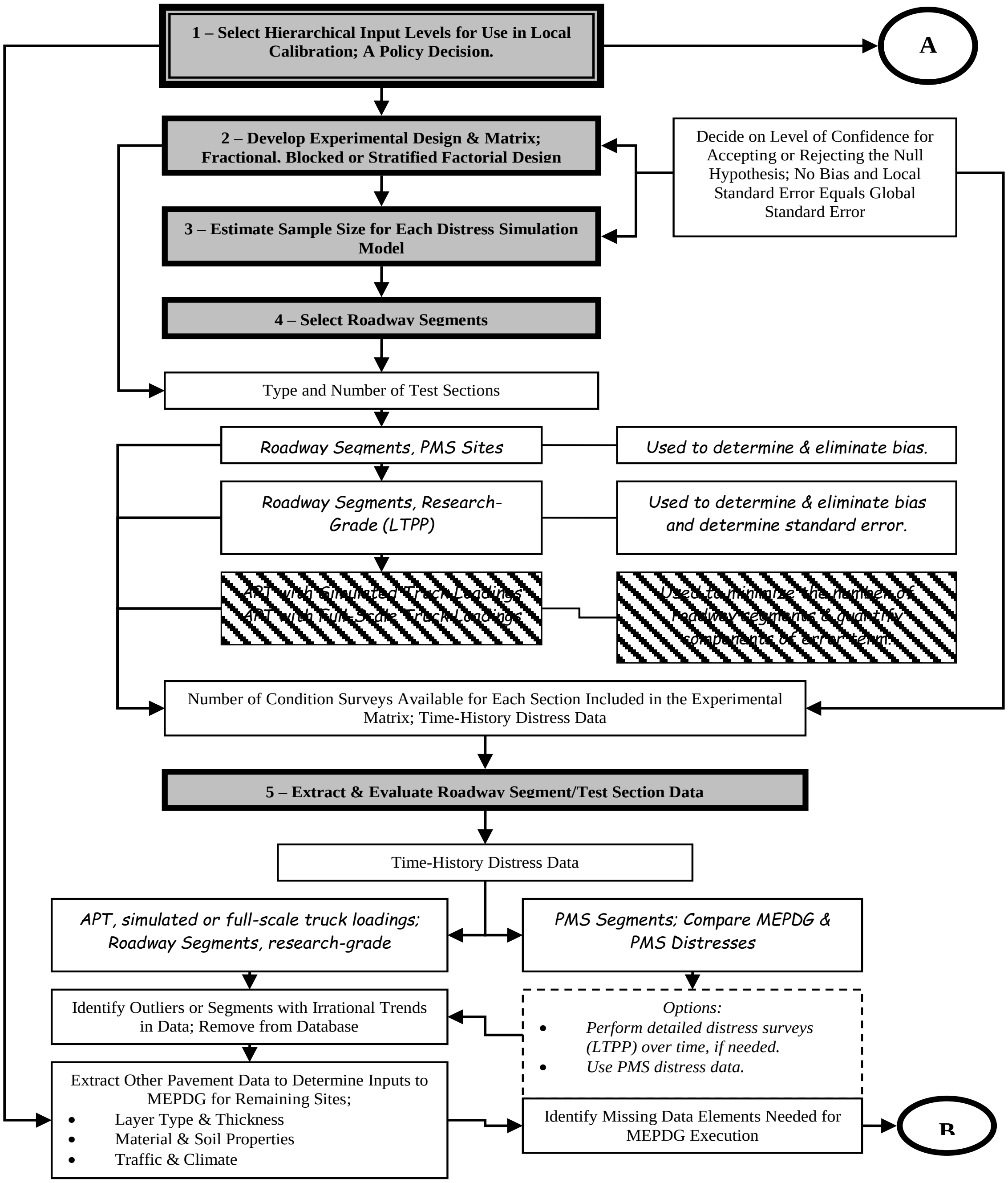

Figure 2-2 Flow chart for the procedure and steps suggested for local calibration: steps 1-5 (NCHRP, 2009)

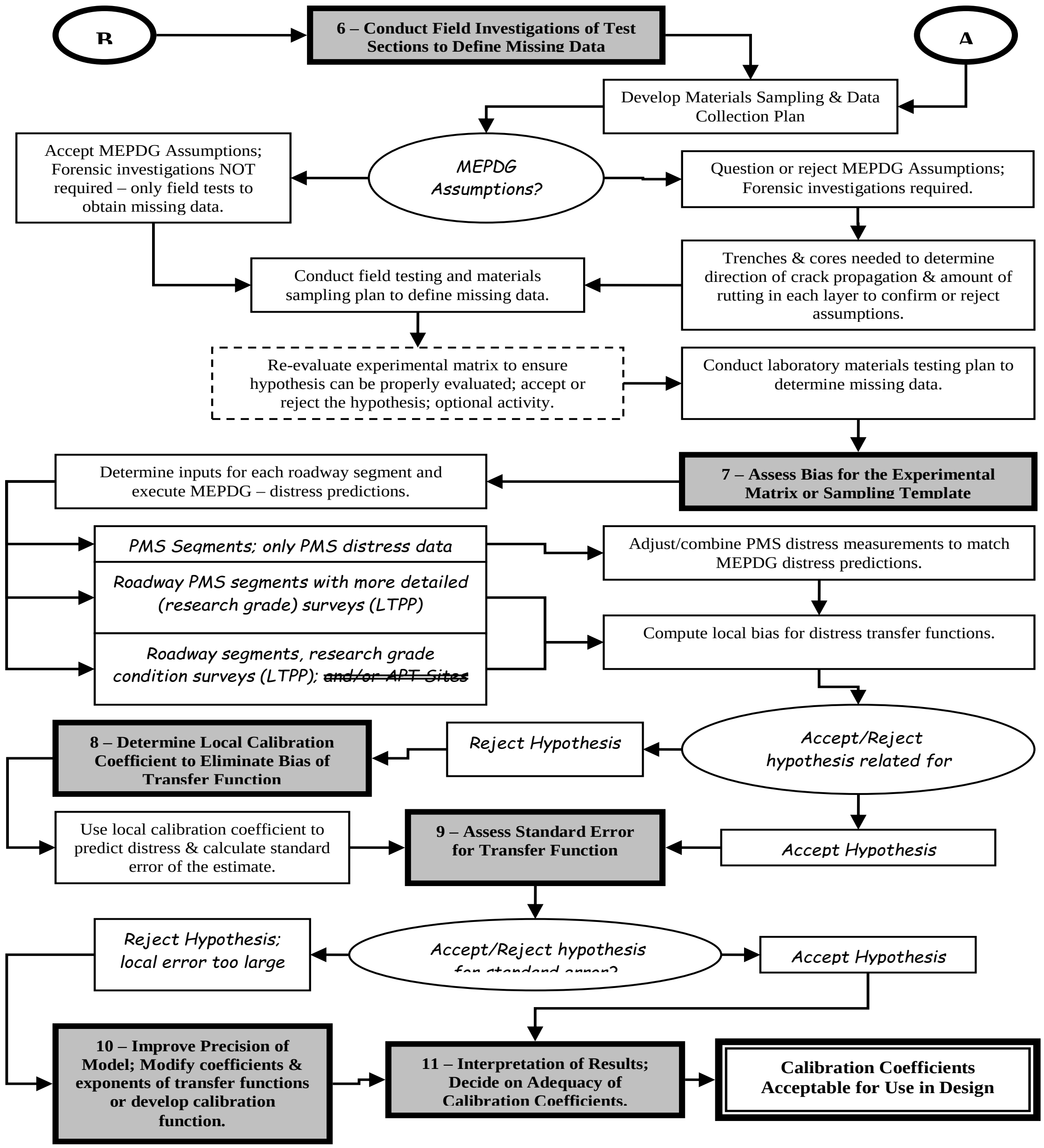

Figure 2-3 Flow chart for the procedure and steps suggested for local calibration: steps 6-11 (NCHRP, 2009)

Step 1: Select Hierarchical Input Level

The MEPDG provides the user with the highest flexibility in obtaining the design inputs for a design project based on its importance and the available resources. In general, the MEPDG considers three hierarchical levels of inputs. Level 1 input represents the highest level of accuracy and lowest level of input errors. Level 1 material input requires laboratory or field testing, such as the dynamic modulus testing of hot mix asphalt concrete, site-specific axle load spectra data collections, or nondestructive deflection testing. Level 1 input is more representative of the agency or project specific materials, traffic, and climatic inputs, thus requiring more resources and time than other levels. Level 2 input represents an intermediate level of accuracy. Inputs are estimated from correlations based on limited laboratory test results or selected from an agency database. Examples include estimating HMA dynamic modulus from binder, aggregate, and mix properties, estimating PCC elastic moduli from compressive strength tests, or using site-specific traffic volume and traffic classification data in conjunction with agency-specific axle load spectra. Level 3 inputs provide the lowest level of accuracy. Inputs typically represent user-selected values or typical averages for the region. Examples include default unbound materials resilient modulus values or default HMA Poisson's ratio for a given mix classes and aggregates used by an agency.

The hierarchical input level to be used in the local validation-calibration process should be consistent with the way the agency intends to determine the inputs for day-to-day use. Some of input level 3 data could be available in the state Department of Transportation (DOT) pavement management system (PMS). It is also important to point out that the calibration using level 1 and 2 input data is dependent upon material and mixture characteristics. Further the linkage of material and mixture characteristics to pavement performance is critical to the level 1 and 2 calibrations. The general information from which the inputs were determined for each input category is discussed in Step 5.

Step 2: Experimental Factorial & Matrix or Sampling Template

A detailed sampling template should be created considering traffic, climate, pavement structure and materials representing local conditions. The number of roadway segments selected for the sampling template should result in a balanced factorial with the same number of replicates within each category.

Step 3: Estimate Sample Size for Each Performance Indicator Prediction Model

The sample size (total number of roadway segments or projects) can be estimated with statistical confidence level of significance. The selection of higher confidence levels can provide more reliable data but increase the number of segments needed. The number of distress observations per segment is dependent on the measurement error or within segment data variability over time (i.e.; higher the within project data dispersion or variability, larger the number of observations needed for each distress). The number of distress measurements made within a roadway segment is also dependent on the within project variability of the design features and site conditions. NCHRP 1-40B project report (NCHRP, 2009) provided the following equation in determination of the number of distress observations:

$$N = \left(\frac{z_{\alpha}\left(s_y\right)}{e_t} \right)^2 \tag{2-1}$$

where, z_{α} = 1.282 for a 90 percent confidence interval; s_y = standard deviation of the maximum true or observed values; and e_t = tolerable bias. The tolerable bias will be estimated from the levels that are expected to trigger some major rehabilitation activity, which are agency dependent. The s_e/s_y value (ratio of the standard error and standard deviation of the measured values) will also be agency dependent.

Step 4: Select Roadway Segments

Roadway segments should be selected to cover a range of distress values that are of similar ages within the sampling template. Roadway segments exhibiting premature or accelerated distress levels, as well as those exhibiting superior performance (low levels of distress over long periods of time), can be used, but with caution. The roadway segments selected for the sampling template when using hierarchal input level 3 data should represent average performance conditions. It is important that the same number of performance observations per age per each roadway segment be available in selecting roadway segments for the sampling template. It would not be good practice to have some segments with ten observations over 10 years with other segments having only two or three observations over 10 years. The segments with one observation per year would have a greater influence on the validation-calibration process than the segments with less than one observation per year.

Step 5: Extract and Evaluate Roadway Segment/Test Section Data

This step is grouped into four activities:

1. Extracting and reviewing the performance data;
2. Comparing the performance indicator magnitudes to the trigger values;
3. Evaluating the distress data to identify anomalies and outliers; and
4. Determining the inputs to the MEPDG.

First, measured time-history distress data should be made from accelerated pavement testing (APT) or extracted from the agency's PMS. In the case of the Oregon DOT, the distress data was extracted from the agency's PMS. The extraction of data from agency PMS should require a prior step of reviewing PMS database to determine whether the measured values are consistent with the values predicted by the MEPDG. NCHRP 1-40B project report (NCHRP, 2009) demonstrated the conversion procedures of pavement distress measurement units between PMS and MEPDG for flexible pavements PMS database of Kansas Department of Transportation (KSDOT) and rigid pavements PMS database of Missouri Department of Transportation (MODOT). These examples in NCHRP 1-40B project report (NCHRP, 2009) are reproduced below.

Kansas DOT (KSDOT) Data Interpretation for MEPDG Use

For the HMA pavement performance data in KSDOT, the measured cracking values are different, while the rutting and International Roughness Index (IRI) values are similar and assumed to be the same. The cracking values and how they were used in the local calibration process are defined below.

Fatigue Cracking. KSDOT measures fatigue cracking in number of wheel path feet per 100 foot sample by crack severity, but do not distinguish between alligator cracking and longitudinal cracking in the wheel path. In addition, reflection cracks are not distinguished separately from the other cracking distresses. The PMS data were converted to a percentage value similar to what is reported in the Highway Performance Monitoring System (HPMS) system from Kansas. In summary, the following equation was used to convert KSDOT cracking measurements to a percentage value that is predicted by the MEPDG

$$FC = \left(\frac{FCR_1(0.5) + FCR_2(1.0) + FCR_3(1.5) + FCR_4(2.0)}{8.0} \right) \qquad (2\text{-}2)$$

All load related cracks are included in one value. Thus, the MEPDG predictions for load related cracking were combined into one value by simply adding the length of longitudinal cracks and reflection cracks for Hot Mix Asphalt (HMA) overlays, multiplying by 1.0 ft, dividing that product by the area of the lane and adding that value to the percentage of alligator cracking predicted by the MEPDG.

Thermal Cracking. Another difference is that KSDOT records thermal cracks as the number of cracks by severity level. The following equation has been used by KSDOT to convert their measured values to the MEPDG predicted value of ft/mile.

$$TC = \left(\frac{TCR_o + TCR_1 + TCR_2 + TCR_3}{(10)(12)(52.8)} \right) \qquad (2\text{-}3)$$

The value of 10 in the above equation is needed because the data are stored with an implied decimal. The value of 12 ft is the typical lane width, and the value of 52.8 coverts from 100 foot sample to a per mile basis. Prior to 1999, KSDOT did not record the number or amount of sealed thermal cracking incidents (TCR_0). As a result, the amount of thermal cracks sometimes goes to “0”.

Missouri DOT (MODOT) Data Interpretation for MEPDG Use

For the PCC pavement performance data in MODOT, the measured thermal cracking values are different from the MEPDG, while the thermal joint faulting and IRI values are similar and assumed to be the same. The thermal cracking values and how they were used in the local calibration process are defined below.

Thermal Cracking. The MEPDG requires the percentage of all Portland Cement Concrete (PCC) slabs with mid panel fatigue thermal cracking. Both MODOT and LTPP describe thermal cracking as cracks that are predominantly perpendicular to the pavement slab centerline. Measured cracking is reported in 3 severity levels (low, medium, and high) and provides distress maps showing the exact location of all thermal cracking identified during visual distress surveys. Thus, the databases contain, for a given number of slabs within a 500-ft pavement segment, the total number of low, medium, and high severity thermal cracking. Since LTPP does not provide details on whether a given slab has multiple cracks, as shown in Figure 2-4, a simple computation of percent slabs with this kind of data can be misleading. Therefore, in order to produce an accurate estimate of percent slab cracked, distress maps or videos prepared as part of distress data collection were reviewed to determine the actual number of slabs with thermal "fatigue" cracking for the 500-ft pavement segments. The total number of slabs was also counted with the percent slabs cracked was defined as follows:

$$PercentSlabsCracked = \left(\frac{Number\,of\ cracked\,slabs}{Total\,number\,of\ slabs}\right)*100 \qquad (2\text{-}4)$$

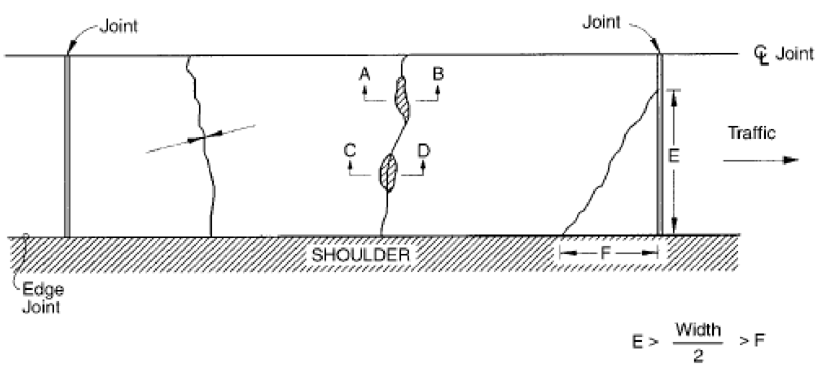

Figure 2-4 LTPP thermal cracking (Miller and Bellinger, 2003)

Thermal Joint Faulting. It is measured and reported by MODOT and LTPP as the difference in elevation to the nearest 1 mm between the pavement surfaces on either side of a thermal joint. The mean joint faulting for all joints within a 500-ft pavement section is reported. This is comparable to the MEPDG predicted faulting.

IRI. The values included in the MODOT PMS database are comparable to the MEPDG predicted IRI.

The second activity of step 5 is to compare the distress magnitudes to the trigger values for each distress. In other words, answer the following question—does the sampling template include values close to the design criteria or trigger value? This comparison is important to provide an answer if the collected pavement distress data could be properly utilized to validate and accurately determine the local calibration values. For example, low values of fatigue cracking measurements comparing to agency criteria is difficult to validate and accurately determine the local calibration values or adjustments for predicting the increase in cracking over time.

The distress data for each roadway segment included in the sampling template should be evaluated to ensure that the distress data are reasonable time-history plots. Any zeros that represent non-entry values should be removed from the local validation-calibration database. Distress data that return to zero values within the measurement period may indicate some type of maintenance or rehabilitation activity. Measurements taken after structural rehabilitation should be removed from the database or the observation period should end prior to the rehabilitation activity. Distress values that are zero as a result of some maintenance or pavement preservation activity, which is a part of the agency's management policy, should be removed but future distress observation values after that activity should be used. If the outliers or anomalies of data can be explained and are a result of some non-typical condition, they should be removed. If the outlier or anomaly cannot be explained, they should remain in the database.

The MEPDG pavement input database related to each selected roadway segment should be prepared to execute the MEPDG software. The existing resource of these input data for level 3 analyses are agency PMS, traffic database, as-built plans, construction database files, etc. If data for level 3 were unavailable or inadequate, the mean value from the specifications was used or the average value determined for the specific input from other projects with similar conditions. The default values of the MEPDG could also be utilized in this case.

Step 6: Conduct Field and Forensic Investigations

Field and forensic investigations could be conducted to check the assumptions and conditions included in the MEPDG for the global (national) calibration effort. These field and forensic investigations include measuring the rutting in the individual layers, determining where the cracks initiated or the direction of crack propagation, and determining permanent curl/warp effective temperature, etc. The field and forensic investigations is not necessary if the agency accepts the assumptions and conditions included in the MEPDG.

Step 7: Assess Local Bias from Global Calibration Factors

The MEPDG software is executed using the global calibration values to predict the performance indicators for each roadway segment selected. The null hypothesis is first checked for the entire sampling matrix. The null hypothesis in equation below is that the average residual error ($e_r = y_{Measured} - x_{predicted}$) or bias is zero for a specified confidence level or level of significance.

$$H_O : \sum_{i=1}^{n} \left(y_{Measured} - x_{\mathrm{Pr}edicted} \right)_i = 0 \tag{2-5}$$

It is helpful for assessment through making plots of a comparison between the predicted ($x_{predicted}$) and the measured values ($y_{Measured}$) and a comparison between the residual errors (e_r) and the predicted values ($x_{predicted}$) for each performance indicator.

Two other model parameters can be also used to evaluate model bias—the intercept (b_o) and slope (m) estimators using the following fitted linear regression model between the measured ($y_{Measured}$) and predicted ($x_{predicted}$) values.

$$\hat{y}_i = b_o + m(x_i) \tag{2-6}$$

The intercept (b_o) and slope (m) estimators can provide not only accuracy of each prediction but also identification of dependent factors such as pavement structure (new construction versus rehabilitation) and HMA mixture type (conventional HMA versus Superpave mixtures) to each prediction. For illustration, Figure 2-6 presents comparison of the intercept and slope estimators to the line of equality for the predicted and measured rut depths using the global calibration values.

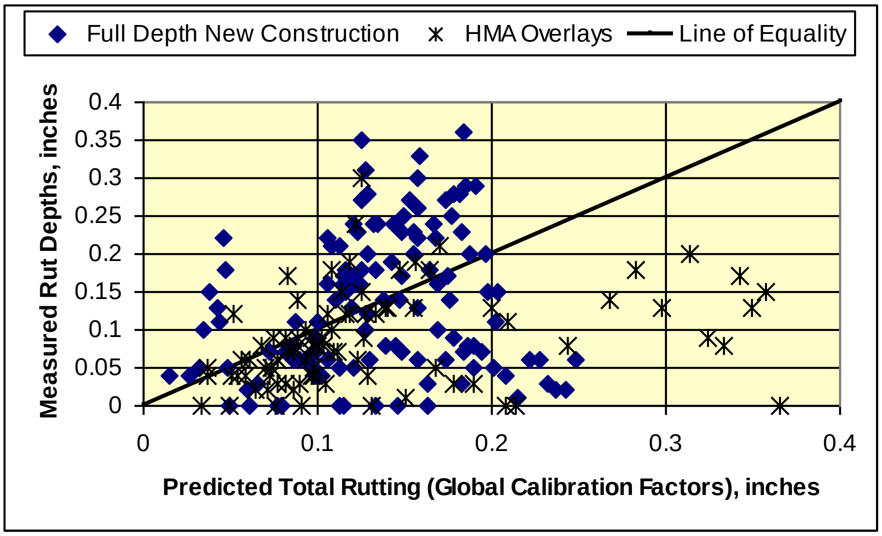

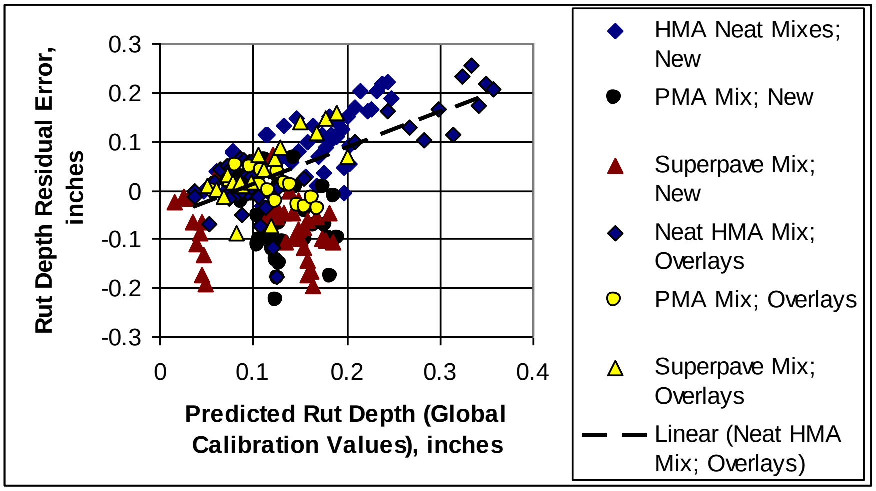

Figure 2-5 Comparison of predicted and measured rut depths using the global calibration in KSDOT study (NCHRP, 2009)

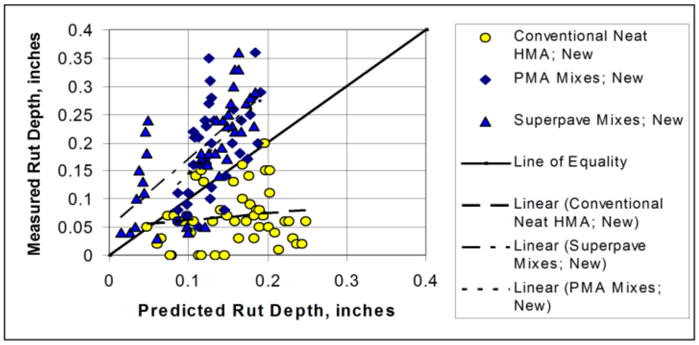

a. Intercept and slope estimators that are dependent on mixture type for the new construction PMS segments.

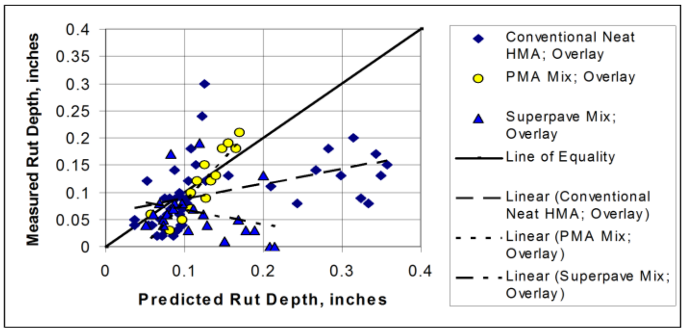

b. Intercept and slope estimators that are dependent on mixture type for the rehabilitation PMS segments.

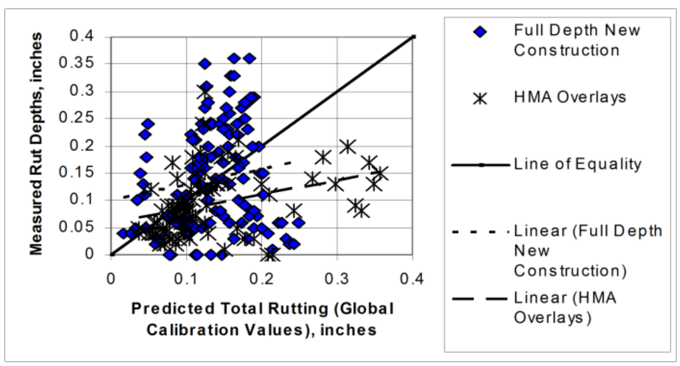

c. Intercept and slope estimators that are structure dependent for the PMS segments.

Figure 2-6 Comparison of the intercept and slope estimators to the line of equality for the predicted and measured rut depths using the global calibration values in KSDOT study (NCHRP, 2009)

Step 8: Eliminate Local Bias of Distress Prediction Models

The MPEDG software includes two sets of parameters for local calibration of most performance indicator transfer functions. One set is defined as agency specific values and the other set as local calibration values. Figure 2-7 shows a screen shot of the tools section where these values can be entered into the software for each performance indicator on a project basis. The default values of the MEPDG performance indicator transfer functions are global calibration values for agency specific values (k_1, k_2, and k_3 in Figure 2-7) and are one for local calibration values (β_1, β_2, and β_3 in Figure 2-7). These parameters are used to make adjustments to the predicted values so that the difference between the measured and predicted values, defined as the residual error, is minimized. Either one can be used with success.

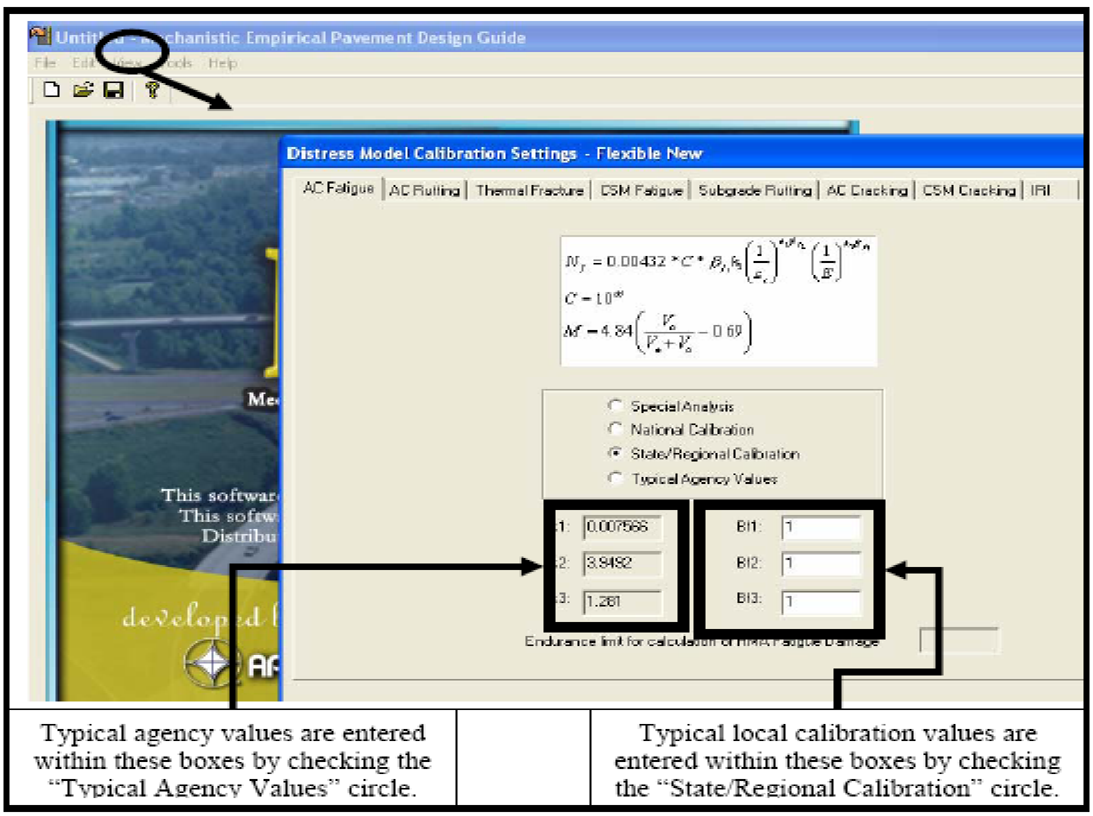

Figure 2-7 Screen shot of the MEPDG software for the local calibration and agency specific values (Von Quintus, 2008b)

NCHRP 1-40B project study (NCHRP, 2009) lists the coefficients of the MEPDG transfer functions or distress and IRI prediction models that should be considered for revising the predictions to eliminate model bias for flexible pavements and HMA overlays. Table 2-1 from NCHRP 1-40B project study (NCHRP, 2009) was prepared to provide guidance in eliminating any local model bias in the predictions. The distress specific parameters can be dependent on site factors, layer parameters, or policies of the agency.

Table 2-1 Calibration parameters to be adjusted for eliminating bias and reducing the standard error of the flexible pavement transfer functions (NCHRP, 2009)

Distress		Eliminate Bias	Reduce Standard Error
Total Rutting	Unbound Materials & HMA Layers	k_1, β_{s1}, or β_{r1}	k_2, k_3, and β_{r2}, β_{r3}
Load Related Cracking	Alligator Cracking	C_2 or k_1	k_2, k_3, and C_1
	Longitudinal Cracking	C_2 or k_1	k_2, k_3, and C_1
	Semi-Rigid Pavements	C_2 or β_{c1}	C_1, C_2, C_4
Non-Load Related Cracking	Transverse Cracking	β_{t3}	β_{t3}
IRI		C_4	C_1, C_2, C_3

The process to eliminate the bias is applied to the globally calibrated pavement performance transfer functions found to result in bias from step 7. The process used to eliminate the bias depends on the cause of that bias and the accuracy desired by the agency. NCHRP 1-40B project study (NCHRP, 2009) addresses three possibilities of bias and the bias elimination procedures corresponding to each possibility reproduced below.

The residual errors are, for the most part, always positive or negative with a low standard error of the estimate in comparison to the trigger value, and the slope of the residual errors versus predicted values is relatively constant and close to zero. In other words, the precision of the prediction model is reasonable but the accuracy is poor. In this case, the local calibration coefficient is used to reduce the bias. This condition generally requires the least level of effort and the fewest number of runs or iterations of the MEPDG with varying the local calibration values to reduce the bias. The statistical assessment described in step 7 should be conducted to the local calibrated pavement performance to check obtaining agency acceptable bias.

The bias is low and relatively constant with time or number of loading cycles, but the residual errors have a wide dispersion varying from positive to negative values. In other words, the accuracy of the prediction model is reasonable, but the precision is poor. In this case, the coefficient of the prediction equation is used to reduce the bias but the value of the local calibration coefficient is probably dependent on some site feature, material property, and/or design feature included in the sampling template. This condition generally requires more runs and a higher level of effort to reduce dispersion of the residual errors. The statistical assessment described in step 7 should be conducted to the local calibrated pavement performance to check obtaining agency acceptable bias.

The residual errors versus the predicted values exhibit a significant and variable slope that is dependent on the predicted value. In other words, the precision of the prediction model is poor and the accuracy is time or number of loading cycles dependent—there is poor correlation between the predicted and measured values. This condition is the most difficult to evaluate because the exponent of the number of loading cycles needs to be considered. This condition also requires the highest level of effort and many more MEPDG runs with varying the local calibration values to reduce bias and dispersion. The statistical assessment described in step 7 should be conducted to the local calibrated pavement performance to check obtaining agency acceptable bias.

Step 9: Assess Standard Error of the Estimate

After the bias is reduced or eliminated for each of the transfer functions, the standard error of the estimate (SEE, S_e) from the local calibration is evaluated in comparison to the SEE from the global calibration. The standard error of the estimate for each globally calibrated transfer function is included under the "Tools" section of the MEPDG software. Figure 2-8 illustrates the comparison of the SEE for the globally calibrated transfer functions to the SEE for the locally calibrated transfer functions.

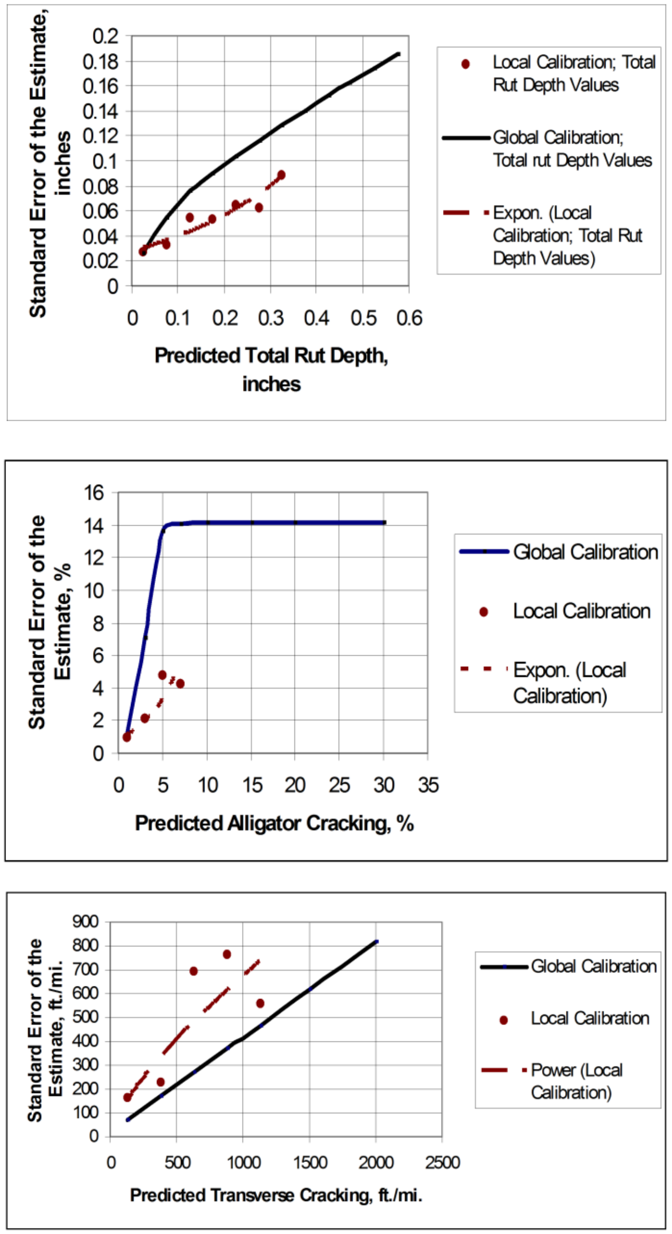

Figure 2-8 Comparison of the standard error of the estimate for the global-calibrated and local-calibrated transfer function in KSDOT study (NCHRP, 2009)

Step 10: Reduce Standard Error of the Estimate

If the SEE from the local calibration is found in step 9 to be statistically different in comparison to the SEE included in the MEPDG for each performance indicator, an statistical analysis of variance (ANOVA) can be conducted to determine if the residual error or bias is dependent on some other parameter or material/layer property for the selected roadway segments. If no correlation would be identified, the local calibration factors determined from step 8 and the SEE values obtained from step 9 could be considered as the final products for the selected roadway segments. If some correlation to some parameters (for example, HMA mixture volumetric properties) would be identified, the local calibration values should be determined for each type in correlated parameters or new calibration function should be developed. NCHRP Project 1-40B and Von Quintus (2008b) documented HMA mixture specific factors used to modify or adjust the MEPDG global calibration factors for the rut depth and the alligator (bottom-up) cracking transfer functions where sufficient data are available.

Step 11: Interpretation of Results and Deciding on Adequacy of Calibration Factors

The purpose of this step is to decide whether to adopt the local calibration values or continue to use the global values that were based on data included in the LTPP program from around the U.S. To make that decision, an agency should identify major differences between the LTPP projects and the standard practice of the agency to specify, construct, and maintain their roadway network. More importantly, the agency should determine whether the local calibration values can explain those differences. The agency should evaluate any change from unity for the local calibration parameters to ensure that the change provides engineering reasonableness.

MEPDG Local Calibration Studies at the State Level

As apart to NCHRP projects, multiple State level research efforts have been being conducted regarding the local calibration of the MEPDG involving each step described in NCHRP 1-40B study. However, not many research studies for MEPDG validation in local sections have been finalized because the MEPDG has constantly been updated through NCHRP projects (2006a; 2006b) after the release of the initial MEPDG software (Version 0.7). This section summarizes up to date MEPDG local calibration research efforts at the State level.

Hot Mix Asphalt Pavements

A study by Galal and Chehab (Galal and Chehab, 2005) in Indiana compared the distress measures of existing HMA overlays over a rubblized PCC slab section using AASHTO 1993 design with the MEPDG (Version 0.7) performance prediction results using the same design inputs. The results indicated that MEPDG provide good estimation to the distress measure except longitudinal (top–down) cracking. They also emphasized the importance of local calibration of performance prediction models.

The Montana DOT conducted the local calibration study of MEPDG for flexible pavements (Von Quintus and Moulthrop, 2007). In this study, results from the NCHRP 1-40B (Von Quintus et al. 2005) verification runs were used to determine any bias and the standard error, and compare that error to the standard error reported from the original calibration process that was completed under NCHRP Project 1-37A (NCHRP, 2004). Bias was found for most of the distress transfer functions. National calibration coefficients included in Version 0.9 of the MEPDG were used initially to predict the distresses and smoothness of the Montana calibration refinement test sections to determine any prediction model bias. These runs were considered a part of the validation process, similar to the process used under NCHRP Projects 9-30 and 1-40B. The findings from this study are summarized for each performance model as shown below:

- *Rutting prediction model*: the MEPDG over-predicted total rut depth because significant rutting was predicted in unbound layers and embankment soils.
- *Alligator cracking prediction model*: the MEPDG fatigue cracking model was found to be reasonable.
- *Longitudinal cracking prediction model*: no consistent trend in the predictions could be identified to reduce the bias and standard error, and improve the accuracy of this prediction model. It is believed that there is a significant lack-of-fit modeling error for the occurrence of longitudinal cracks.
- *Thermal cracking prediction model*: the MEPDG prediction model with the local calibration factor was found to be acceptable for predicting thermal cracks in HMA

pavements and overlays in Montana.

- *Smoothness prediction model*: the MEPDG prediction equations are recommended for use in Montana because there are too few test sections with higher levels of distress in Montana and adjacent States to accurately revise this regression equation.

Von Quintus (Von Quintus, 2008b) summarized the flexible pavement local calibration value results of the MEPDG from NCHRP project 9-30, 1-40 B, and Montana DOT studies listed in Table 2-2. These results originally from Von Quintus (Von Quintus, 2008b) are presented in Table 2-3 to Table 2-5 for the rut depth, fatigue cracking, and thermal cracking transfer functions, respectively. These could be useful reference for states having similar conditions of studied sites. The detailed information of studied sites is described elsewhere by Von Quintus (Von Quintus, 2008b).

Table 2-2 Listing of local validation-calibration projects (Von Quintus, 2008b)

Project Identification	Transfer Functions Included in the Local Validation and/or Calibration Efforts for Each Project				
	Rut Depths	Area Cracking	Longitudinal Cracking	Thermal Cracking	Smoothness or IRI
NCHRP Projects 9-30 & 1-40B; *Local Calibration Adjustments for HMA Distress Prediction Models in MEPDG Software*, (Von Quintus, et al., 2005a & b)	√	√	√		
Montana DOT, *MEPDG Flexible Pavement Performance Prediction Models for Montana*, (Von Quintus & Moulthrop, 2007a & b)	√	√	√	√	√
NCHRP Project 1-40B, *Examples Using Recommended Practice for Local Calibration of MEPDG Software*, Kansas Pavement Management Data, (Von Quintus, et al., 2008b)	√	√		√	√
NCHRP Project 1-40B, *Examples Using Recommended Practice for Local Calibration of MEPDG Software*, LTPP SPS-1 and SPS-5 Projects, (Von Quintus, et al., 2008b)	√	√		√	√

Table 2-3 Summary of local calibration values for the rut depth transfer function (Von Quintus, 2008b)

Project Identification		Unbound Materials/Soils, β_{s1}: Fine-Grained	Unbound Materials/Soils, β_{s1}: Coarse-Grained	HMA Calibration Values: β_{r1}	HMA Calibration Values: β_{r3}	HMA Calibration Values: β_{r2}
NCHRP Projects 9-30 & 1-40B; Verification Studies, Version 0.900 of the MEPDG.		0.30	0.30	Values dependent on volumetric properties of HMA; the values below represent the overall range.		
		Insufficient information to determine effect of varying soil types.		6.9 to 10.8	0.65 to 0.90	0.90 to 1.10
Montana DOT; Based on version 0.900 of the MEPDG		0.30	0.30	Values dependent on the volumetric properties of HMA; the values below represent overall averages.		
				7.0	0.70	1.13
Kansas DOT; PM Segments; HMA Overlay Projects; All Mixtures (Version 1.0)		0.50	0.50	1.5	0.95	1.00
Kansas PM Segments; New Construction	Convent.	0.50	0.50	1.5	0.90	1.00
	Superpave			1.5	1.20	1.00
	PMA			2.5	1.15	1.00
LTPP SPS-1 & SPS-5 Projects built in accordance with specification; conventional HMA mixtures (Version 1.0).		0.50	0.50	Value dependent on the air void & asphalt content		1.00
				1.25 to 1.60	0.90 to 1.15	1.00
LTPP SPS-1 Projects with anomalies or construction difficulties, unbound layers.		Values dependent on density and moisture content; values below represent the range found.		---	---	---
		0.50 to 1.25	0.50 to 3.0			

Table 2-4 Summary of local calibration values for the area fatigue cracking transfer function (Von Quintus, 2008b)

Project Identification		β_{f1}	β_{f2}	β_{f3}	C_2
NCHRP Projects 9-30 & 1-40B; Verification Studies, Version 0.900 of the MEPDG		Values dependent on the volumetric properties.			
		0.75 to 10.0	1.00	0.70 to 1.35	1.0 to 3.0
Montana DOT; Based on version 0.900 of the MEPDG, with pavement preservation treatments		Values dependent on the volumetric properties.			
		13.21	1.00	1.25	1.00
Northwest Sites; Located in States Adjacent to Montana, without pavement preservation treatments		Values dependent on the volumetric properties.			
		1.0 to 5.0	1.00	1.00	1.0 to 3.0
Kansas DOT; PM Segments; HMA Overlay Projects; All HMA Mixtures		0.05	1.00	1.00	1.00
Kansas DOT; PM Segments; New Construction	Conventional HMA Mixes	0.05	1.00	1.00	1.00
	PMA	0.005	1.00	1.00	1.00
	Superpave	0.0005	1.00	1.00	1.00
Mid-West Sites	LTPP SPS-1 Projects built in accordance with specifications	0.005	1.00	1.00	1.00
	LTPP SPS-1 Projects with anomalies or production difficulties	1.00	1.00	1.00	1.0 to 4.0
	LTPP SPS-5 Projects; Debonding between HMA Overlay and Existing Surface	0.005	1.00	1.00	1.0 to 4.0

Table 2-5 Summary of the local calibration values for the thermal cracking transfer function (Von Quintus, 2008b)

Project Identification		β_{t1}	β_{t2}	β_{t3}
Montana DOT; application of pavement preservation treatments.		---	---	0.25
Northwest Sites, located in states adjacent to Montana, but without pavement preservation treatments; appears to be agency dependent.		---	---	1.0 to 5.0
Kansas PM Segments; Full-Depth Projects	PMA	---	---	2.0
	Conventional	---	---	2.0
	Superpave	---	---	3.5
Kansas PMS Segments; HMA Overlay Projects	PMA	---	---	2.0
	Conventional	---	---	7.5
	Superpave	---	---	7.5
LTPP Projects; HMA produced in accordance with specifications	Conventional	---	---	Dependent on Asphalt Content & Air Voids
LTPP Projects; Severely aged asphalt	Conventional	---	---	7.5 to 20.0

Kang (Kang et al., 2007) prepared a regional pavement performance database for a Midwest implementation of the MEPDG. They collected input data required by the MEPDG as well as measured fatigue cracking data of flexible and rigid pavements from Michigan, Ohio, Iowa and Wisconsin State transportation agencies. They reported that the gathering of data was labor-intensive because the data resided in various and incongruent data sets. Furthermore, some pavement performance observations included temporary effects of maintenance and those observations must be removed through a tedious data cleaning process. Due to the lack of reliability in collected pavement data, the calibration factors were evaluated based on Wisconsin data and the distresses predicted by national calibration factors were compared to the field collected distresses for each state except Iowa. This study concluded that the default national calibration values do not predict the distresses observed in the Midwest. Therefore, this reinforces the reason to collect local data from Oregon for the purpose of this study and calibrate the MEPDG for local conditions. The collection of more reliable pavement data is recommended for a future study.

Schram and Abdelrahman (Schram and Abdelrahman, 2006) attempted to calibrate two of the MEPDG IRI models for the Jointed Plain Concrete Pavement (JPCP) and the HMA overlays of PCC pavements at the local project-level using Nebraska Department of Roads (NDOR) pavement management data. The focused dataset was categorized by annual daily truck traffic (ADTT) and surface layer thickness. Three categories of ADTT were considered: low (0 – 200 trucks/day), medium (201 – 500 trucks/day), and high (over 500 trucks/day). The surface layer thicknesses considered ranged from 6 inches to 14 inches for JPCP and 0 to 8 inches for HMA layers. Results showed that project-level calibrations reduced default model prediction error by nearly twice that of network-level calibration. Table 2-6 and Table 2-7, as reported from this study, contain coefficients for the smoothness model of HMA overlays of rigid pavements and JPCP.

Table 2-6 HMA overlaid rigid pavements' IRI calibration coefficients for surface layer thickness within ADTT (Schram and Abdelrahman, 2006)

ADTT	Thickness	C1	C2	C3	N	R^2	SEE (m/km)
Low	2"-3"	0.1318	0.0018	0.3971	3	0.994	0.02
	4"-5"	0.0704	-0.0048	-2.8771	16	0.813	0.11
	5"-6"	-0.0038	0.2409	-4.6360	5	0.039	1.15
Medium	2"-3"	0.0639	0.1337	-0.7896	21	0.612	0.5
	3"-4"	0.0733	0.0282	1.4725	65	0.532	0.36
	4"-5"	0.0781	-0.0032	1.1116	82	0.546	0.31
	5"-6"	0.0649	0.0169	3.5543	84	0.535	0.31
	6"-7"	0.0794	-0.0312	4.3652	31	0.888	0.17
	7"-8"	0.0674	-0.0164	1.7122	19	0.674	0.13
	8"-9"	0.0683	0.0192	-3.6231	13	0.936	0.1
High	0"-1"	0.2019	0.1158	-10.0646	27	0.392	0.45
	2"-3"	0.1866	0.0498	-16.7082	19	0.565	0.6
	3"-4"	0.1835	-0.0579	8.1863	32	0.010	0.9
	4"-5"	0.1170	-0.0100	1.4057	101	0.299	0.51
	5"-6"	0.2422	0.0371	-23.4448	62	0.713	0.85
	6"-7"	0.0756	0.0127	0.9250	64	0.597	0.22
	7"-8"	0.0604	0.0574	-2.4936	7	0.624	0.2
	8"-9"	0.0578	0.0706	-10.9179	28	0.103	0.25
	9"-10"	0.1005	-0.0001	-0.5216	8	0.845	0.13

Table 2-7 JPCP IRI calibration coefficients for surface layer thickness within ADTT (Schram and Abdelrahman, 2006)

ADTT	Thickness	C1	C2	C3	C4	N	R^2	SEE (in/mi)
Low	6"-7"	0.0000	0.0000	1.0621	74.8461	33	0.434	26.885
	7"-8"	0.0000	0.0000	1.9923	46.9256	37	0.961	8.235
	8"-9"	0.8274	0.0000	0.0000	86.9721	39	0.904	14.465
	9"-10"	0.3458	0.0000	1.5983	64.3453	110	0.537	26.230
	10"-11"	0.0300	0.0000	3.4462	10.7893	37	0.893	17.280
	11"-12"	--	--	--	--	--	--	--
	12"-13"	--	--	--	--	--	--	--
	13"-14"	--	--	--	--	--	--	--
	14"-15"	--	--	--	--	--	--	--
Medium	6"-7"	0.0000	0.0000	4.1422	0.0000	3	0.966	5.094
	7"-8"	0.0000	1.5628	0.0000	71.9009	22	0.968	9.952
	8"-9"	0.0000	0.0000	1.7162	53.0179	122	0.291	40.537
	9"-10"	0.1910	0.0000	0.9644	89.3990	609	0.686	24.945
	10"-11"	0.0000	0.0000	2.0945	73.1246	314	0.812	18.535
	11"-12"	0.0000	0.0090	1.3617	100.0000	27	0.792	10.166
	12"-13"	--	--	--	--	--	--	--
	13"-14"	0.0000	0.0100	2.2226	24.9354	4	0.924	3.948
	14"-15"	--	--	--	--	--	--	--
High	6"-7"	--	--	--	--	--	--	--
	7"-8"	--	--	--	--	--	--	--
	8"-9"	0.0000	0.1376	0.4352	79.5526	46	0.151	48.576
	9"-10"	0.1561	0.0000	1.1024	62.9556	81	0.333	31.255
	10"-11"	0.0000	0.0000	1.6344	100.0000	228	0.653	22.295
	11"-12"	0.1125	1.8207	1.1678	100.0000	29	0.739	13.366
	12"-13"	0.0000	0.0000	1.5331	100.0000	151	0.719	17.724
	13"-14"	0.0100	0.0100	0.5184	0.0000	4	0.623	1.728
	14"-15"	0.1904	0.0000	2.1387	51.4053	146	0.838	9.018

Muthadi and Kim (Muthadi and Kim, 2008) performed the calibration of the MEPDG for HMA pavements located in North Carolina (NC) using version 1.0 of the MEPDG software. Two distress models, rutting and alligator cracking, were used for this effort. A total of 53 pavement sections were selected from the LTPP program and the NC DOT databases for the calibration and validation process. Based on calibration procedures suggested by the NCHRP 1-40B study, the flow chart was made for this study. The verification results of the MEPDG performance models with national calibration factors showed bias (systematic difference) between the measured and predicted distress values. The Microsoft Excel Solver program was used to minimize the sum of the squared errors (SSE) of the measured and the predicted rutting or cracking by varying the coefficient parameters of the transfer function. Table 2-8 lists local calibration factors of rutting and alligator cracking transfer functions obtained in this study. This study concluded that the standard error for the rutting model and the alligator cracking model is significantly less after the calibration.

Table 2-8 North Carolina local calibration factors of rutting and alligator cracking transfer functions (Muthadi and Kim, 2008)

Recalibration	Calibration Coefficient	National Calibration	National Recalibration	Local Calibration
Rutting				
AC	k_1	−3.4488	−3.35412	−3.41273
	k_2	1.5606	1.5606	1.5606
	k_3	0.479244	0.479244	0.479244
GB	β_{GB}	1.673	2.03	1.5803
SG	β_{SG}	1.35	1.67	1.10491
Fatigue				
AC	k_1	0.00432	0.007566	0.007566
	k_2	3.9492	3.9492	3.9492
	k_3	1.281	1.281	1.281
	C_1	1	1	0.437199
	C_2	1	1	0.150494

The Washington State DOT (Li et al. 2009) developed procedures to calibrate the MEPDG (version 1.0) HMA pavement performance models using data obtained from the Washington State Pavement Management System (WSPMS). Calibration efforts were concentrated on the asphalt mixture fatigue damage, longitudinal cracking, alligator cracking, and rutting models. There were 13 calibration factors to be considered in the four related models. An elasticity analysis was conducted to describe the effects of those calibration factors on the pavement distress models, i.e., the higher the absolute value of elasticity, the greater impact the factor has on the model. The calibration results of typical Washington State HMA pavement systems determined from this study presents in Table 2-9. This study also reported that a version 1.0 of the MEPDG software bug does not allow calibration of the roughness model.

Table 2-9 Local calibrated coefficient results of typical Washington State flexible pavement systems (Li et al., 2009)

Calibration Factor		Default	Calibrated Factors
AC Fatigue	B_{f1}	1	0.96
	B_{f2}	1	0.97
	B_{f3}	1	1.03
Longitudinal cracking	C1	7	6.42
	C2	3.5	3.596
	C3	0	0
	C4	1000	1000
Aligator cracking	C1	1	1.071
	C2	1	1
	C3	6000	6000
AC Rutting	B_{r1}	1	1.05
	B_{r2}	1	1.109
	B_{r3}	1	1.1
Subgrade Rutting	B_{s1}	1	0
IRI	C1	40	–
	C2	0.4	–
	C3	0.008	–
	C4	0.015	–

Similar to the study conducted in NC (Muthadi and Kim 2008), Banaerjee (Banaerjee et al., 2009) minimized the SSE between the observed and the predicted surface permanent deformation to determine the coefficient parameters of HMA permanent deformation performance model after values based on expert knowledge assumed for the subgrade permanent deformation calibration factors (β_{s1}) and the HMA mixture temperature dependency calibration factors (β_{r2}). Pavement data from the Texas SPS-1 and SPS-3 experiments of the LTPP database were used to run the MEPDG and calibrate the guide to Texas conditions. The set of state-default calibration coefficients for Texas was determined from joint minimization of the SSE for all the sections after the determination of the Level 2 input calibration coefficients for each section. The results of calibration factors as obtained from this study are given in Figure 2-9. Souliman (Souliman et al., 2010) also presented the calibration of the MEPDG (Version 1.0) predictive models for flexible pavement design in Arizona conditions. This calibration was performed using 39 Arizona pavement sections included in the LTPP database. The results of calibration factors as obtained from this study are given in Table 2-10.

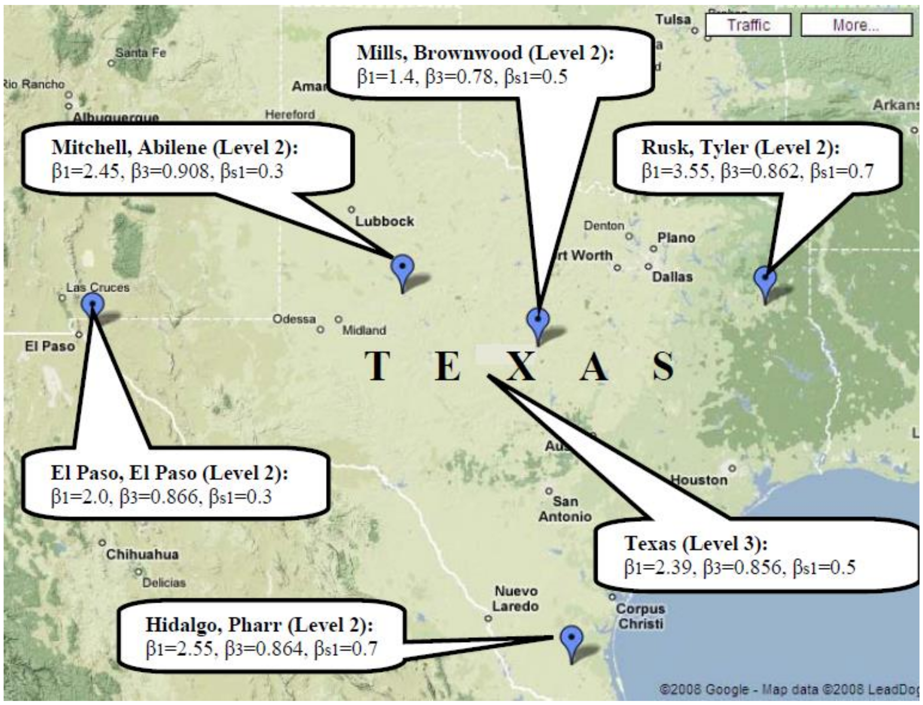

Figure 2-9 Regional and State level calibration coefficients of HMA rutting depth transfer function for Texas (Banerjee et al., 2009)

Hoegh (Hoegh et al., 2010) utilized time history rutting performance data for pavement sections at the Minnesota Department of Transportation (Mn DOT) full-scale pavement research facility (MnROAD) for an evaluation and local calibration of the MEPDG rutting model. Instead of an adjustment of the calibration parameters in the current MEPDG rutting model, a modified rutting model was suggested to account for the forensic and predictive evaluations on the local conditions. This study demonstrated that the current MEPDG subgrade and base rutting models grossly overestimate rutting for the MnROAD test sections.

Some type of maintenance or rehabilitation activity can make actual distress measurements decrease in distress time-history plots (Kim et al., 2010). Banerjee (Banerjee et al., 2010) found that the calculation factors of the MEPDG permanent deformation performance models are influenced by maintenance strategies. Liu (Liu et al., 2010) suggested historical pavement performance model to account for rehabilitation or maintenance activity using piecewise approximation. The whole pavement serviceable life was divided into three zones: Zone 1 for the early age pavement distress, Zone 2 in rehabilitation stage, and Zone 3 for over-distressed situations. The historical pavement performance data were regressed independently in each time zone. This approach is able to accurately predict the pavement distress progression trends in each individual zone by eliminating the possible impacts from the biased data in the other zones. It is also possible to compare the pavement distress progression trends in each individual zone with the MEPDG incremental damage approach predictions.

Table 2-10 Calibration coefficients of the MEPDG HMA pavement distress models in Arizona conditions (Souliman et al., 2010)

MEPDG Model	Coefficients before Calibration	Coefficients after Calibration	Net Effect of Calibration
Alligator Fatigue Transfer Function	$\beta_{f1} = 1$	$\beta_{f1} = 0.729$	Increased prediction
	$\beta_{f2} = 1$	$\beta_{f2} = 0.8$	
	$\beta_{f3} = 1$	$\beta_{f3} = 0.8$	
	$C_1 = 1.0$	$C_1 = 0.732$	
	$C_2 = 1.0$	$C_2 = 0.732$	
Longitudinal Fatigue Transfer Function	$\beta_{f1} = 1$	$\beta_{f1} = 0.729$	Decreased prediction
	$\beta_{f2} = 1$	$\beta_{f2} = 0.8$	
	$\beta_{f3} = 1$	$\beta_{f3} = 0.8$	
	$C_1 = 7.0$	$C_1 = 1.607$	
	$C_2 = 3.5$	$C_2 = 0.803$	
AC Rutting Model	$\beta_{r1} = 1$	$\beta_{r1} = 3.63$	Increased prediction
	$\beta_{r2} = 1$	$\beta_{r2} = 1.1$	
	$\beta_{r3} = 1$	$\beta_{r3} = 0.7$	
Granular base Rutting Model	$\beta_{gb} = 1$	$\beta_{gb} = 0.111$	Decreased prediction
Subgrade Rutting Model	$\beta_{sg} = 1$	$\beta_{sg} = 1.38$	Increased prediction
Roughness Model	$C_1 = 40$	$C_1 = 5.455$	Decreased prediction
	$C_2 = 0.4$	$C_2 = 0.354$	
	$C_3 = 0.008$	$C_3 = 0.008$	
	$C_4 = 0.015$	$C_4 = 0.015$	

Mamlouk and Zapata (Mamlouk and Zapata, 2010) discussed differences between the Arizona Department of Transportation (ADOT) PMS data and the LTPP database used in the original development and national calibration of the MEPDG distress models. Differences were found between the following: rut measurements, asphalt cracking, IRI, and all layer backcalculated moduli found from NDT measurements done by ADOT and those of the LTPP. Differences in distress data include types of data measured, types of measuring equipment, data processing methods, units of measurements, sampling methods, unit length of pavement section, number of runs of measuring devices, and survey manuals used. Similar findings were reported in NC DOT PMS by Corley-Lay (Corley-Lay et al., 2010). Table 2-11 summarizes the findings of agency's efforts on calibration of performance prediction models for HMA pavements.

Table 2-11 Summary of calibration effort conducted by agencies

Model/ Agency	*Rutting*	*Alligator (Bottom-up)*	*Longitudinal (Top-down)*	*Transverse (Thermal)*	*Roughness*
Arkansas DOT	Good	Good	Poor	Poor	-
Arizona DOT	Good	Good	Poor	N/A	Poor
Minnesota DOT	Good	-	-	-	-
North Carolina DOT	Good	Good	-	-	-
Montana DOT	Good	Average	Poor	Average	Good
Nebraska DOT	-	-	-	-	Good
Washington DOT	Good	Average	Average	Average	Poor

Portland Cement Concrete Pavements

The Washington State DOT (Li et al., 2006) developed procedures to calibrate the MEPDG (Version 0.9) PCC pavement performance models using data obtained from the WS PMS. Some significant conclusions from this study are as follows: (a) WSDOT PCC pavement performance prediction models require calibration factors significantly different from default values; (b) the MEPDG software does not model longitudinal cracking of PCC pavement, which is significant in WSDOT pavements; (c) WS PMS does not separate longitudinal and thermal cracking in PCC pavements, a deficiency that makes calibration of the software's thermal cracking model difficult; and (d) the software does not model studded tire wear, which is significant in WS DOT pavements. This study also reported that: (a) the calibrated software can be used to predict future deterioration caused by faulting, but it cannot be used to predict cracking caused by the thermal or longitudinal cracking issues in PCC pavement, and (b) with a few improvements and resolving software bugs, the MEPDG software can be used as an advanced tool to design PCC pavements and predict future pavement performance. The local calibration results of typical Washington State PCC pavement systems determined from this study are presented in Table 2-12.

Table 2-12 Calibration coefficients of the MEPDG (Version 0.9) PCC pavement distress models in the State of Washington (Li et al., 2006)

Calibration Factor		Default for New Pavements	Undoweled	Undoweled – MP[a]	DBR[b,c]
Cracking	C_1	2	2.4	2.4	2.4
	C_2	1.22	1.45	1.45	1.45
	C_4	1	0.13855	0.13855	0.13855
	C_5	-1.68	-2.115	-2.115	-2.115
Faulting	C_1	1.29	0.4	0.4	0.934
	C_2	1.1	0.341	0.341	0.6
	C_3	0.001725	0.000535	0.000535	0.001725
	C_4	0.0008	0.000248	0.000248	0.0004
	C_5	250	77.5	77.5	250
	C_6	0.4	0.0064	0.064	0.4
	C_7	1.2	2.04	9.67	0.65
	C_8	400	400	400	400
Roughness[d]	C_1	0.8203	0.8203	0.8203	0.8203
	C_2	0.4417	0.4417	0.4417	0.4417
	C_3	1.4929	1.4929	1.4929	1.4929
	C_4	25.24	25.24	25.24	25.24

Notes:

a. Mountain pass climate
b. Dowel bar retrofitted
c. DBR calibration factors are the same as default "restoration" values in NCHRP 1-37A software
d. Roughness calibration factors are the same as the default values

Khazanovich (Khazanovich et al., 2008) evaluated the MEPDG PCC pavement performance prediction models for the design of low-volume concrete pavements in Minnesota. It was found that the faulting model in versions 0.8 and 0.9 of the MEPDG produced acceptable predictions, whereas the cracking model had to be adjusted. The cracking model was recalibrated using the design and performance data for 65 pavement sections located in Minnesota, Iowa, Wisconsin, and Illinois. The recalibrated coefficients of the 0.8 and 0.9 versions of the MEPDG for cracking model predictions in this study are (1) $C_1 = 1.9875$, (2) $C_2 = -2.145$. Since the MEPDG software evaluated in this study was not a final product, the authors recommended that these values should be updated for the final version of the MEPDG software.

Bustos (Bustos et al., 2009) attempted to adjust and calibrate the MEPDG PCC pavement distress models to Argentina conditions. A sensitivity analysis of distress model transfer functions was conducted to identify the most important calibration coefficient. The C_6 of joint faulting model transfer function and the C_1 or C_2 of cracking model transfer function were the most sensitive coefficients.

Top-Down Cracking

Background

It have been well recognized that cracking of hot-mix asphalt (HMA) pavements is a major mode of premature failure. Currently, four major mode of failure associated with HMA cracking are identified: (Birgisson et al., 2002, Von Quintus and Moulthrop, 2007) 1) fatigue cracking, which starts at the bottom of the HMA pavement and propagates upward to the surface of the pavement, 2) top-down cracking, initiating at the top of the asphalt pavement layer in a direction along the wheel path and propagating upward, 3) thermal cracking, and 4) reflective cracking, in which existing cracks or joints cause stress concentrations that result in crack propagation through an HMA overlay.

Traditionally, most flexible pavement design methods consider fatigue cracking initiating at the bottom of the HMA layer and propagating upward as the most critical criteria for the fatigue failure of HMA pavements. However, recent research has suggested that premature pavement fatigue failure initiates at the surface of HMA pavement and propagates downward, which is known as top-down cracking (shown in Figures 2-10 and 2-11). The only way to differentiate top-down cracking form bottom-up cracking is to take cores and trench sections. For years pavement engineers within the Washington State Department of Transportation (WSDOT) have observed that asphalt concrete pavements in State of Washington have displayed longitudinal and fatigue cracks (multi-connected) that appear to crack from the top of the pavement and propagate downward. Often, the cracks stop at the interface between the wearing course and the underlying bituminous layers (a depth of about 50 mm).The top-down cracking was observed in thicker sections with thinner sections cracking full depth. Top-down cracking generally started within three to eight years of paving for pavement sections that were structurally adequate and were designed for adequate ESALs (Uhlmeyer et al., 2000).

In July 1997, a section o of I-25 between Colorado State Highway 7 and 120th Avenue near Denver was rehabilitated by cold milling the existing surface to a depth of 3 inch. and replacing with 3 inch. new hot mix asphalt. The 3/4 inch. (19 mm) mixture contained asphalt content of 4.8% and asphalt grade of PG 76-28. It is important to note that the project received bonus for material quality and smoothness and the mixture passed all torture tests (Hamburg and French Wheel Rutter) in the Colorado Department of Transportation’s European Laboratory. Longitudinal cracks appeared in the outside lanes of both the north and southbound directions within 1 year of the project completion. The severity of the cracking ranged from low to medium and in some locations high. The occurrence of this premature cracking followed a series of investigations. The first investigation revealed that two of three cores taken over the top of existing longitudinal cracks were observed reflecting cracks through from the underlying pavement. It was identified that the reflecting cracks were due to the presence of moisture and traffic. After the first project, a statewide evaluation was conducted to identify the extent of this distress in other pavements. As a result, 28 projects were evaluated throughout the state of Colorado and 18 projects displayed top-down cracking (Harmelink et al., 2008)

A study by Myers et al.(1998) in Florida reported that fatigue failure of HMA pavement in Florida was mainly caused by top-down cracking A more recent study by Wang et al. (2007) revealed that 90% cracking encountered in Florida HMA pavements were recognized as top-down cracking. This scenario is not unique to Florida. Similar results have been reported in other states and countries, including Indiana, Washington, India, Japan, Kenya, South Africa, France, Netherlands, and United Kingdom (Kim and Underwood, 2003).

Figure 2-10 Lane exhibiting surface initiated top-down cracking in both wheelpaths (Myers et al., 2000)

Figure 2-11 Core extracted from wheelpath shows top-down cracking (Myers et al., 2000)

Stages of Top-Down Cracking

Top-down cracking in hot mix asphalt pavements initiates at the pavement surface and propagates downward, sometimes throughout the entire depth of the asphalt pavement. There are three stages recognized associated with initiation and propagation of top-down cracks. (Svasdisant et al., 2002). At initial stage, a single short longitudinal crack appears just outside the wheelpath. Over time, the top-down cracks grow into a second stage where the longitudinal short cracks grow longer and sister cracks develop parallel to and within 0.3 to 1 meter (1 to 3 feet) from the original cracks. Finally, the top-down cracks merge into a third stage where the parallel longitudinal cracks are connected through short transverse top-down cracks. Figure 2-12 illustrates the three stages mentioned earlier where A, B, and C represent first, second and third stages, respectively.

Causes and Mechanisms of Top-down Cracking

Svasdisant et al. (2002) conducted field and laboratory investigations on flexible and rubblized pavements exhibiting top down cracking. Detailed mechanistic analyses were conducted using the engineering characteristics obtained from field and laboratory test results to determine the potential for top down cracking. In the mechanistic analysis, 3-D finite element method using the ABAQUS, the CHEVRONX (a closed-form solution) and the MICHPAVE (a liner/nonlinear 2-D finite element) computer programs were used. The conclusions of the study are as follows:

- Most top down cracking are observed just outside the wheelpaths and progress in three stages.
- Surface radial tensile stress induced by wheel load and enhanced by differential stiffness due to construction (poor compaction and segregation), temperature and aging can cause top down cracking,
- Aging of asphalt binder reduces the tensile strength and tensile strain at failure of the asphalt mixture, and
- The locations of the maximum surface tensile stress predicted by the mechanistic analysis correspond very well to the locations of the filed observed top down cracking.

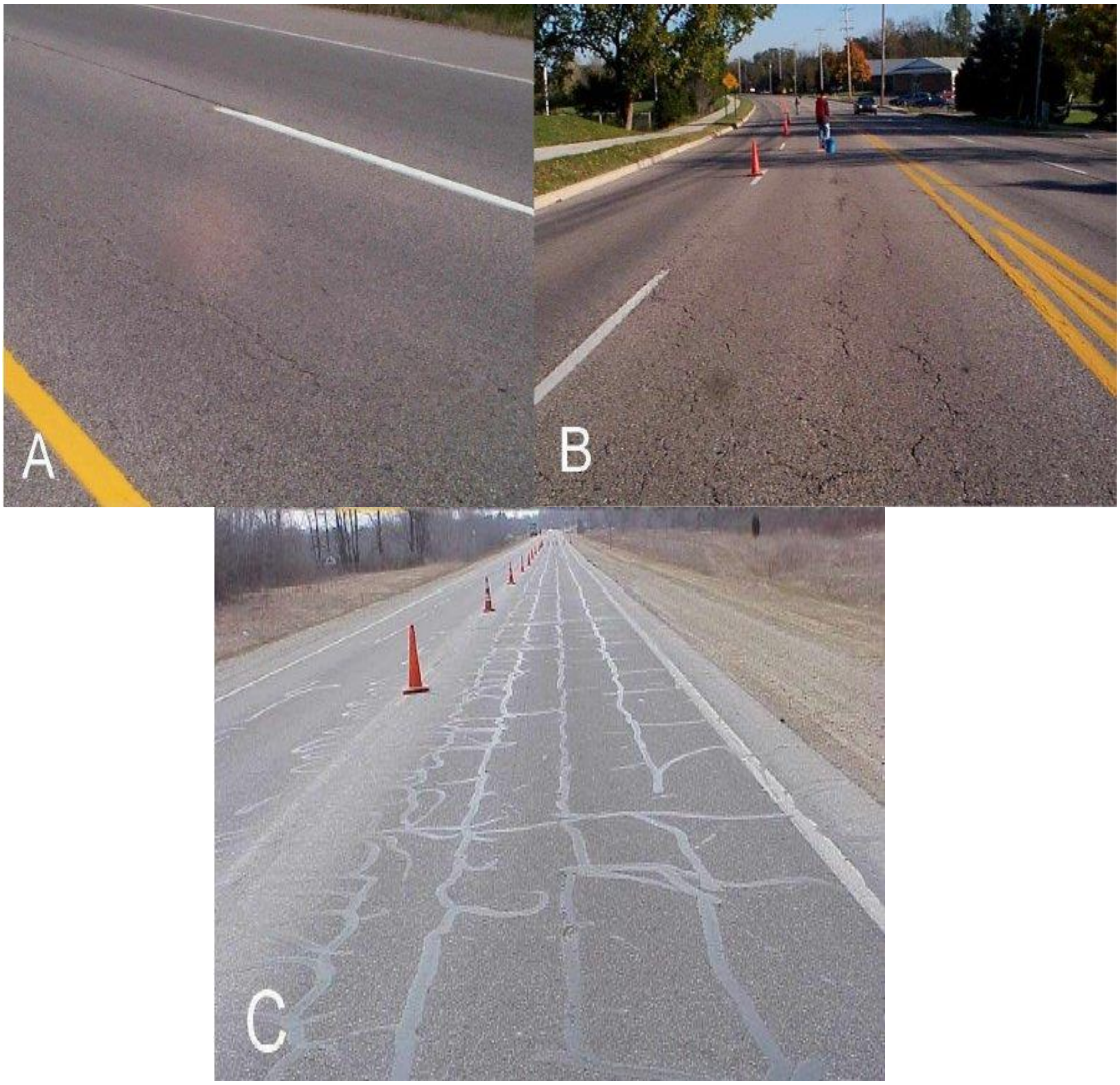

Figure 2-12 Photographs illustrating the development of top-down cracking (Svasdisant et al., 2002)

Baladi et al. (2002) studied the effects of segregation on the initiation and propagation of top down cracking in flexible pavements. Both field and forensic investigation were conducted and it was confirmed that top down cracking initiates in segregated areas. The results from the mechanistic analysis revealed that segregated areas are susceptible to fatigue cracking manifested as top down cracking.

Nunn (1998) reported that surface initiated cracks, either longitudinal or transverse, were observed about 10 years after construction in UK motorways. He observed that there was no evidence of fatigue cracking in the lower bituminous base layers with thickness exceeding 180 mm-only the wearing course. The transverse cracks were related to low binder penetration values (typically about 15). He noted that the surface initiated cracking was due to horizontal tensile stresses generated by truck tires at the top of asphalt surface. Wide based tires generated the highest tensile stresses. Nunn (1998) concluded based on the work performed in the Netherlands that for asphalt thickness greater than 160 mm, cracks initiated at the pavement surface and eventually penetrated to a depth of about 100 mm. He also stated that full depth cracks were observed with thinner pavement sections.

Myers et al. (1998) observed that surface initiated cracking predominates in Florida five to ten years after construction. Based on the computer modeling, they found out that tensile stresses under the treads of the tire-not the tire edges-were the primary cause of the cracks. Further, they stated that wide based tires caused the highest tensile stresses, which confirmed the results conducted by Nunn (1998). They concluded that surface initiated cracking is not a structural design issue but more related to mixture composition. They suggested that more fracture resistant mixtures be used to improve the surface initiated cracking performance of the pavement. Gerritsen et al. (1987) observed that pavements in Netherlands were experiencing premature cracking in the wearing course. These surface cracks which did not extend into the lower bituminous base layers, occurred both inside and outside the wheelpath areas, and in some cases, soon after the construction. They reported that the surface cracking outside of the wheelpaths had low mix strength characteristics at low temperature and the surface cracks in the wheelpaths areas were largely due to radial shear forces under truck tires near the tire edges. They concluded that both load and thermal related effects could be attributed to the observed surface cracking. Their recommendation was to increase the binder film thickness to reduce early age hardening of the mixtures.

Dauzats et al. (1987) reported that surface initiated cracks, either longitudinal or transverse, were observed in France and occurred typically three to five years after paving. They found that these types of surface cracks were initially caused by thermal stresses and then further propagated by traffic loads. They noted that a rapid hardening of the mix binder likely contributed to this type of pavement distress.

Studies based on measured tire/pavement contact pressures by De Beer et al. (1997) and Himeno et al. (1997) and instrumented pavements by Dai et al. (1997) in MinnRoad supported the view that truck tires were a primary cause of top-down cracking in asphalt concrete wearing courses.

In a study by Harmelink et al. (2008), 28 projects were evaluated from a wide geographical area of Colorado and 18 sites out of 28 sites were judged exhibiting top down cracking. Of these 18 sites, 12 had visual evidence of segregation observed at the bottom of the upper pavement lift as shown in Figure 2-13, that was not visible on the surface. Other factors included percentage of air voids in the pavement, volume of effective asphalt binder, and physical properties of the asphalt binder.

A study conducted by the Illinois Department of Transportation (IDOT) in 1993 detailed the history and investigation of longitudinal cracks in asphalt pavements. The study indicated that there is a high degree of correlation between the outside edges of the conveyors on the paver and the longitudinal cracking in the pavement. Two pavers were identified in the study that demonstrated the correlation between the longitudinal cracking in the pavement and the outside edges of the conveyor slats.

A micromechanics study on top-down cracking based on the material's microstructure by Wang et al. (2003) indicated that top-down cracking may not necessarily initiate only at the pavement surface. It may also initiate at some distance down from the pavement surface. They concluded that both tensile-type and shear-type cracking could initiate top-down cracking. They also concluded that when the mastic is weaker or the pavement surface temperature is higher, top-down cracking most likely initiate. Therefore, a mix sensitive to rutting may also be sensitive to top-down cracking.

Myers et al. (2001) concluded that top-down cracking can be initiated by traffic induced stresses, temperature changes, or due to their combined effect. Temperature and modulus gradients are assumed to be critical to the top-down cracking initiation and propagation.

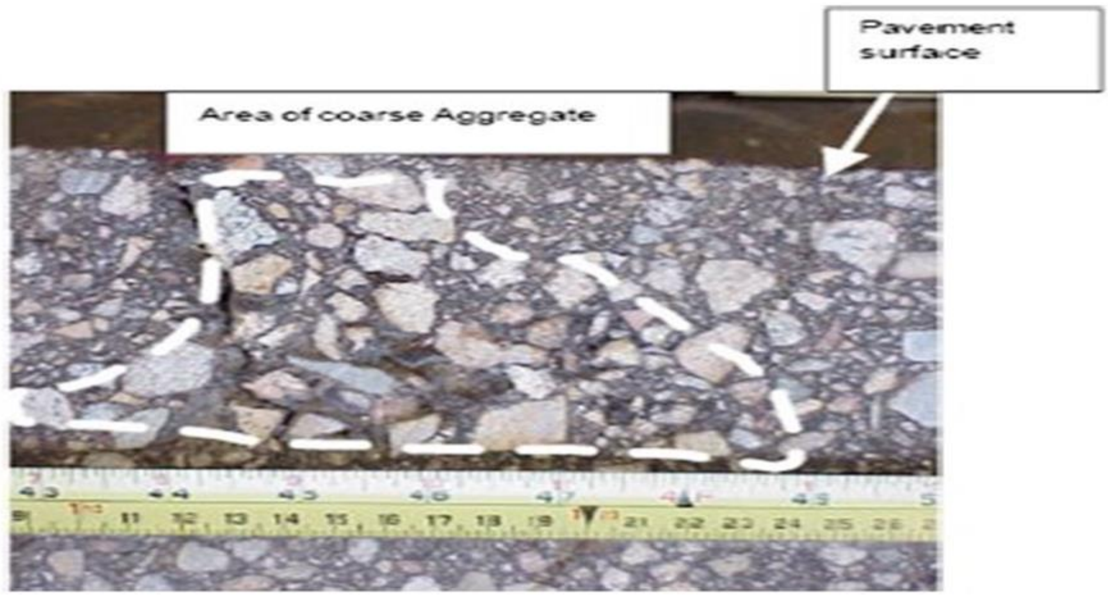

Figure 2-13 Segregation at the Bottom of Pavement lift (Harmelink et al., 2008)

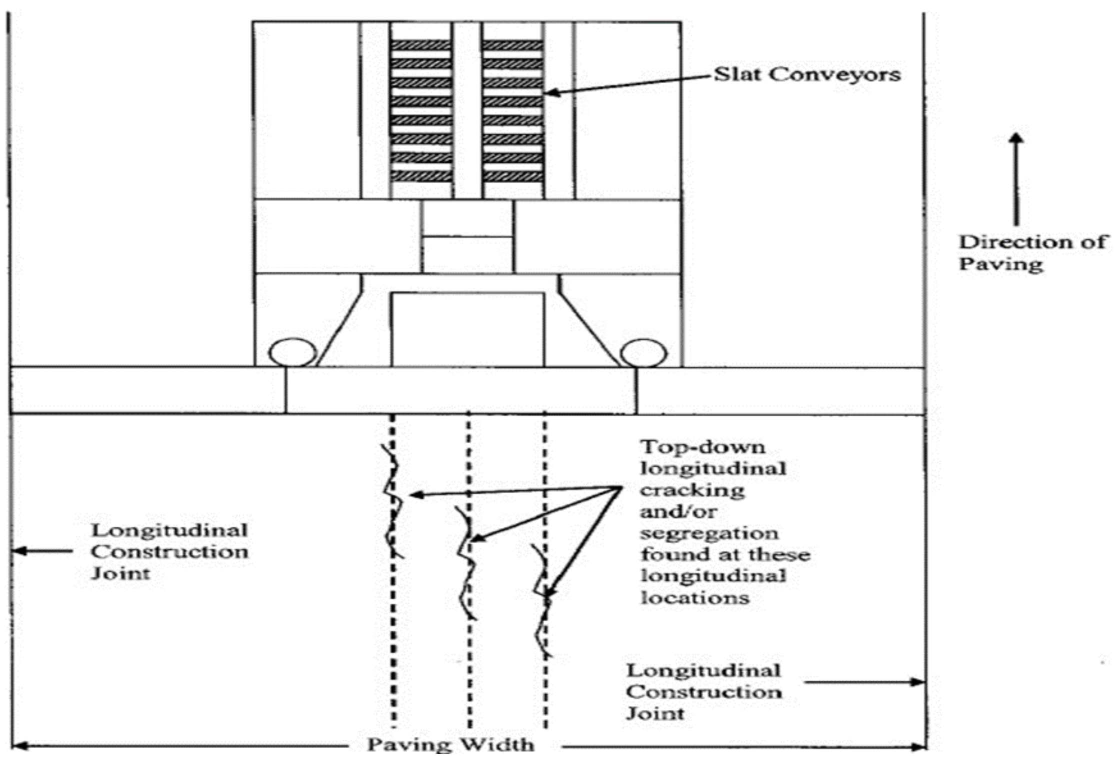

Figure 2-14 Paver top view and associated top-down longitudinal cracks (Harmelink et al., 2008)

Baladi et al. (2003) concluded that a segregated area in pavement due to poor construction is more prone to top-down cracking along with raveling. They also mentioned that differential stiffness between HMA courses cause a significant increase in load-induced surface tensile stresses. Nighttime temperatures produce the highest magnitude of surface tensile stress.

A study by Freitas et al. (2005) concluded that air voids, segregation and binder content have a significant effect on the top-down cracking for all temperatures. They also found that higher temperature and rutted surface contributes significantly to top-down cracking initiation. El-Basyouny and Witczak (2005) stated that top-down cracking is caused by extremely large contact pressures at the tire edge-pavement interface in combination with highly aged thin surface layer that have become oxidized.

A study by Sridhar et al. (2008) on the Indian Highways indicated that temperature, especially in combination with heavy axle loading, was a critical parameter influencing the top-down cracking susceptibility of the HMA layer. H. Wang and I.L. Al-Qadi (2010) concluded that at high temperatures, shear-induced top-down cracking could initiate from some distance below the pavement surface in conjunction with the distortional deformation. They also indicated that negative temperature gradient in the HMA layer and debonding under the surface layer could lead to premature top-down cracking. Ozer et al. (2011) stated that several factors contribute to the top-down cracking such as, heavy traffic and thermal loads, stiffness gradients due to binder aging, variation in bituminous characteristics between lifts, and bituminous material segregation. There are various opinions related to mechanisms that causes top-down cracking, but there are no conclusive data to suggest that one is more applicable than the other one is (Von Quintus and Moulthrop, 2007). Based on the literature review aforementioned, the following factors are considered to be contributing to top-down cracking initiation and propagation:

- high tire and contact pressures and/or heavy wheel loads
- severe aging of the binder near the surface resulting in large modulus gradients
- combination of thermal stresses with those induced from heavy wheel loads
- mixture properties, including binder type and content, air voids, and aggregate gradation
- construction quality, including segregation and compaction procedures
- climatic conditions as well as structural conditions, including layer thickness

Top-down Cracking Model Used in M-EPDG

Over the last 3 to 4 decades of pavement technology, fatigue cracking has been assumed to normally initiate at the bottom of the asphalt layer and propagate to the surface (bottom-up cracking). However, numerous recent worldwide studies have also concluded that fatigue cracking may also initiate from the top of the surface and propagate downward which is known as top-down cracking. This type of cracking is not as well defined from a mechanistic viewpoint as the more classical bottom-up cracking. However, it is a reasonable engineering assumption, with the current state of knowledge, that this distress may be due to critical tensile and/or shear stresses developed at the pavement surface and, perhaps, caused by extremely large contact pressures at the tire edge-pavement interface; coupled with highly aged (stiff) thin surface layer that have become oxidized. In this initial mechanistic attempt to model top-down cracking in the Design Guide; the failure mechanism for this distress is hypothesized to be a result of tensile surface strains leading to fatigue cracking at the pavement surface.

The MEPDG predicts both bottom-up and top-down fatigue cracks using an incremental damage index approach. Alligator cracks are assumed to initiate at the bottom of HMA layers, while longitudinal cracks are assumed to initiate at the surface of the pavement. For both load related cracking models, the approach to calculate the allowable number of axle-load applications needed for the incremental damage index is shown using Equation 2-7.

$$N_{f-HMA} = k_{f1}(C)(C_H)\beta_{f1}(\varepsilon_t)^{k_{f2}\beta_{f2}}(E_{HMA})^{k_{f3}\beta_{f3}} \qquad (2-7)$$

where:

N_{f-HMA} = Allowable number of axle-load applications for a flexible pavement and HMA overlayers

ε_t = Tensile strain at critical locations and calculated by the structural response model, in./in.

E_{HMA} = Dynamic modulus of the HMA measured in compression, psi

k_{f1}, k_{f2}, k_{f3} = Global field calibration parameters (from the NCHRP 1-40D re-calibration; kf1=0.007566, kf2=-3.9492, and kf3=-1.281), and

$\beta_{f1}, \beta_{f2}, \beta_{f3}$ = Local or mixture specific field calibration constants; for the global calibration effort, these constants were set to 1.0

C = Correction factor, 10^M, when:

$$M = 4.84\left(\frac{V_{be}}{V_a + V_{be}} - 0.69\right)$$

V_a = Percent air voids in the HMA mixture (in situ only, not mixture design)

V_{be} = Effective asphalt content by volume, percent

C_H = Thickness correction term, depending on type of cracking:

For bottom-up or alligator cracking:

$$C_H = \frac{1}{0.000398 + \frac{0.003602}{1+e^{(11.02-3.49H_{HMA})}}}$$

H_{HMA} = Total HMA thickness, in.

For top-down or longitudinal cracking:

$$C_H = \frac{1}{0.01 + \frac{12.00}{1+e^{(15.676-2.8186H_{HMA})}}}$$

H_{HMA} = Total HMA thickness, in.

Using the calculation for allowable number of axle-load applications shown above, the MEPDG calculates an incremental damage index (ΔDI) to predict the load related cracking. The incremental damage index (DI) is calculated for each axle load interval for each axle type and truck type that is applied within a month that is subdivided into five average temperatures. The cumulative damage index is determined by summing the incremental damage indices (refer to Equation 2-8).

$$DI = \sum (\Delta DI)_{j,m,l,p,T} = \sum \left(\frac{n}{N_{f-HMA}}\right)_{j,m,l,p,T} \qquad (2-8)$$

where:

n = Actual number of axle load applications within a specific time period

N_{f-HMA} = Allowable number of axle load applications for a flexible pavement and HMA overlays to fatigue cracking

j = Axle-load interval

m = Axle-load type (single, tandem, tridem, quad, or special axle configuration)

l = Truck type using the truck classification groups included in the M-EPDG

p = Month

T = Median temperature for the five temperature intervals used to subdivide Each month

The MEPDG calculates the amount of alligator area cracking and the length on LCWP based on the incremental damage index that are summed with time and different truck loadings (Equation 2-8). Different relationships were developed between the amounts of cracking and damage indices. Equation 2-9 is the relationship to predict area alligator cracking based on total lane area, while Equation 2-10 is the relationship to predict length of longitudinal cracking in the wheel paths.

Bottom initiated fatigue cracks:

$$FC_{Bottom} = \left(\frac{1}{60}\right)\left(\frac{C_4}{1 + e^{\left(C_1 C_1^* + C_2 C_2^* Log(DI_{Bottom} * 100)\right)}}\right) \qquad (2-9)$$

where:

FC_{Bottom} = Bottom initiated fatigue cracks, percent of total lane area

C_4 = Calibration coefficients of 6,000

C_1 = Calibration coefficients of 1.00

C_2 = Calibration coefficients of 1.00

C_1^* = $-2C_2^*$

C_2^* = $-2.40874 - 39.748\,(1 + H_{HMA})^{-2.856}$

H_{HMA} = Total HMA thickness, in.

DI_{Bottom} = Bottom incremental damage index

Surface initiated fatigue cracks:

$$FC_{Top} = 10.56\left(\frac{C_4}{1 + e^{(C_1 - C_2 Log DI_{Top})}}\right) \qquad (2-10)$$

where:

FC_{Top} = Surface initiated longitudinal cracks, ft/mile

C_4 = Calibration coefficients of 1,000

C_1 = Calibration coefficients of 7.00

C_2 = Calibration coefficients of 3.5

DI_{Top} = Surface incremental damage index

Energy Ratio Concept

Energy ratio is used to evaluate the asphalt mixture's resistance to cracking. Roque et al. (2006) performed an extensive study on 27 pavement sections collected from cracked and uncracked sections throughout the state of Florida to evaluate the top down cracking in flexible pavements, as shown in Figure 2-15.

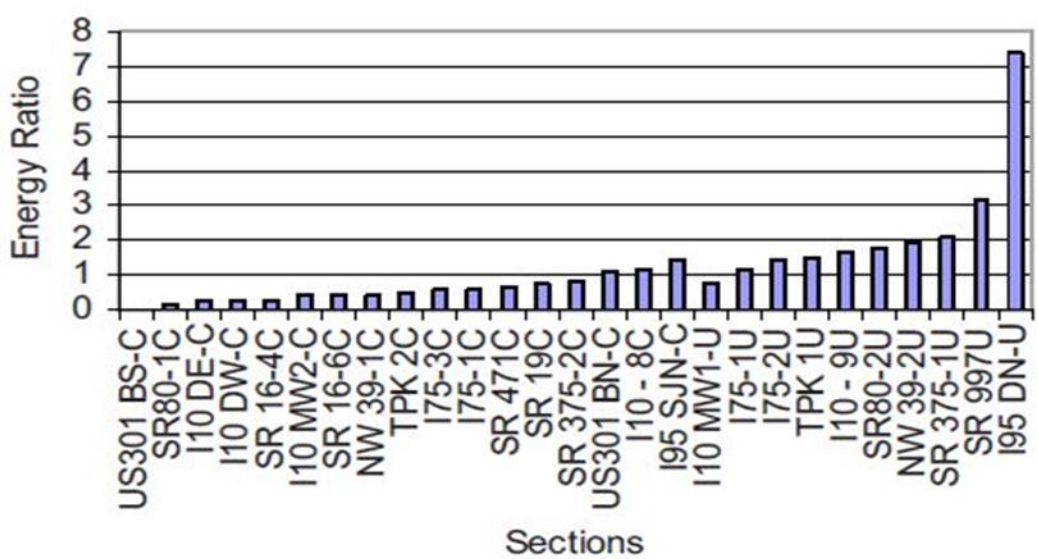

Figure 2-15 Energy ratio for 27 field test sections in Florida (Kim et al., 2009)

All the cracked sections, as represented by "C" in Figure 2-15, showed top down cracking. All the uncracked sections in Figure 2-6 are represented by "U". Based on a parameter called energy ratio, Roque et al. (2004) suggested a simple form of a crack model through the evaluation of known top-down cracking performance data. The higher the value of energy ratio, the better the top down cracking performance of the pavement. The energy ratio (ER) is given by the following equation:

$$ER = \frac{DCSE_f.[7.294.10^{-5}.\sigma^{-3.1}(6.36-S_t)+2.46.10^{-8}}{m^{2.98}.D_1} \qquad (2-11)$$

Where $DCSE_f$ is dissipated creep strain energy at failure, σ is the tensile stress obtained at the bottom of the asphalt layer using elastic layer analysis, m and D_1 are power function parameters. The parameters required for the top down cracking model can be obtained from resilient modulus, creep compliance and tensile strength tests. The resilient modulus, M_r is determined from the stress-strain curve obtained in resilient modulus test. The power function parameters are obtained by fitting the creep compliance curve performed using a constant load control load. The tensile strength and dissipated creep strain energy at failure are determined from the stress-strain curve of a given mixture from the strength test. Figure 2-16 shows the description of parameters determined for top down cracking model.

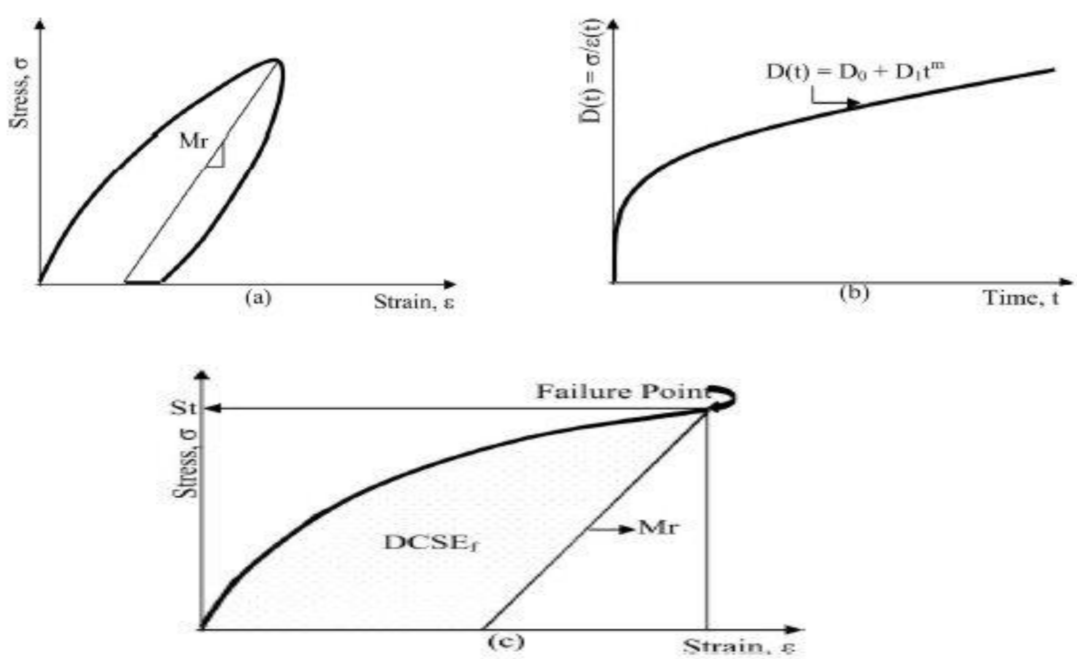

Figure 2-16 Description of parameters obtained from (a) resilient modulus, (b) creep compliance, and (c) strength tests (Kim et al., 2009)

Kim et al. (2009) found that tensile strain obtained at the top is inversely related to energy ratio, if the identified tensile strain at top is a primary cause of top down cracking. Figure 2-17 shows the linear relationship between energy ratio and inverse tensile strain at top at the 50-loading cycle. The study indicated that the tensile strain at the top of asphalt layer is a primary factor affecting the top down cracking performance.

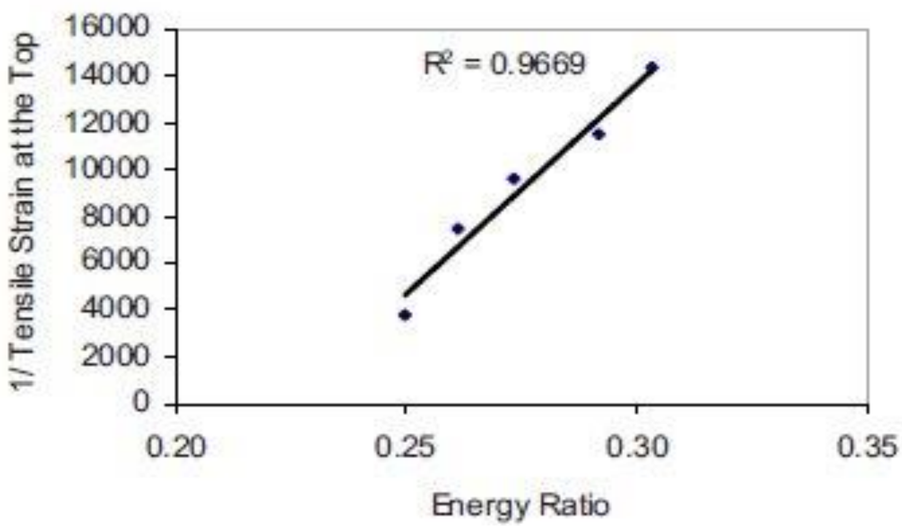

Figure 2-17 Inverse tensile strain at top of the asphalt layer versus energy ratio (Kim et al., 2009)

Prevention and Rehabilitation of Top-down Cracking

Pellinen et al. (2004) reported recommendations related to the prevention of top-down cracking in terms of material selection, material properties and construction practices:

- In-situ air voids content should be reduced below or equal to 7% by requiring tougher density specification.
- The amount of fines in the asphalt mixture is recommended to limit to 5% to 6%.
- No changes for binder grade at this point
- Non-uniformities in the material properties should be prevented by enhancing construction practices and QC/QA work including prevention of segregation during paving.

Emery (2006) reported the two major potential solutions for top-down cracking focus on the most controllable factors:

- "*improved heavy vehicle loadings control (weigh-in motion scales for instance - difficult but imperative for developing countries) and appropriate mechanical, axle and tire technology implementation (suspension systems and tires properly matched, inflated and kept in good operating condition - very difficult, but again imperative for developing countries); and*
- *improved renewable, specialized asphalt surface courses (open graded friction course, stone mastic asphalt and Superpave, for instance) with good permanent deformation (rutting) resistance, and enhanced tensile and shear stress endurance*".

Before rehabilitation strategy, top-down cracking should be distinguished from bottom-up cracking based on the knowledge of the thickness of the pavement structure and the pattern of cracking. Top-down cracking manifests itself as a longitudinal cracking in the wheelpath area or in the center of the lane. If layer thickness is above 200 mm it is unlikely that cracks will penetrate deeper than through the surface layer in the pavement. Coring from a few locations in the pavement and examining cracks can be used to verify the top-down cracking. A structural analysis based on falling weight deflectometer (FWD) testing must be performed to confirm that the cracking has not weakened the pavement structure. If the pavement structural capacity is good, then the pavement can be rehabilitated by milling and replacing the surface mix. The selection of the materials for rehabilitation strategy should be based on the structural capacity of the pavement. The material selection for rehabilitation should follow the recommendations given to prevent top-down cracking (Pellinen et al., 2004).

Segregation was apparent around the top down cracking studied by Harmelink et al. (2008). As moisture infiltrates these cracks, progressive deterioration of the pavement around the cracks will occur. Therefore, sealing the cracks should reduce the moisture infiltration if the crack has not widened significantly. Other forms of rehabilitation discussed include milling the affected area surrounding the crack and replacing with hot mix asphalt. However, this repair method has not been successful in the past (Shuler, 2007) and is discouraged due to the creation of two longitudinal cracks adjacent to the crack being repaired.

Harmelink et al. (2008) concluded that the occurrence of top down cracking reduced through the changes to the Superpave mix design process during 2003. The changes included an increase in the asphalt binder content in the mix; which appeared to reduce the potential for segregation. This increase in binder content was accomplished by reducing the number of design gyrations as a function of traffic volume.

Uhlmeyer et al. (2000) studied top-down cracking in the State of Washington and reported that rehabilitation strategy for top-down cracking should be based on the severity of cracking. If the pavement surface is cracking within the top lift, possibly caused by stripping, rotomilling the top lift of asphalt and inlaying would be the preferred rehabilitation option. For some longitudinal cracking, pavement repair prior to overlaying or just overlaying the roadway may be the best choice depending upon the severity of the cracks. Rehabilitation for full depth cracked areas, depending upon the severity of distress, may require removal and replacement of fatigued pavement.

CHAPTER 3 - RESEARCH PLAN DEVELOPMENT

Local Calibration of the MEPDG Prediction Models

Introduction

The research plan developed for calibrating the MEPDG generally followed the flow chart recommended by Von Quintus et al. (2009) with some modifications as outlined in Figures 3-1 and 3-2 summarized below.

It is important to point out that since Accelerated Pavement Testing (APT) does not exist in Oregon, this has been struck out in Figures 3-1 (step 4) and 3-2 (step 7). Further, the research team did forensic investigation only in so far as to determine the type of load related cracking, e.g. top-down as compared to bottom-up cracking, via coring at the end of cracks.

The data mining of Oregon DOT databases included identifying pavement types with varying levels of distresses, as well as historical mix design, structural design, and traffic information for rehabilitated pavements. The research team pursued obtaining pavement sections with a range of distress levels for the types of pavement types for cracking and rutting. Further challenging the research team in this endeavor is understanding the differences between materials used historically as compared to those being used today (e.g. pre-Superpave mixes as compared to Superpave). It was necessary to plan for conducting distress surveys in accordance with the FHWA Long Term Pavement Performance (LTPP) publication *Data Collection Guide For Long Term Pavement Performance* for calibrating the simulated outcomes of the MEPDG. The pavement test sections needed to cover a range of climatic conditions from coastal areas (western Oregon) to central and eastern Oregon, a range of trafficking levels, and typically used materials. The research team segmented the trafficking levels into two categories: low volume (less than 10 million Equivalent Single Axle Load (ESALs)), and high volume (greater than 10 million ESALs). This was based upon the changes in the mix design criteria which includes the materials specified in the various design levels.

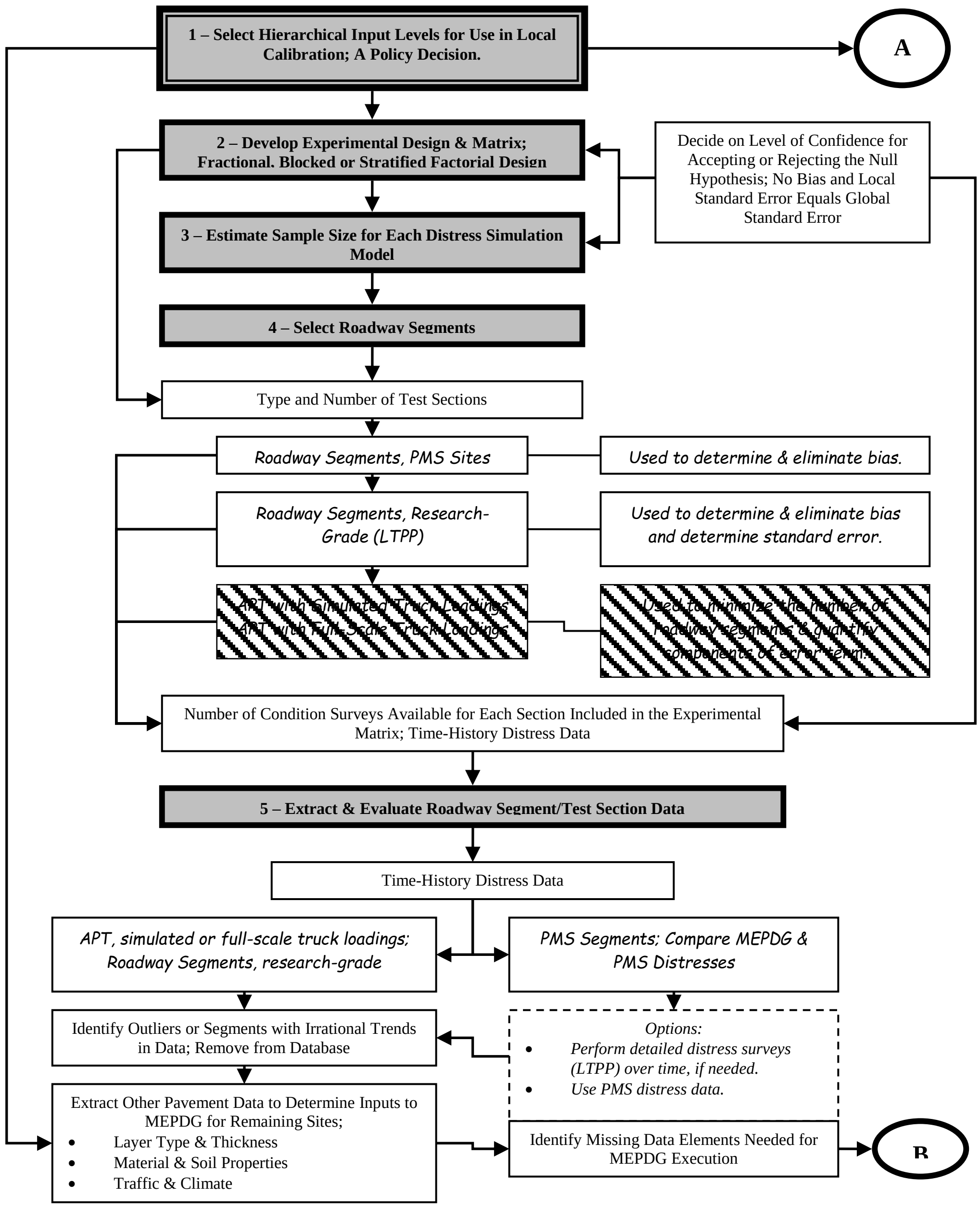

Figure 3-1 Flow chart for the procedure and steps suggested for local calibration: steps 1-5 (Von Quintus et al., 2009

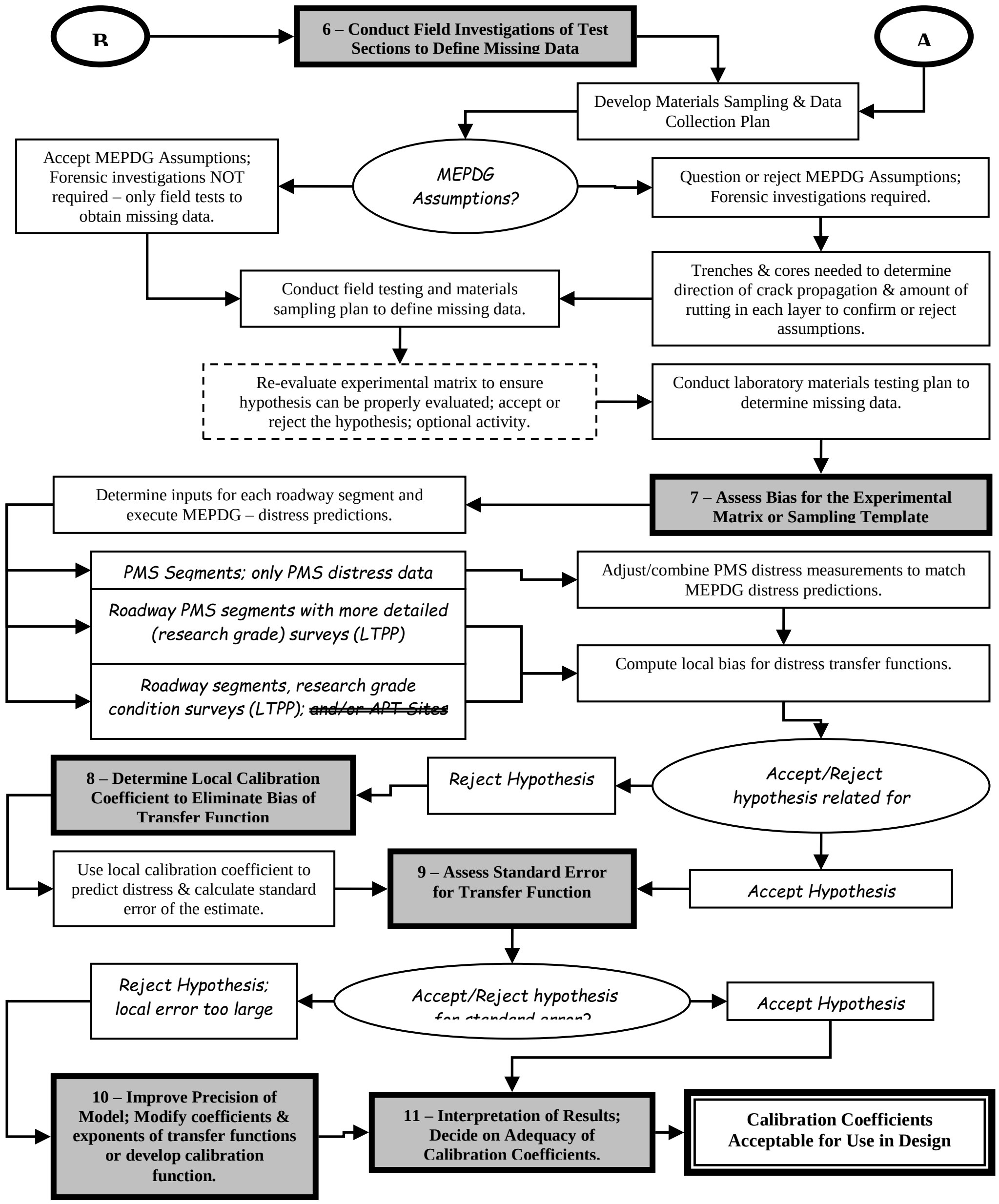

Figure 3-2 Flow chart for the procedure and steps suggested for local calibration: steps 6-11 (Von Quintus et al., 2009)

Development of Calibration Plan

The calibration of the MEPDG needed to consider a number of different factors including the following:

- Pavement type/structure,
- Pavement age,
- Pavement performance,
- Trafficking level, and
- Region (climatic variation).

A brief discussion of the identified factors ensues to illustrate the importance of these factors in the experimental plan.

Pavement Type

There are five primary pavement types in Oregon consisting of hot mix asphalt over aggregate base (HMA/Agg), HMA inlay or overlay over aggregate base (HMA/HMA/Agg), HMA inlay or overlay over cement treated base (HMA/HMA/CTB), continuously reinforced concrete pavement (CRCP), and HMA overlay of CRCP (HMA/CRCP). Open-graded friction coarse mixes are often used as surface mixes in lieu of dense-graded ones and they needed to be considered. Also, polymer modified asphalt binders have only been used for the past five years and the longer term performance aspects may not exist in older pavement sections. The primary pavement types included in the calibration were HMA over aggregate base, HMA inlay or overlay over aggregate base, HMA inlay or overlay over cement treated base, HMA overlay of CRCP, and CRCP.

Pavement Age and Performance

The pavement performance at various ages is critical to calibrating the MEPDG. The three primary distresses targeted for HMA pavement types were HMA rutting, fatigue cracking, and thermal cracking. The MEPDG considers two types of fatigue cracking: the classical bottom-up (alligator) and top-down (longitudinal). Most pavement management systems do not delineate between the two types of fatigue cracking, thus the research team attempted to identify whether the cracking was bottom- up or top-down. It was important for rutting to be delineated between material shear flow as compared to wear rutting of open-graded friction coarse mixes. Based upon discussion with the Technical Advisory Committee (TAC), subgrade rutting is not a problem in Oregon and thus it was not reasonable to identify pavements with a range in performance for this distress. The performance characteristics for CRCP are cracking and surface defects. Cracking in CRCP includes durability (D), longitudinal cracking, thermal cracking, punch-outs (with crack width for calibration), and determine the international roughness index. Whereas surface defects are map cracking/scaling, polishing, and pop-outs.

Trafficking Level

The trafficking levels are important to identify as varying materials are used depending upon a pavements design level. As an example, varying amounts of RAP are allowable depending upon the ESAL design level as the number of design gyrations. The research team's initial thinking was that two trafficking levels be considered: 1. less than 10million ESALs, and 2. more than 10million ESALs. This would delineate the higher quality aggregates and the use of polymer modified binder in high volume roads, and have the HMA overlays of cold mixes in low volume roads. Also, CRCP only occurs in high volume roads.

Region (Climatic Variation)

Oregon has vastly different climatic conditions that occur on the Coast as compared to in the Valley and on the Eastern portion of the state. As a result, the research team considered three different regions, however, not all pavement types necessarily occur in each region.

Initial Field Experimental Plan

The developed initial field experimental plan that considered the factors addressed above was developed and pursued is represented in Table 3-1. The plan included the three aforementioned regions (Coastal, Valley, and Eastern), the five primary types of pavements (HMA over aggregate base = HMA/Agg, HMA inlay or overlay over aggregate base= HMA/HMA/Agg, HMA inlay or overlay over cement treated base=HMA/HMA/CTB, HMA overlay of CRCP=HMA/CRCP, and CRCP), low and high trafficked roads, and three different levels of pavement performance (very good-excellent, as expected, and inadequate). Each experimental block has three replicate locations for condition surveys to be conducted within a selected roadway section. As an example, X_{011} represent section 01, location 1. The three locations were randomly selected within the segment length using a random number generator and then normalized. To simplify the coordination of the condition surveys, only one traffic direction underwent condition surveys and again the direction was randomly selected. The draft experimental plan called for identifying 36 pavement sections for conducting condition surveys for a total of 108 pavement condition surveys.

Field Experimental Plan

The research team in coordination with the Oregon DOT updated the experimental plan to reflect the needs to best calibrate the MEPDG. This updated field plan is reflected in Table 3-2 on the ensuing page. It is important to point out that all of these pavements had at least three pavement condition surveys conducted on three randomly selected 500 foot sections. In some instances, the initial random sections needed to be adjusted for safety reasons, e.g. avoiding intersections and on or off ramps for divided roadways as well as bridge structures. In a couple of instances, it was necessary to shorten the survey section length from 500 to 300 feet, because the overall pavement section was less than one mile, yet the surveyed sections did represent a substantial percentage of the overall pavement. Where the pavement being surveyed was less than 0.5 mile, the entire pavement was surveyed.

Table 3-1 Draft field experimental plan

		Region								
		Coastal			Valley			Eastern		
Traffic	Pavement Performance	HMA/Agg, HMA/HMA/CTB	HMA/HMA/Agg	HMA/CRCP, CRCP	HMA/Agg, HMA/ HMA/CTB	HMA/HMA/Agg	CRCP	HMA/Agg, HMA/HMA/CTB	HMA/HMA/Agg	HMA/ CRCP, CRCP
Low Volume	Very Good-Excellent	X_{011}, X_{012}, X_{013}	X_{021}, X_{022}, X_{023}		X_{031}, X_{032}, X_{033}	X_{041}, X_{042}, X_{043}		X_{051}, X_{052}, X_{053}	X_{061}, X_{062}, X_{063}	
	As Expected	X_{071}, X_{072}, X_{073}	X_{081}, X_{082}, X_{083}		X_{091}, X_{092}, X_{093}	X_{101}, X_{102}, X_{103}		X_{111}, X_{112}, X_{113}	X_{121}, X_{122}, X_{123}	
	Inadequate	X_{131}, X_{132}, X_{133}	X_{141}, X_{142}, X_{143}		X_{151}, X_{152}, X_{153}	X_{161}, X_{162}, X_{163}		X_{171}, X_{172}, X_{173}	X_{181}, X_{182}, X_{183}	
High Volume	Very Good-Excellent	X_{191}, X_{192}, X_{193}		X_{201}, X_{202}, X_{203}	X_{211}, X_{212}, X_{213}		X_{221}, X_{222}, X_{223}	X_{231}, X_{232}, X_{233}		X_{241}, X_{242}, X_{243}
	As Expected	X_{251}, X_{252}, X_{253}		X_{261}, X_{262}, X_{263}	X_{271}, X_{272}, X_{273}		X_{281}, X_{282}, X_{283}	X_{291}, X_{292}, X_{293}		X_{301}, X_{302}, X_{303}
	Inadequate	X_{311}, X_{312}, X_{313}		X_{321}, X_{322}, X_{323}	X_{331}, X_{332}, X_{333}		X_{341}, X_{342}, X_{343}	X_{351}, X_{352}, X_{353}		X_{361}, X_{362}, X_{363}

Table 3-2 Pavement sections surveyed

		Region								
		Coastal		Valley				Eastern		
Traffic	Pavement Performance	HMA/HMA/Agg	HMA/HMA/CTB	HMA/HMA/Agg	HMA/Agg	CRCP/stab or unstab	HMA/CRCP	HMA/HMA/Agg	HMA/Agg	CRCP/stab or unstab
Low Volume	Very good-Excellent	US 101: Neptune Dr-Camp Rilea	US 101: NCL Bandon-June Ave, US 101: Sutton Creek-Munsel Lake Rd	US 20: Sweet Home-18th Ave, OR 34: Wcl Lebanon-RXR X-ing,				US 730: I-84 Canal Rd, OR 201: Washington Ave-Airport Way, OR 140: Jct Hwy 019-Bowers Bridges Creek		
	As expected	US 101:Tillamook Couplet (SB), US 101: Wilson R.-Tillamook Couplet	US 101:Elk Hill Rd-Port Orford	OR 99 E:Albany Ave-Calapooia St				US 97: Weighb St-Crawford Rd, US 20: MP 10.3-MP 12.5	US 26: Prairie City-Dixie Summit, US 26: Prairie City Section, US 395: Jct Hwy 2-Hwy 33	
	Inadequate	US 101: Dooley Br-Jct Hwy 047, US 101: Florida Ave-Washington Ave			OR 221: N. Salem-Orchard Heights Rd			US730: Canal Rd-Umatilla Bridge		
High Volume	Very good-Excellent			US 30: Cornelius Pass Rd-Begin JCP, OR 120: End Jcp-Beg Hwy 081			I-5:Wilsonville Intch-Tualatin R	US 97: S. Century Dr-MP 161		
	As expected			OR 569: Hwy 091-Willametter R. (EB)	OR 99W: Marys R-Kiger Island Dr, OR 99W: N. Sherwood-SW 12th St.	I-5:Corvallis/Lea non Interchange-N. Albany	I-5: Haysville Intch to Woodburn	US 97: Madras Couplet-Hwy 360		I-84:N. Powder-Baldock Slough, I-84: N. FK Jocobsen Gulch-Malheur River (WB)
	Inadequate			I-5: Azalea-Canyonville, OR 99W: Brustschr St. -Jct Hwy 151,	OR 22: End Hwy 072-I-5 NB Ramps		I-84: NE Union Ave-S. Banfield Intch	I-84: N.FK Jocobsen Gulch-Malheur River (EB), US 97: N. Chiloquin Intch-Williamson Dr		I-84: Stanfield Int-Pendleton,

Top-Down Cracking

Experimental Plan and Site Selection

The proposed experimental plan summarized in Table 3-3 below represents sampling 10 pavements, 6 with top-down cracking and 4 without top-down cracking. ODOT pavement management databases have been explored to identify top performers and early failures. Database investigation also included reviewing pavement designs, mix designs and construction history. This represents a factorial plan based upon the main effects- with and without top-down cracking, and ESAL level (low vs. high trafficking levels). Each of the pavements with top-down cracking would need 10 cores of 6-inch diameter, 5 next to a crack and 5 away from the crack. Prior to removing the 10 cores, the top-down cracking would need to be verified by coring on a crack. Overall, this would allow for determination of what led to the crack initiation and propagation at a particular location and thus identify potential differences within the same pavement section. Sampling pavements that have not undergone top-down cracking, 5 6-inch diameter cores, will allow for comparison of good performing pavements as compared to ones that are experiencing inadequate performance. These comparisons will allow for determining the mechanisms leading to good performing pavements and those experiencing top down cracking. Table 3-4 illustrates the designation of the pavement sections that will be used in this study.

Table 3-3 Proposed experimental plan

Pavement Performance	Location	ESAL Level							
		Low Volume Traffic				High Volume Traffic			
		Proposed Candidates				Proposed Candidates			
		Name	Highway Number	Begin MP	End MP	Name	Highway Number	Begin MP	End MP
Pavements with Top-Down Cracking	Next To Crack	OR221	150	17.3	20.15	OR99EB	072	0.47	3.41
		OR238	272	38.09	38.75	OR99W	091	21.8	23.76
		OR140	270	53.6	53.79	OR99	091	108.82	109.65
	Away From Crack	OR221	150	17.3	20.15	OR99EB	072	0.47	3.41
		OR238	272	38.09	38.75	OR99W	091	21.8	23.76
		OR140	270	53.6	53.79	OR99*	091	108.82	109.65
Pavements without Top-Down Cracking	N/A	OR22	162	12.11	13.8	US20	007	1.11	2.29
						US97	004	114.25	115.2
						OR99	091	108.82	109.65

* Denotes bad (cracked) performing section of OR99

Table 3-4 Designation of the test sections in the study

Test Section	Route	Cracking	Designation Used in this Study
OR22:Sublimity Intchg Sect (RW2-WB)	OR22	NO	OR22-U
OR238: Beg. Div Hwy-Jct Hwy 063	OR238	YES	OR238-C
OR 99W:Brutscher St-Jct Hwy 151	OR99W	YES	OR99W-C
OR 221: N. Salem-Orchard Heights Rd	OR221	YES	OR221-C
OR 99EB: Jct Hwy 001-Comm. St.	OR99EB	YES	OR99EB-C
US97: NW Wimp Way-Terrebonne	US97	NO	US97-U
US20: NE 11th St-Purcell Blvd	US20	NO	US20-U
OR 140: Aspen Lake Rd-Boat Landing	OR140	YES	OR140-C
OR99: Junction City 1 (Cracked)	OR99	YES	OR99*-C
OR99: Junction City 1 (Uncracked)	OR99	NO	OR99-U

Field Work Plan

This phase included field work including identification of pavements with and without top-down cracking, and field sampling. It is difficult to identify pavements with top-down cracking through examining pavement performance records and only through forensic field study that includes coring, can identify top-down cracking. Thus candidate pavements for top-down cracking evaluation would likely need to be identified through a combination of paper records review, discussion with ODOT personnel, as well as utilizing information gathered from the recently completed M-E Pavement Design Guide calibration project. Once pavements that have been identified as top-down cracking candidates, field sampling via coring will be done for subsequent assessment. It is important to verify top-down cracking via sampling on top of cracks as well as sampling next to the crack and well away for the cracks. Before coring is done, field condition survey and falling weight deflectometer (FWD) testing will be conducted. Also, dynamic cone penetrometer (DCP) testing on base/subbase as well as geoprobe samples up to 4 feet deep at core locations after coring. This field testing information will subsequently be used to assess the adequancy of the pavement structure. Visible assessment of drainage conditions will also done on site. In this phase the following tasks are to be completed:

- Field condition survey compatible with MEPDG
- FWD testing to assess the adequancy of the pavement structure

- Field sampling-10 cores from each pavement with top-down cracking and 5 cores from each pavement without top-down cracking
- DCP testing and geoprobe samples at core locations after coring

Laboratory Testing Plan

Laboratory testing on the extracted asphalt mixture cores will include dynamic modulus and indirect tensile strength testing in a diametrical test configuration over a range of temperatures and at multiple frequencies. The binder will then be extracted and recovered from the cores for subsequent rheological testing for binder grade determination. The binder grading will include dynamic shear rheometer and bending beam rheometer testing for grade determination. Further, the recovered aggregate will be tested for gradation, and coarse and fine aggregate angularity. Table 3-5 lists all the tests that will be performed on the asphalt cores, and extracted asphalt binder and aggregate.

Table 3-5 Tests on asphalt mix cores and asphalt binder

Test Name	Standard Be Used
Bulk Specific Gravity & Density of Asphalt Mix Cores	AASHTO T 166-93
Dynamic Modulus (E^*)	AASHTO T342-11
Indirect Tensile Strength (ITS)	AASHTO T322-07
Theoretical Maximum Specific gravity of Asphalt Mix	AASHTO T 209-94
Binder Recover & Extraction	AASHTO T319-08
Dynamic Shear Rheometer (DSR)	AASHTO T315
Bending Beam Rheometer (BBR)	AASHTO T313
Aggregate Gradation	AASHTO T 27-93

Upon completion of the tests on asphalt mix cores and asphalt binder, gradation analysis on removed unbound base materials will be performed for subsequent comparison to construction records and material design specifications in place at the time of construction. This will allow for determination whether or not fines have migrated into the unbound base materials and adversely affecting their performance.

CHAPTER 4 - LOCAL CALIBRATION OF THE FATIGUE CRACKING MODEL OF THE MEPDG FOR PAVEMENT REHABILITATION IN OREGON

Md S. Rahman[1 2], R. Christopher Williams[3], and Todd Scholz[4]

A paper accepted for presentation at the *Transportation Research Board* Annual Meeting, January, 2013

Abstract

The performance prediction models within the AASHTO Mechanistic-Empirical Pavement Design Guide (MEPDG) were calibrated primarily using design inputs and performance data largely from the national Long-Term Pavement Performance (LTPP) program. Before implementing the MEPDG at the state level, performance (distress) prediction models warrant detailed validation and calibration because of potential differences between national and local conditions. The Oregon Department of Transportation (ODOT) is in the process of implementing the new MEPDG for new pavement sections. However, the vast majority of pavement work conducted by ODOT involves rehabilitation of existing pavements.

---

[1] Ph.D. Candidate, Department of Civil, Construction & Environmental Engineering, Ames, IA 50011. PH: 515 817 3774, E-mail: msrahman@iastate.edu

[2] Primary researcher and author

[3] Professor, Department of Civil, Construction & Environmental Engineering, Ames, IA 50011. PH: 515 294 4419, Fax: 515 294 8216, E-mail: rwilliam@iastate.edu

[4] Assistant Professor, School of Civil and Construction Engineering, Corvallis, OR 97331. PH: 541 737 2056, Fax: 541 737 3052, E-mail: todd.scholz@oregonstate.edu

Hot mix asphalt concrete (AC) overlays are the preferred rehabilitation treatment for both flexible and rigid pavements in Oregon. However, like new work sections, AC overlays are also susceptible to fatigue cracking (alligator cracking and longitudinal cracking), rutting, and thermal cracking. Additional work is therefore needed to calibrate the design process for rehabilitation of existing pavement structures. A detailed comparison of predictive and measured distresses was made using recently MEPDG released software Darwin M-E (version 1.1). It was found that Darwin M-E predictive distresses did not accurately reflect measured distresses, calling for a local calibration of performance prediction models is warranted. While the local calibration of rutting and thermal cracking prediction models is currently underway, alligator (bottom-up) cracking and longitudinal (top-down) cracking models were calibrated. The Microsoft Excel Solver was employed to optimize the calibration coefficients by minimizing the sum of the squared errors (SSR) between the predictive and measured distresses. A comparison was made between the results before and after the calibration to assess the improvement in accuracy of the distress prediction models provided by the local calibration. Both alligator cracking and longitudinal cracking models were improved by local calibration. However, there was a high degree of variability between the predicted and measured distresses, especially for longitudinal cracking, even after the calibration. It is recommended that additional sites, which would contain more detailed inputs (mostly Level 1), be established to be included in the future calibration efforts and thus, improve the accuracy of the prediction models.

Introduction

The new Mechanistic-Empirical Pavement Design Guide (MEPDG) and software were developed through the National Cooperative Highway Research Program (NCHRP) 1-37A project in recognition of the limitations of the current American Association of State Highway and Transportation Officials (AASHTO) Design Guide (NCHRP, 2004). It represents a transitioning of the empirically-based pavement design to a mechanistic-empirical procedure that combines the strengths of advanced analytical modeling and observed field performance. The pavement performance prediction models in the MEPDG were calibrated primarily using design inputs and performance data largely from the national Long-Term Pavement Performance

(LTPP) database. However, these performance prediction models warrant detailed validation and calibration because of potential differences between national and local conditons. Therefore, it is necessary to calibrate these performance prediction models for implementation in local conditions by taking into account local material properties, traffic patterns, environmental conditions, construction, and maintenance activities.

The importance of local calibration of performance prediction models contained in MEPDG is well-documented by different transportation agencies throughout the United States. Hall et al. (2011) conducted a local calibration of performance prediction models in MEPDG for Arkansas. While rutting and alligator (bottom-up) cracking models were successfully calibrated, longitudinal (top-down) cracking and transverse cracking models were not calibrated due to the nature of data (Hall et al., 2011). Souliman et al. (2010) calibrated distress models for alligator cracking, longitudinal cracking, rutting, and roughness for flexible pavements for Arizona using 39 LTPP pavement sections. It was found that national calibrated MEPDG under predicted alligator cracking and AC rutting while the longitudinal cracking and the subgrade rutting were over predicted. A significant improvement of performance prediction for alligator cracking and AC rutting resulted after calibration; however, only marginal improvement was realized for longitudinal cracking and roughness models (Souliman et al., 2010). Hoegh et al. (2010) conducted a local calibration of the rutting model for MnROAD test sections. They concluded that the locally calibrated model greatly improved the MEPDG rutting prediction for various pavement designs in MnROAD conditions (Hoegh et al., 2010). A study by Von Quintus (2008) found that the measurement error of the performance data had the greatest effect on the precision of MEPDG performance models (Von Quintus, 2008a, and Von Quintus, 2008b). MEPDG performance models were verified for Iowa using Pavement Management Information System (PMIS) data (Kim et al., 2010). Systematic differences were observed for rutting and cracking models. Muthadi and Kim (2008) performed the MEPDG calibration for flexible pavements located in North Caorlina (NC) using version 1.0 of the MEPDG software. Two distress models, rutting and alligator cracking, were used for this effort. This study concluded that the standard errors for the rutting model and the alligator cracking model were significantly lower after the calibration (Muthadi and Kim, 2008).

The properly calibrated MEPDG will enable more economical designs as well as potentially linking pavement design with actual material characteristics-, and construction processes. Further, as newer technologies and materials are developed, characterization of their material properties will expedite their use in the MEPDG. Several examples exist including the use of warm mix asphalt, post consumer asphalt roofing shingles in asphalt mixtures, and the evaluation of other technologies such as additives and modifiers

The Need for Local Calibration

The Oregon Department of Transportation (ODOT) is in the process of implementing the new Mechanistic-Empirical pavement design guide (MEPDG) for new pavement sections. Internally, ODOT has been evaluating the MEPDG for new sections for both flexible and rigid interstate pavement sections. Work is also currently being conducted at Oregon State University to develop design inputs and evaluate the three principal pavement performance models (e.g., fatigue cracking, rutting, and thermal cracking models) that are integral to the design process of new work sections for asphalt concrete (AC) pavement structures. However, the vast majority of pavement work conducted by ODOT involves rehabilitation of existing pavements. Additional work is therefore needed to calibrate the design process for rehabilitation of existing pavement structures.

Asphalt mix overlays are the preferred rehabilitation treatment for both flexible and rigid pavements in Oregon. However, like new work sections, overlays are also susceptible to fatigue cracking, rutting, and thermal cracking- thus, the need to include these forms of distresses in the calibration process.

Development of Calibration Plan and Test Sections

The research plan developed for calibrating the MEPDG generally followed the flow chart recommended by Von Quintus et al. (2009). The general procedures and steps employed for calibration of MEPDG as outlined in Figure 4-1 are summarized below.

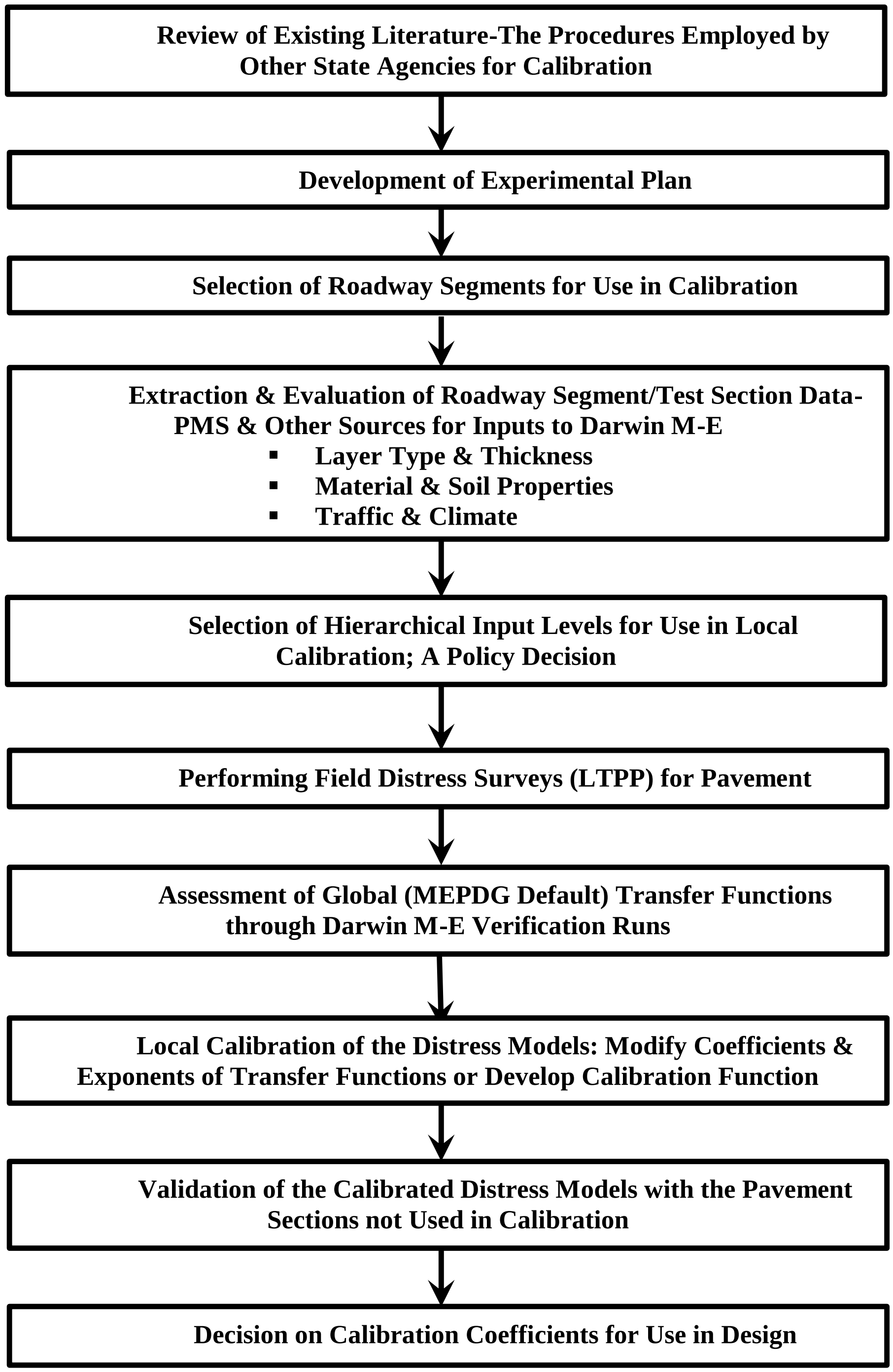

Figure 4-1 Flow chart for the procedure and steps employed for local calibration

It is important to point out that since Accelerated Pavement Testing (APT) does not exist in Oregon, this has been struck out in Figure 1. Further, the research team did forensic investigation only in so far as to determine the type of load related cracking, (e.g. top-down as compared to bottom-up cracking, via coring at the end of cracks and to verify pavement structures).

The data mining of Oregon DOT databases included identifying pavement types with varying levels of distresses, as well as historical mix design, structural design, and traffic information for rehabilitated pavements. The research team pursued obtaining pavement sections with a range of distress levels for the types of pavement types for cracking and rutting. Further challenging the research team in this endeavor was understanding the differences between materials used historically as compared to those being used today (e.g., pre-Superpave mixes as compared to Superpave mixes). Field condition surveys were conducted via distress surveys in accordance with the FHWA Long Term Pavement Performance (LTPP) publication *Data Collection Guide For Long Term Pavement Performance* for calibrating the simulated outcomes of the MEPDG. The pavement test sections also covered a range of climatic conditions from coastal areas (western Oregon) to central and eastern Oregon, a range of trafficking levels, and typically used materials. The research team segmented the trafficking levels into two categories: low volume (less than 10 million Equivalent Single Axle Load (ESALs)), and high volume (greater than 10 million ESALs). This was based upon the changes in the mix design criteria which included the materials specified in the various design levels.

The calibration of the MEPDG thus considered a number of different factors including the following:

- Pavement type/structure,
- Pavement age,
- Pavement performance,
- Trafficking level, and
- Region (climatic variation).

There are five primary pavement types in Oregon consisting of hot mix asphalt over aggregate base (HMA/Agg), HMA inlay or overlay over aggregate base (HMA/HMA/Agg), HMA inlay or overlay over cement treated base (HMA/HMA/CTB), continuously reinforced concrete pavement (CRCP), and HMA overlay of CRCP (HMA/CRCP). The primary pavement types included in the calibration were HMA over aggregate base, HMA inlay or overlay over aggregate base, HMA inlay or overlay over cement treated base, and HMA overlay of CRCP. The three primary distresses targeted for the HMA pavement types were HMA rutting, fatigue cracking, and thermal cracking. The MEPDG considers two types of fatigue cracking: the classical alligator (bottom-up) cracking and longitudinal (top-down) cracking. Most pavement management systems do not delineate between the two types of fatigue cracking, thus the research team identified whether the cracking was bottom-up or top-down via field coring. The trafficking levels are important to identify as varying materials are used depending upon a pavements design level. The research team's initial thinking was that two trafficking levels be considered: 1) less than 10million ESALs, and 2) more than 10million ESALs. Oregon has vastly different climatic conditions that occur on the Coast as compared to in the Valley and on the Eastern portion of the state. As a result, the research team considered three different regions.

The factors listed above were incorporated in the field experimental plan developed in this calibration effort as shown in Table 4-1. The plan included the three aforementioned regions (Coastal, Valley, and Eastern), the four primary types of pavements (HMA over aggregate base = HMA/Agg, HMA inlay or overlay over aggregate base=HMA/HMA/Agg, HMA inlay or overlay over cement treated base=HMA/HMA/CTB, HMA overlay of CRCP=HMA/CRCP), low and high trafficked roads, and three different levels of pavement performance (very good-excellent, as expected, and inadequate). It is important to point out that no high volume roads were identified in coastal region, thus leaving the appropriate block empty along with other empty blocks as evident in Table 4-1. In Table 4-1, one block does not necessarily mean one pavement section included in the calibration study. For instance, two pavement sections separated by comma (,)-US 101: NCL Bandon-June Ave and US 101: Sutton Creek-Munsel Lake Rd- are located in one block (Coastal Region, Low Volume Traffic, Very good-Excellent Pavement Performance, and HMA/HMA/CTB Pavement Structure).

Table 4-1 Field experimental plan

		Region						
		Coastal		Valley			Eastern	
Traffic	Pavement Performance	HMA/HMA/Agg	HMA/HMA/CTB	HMA/HMA/Agg	HMA/Agg	HMA/CRCP	HMA/HMA/Agg	HMA/Agg
Low Volume	Very good-Excellent	US 101: Neptune Dr-Camp Rilea	US 101: NCL Bandon-June Ave, US 101: Sutton Creek-Munsel Lake Rd	US 20: Sweet Home-18th Ave, OR 34: Wcl Lebanon-RXR X-ing, OR 140: Jct Hwy 019-B.B.Creek			US 730: I-84 Canal Rd, OR 201: Washington Ave-Airport Way	
	As expected	US 101:Tillamook Couplet (SB), US 101: Wilson R.-Tillamook Couplet	US 101:Elk Hill Rd-Port Orford	OR 99 E:Albany Ave-Calapooia St			US 97: Weighb St-Crawford Rd (NB), US 97: Weighb St-Crawford Rd (SB),US 20: MP 10.3-MP 12.5	US 26: Prairie City-Dixie Summit, US 26: Prairie City Section, US 395: Jct Hwy 2-Hwy 33
	Inadequate	US 101: Dooley Br-Jct Hwy 047, US 101: Florida Ave-Washington Ave			OR 221: N. Salem-Orchard Heights Rd		US730: Canal Rd-Umatilla Bridge	
High Volume	Very good-Excellent			US 30: Cornelius Pass Rd-Begin JCP, OR 120: End Jcp-Beg Hwy 081		I-5:Wilsonville Intch-Tualatin R	US 97: S. Century Dr-MP 161	
	As expected			OR 569: Hwy 091-Willametter R. (EB)	OR 99W: Marys R-Kiger Island Dr, OR 99W: N. Sherwood-SW 12th St.	I-5: Haysville Intch to Woodburn	US 97: Madras Couplet-Hwy 360	
	Inadequate			I-5: Azalea-Canyonville, OR 99W: Brustschr St. -Jct Hwy 151, US 97: N. Chiloquin Intch-W. DR	OR 22: End Hwy 072-I-5 NB Ramps	I-84: NE Union Ave-S. Banfield Intch	I-84: N.FK Jocobsen Gulch-Malheur River (EB)	

Each pavement section had three replicate locations for condition surveys conducted within a selected roadway section. The three locations, typically 500 feet each, were randomly selected using a random number generator and normalized over the section length. Condition surveys were conducted in, - only one traffic direction to simplify the coordination of surveys (i.e., work zone setup, etc.). The experimental plan included 38 pavement sections for a total of 114 pavement condition surveys. The locations of the pavement sections surveyed are shown in Figure 4-2. A total of 44 pavement sections were surveyed; 4 were CRCP and 2 were dropped out from the calibration due to lack of availability of data, thus leaving 38 pavement sections available for calibration study.

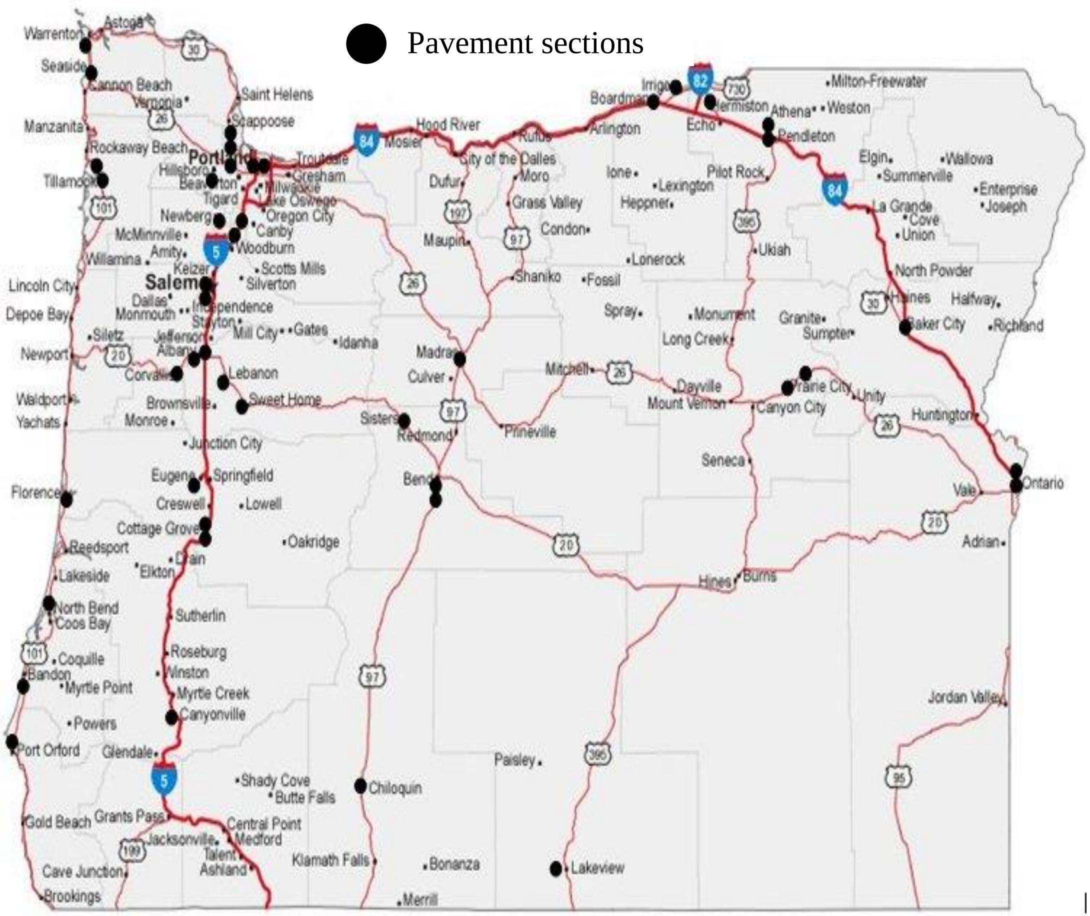

Figure 4-2 Locations of pavement sections in calibration study

Data Preparation for Calibration

The quality of the data required for the MEPDG plays a major role in the calibration accuracy. Data collection included five main categories: materials, traffic, climatic, pavement structure, and pavement performance data. ODOT's Pavement Management System (PMS) database was used for condition surveys. Furthermore, ODOT' electronic database what ODOT refers to as V-files was mined for the pavement structures used in the calibration study.

Traffic

The traffic data required for Darwin M-E includes Average Annual Daily Truck Traffic (AADTT), vehicle class distribution, growth rate, axle load distribution, number of axles per truck, hourly and monthly adjustment, lateral wander, and wheelbase. AADTT and growth rate data were derived from http://highway.odot.state.or.us/cf/highwayreports/traffic_parms.cfm and lane distribution factor (LDF) from ODOT maintained website http://www.tripcheck.com/Pages/CamerasBend.asp.

The AADTT ranged from 310 to 17,780 vehicles per day and growth rates from 0 to 3%. The lane distribution factor (LDF) for the driving lane was estimated as pavement performance (pavement distresses) of the driving lane was used in the calibration study. Table 4-2 shows the LDF for pavements with different number of lanes in one direction. Darwin M-E default values were used for vehicle class distribution, axle load distribution, number of axles per truck, hourly and monthly adjustment, lateral wander, and wheelbase.

Table 4-2 Lane distribution factor (LDF)

No of lanes in one direction	LDF
1	1
2	0.90
3	0.50
4	0.12

Climate

For each of the pavement sections, the latitude, longitude, and elevation were derived from Google Earth software using the project location. Depth of water table for each section was extracted from the Web Soil Survey of the United States Department of Agriculture (USDA) or the National Water Information System of the United States Geological Survey (USGS). This information was used to generate the climatic data for each pavement section.

Materials and Pavement Structure

Information regarding layer thicknesses and HMA mixture properties, such as binder type, gradation, volumetric properties, base, and subgrade type that are necessary for Level 3 were provided by Oregon State University (OSU) in combination with ODOT. Other default values recommended by Darwin M-E were used for Poisson’s ratio, thermal properties of the asphalt mixtures, base and subgrade properties.

Performance Data

Since ODOT distress measurement system is not compatible with MEPDG defined distresses, field condition surveys were conducted to obtain pavement performance (pavement distresses) data. The field condition distress surveys were conducted according to the FHWA Long Term Pavement Performance (LTPP) publication *Data Collection Guide for Long Term Pavement Performance* (Miller and Bellinger, 2003). It is important to point out that the vast majority of the pavements had condition surveys conducted on three randomly selected 500-foot sections and the data utilized for calibration were the average of the three condition surveys. Longitudinal (top-down) cracking and thermal cracking were reported linear feet per mile while for alligator (bottom-up) cracking, the linear feet of cracking recorded in the field distress surveys were converted a percentage of the surveyed section for calibrating with Darwin M-E as the software estimates the percentage of a sections’-cracked area. Similar to the national calibration, low, medium, and high severity cracking were summed up without adjustment for both alligator cracking and longitudinal cracking. For transverse cracking, low, medium, and high severity cracking were summed up using the same weighting function in the national calibration that is shown in the following equation (ARA, 2004).

$$Transverse\ Cracking\ (TC) = \frac{Low\ severity\ TC + 3 * Medium\ severity\ TC + 5 * High\ severity\ TC}{9} \qquad (4-1)$$

Discussion of Results

Verification

The input data required for Darwin M-E were prepared for verification runs. The verification runs were done with the national-default calibration coefficients. Figure 4-3 illustrates the comparison of predicted and measured total rutting, transverse cracking, alligator cracking, and longitudinal cracking. The red dotted line used throughout the paper represents the line of equality. Figure 4-4 shows the difference between predicted and actual distresses (Residual=Predicted-Measured) as a function of total AC (existing AC+ AC overlay) thickness, for total rutting, alligator cracking, and longitudinal cracking. From the verification runs, it was observed that the predicted distresses did not match well with the measured distresses, suggesting an extensive local calibration was required. From Figure 4-3 (a), it is evident that Darwin M-E over predicted total rutting compared to the measured total rutting. The subgrade rutting predicted by Darwin M-E ranged from 31% to 100% of total rutting, with an average value of 68%. Base rutting predicted ranged from 0% to 16% of total rutting, with an average of 8%. So, most of the rutting predicted by Darwin M-E came from the subgrade, which supports the study findings conducted by the Montana DOT (Von Quintus and Moulthrop, 2007). The Montana DOT conducted the local calibration study of MEPDG for flexible pavements. They concluded that the rutting prediction model in the MEPDG over-predicted total rut depth because significant rutting was predicted in unbound layers and embankment soils. A study by Hoegh et al. (2010) demonstrated that current MEPDG subgrade and base rutting models grossly overestimated rutting for the MnROAD test sections.

The Coastal and Valley regions of Oregon do not experience low-temperature thermal cracking (transverse cracking). But, the Eastern region displays a considerable amount of thermal cracking. It is shown in Figure 4-3 (b) that Darwin M-E predicted no thermal cracking even in the Eastern region. While Darwin M-E predicted no alligator cracking (Figure 4-3 (c)) for all the sections considered, a high variability between predicted and measured longitudinal cracking was observed, as shown in Figure 4-3 (d).

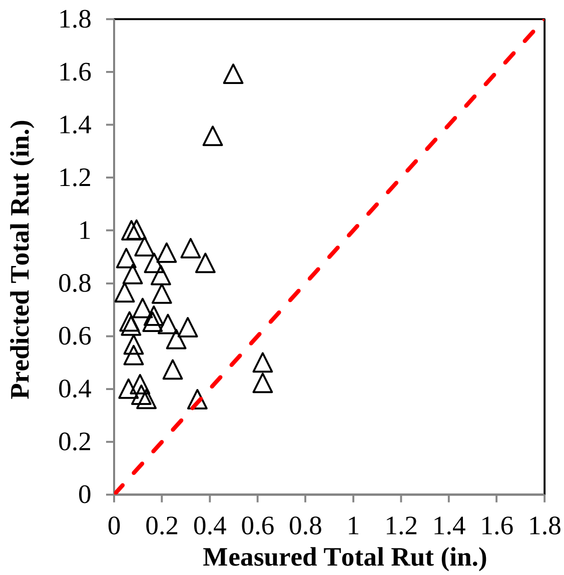

(a)

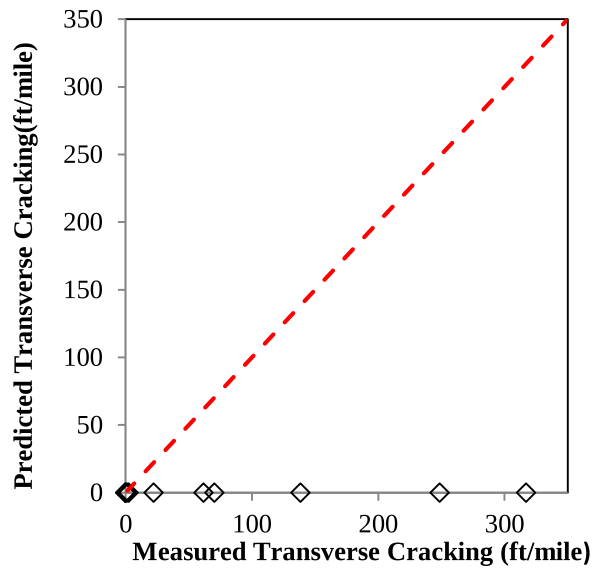

(b)

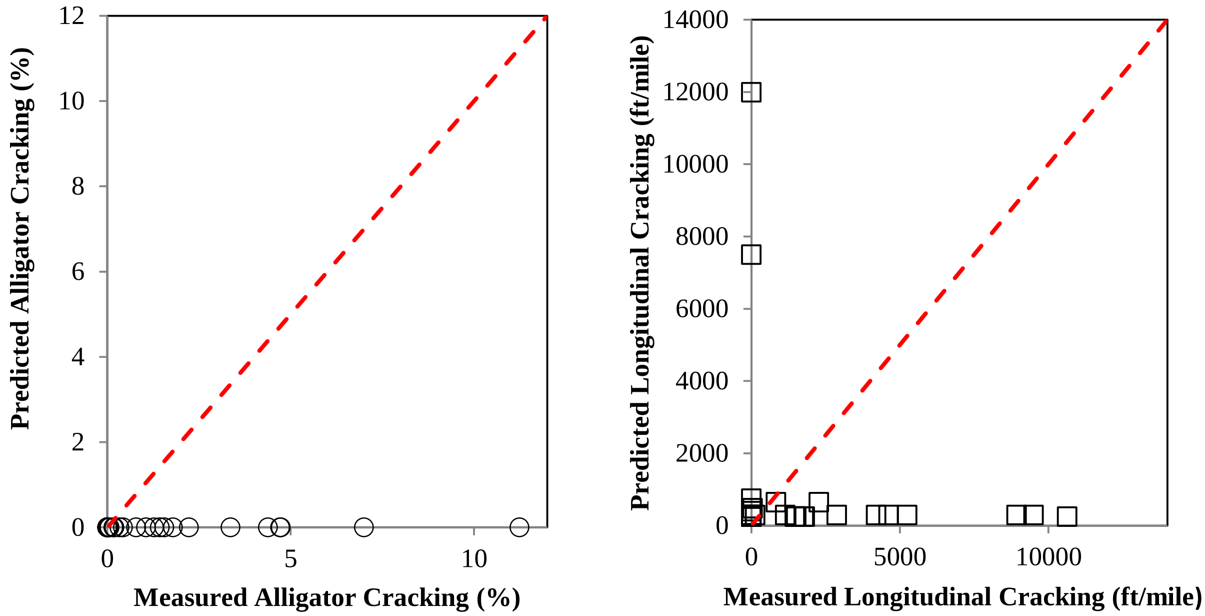

(c) **(d)**

Figure 4-3 Comparison between predicted and measured distresses with Darwin M-E default coefficients: (a) total rutting, (b) transverse cracking, (c) alligator Cracking, and (d) longitudinal cracking.

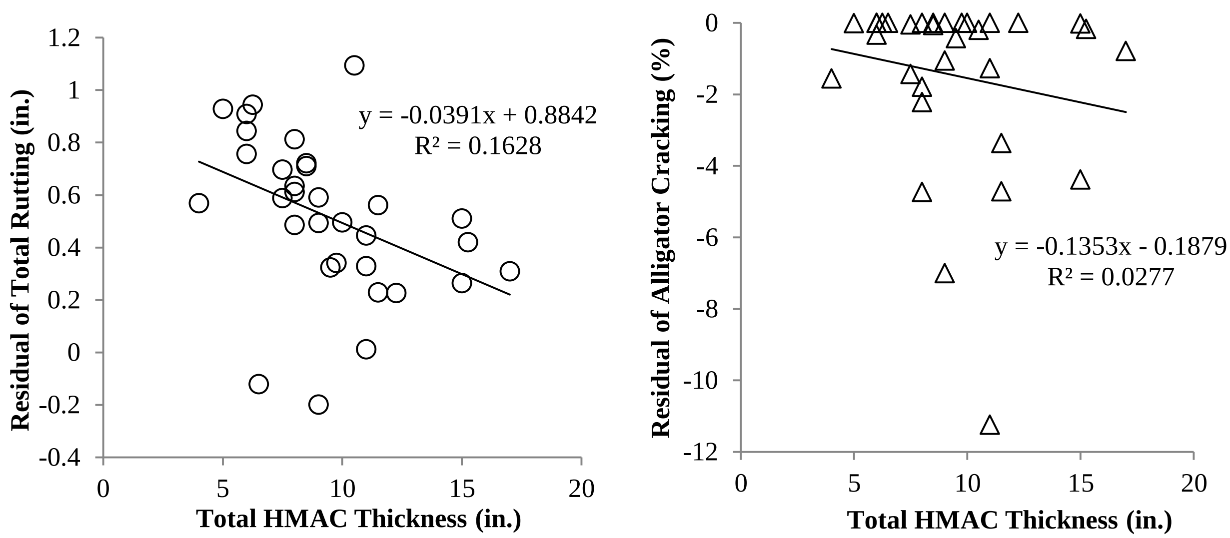

(a) **(b)**

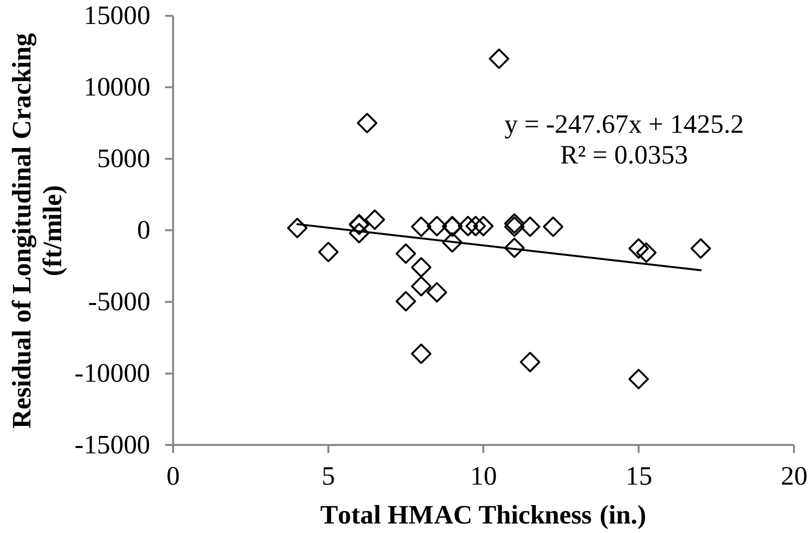

(c)

Figure 4-4 Residual of predicted and measured distresses versus total HMAC thickness: (a) total rutting, (b) alligator cracking, and longitudinal cracking

Calibration

Both alligator (bottom-up) and longitudinal (top-down) cracking prediction models were calibrated. The Darwin M-E predicts both bottom- and surface-initiated fatigue cracks using an incremental damage index approach. Alligator cracks are assumed to initiate at the bottom of HMA layers, while longitudinal cracks are assumed to initiate at the surface of the pavement. The damage is calculated as the ratio of the cumulative load repetitions from traffic to the allowable number of load repetitions as shown in Equation 4-2.

$$DI = \sum (\Delta DI)_{j,m,l,p,T} = \sum \left(\frac{n}{N_{f-HMA}}\right)_{j,m,l,p,T} \qquad (4-2)$$

where,

n = Actual number of axle load applications within a specific time period,

N_{f-HMA} = Allowable number of axle load applications for a flexible pavement and HMA overlays to fatigue cracking,

j = Axle-load interval,

m = Axle-load type (single, tandem, tridem, quad, or special axle configuration),
l = Truck type using the truck classification groups included in the M-EPDG,
p = Month, and
T = Median temperature for the five temperature intervals used to subdivide each month.

The Darwin M-E calculates the amount of alligator area cracking and the length of longitudinal cracking based on the incremental damage index. The damage transfer functions used in the Darwin M-E for alligator cracking and longitudinal cracking are shown in Equations 4-3 and 4-4, respectively.

$$FC_{Bottom} = \left(\frac{C_3}{1 + e^{\left(C_1 C_1^* + C_2 C_2^* Log(DI_{Bottom})\right)}}\right) * \left(\frac{1}{60}\right) \qquad (4-3)$$

where,

FC_{Bottom} = Alligator cracking, percent of total lane area,
C_1 = Calibration coefficient,
C_2 = Calibration coefficient,
C_1^* = $-2C_2^*$,
C_2^* = $-2.40874 - 39.748\ (1 + H_{HMA})^{-2.856}$
H_{HMA} = Total HMAC thickness, in.,
C_3 = Calibration factor, 6000 and
DI_{Bottom} = Bottom incremental damage, %.

$$FC_{Top} = \left(\frac{C_4}{1 + e^{(C_1 - C_2 * Log(DI_{Top}))}}\right) * 10.56 \qquad (4-4)$$

where,

FC_{Top} = Longitudinal cracking, ft/mile,
C_1 = Calibration coefficient,
C_2 = Calibration coefficient,
C_4 = Calibration factor, 1000, and
DI_{Top} = Surface incremental damage, %.

Both alligator cracking and longitudinal cracking transfer functions have two calibration coefficients; C_1 and C_2. Both the transfer functions used in Darwin M-E for alligator cracking and longitudinal cracking were calibrated by minimizing the sum of standard error between predicted and measured values using Equation 4-5:

$$Sum\ of\ Standard\ Error\ (SSR) = \sum_{i=1}^{N}(Predicted\ distress - Measured\ distress)^2 \quad (4-5)$$

The Solver function within Microsoft Excel was employed to optimize the calibration coefficients in the alligator cracking and longitudinal cracking models. The calibrated coefficients for both alligator and longitudinal cracking models are shown in Table 4-3.

Table 4-3 Calibration factors for fatigue prediction models in the Darwin M-E

Calibration Factor	**Darwin M-E Default Value**	**Calibrated Value**
Alligator cracking		
C_1	1	0.560
C_2	1	0.225
C_3	6000	6000
Longitudinal cracking		
C_1	7	1.453
C_2	3.5	0.097
C_3	0	0
C_4	1000	1000

Figure 4-5 illustrates a comparison of the predicted and measured alligator cracking and longitudinal cracking before and after calibration. Both alligator cracking and longitudinal cracking models were improved by calibration. However, there was a high degree of variability between the predicted and measured distresses, especially for longitudinal cracking, even after the calibration. There is a continuing concern regarding the accuracy of prediction of longitudinal cracking model. Based on the findings from the NCHRP 9-30 study, it was noted that longitudinal cracking be dropped from the local calibration guide development in NCHRP 1-40B study due to lack of accuracy in the predictions (Von Quintus, 2008a, and Von Quintus, 2008b). The Montana DOT conducted the local calibration study of MEPDG for flexible pavements. Regarding the longitudinal cracking prediction model they concluded that no consistent trend in the predictions could be identified to reduce the bias and standard error, and improve the accuracy of this prediction model. It is believed that there is a significant lack-of-fit modeling error for the occurrence of longitudinal cracks (Von Quintus and Moulthrop, 2007). A study by Galal and Chehab (2005) in Indiana indicated that MEPDG provided good estimation to the distress measure except longitudinal cracking.

It is important to point out that only one year of distress data for each pavement section considered in this study were available in this verification and calibration process. Moreover, many default values recommended by the Darwin M-E were used in this study due to the unavailability of data. It is recommended that additional sites be established to include in the future calibration efforts and thus, improve the accuracy of the predictive models.

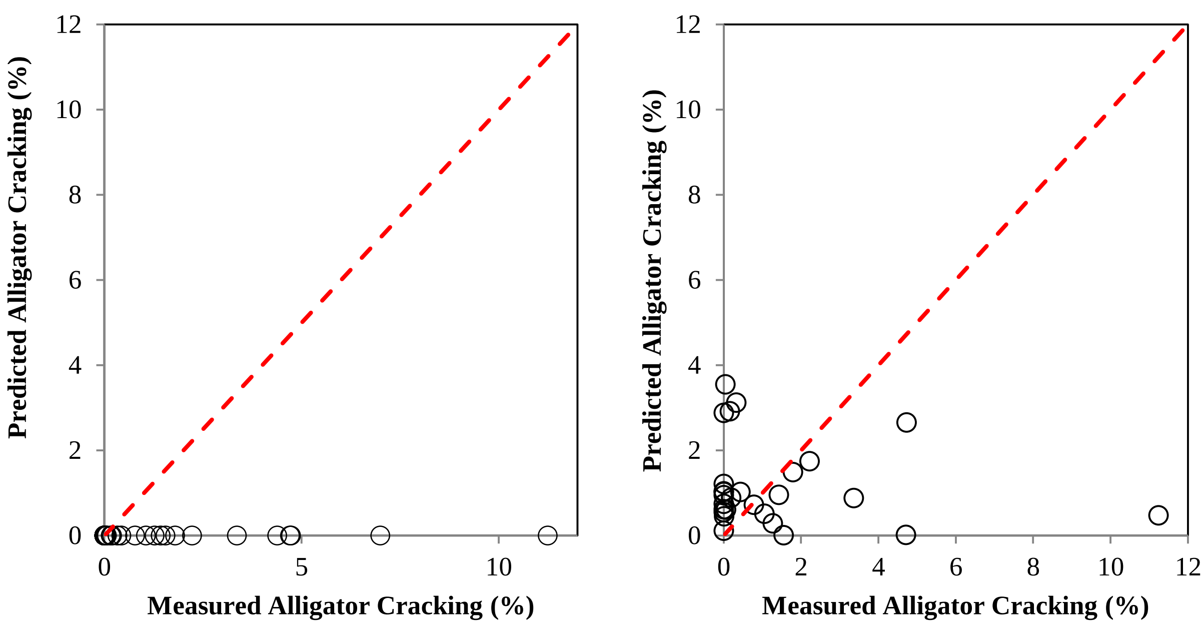

(a) **Before Calibration** **(b) After Calibration**

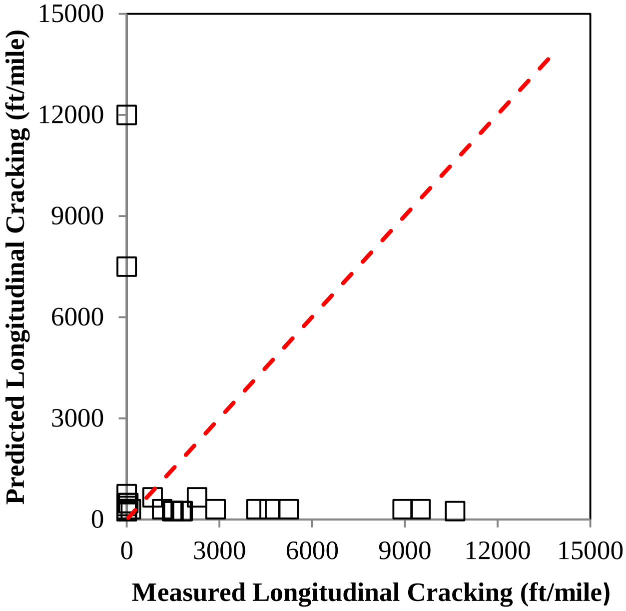

(c) Before Calibration

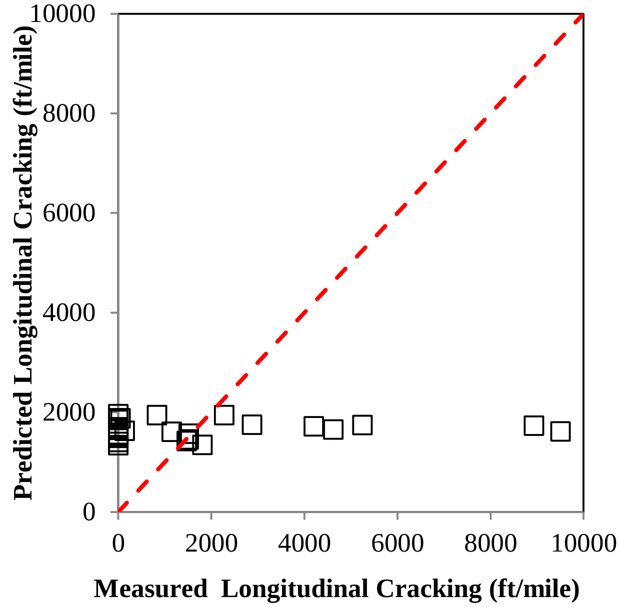

(d) After Calibration

Figure 4-5 Comparison of predicted and measured distresses for Darwin M-E default (a, c) and calibrated models (b, d)

Validation

Calibrated models are needed to be validated to confirm that the locally calibrated performance prediction models can produce robust and accurate predictions for cases other than those used for model calibration. The calibrated models were validated by running the Darwin M-E on the remaining projects that were not included in the calibration process to compare predicted and measured performance. Figure4- 6 shows the comparison of the predicted and measured performance. It is observed that local calibration significantly reduced the difference between predicted and measured distresses. However, it is recommended that additional sites be established in the future calibration effort to further reduce this difference.

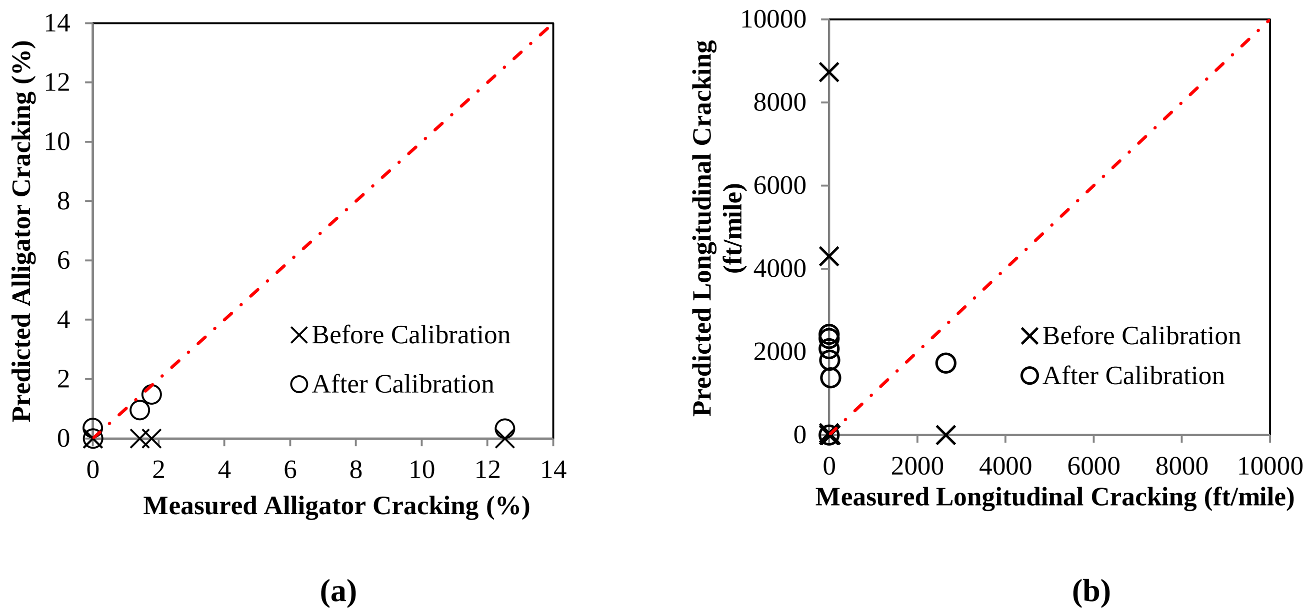

Figure 4-6 Comparisons of national (before calibration) and calibrated performance models for (a) alligator cracking and (b) longitudinal cracking

Conclusions and Recommendations

This paper presents the findings for initial calibration of the Darwin M-E alligator cracking and longitudinal cracking models of HMAC rehabilitation of the existing pavements for Oregon. The following conclusions and recommendations are made from this study:

- Predicted distresses using the Darwin M-E default calibration coefficients did not match well with actual distresses observed during the condition surveys, suggesting extensive local calibration is required for Oregon conditions. Further, it was observed that most of the rutting predicted by Darwin M-E occurred in the subgrade.
- Both alligator cracking and longitudinal cracking models were improved by local calibration. However, there was a high degree of variability between the predicted and measured distresses, especially for longitudinal cracking, even after the calibration. It is recommended that additional sites be established to include in future calibration efforts and thus, to improve the accuracy of the prediction models.

- The availability and quality of data (materials, construction, and performance data) required for Darwin M-E are critical for local calibration. It is recommended that more detailed inputs (Level 1 mostly) be established for future calibration efforts, which will help reduce a significant amount of input error and, thus, may improve the accuracy of prediction models.
- It always remains a challenge to delineate between alligator (bottom-up) cracking and longitudinal (top-down) cracking as it is not practical to take cores or trenches at each single crack to distinguish between alligator cracking and longitudinal cracking. Therefore, there could be measurement error, which may affect the calibration effort.
- There remains a question regarding the usability of longitudinal cracking and thermal cracking models, as was supported by previous research. Currently, improved thermal cracking models are being developed through FHWA pooled-fund studies. And, a NCHRP project 01-52 is underway to improve the longitudinal cracking model (http://apps.trb.org/cmsfeed/TRBNetProjectDisplay.asp?ProjectID=3152). Therefore, it is recommended that longitudinal cracking and thermal cracking models be recalibrated once these models are improved by MEPDG.
- Although Oregon DOT has an extensive PMS database, most of the PMS data, especially pavement distress data, do not directly support the MEPDG. The difference between the distress measurement techniques of the ODOT and the MEPDG poses direct challenges to the implementation and local calibration efforts for the MEPDG. It is recommended that ODOT adopts the MEPDG (LTPP) standard procedure, at least for the sections to be used in the future calibration effort. By doing so, a significant amount of measurement error and input error can be reduced. And, the accuracy of performance prediction models can be improved.

Acknowledgments

This study was sponsored by the Oregon Department of Transportation (ODOT) and the Federal Highway Administration (FHWA) under project, “Mechanistic Design Guide Calibration for Pavement Rehabilitation”. The authors gratefully acknowledge Oregon State University and

ODOT engineers for all the technical assistance and data provided. The contents of this paper reflect the views of the authors, who are responsible for the accuracy of the facts and data presented herein, and do not necessarily reflect the official policies of the ODOT and Iowa State University. This paper does not constitute a standard, specification, or regulation.

References

AASHTO. (1993). *AASHTO guide for design of pavement structures*, Washington, D.C.

ARA, Inc., ERES Consultants Division. (2004). "Guide for Mechanistic–Empirical Design of New and Rehabilitated Pavement Structures". *Final report, NCHRP Project 1-37A*. Transportation Research Board of the National Academies, Washington, D.C. http://www.trb.org/ mepdg/guide.htm.

Galal, K. A., and Chehab, G. R. (2005). "Implementing the mechanistic-empirical design guide procedure for a Hot-Mix Asphalt-rehabilitated pavement in Indiana". In *Transportation Research Record: Journal of the Transportation Research Board, No. 1919*, TRB, National Research Council, Washington, D.C., pp. 121-133.

Hall, K.D., Xiao, D. X., and Wang, K.C.P. (2011). "Calibration of the MEPDG for flexible pavement design in Arkansas". In *Transportation Research Record: Journal of the Transportation Research Board, No. 2226*, TRB, National Research Council, Washington, D.C., pp. 135-141.

Hoegh, K., Khazanovich, L., and Jensen, M. R. (2010). "Local calibration of MEPDG rutting model for MnROAD test sections", DVD. *Presented at the 89th Annual Meeting of the Transportation Research Board*. Washington, DC: Transportation Research Board.

Kim, S., Ceylan, H., Gopalakrishnan, K., Smadi, O., Brakke, C., and Behnami, F. (2010). "Verification of MEPDG performance predictions using pavement management information system (PMIS)", DVD. *Presented at the 89th Annual Meeting of the Transportation Research Board*. Washington, DC: Transportation Research Board.

Miller, J. S., and W. Y. Bellinger. (2003). "Distress Identification Manual for the Long-Term Pavement Performance Program". *FHWA-RD-03-031*. FHWA, U.S. Department of Transportation.

Muthadi, N. R. (2007). *Local Calibration of the MEPDG for Flexible Pavement Design*. M.S thesis. North Carolina State University.

Muthadi, N. R., and Kim, R. (2008). “Local calibration of mechanistic-empirical pavement design guide for flexible pavement design”. *In Transportation Research Record: Journal of the Transportation Research Board, No. 2087,* TRB, National Research Council, Washington, D.C., pp. 131-141.

National Cooperative Highway Research Program (NCHRP). (2004). “Guide for Mechanistic-Empirical Design of New and Rehabilitated Pavement Structures”. *Draft Final Report NCHRP Project 1-37A,* Transportation Research Board, National Research Council, Washington, D.C.

Souliman, M. I., Mamlouk, M. S., El-Basyouny, M. M., and Zapata, C. E. (2010). “Calibration of the AASHTO MEPDG for flexible pavement for Arizona conditions”, DVD. *Presented at the 89th Annual Meeting of the Transportation Research Board*. Washington, DC: Transportation Research Board.

Von Quintus, H. L. and Moulthrop, J. S. (2007). “Mechanistic-Empirical Pavement Design Guide Flexible Pavement Performance Prediction Models: Volume I- Executive Research Summary”. *FHWA/MT-07-008/8158-1*. Texas: Fugro Consultants, Inc.

Von Quintus, H. L. (2008a). “MEPDG Overview & National Perspective”. *Presented at North-Central MEPDG User Group*, Ames, IA.

Von Quintus, H. L. (2008b). “Local calibration of MEPDG—an overview of selected studies”. *Presented at 2008 AAPT Symposium Session: Implementation of the New MEPDG*, Philadelphia, PA.

Von Quintus, H. L., Darter, M. I., and Mallela, J. (2009a). “Recommended Practice for Local Calibration of the M-E Pavement Design Guide”. *National Cooperative Highway Research Program Project 1- 40B Manual of Practice*, Washington, DC: Transportation Research Board, National Research Council.

Von Quintus, H. L., Darter, M. I., and Mallela, J. (2009b). “Examples Using the Recommended Practice for Local Calibration of the MEPDG Software”. *National Cooperative Highway Research Program Project 1- 40B Manual of Practice (under review)*, Washington, DC: Transportation Research Board, National Research Council.

CHAPTER 5 - LOCAL CALIBRATION OF THE PERFORMANCE PREDICTION MODELS IN THE DARWIN M-E FOR PAVEMENT REHABILITATION IN OREGON

Md S. Rahman[1 2], R. Christopher Williams[3], and Todd Scholz[4]

A paper to be submitted to the *Transportation Engineering Journal,* published by the American Society of Civil Engineers (ASCE)

Abstract

The Oregon Department of Transportation (ODOT) is in the process of implementing the recently introduced AASHTO Mechanistic-Empirical Pavement Design Guide (MEPDG) for new pavement sections. However, the vast majority of pavement work conducted by ODOT involves rehabilitation of existing pavements. Hot mix asphalt (HMA) overlays are the preferred rehabilitation treatment for both flexible and rigid pavements in Oregon. However, like new work sections, HMA overlays are also susceptible to fatigue cracking (alligator cracking and longitudinal cracking), rutting, and thermal cracking. Additional work was therefore needed to calibrate the design process for rehabilitation of existing pavement structures. 38 pavement

---

[1] Ph.D. Candidate, Department of Civil, Construction & Environmental Engineering, Ames, IA 50011. PH: 515 817 3774, E-mail: msrahman@iastate.edu

[2] Primary researcher and author

[3] Professor, Department of Civil, Construction & Environmental Engineering, Ames, IA 50011. PH: 515 294 4419, Fax: 515 294 8216, E-mail: rwilliam@iastate.edu

[4] Assistant Professor, School of Civil and Construction Engineering, Corvallis, OR 97331. PH: 541 737 2056, Fax: 541 737 3052, E-mail: todd.scholz@oregonstate.ed

sections throughout Oregon were included in this calibration study. A detailed comparison of predictive and measured distresses was made using the MEPDG released software Darwin M-E (Version 1.1). It was found that Darwin M-E predictive distresses did not accurately reflect measured distresses, calling for a local calibration of performance prediction models was warranted. Four distress prediction models (rutting, alligator cracking, longitudinal cracking, and thermal cracking) of the HMA overlays were calibrated for Oregon conditions. A comparison was made between the results before and after the calibration to assess the improvement in accuracy of the distress prediction models provided by the local calibration. While the thermal cracking model could not be calibrated, the locally calibrated models of rutting, alligator cracking, and longitudinal cracking provided better predictions with lower bias and standard error than the nationally (default) calibrated models. However, there was a high degree of variability between the predicted and measured distresses, especially for longitudinal cracking, even after the calibration. It is believed that there is a significant lack-of-fit modeling error for the occurrence of thermal cracks. The Darwin M-E calibrated models of rutting and alligator cracking can be implemented, however, it is recommended that additional sites, which would contain more detailed inputs (mostly Level 1), be established and be included in the future calibration efforts and thus, further improve the accuracy of the prediction models.

Key Words: Hot mix asphalt, Rehabilitation, MEPDG, Darwin M-E, Pavement design, Performance prediction models, Verification and Calibration

Introduction

The new Mechanistic-Empirical Pavement Design Guide (MEPDG) and software were developed through the National Cooperative Highway Research Program (NCHRP) 1-37A project in recognition of the limitations of the current American Association of State Highway and Transportation Officials (AASHTO) Design Guide (NCHRP, 2004). It represents a transitioning of the empirically-based pavement design to a mechanistic-empirical procedure that combines the strengths of advanced analytical modeling and observed field performance. The pavement performance prediction models in the MEPDG were calibrated primarily using design inputs and performance data largely from the national Long-Term Pavement Performance (LTPP) database. However, these performance prediction models warrant detailed calibration and validation because of potential differences between national and local conditons. Therefore, it is necessary to calibrate these performance prediction models for implementation in local conditions by taking into account local material properties, traffic patterns, environmental conditions, construction, and maintenance activities.

The importance of local calibration of performance prediction models contained in MEPDG is well-documented by different transportation agencies throughout the United States. Hall et al. (2011) conducted a local calibration of performance prediction models in MEPDG for Arkansas. While rutting and alligator (bottom-up) cracking models were successfully calibrated, longitudinal (top-down) cracking and transverse cracking models were not calibrated due to the nature of the data. Souliman et al. (2010) calibrated distress models for alligator cracking, longitudinal cracking, rutting, and roughness for flexible pavements for Arizona using 39 LTPP pavement sections. It was found that national calibrated MEPDG underpredicted alligator cracking and AC rutting while the longitudinal cracking and the subgrade rutting were overpredicted. A significant improvement of performance prediction for alligator cracking and AC rutting resulted after calibration; however, only marginal improvement was realized for longitudinal cracking and roughness models. Hoegh et al. (2010) conducted a local calibration of the rutting model for MnROAD test sections. They concluded that the locally calibrated model greatly improved the MEPDG rutting prediction for various pavement designs for Minnesota conditions. A study by Von Quintus (2008) found that the measurement error of the performance data had the greatest effect on the precision of MEPDG performance models. Kim et al. (2010) verified MEPDG performance models for Iowa using Pavement Management Information System (PMIS) data. Systematic differences were observed for rutting and cracking models. Muthadi and Kim (2008) performed the MEPDG calibration for flexible pavements located in North Caorlina (NC) using version 1.0 of the MEPDG software. Two distress models, rutting and alligator cracking, were used for this effort. This study concluded that the standard errors for the rutting model and the alligator cracking model were significantly lower after the calibration.

A properly calibrated MEPDG will enable more economical designs as well as potentially linking pavement design with actual material characteristics-, and construction processes. Further, as newer technologies and materials are developed, characterization of their material properties will expedite their use in the MEPDG. Several examples exist including the use of warm mix asphalt, post-consumer asphalt roofing shingles in asphalt mixtures, and the evaluation of other technologies such as additives and modifiers.

The Need for Local Calibration

The Oregon Department of Transportation is in the process of implementing the new MEPDG for new pavement sections. Internally, ODOT has been evaluating the MEPDG for new sections for both flexible and rigid interstate pavement sections. Work is also currently being conducted at Oregon State University to develop design inputs and evaluate the three principal pavement performance models (e.g., fatigue cracking, rutting, and thermal cracking models) that are integral to the design process of new work sections for asphalt concrete (AC) pavement structures. However, the vast majority of pavement work conducted by ODOT involves rehabilitation of existing pavements. Additional work is therefore needed to calibrate the design process for rehabilitation of existing pavement structures.

Asphalt mix overlays are the preferred rehabilitation treatment for both flexible and rigid pavements in Oregon. However, like new work sections, overlays are also susceptible to fatigue cracking, rutting, and thermal cracking- thus, the need to include these forms of distresses in the calibration process.

Development of Calibration Plan and Test Sections

The research plan developed for calibrating the MEPDG generally followed the flow chart recommended by Von Quintus et al. (2009). The general procedures and steps employed for calibration of MEPDG as outlined in Figure 5-1 are summarized below.

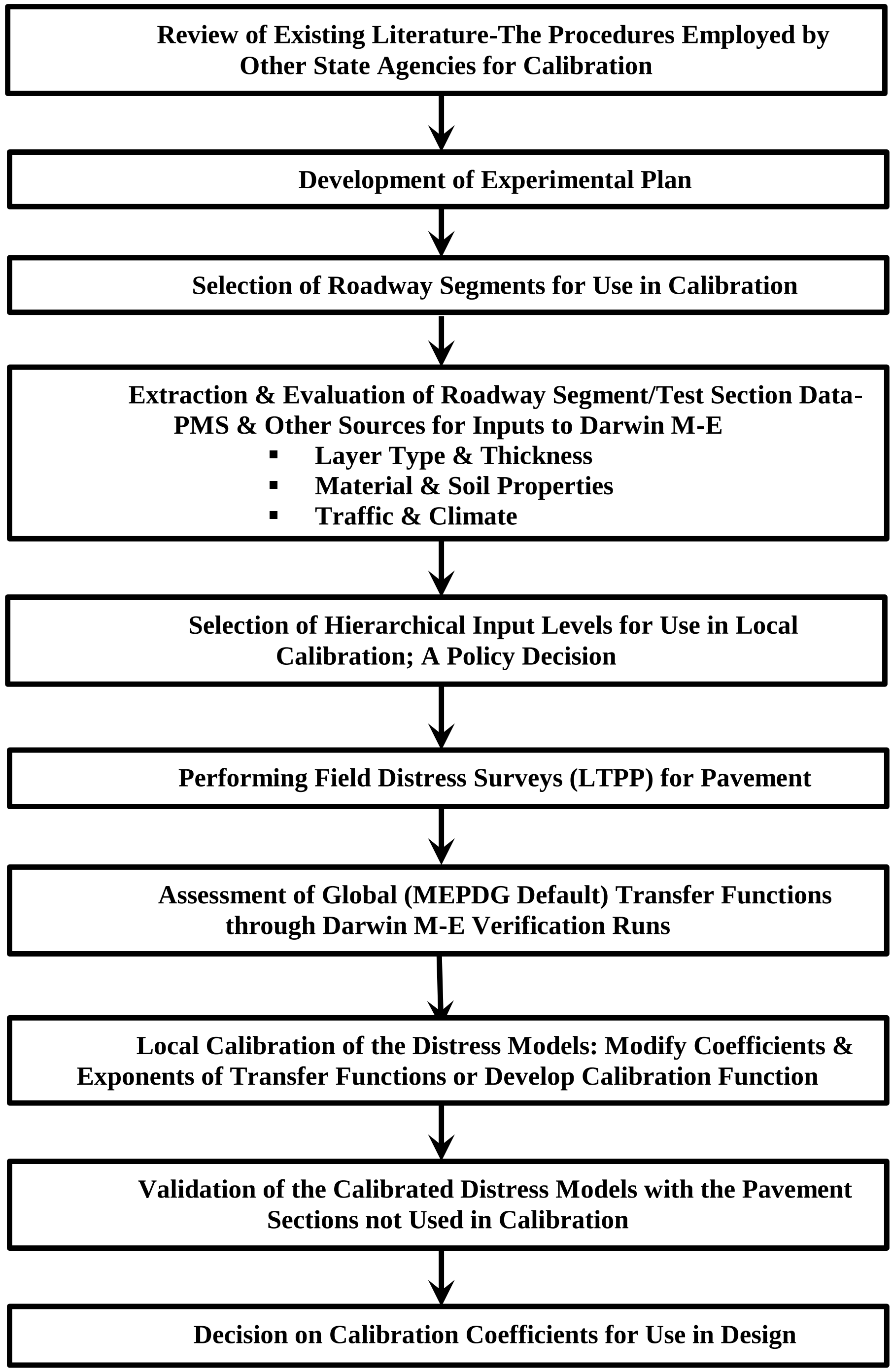

Figure 5-1 Flow chart for the procedure and steps employed for local calibration

It is important to point out that Accelerated Pavement Testing (APT) does not exist in Oregon. Further, the research team did forensic investigation only in so far as to determine the type of load related cracking, (e.g. top-down as compared to bottom-up cracking, via coring at the end of cracks and to verify pavement structures).

The data mining of Oregon DOT databases included identifying pavement types with varying levels of distresses, as well as historical mix design, structural design, and traffic information for rehabilitated pavements. The research team pursued obtaining pavement sections with a range of distress levels for the types of pavement types for cracking and rutting. Further challenging the research team in this endeavor was understanding the differences between materials used historically as compared to those being used today (e.g., pre-Superpave mixes as compared to Superpave mixes). Field condition surveys were conducted via distress surveys in accordance with the FHWA Long Term Pavement Performance (LTPP) publication *Data Collection Guide For Long Term Pavement Performance (2003)* for calibrating the simulated outcomes of the MEPDG. The pavement test sections also covered a range of climatic conditions from coastal areas (western Oregon) to central and eastern Oregon, a range of trafficking levels, and typically used materials. The research team segmented the trafficking levels into two categories: low volume (less than 10 million Equivalent Single Axle Load (ESALs)), and high volume (greater than 10 million ESALs). This was based upon the changes in the mix design criteria which included the materials specified in the various design levels.

The calibration of the MEPDG thus considered a number of different factors including the following:

- Pavement type/structure,
- Pavement age,
- Pavement performance,
- Trafficking level, and
- Region (climatic variation).

There are five primary pavement types in Oregon consisting of hot mix asphalt over aggregate base (HMA/Agg), HMA inlay or overlay over aggregate base (HMA/HMA/Agg), HMA inlay or overlay over cement treated base (HMA/HMA/CTB), continuously reinforced concrete pavement (CRCP), and HMA overlay of CRCP (HMA/CRCP). The primary pavement types included in the calibration were HMA over aggregate base, HMA inlay or overlay over aggregate base, HMA inlay or overlay over cement treated base, and HMA overlay of CRCP. The three primary distresses targeted for the HMA pavement types were HMA rutting, fatigue cracking, and thermal cracking. The MEPDG considers two types of fatigue cracking: the classical alligator (bottom-up) cracking and longitudinal (top-down) cracking. Most pavement management systems do not delineate between the two types of fatigue cracking, thus the research team identified whether the cracking was bottom-up or top-down via field coring. The trafficking levels are important to identify as varying materials are used depending upon a pavements design level. The research team's initial thinking was that two trafficking levels be considered: 1) less than 10million ESALs, and 2) more than 10million ESALs. Oregon has vastly different climatic conditions that occur on the Coast as compared to in the Valley and on the Eastern portion of the state. As a result, the research team considered three different regions.

The factors listed above were incorporated in the field experimental plan developed in this calibration effort as shown in Table 5-1. The plan included the three aforementioned regions (Coastal, Valley, and Eastern), the four primary types of pavements (HMA over aggregate base = HMA/Agg, HMA inlay or overlay over aggregate base=HMA/HMA/Agg, HMA inlay or overlay over cement treated base=HMA/HMA/CTB, HMA overlay of CRCP=HMA/CRCP), low and high trafficking levels, and three different levels of pavement performance (very good-excellent, as expected, and inadequate). It is important to point out that no high volume roads were identified in the coastal region, thus leaving the appropriate block empty along with other empty blocks as evident in Table 5-1. In Table 5-1, one block does not necessarily mean one pavement section included in the calibration study. For instance, two pavement sections separated by a comma (,)-US 101: NCL Bandon-June Ave and US 101: Sutton Creek-Munsel Lake Rd- are located in one block (Coastal Region, Low Volume Traffic, Very good-Excellent Pavement Performance, and HMA/HMA/CTB Pavement Structure).

Table 5-1 Field experimental plan

		Region						
		Coastal		Valley			Eastern	
Traffic	Pavement Performance	HMA/HMA/Agg	HMA/HMA/CTB	HMA/HMA/Agg	HMA/Agg	HMA/CRCP	HMA/HMA/Agg	HMA/Agg
Low Volume	Very good-Excellent	US 101: Neptune Dr-Camp Rilea	US 101: NCL Bandon-June Ave, US 101: Sutton Creek-Munsel Lake Rd	US 20: Sweet Home-18th Ave, OR 34: Wcl Lebanon-RXR X-ing			US 730: I-84 Canal Rd, OR 201: Washington Ave-Airport Way, OR 140: Jct Hwy 019-B.B.Creek	
	As expected	US 101:Tillamook Couplet (SB), US 101: Wilson R.-Tillamook Couplet	US 101:Elk Hill Rd-Port Orford	OR 99 E:Albany Ave-Calapooia St			US 97: Weighb St-Crawford Rd (NB), US 97: Weighb St-Crawford Rd (SB),US 20: MP 10.3-MP 12.5	US 26: Prairie City-Dixie Summit, US 26: Prairie City Section, US 395: Jct Hwy 2-Hwy 33
	Inadequate	US 101: Dooley Br-Jct Hwy 047, US 101: Florida Ave-Washington Ave			OR 221: N. Salem-Orchard Heights Rd		US730: Canal Rd-Umatilla Bridge	
High Volume	Very good-Excellent			US 30: Cornelius Pass Rd-Begin JCP, OR 120: End Jcp-Beg Hwy 081		I-5:Wilsonville Intch-Tualatin R	US 97: S. Century Dr-MP 161	
	As expected			OR 569: Hwy 091-Willametter R. (EB)	OR 99W: Marys R-Kiger Island Dr, OR 99W: N. Sherwood-SW 12th St.	I-5: Haysville Intch to Woodburn	US 97: Madras Couplet-Hwy 360	
	Inadequate			I-5: Azalea-Canyonville, OR 99W: Brustschr St. -Jct Hwy 151	OR 22: End Hwy 072-I-5 NB Ramps	I-84: NE Union Ave-S. Banfield Intch	I-84: N.FK Jocobsen Gulch-Malheur River (EB), US 97: N. Chiloquin Intch-W. DR	

Each pavement section had three replicate locations for condition surveys conducted within a selected roadway section. The three locations, typically 150 meters each, were randomly selected using a random number generator and normalized over the section length. Condition surveys were conducted in, - only one traffic direction to simplify the coordination of surveys (i.e., work zone setup, etc.). The experimental plan included 38 pavement sections for a total of 114 pavement condition surveys. The locations of the pavement sections surveyed are shown in Figure 5-2. A total of 44 pavement sections were surveyed; 4 were CRCP and 2 were dropped out from the calibration due to lack of availability of data, thus leaving 38 pavement sections available for the calibration study.

Figure 5-2 Locations of pavement sections used in calibration study

Data Preparation for Calibration

The quality of the data required for the MEPDG plays a major role in the calibration accuracy. Data collection included five main categories: materials, traffic, climatic, pavement structure, and pavement performance data. ODOT's Pavement Management System (PMS) database was used for condition surveys. Furthermore, ODOT's electronic database what ODOT refers to as V-files was mined for the pavement structures used in the calibration study.

Traffic

The traffic data required for Darwin M-E includes Average Annual Daily Truck Traffic (AADTT), vehicle class distribution, growth rate, axle load distribution, number of axles per truck, hourly and monthly adjustment, lateral wander, and wheelbase. AADTT and growth rate data were derived from http://highway.odot.state.or.us/cf/highwayreports/traffic_parms.cfm and lane distribution factor (LDF) from ODOT maintained website http://www.tripcheck.com/Pages/CamerasBend.asp.

The AADTT ranged from 310 to 17,780 vehicles per day and growth rates from 0 to 3%. The lane distribution factor (LDF) for the driving lane was estimated as pavement performance (pavement distresses) of the driving lane was used in the calibration study. Table 5-2 shows the LDF for pavements with different number of lanes in one direction. Darwin M-E default values were used for vehicle class distribution, axle load distribution, number of axles per truck, hourly and monthly adjustment, lateral wander, and wheelbase.

Table 5-2 Lane distribution factor (LDF)

No of lanes in one direction	LDF
1	1
2	0.90
3	0.50
4	0.12

Climate

For each of the pavement sections, the latitude, longitude, and elevation were derived from Google Earth software using the project location. Depth of water table for each section was extracted from the Web Soil Survey of the United States Department of Agriculture (USDA) or the National Water Information System of the United States Geological Survey (USGS). This information was used to generate the climatic data for each pavement section.

Materials and Pavement Structure

Information regarding layer thicknesses and HMA mixture properties, such as binder type, gradation, volumetric properties, base, and subgrade type that are necessary Darwin M-E were provided by Oregon State University (OSU) in combination with ODOT. Other default values recommended by Darwin M-E were used for Poisson’s ratio, thermal properties of the asphalt mixtures, base and subgrade properties.

Performance Data

Since the ODOT distress measurement system is not compatible with the MEPDG defined distresses, field condition surveys were conducted to obtain pavement performance (pavement distresses) data. The field condition distress surveys were conducted according to the FHWA Long Term Pavement Performance (LTPP) publication *Data Collection Guide For Long Term Pavement Performance* (Miller et al., 2003). It is important to point out that the vast majority of the pavements had condition surveys conducted on three randomly selected 150-meter sections and the data utilized for calibration were the average of the three condition surveys. In a couple of instances, it was necessary to shorten the survey section length from 150 to 90 meters, because the overall pavement section was less than 1.5 kilometer, yet the surveyed sections did represent a substantial percentage of the overall pavement. Where the pavement being surveyed was less than 0.8 kilometer, the entire pavement was surveyed. Longitudinal (top-down) cracking and thermal cracking were reported as linear meter per kilometer while for alligator (bottom-up) cracking, the linear meter of cracking recorded in the field distress surveys were converted a percentage of the surveyed section for calibrating with Darwin M-E as the software estimates the percentage of a section's cracked area. Similar to the national calibration, low, medium, and high severity cracking were summed up without adjustment for both alligator cracking and longitudinal cracking. For transverse cracking, low, medium, and high severity cracking were summed up using the same weighting function in the national calibration that is shown in the following equation (ARA, 2004).

$$Transverse\ Cracking\ (TC) = \frac{Low\ severity\ TC + 3 * Medium\ severity\ TC + 5 * High\ severity\ TC}{9} \quad (5\text{-}1)$$

Discussion of Results

Verification

The input data required for Darwin M-E were prepared for verification runs. The verification runs were done with the national-default (Darwin M-E default) calibration coefficients. Figure 5-3 illustrates the comparison of predicted and measured total rutting, transverse cracking, alligator cracking, and longitudinal cracking. The red dotted line used throughout the paper represents the line of equality. Figure 5-4 shows the difference between predicted and actual distresses (Residual=Predicted-Measured) as a function of total AC (existing AC+ AC overlay) thickness, for total rutting, alligator cracking, and longitudinal cracking. From the verification runs, it was observed that the predicted distresses did not match well with the measured distresses, suggesting an extensive local calibration was required. From Figure 5-3 (a), it is evident that Darwin M-E overpredicted total rutting compared to the measured total rutting. The subgrade rutting predicted by Darwin M-E ranged from 31% to 100% of the total rutting, with an average value of 68%. The base rutting prediction ranged from 0% to 16% of total rutting, with an average of 8%. So, most of the rutting predicted by Darwin M-E came from the subgrade, which supports a study's findings conducted by the Montana DOT (Von Quintus and Moulthrop, 2007). The Montana DOT conducted the local calibration study of MEPDG for flexible pavements. They concluded that the rutting prediction model in the MEPDG overpredicted the total rut depth because significant rutting was predicted in unbound layers and embankment soils. A study by Hoegh et al. (2010) demonstrated that the current MEPDG subgrade and base rutting models grossly overestimated rutting for MnROAD test sections.

The Coastal and Valley regions of Oregon do not experience low-temperature thermal cracking (transverse cracking). But, the Eastern region displays a considerable amount of thermal cracking. It is shown in Figure 5-3 (b) that Darwin M-E predicted no thermal cracking even in the Eastern region. While Darwin M-E predicted no alligator cracking (Figure 5-3 (c)) for all the sections considered, a high variability between predicted and measured longitudinal cracking was observed, as shown in Figure 5-3 (d).

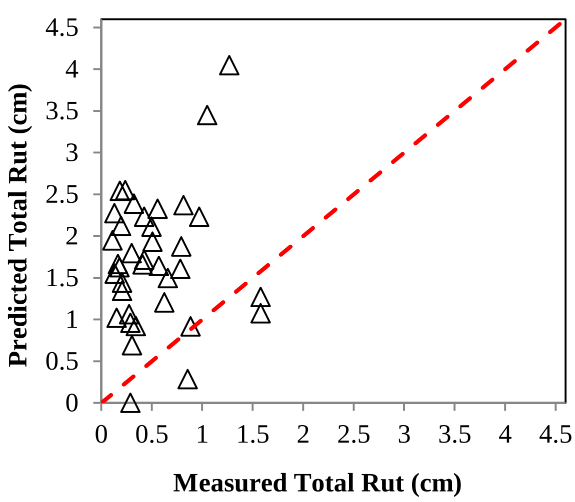

(a)

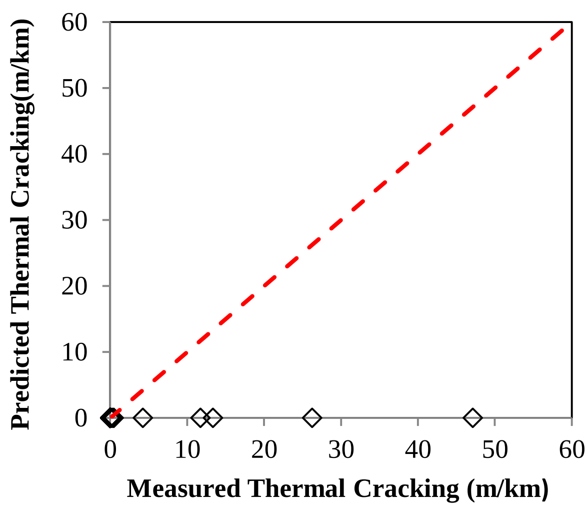

(b)

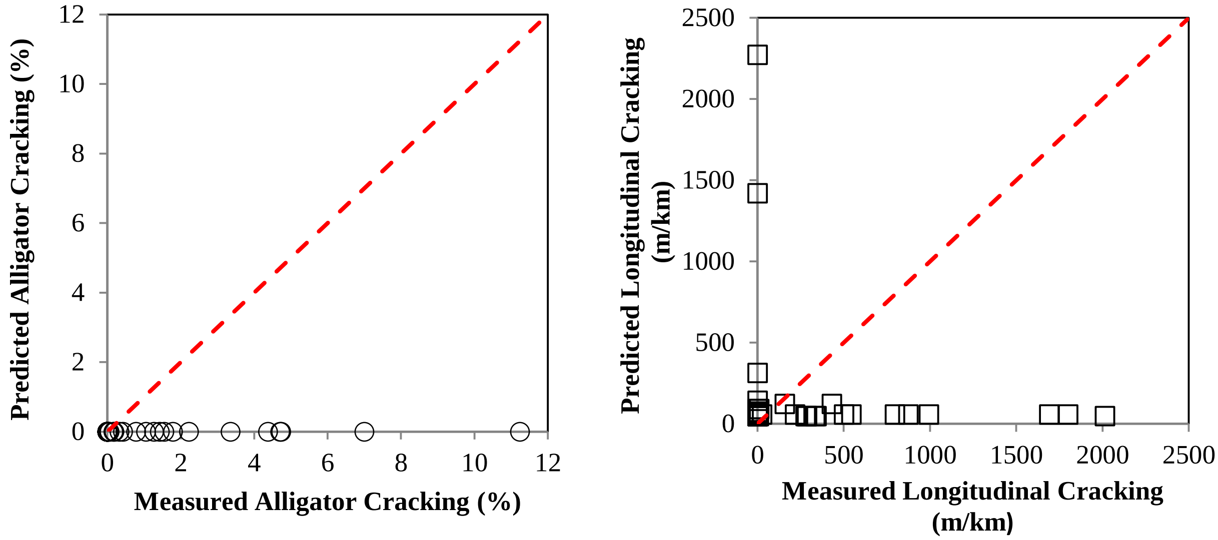

(c) (d)

Figure 5-3 Comparison between predicted and measured with Darwin M-E default coefficients: (a) total Rutting, (b) transverse cracking, (c) alligator cracking, and (d) longitudinal cracking.

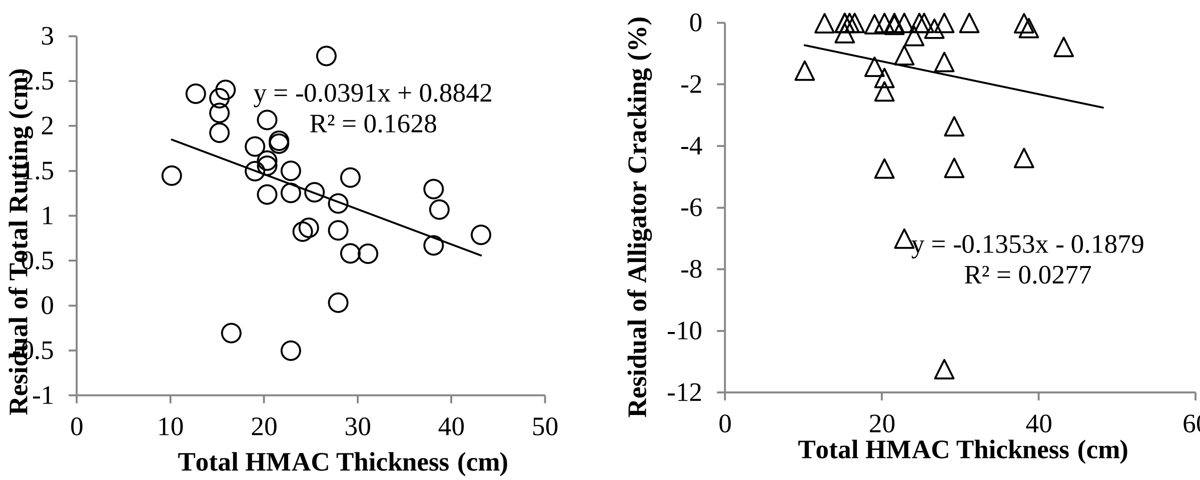

(a) (b)

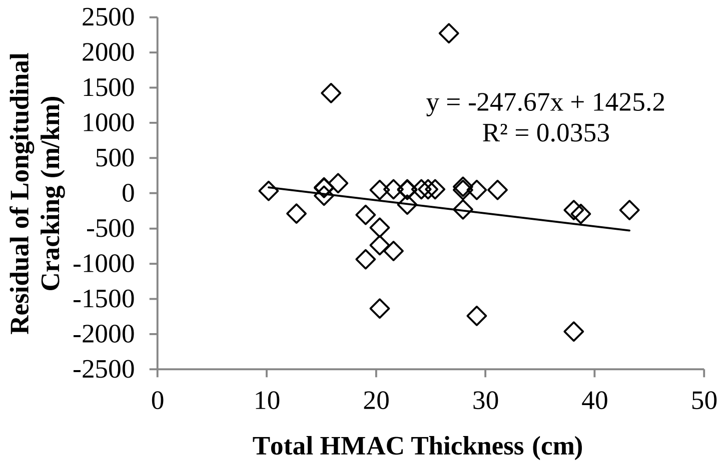

(c)

Figure 5-4 Residual of predicted and measured distresses versus total HMAC thickness: (a) total rutting, (b) alligator cracking, and (c) longitudinal cracking.

(Note: Residual=Predicted-Measured)

Calibration

The importance of local calibration of performance prediction models contained in Darwin M-E is well-documented by different transportation agencies throughout the United States. From the verification runs, it was observed that the predicted distresses did not match well with the measured distresses, suggesting an extensive local calibration was required. The following section discusses the calibration process of the performance prediction models.

Rutting Model Calibration

Rutting (or permanent deformation) is one of the most important load associated pavement distresses in hot mix asphalt concrete (AC) pavement systems. A rut is a depression in the wheel path of an AC pavement, caused by the accumulation of permanent strains in all or some of the layers in the pavement structure. The Darwin M-E predicts rutting in AC layer, base, and subgrade individually. Then the total rut is calculated by summing the rutting in the AC layer, base, and subgrade as shown in equation (5-2):

$$Total\ Rutting = AC\ Rutting + Base\ Rutting + Subrage\ Rutting \qquad (5\text{-}2)$$

Where *Total Rutting* is the predicted total rutting due to the subgrade, base, and AC layer, *AC Rutting* is the predicted rutting in the AC layer only, *Base Rutting* is the predicted rutting in the base layer only, and *Subgrade Rutting* is the predicted rutting in the subgrade only.

The Darwin M-E field-calibrated mathematical equation that is used to predict rutting in the AC layer is of the form:

$$\Delta_{p(HMA)} = \varepsilon_{p(HMA)} h_{HMA} = \beta_{r1} k_z \varepsilon_{r(HMA)} 10^{k_1} n^{k_2 \beta_{r2}} T^{k_3 \beta_{r3}} \quad \textit{(5-3)}$$

where,

$\Delta_{p\ (HMA)}$	= Accumulated permanent or plastic deformation in the AC layer/sublayer, in
$\varepsilon_{p\ (HMA)}$	= Accumulated permanent or plastic axial strain in the AC layer/sublayer, in/in
h_{HMA}	= Thickness of the AC layer/sublayer, in
n	= Number of axle load repetitions
T	= Mix or pavement temperature, °F
k_z	= Depth confinement factor
$k_{1,2,3}$	= Global field calibration parameters (from the NCHRP 1-40D recalibration; k1 =-3.35412, k2 =1.5606, k3 =0.4791)
$\beta_{r1,r2,r3}$	= Local or mixture field calibration constants; for the global calibration, these constants were all set to 1.0

$$k_z = (C_1 + C_2 D)0.328196^D \quad \textit{(5-4)}$$

$$C_1 = -0.1039(H_{HMA})^2 + 2.4868H_{HMA} - 17.342 \quad \textit{(5-5)}$$

$$C_2 = 0.0172(H_{HMA})^2 - 1.7331H_{HMA} + 27.428 \quad \textit{(5-6)}$$

D = Depth below the surface, in

H_{HMA} = Total HMA thickness, in

Equation (5-7) shows the field-calibrated mathematical equation used to calculate plastic vertical deformation within all unbound pavement sublayers and the foundation or embankment soil.

$$\delta_a(N) = \beta_{s1} k_1 \varepsilon_v h_{soil} \left(\frac{\varepsilon_o}{\varepsilon_r}\right) e^{-(\frac{\rho}{n})^{\beta}} \qquad \textit{(5-7)}$$

where,

$\delta_a(N)$ = Permanent or plastic deformation for the layer/sublayer, in

n = Number of axle load applications

ε_o = Intercept determined from laboratory repeated load permanent deformation tests, in/in

ε_r = Resilient strain imposed in laboratory test to obtain material properties *εo*, *β*, and ρ, in/in

ε_v = Average vertical resilient or elastic strain in the layer/sublayer and calculated by the structural response model, in/in

h_{soil} = Thickness of the unbound layer/sublayer, in

k_1 = Global calibration coefficients; *k1*=2.03 for granular materials and 1.35 for fine-grained materials

β_{s1} = Local calibration constant for the rutting in the unbound layers (base or subgrade); the local calibration constant was set to 1.0 for the global calibration effort. Note that *βs1* represents subgrade layer while *βB1* represents base layer.

$$Log\beta \quad = -0.61119 - 0.017638\ (W_c) \qquad \textit{(5-8)}$$

$$\rho \quad = 10^9 \left(\frac{C_o}{(1-(10^9)^{\beta})}\right)^{\frac{1}{\beta}} \qquad \textit{(5-9)}$$

$$C_o \quad = Ln\left(\frac{a_1 M_r^{b_1}}{a_9 M_r^{b_9}}\right) = 0.0075 \qquad \textit{(5-10)}$$

where:

W_c = Water content, percent

M_r = Resilient modulus of the unbound layer or sublayer, psi

$a_{1,9}$ = Regression constants; *a1*=0.15 and *a9*=20.0

$b_{1,9}$ = Regression constants; *b1*=0.0 and *b9*=0.0.

As discussed earlier, there are five calibration factors (three for AC layers, one for the unbound granular base, and one for the subgrade layers) in the rutting (permanent deformation) model calibration. It is important to point out that in Oregon, rutting in base and subgrade layers is not a problem, most of the rutting coming from the AC layers only. Therefore, calibration factors for base and subgrade layers were set to 0.

Iterative runs of the Darwin M-E using discrete calibration coefficients were employed to optimize the AC rutting model. The first step involved the simulation runs using the Darwin M-E software for a combination of βr2 and βr3 on the asphalt model only. Table 5-3 lists the possible combinations of βr2 and βr3 calibration values. And Figure 5-5 shows the sum of squared error (SSE) between predicted and measured rutting variation compared to combination values for βr2 and βr3. As seen from Figure 5-5, a combination values for βr2 and βr3 was found to be 1 and 0.9 which minimized the SSE. After βr2 and βr3 calibration values were chosen, the value for βr1 was estimated using the Solver function within Microsoft Excel to further reduce the SSE. Table 5-4 shows the adjusted calibration coefficients. Figure 5-6 illustrates a comparison of the predicted and measured rutting before and after calibration. Before calibration, the standard error of the estimate (SEE) of the rutting model was found to be 1.443 cm. SEE was reduced to 0.457 cm after calibration, indicating an almost 70% increase in accuracy of the prediction.

Table 5-3 All combinations of calibration values for rutting model

Trial Number	**βr2**	**βr3**
1	0.8	0.8
2		0.9
3		1
4		1.2
5	1	0.8
6		0.9
7		1
8		1.2
9	1.2	0.8
10		0.9
11		1
12		1.2

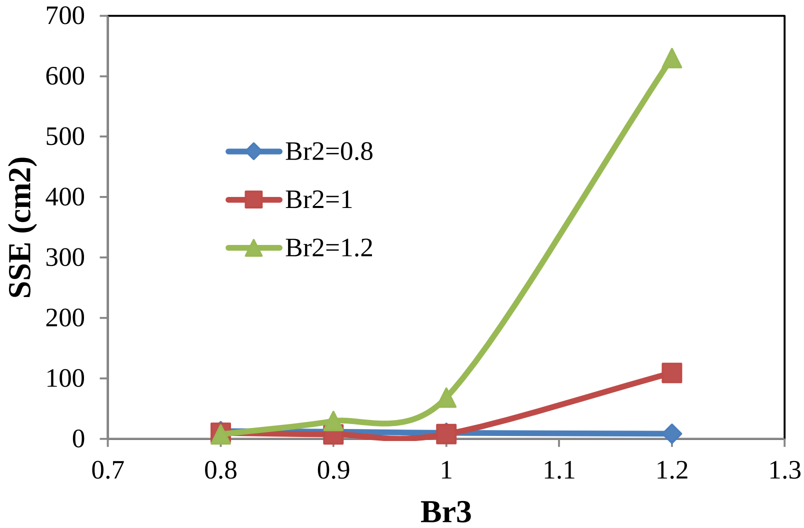

Figure 5-5 Sum of squared error (SSE) variation with βr2 and βr3

Table 5-4 Summary of calibration factors

Calibration Factor	Default Value	Calibrated Valued
AC Rutting		
βr1	1	1.48
βr2	1	1
βr3	1	0.9
Base Rutting		
βs1	1	0
Subrage Rutting		
βs1	1	0

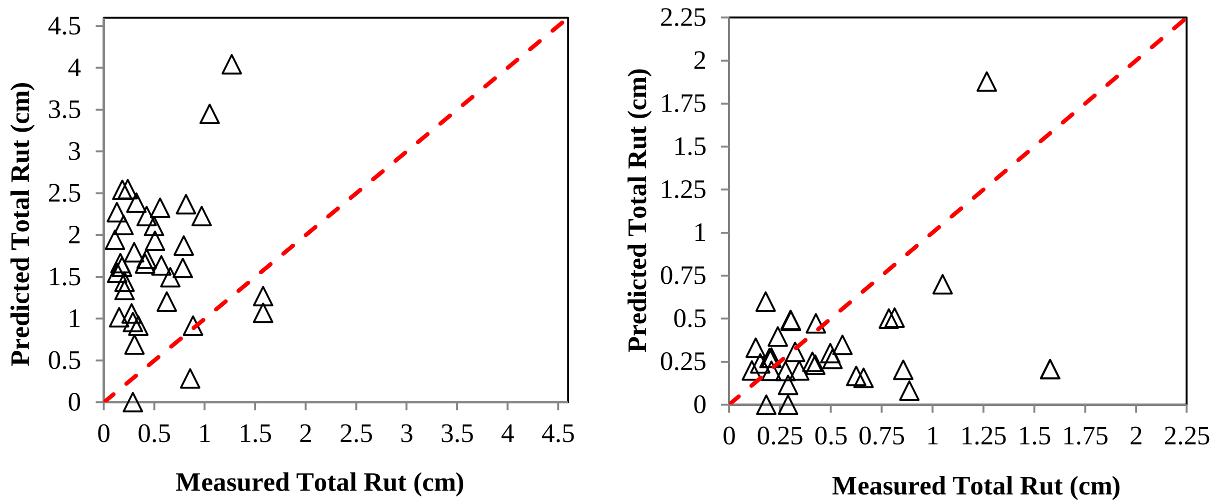

(a) Before Calibration **(b) After Calibration**

Figure 5-6 Comparison of predicted and measured Rutting (a) before calibration and (b) after calibration

Fatigue Cracking Model Calibration

Both alligator (bottom-up) and longitudinal (top-down) cracking prediction models were calibrated. The Darwin M-E predicts both bottom- and surface-initiated fatigue cracks using an incremental damage index approach. Alligator cracks are assumed to initiate at the bottom of HMA layers, while longitudinal cracks are assumed to initiate at the surface of the pavement. The damage is calculated as the ratio of the cumulative load repetitions from traffic to the allowable number of load repetitions as shown in Equation (5-11).

$$DI = \sum (\Delta DI)_{j,m,l,p,T} = \sum \left(\frac{n}{N_{f-HMA}} \right)_{j,m,l,p,T} \tag{5-11}$$

where,

n = Actual number of axle load applications within a specific time period

N_{f-HMA} = Allowable number of axle load applications for a flexible pavement and HMA overlays to fatigue cracking

j = Axle-load interval

m = Axle-load type (single, tandem, tridem, quad, or special axle configuration)

l = Truck type using the truck classification groups included in the M-EPDG

p = Month

T = Median temperature for the five temperature intervals used to subdivide each month

The Darwin M-E calculates the amount of alligator area cracking and the length of longitudinal cracking based on the incremental damage index. The damage transfer functions used in the Darwin M-E for alligator cracking and longitudinal cracking are shown in Equations (5-12) and (5-13), respectively.

$$FC_{Bottom} = \left(\frac{C_3}{1 + e^{\left(C_1 C_1^* + C_2 C_2^* Log(DI_{Bottom})\right)}}\right) * \left(\frac{1}{60}\right) \tag{5-12}$$

where,

FC_{Bottom} = Alligator cracking, percent of total lane area

C_1 = Calibration coefficient

C_2 = Calibration coefficient

C_1^* = $-2C_2^*$

C_2^* = $-2.40874 - 39.748\ (1 + H_{HMA})^{-2.856}$

H_{HMA} = Total HMAC thickness, in

C_3 = Calibration factor, 6000 and

DI_{Bottom} = Bottom incremental damage, %.

$$FC_{Top} = \left(\frac{C_4}{1 + e^{\left(C_1 - C_2 * Log(DI_{Top})\right)}}\right) * 10.56 \tag{5-13}$$

where,

FC_{Top} = Longitudinal cracking, ft/mile

C_1 = Calibration coefficient

C_2	= Calibration coefficient
C_4	= Calibration factor, 1000
DI_{Top}	= Surface incremental damage, %.

Both alligator cracking and longitudinal cracking transfer functions have two calibration coefficients; C_1 and C_2. Both the transfer functions used in Darwin M-E for alligator cracking and longitudinal cracking were calibrated by minimizing the sum of standard error (SSE) between predicted and measured values using Equation (5-14):

$$Sum\ of\ Standard\ Error\ (SSE) = \sum_{i=1}^{N} (Predicted\ distress - Measured\ distress)^2 \quad (5\text{-}14)$$

The Solver function within Microsoft Excel was employed to optimize the calibration coefficients in the alligator cracking and longitudinal cracking models. The calibrated coefficients for both alligator and longitudinal cracking models are shown in Table 5-5.

Table 5-5 Calibration factors for fatigue prediction models in the Darwin M-E

Calibration Factor	**Darwin M-E Default Value**	**Calibrated Value**
Alligator cracking		
C_1	1	0.560
C_2	1	0.225
C_3	6000	6000
Longitudinal cracking		
C_1	7	1.453
C_2	3.5	0.097
C_3	0	0
C_4	1000	1000

Figure 5-7 illustrates a comparison of the predicted and measured alligator cracking and longitudinal cracking before and after calibration. Both alligator cracking and longitudinal cracking models were improved by calibration. However, there was a high degree of variability between the predicted and measured distresses, especially for longitudinal cracking, even after the calibration. For alligator cracking, SEE values were found to be 3.384 (before calibration) and 2.144 (after calibration) while SEE values of 682 m/km (before calibration) and 486 m/km (after calibration) were found for longitudinal cracking. There is a continuing concern regarding the accuracy of the prediction of the longitudinal cracking model. Based on the findings from the NCHRP 9-30 study, it was noted that longitudinal cracking should be dropped from the local calibration guide development in NCHRP 1-40B study due to lack of accuracy in the predictions (Von Quintus et al., 2009). The Montana DOT conducted the local calibration study of MEPDG for flexible pavements. Regarding the longitudinal cracking prediction model, they concluded that no consistent trend in the predictions could be identified to reduce the bias and standard error, and improve the accuracy of this prediction model. It was believed that there is a significant lack-of-fit modeling error for the occurrence of longitudinal cracks (Von Quintus and Moulthrop, 2007). A study by Galal and Chehab (2005) in Indiana indicated that the MEPDG provided good estimation to the distresses measured except longitudinal cracking.

It is important to point out that only one year of distress data for each pavement section considered in this study were available in this verification and calibration process. Moreover, many default values recommended by the Darwin M-E were used in this study due to the unavailability of data. It is recommended that additional sites be established to include in the future calibration efforts and thus, improve the accuracy of the predictive models.

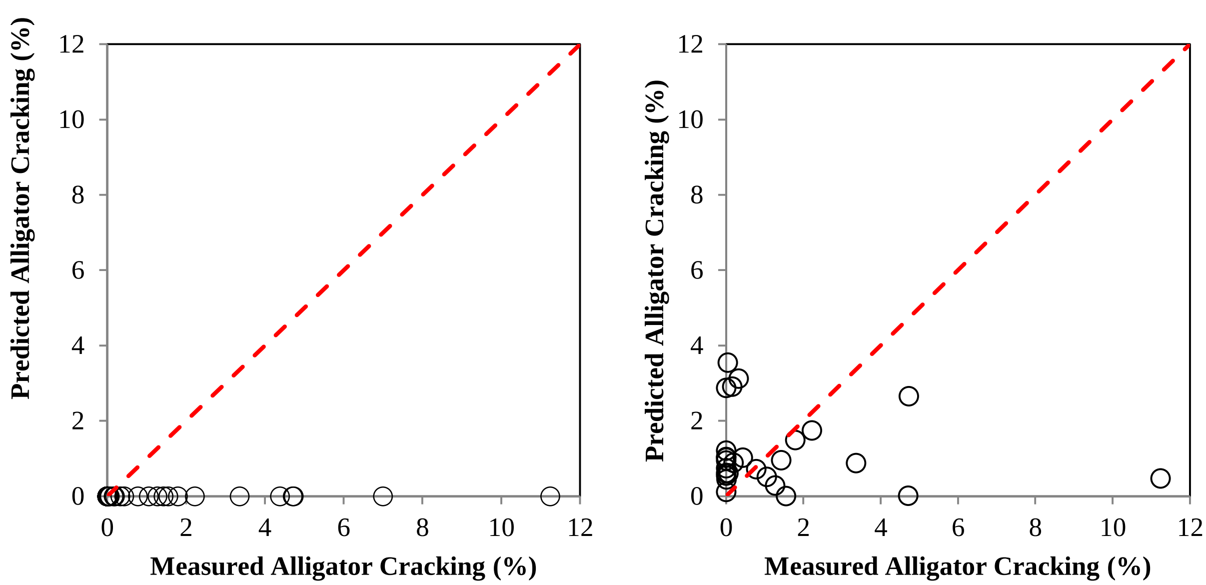

(a) Before Calibration **(b) After Calibration**

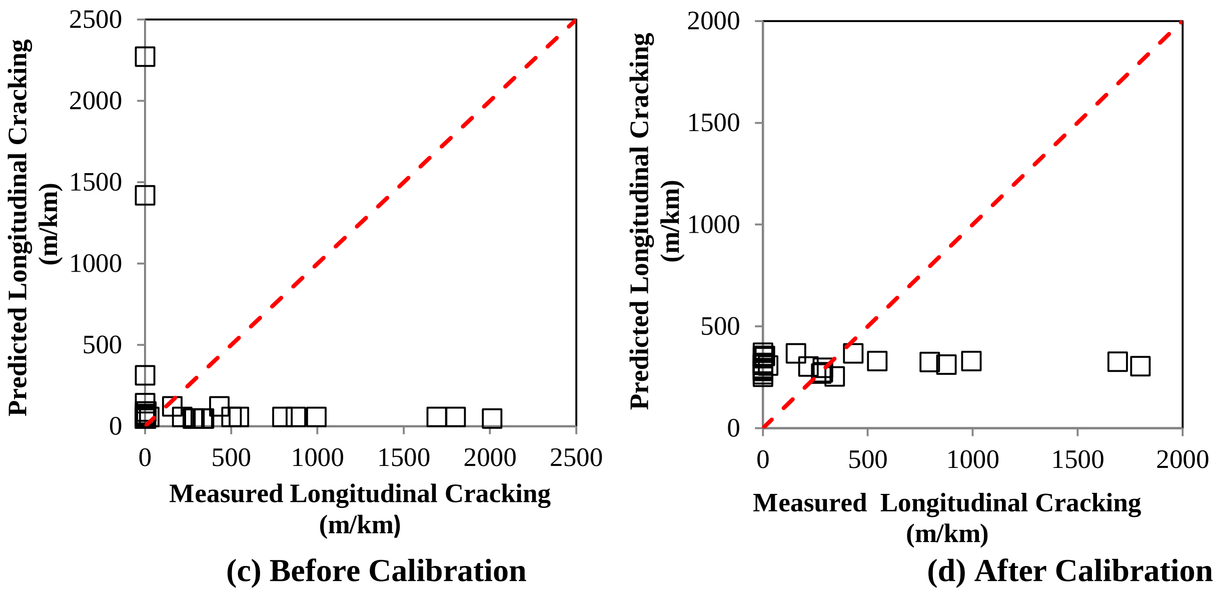

Figure 5-7 Comparison of predicted and measured distresses for Darwin M-E default (a, c) and calibrated models (b, d)

Thermal Cracking Model Calibration

There is one calibration factor (k) in the thermal (transverse) cracking model. Iterative runs of the Darwin M-E using discrete coefficients were employed to optimize the thermal cracking model. The default (nationally calibrated) value of k for Level 3 is 1.5. In the iterative runs, the value of k ranged from 1.5 to 12.5, where most of the thermal cracking predicted were almost zero for k up to 7.5. At k=12, thermal cracks were highly over predicted by Darwin M-E, however, a reasonable estimate of thermal cracking were found at k=10.

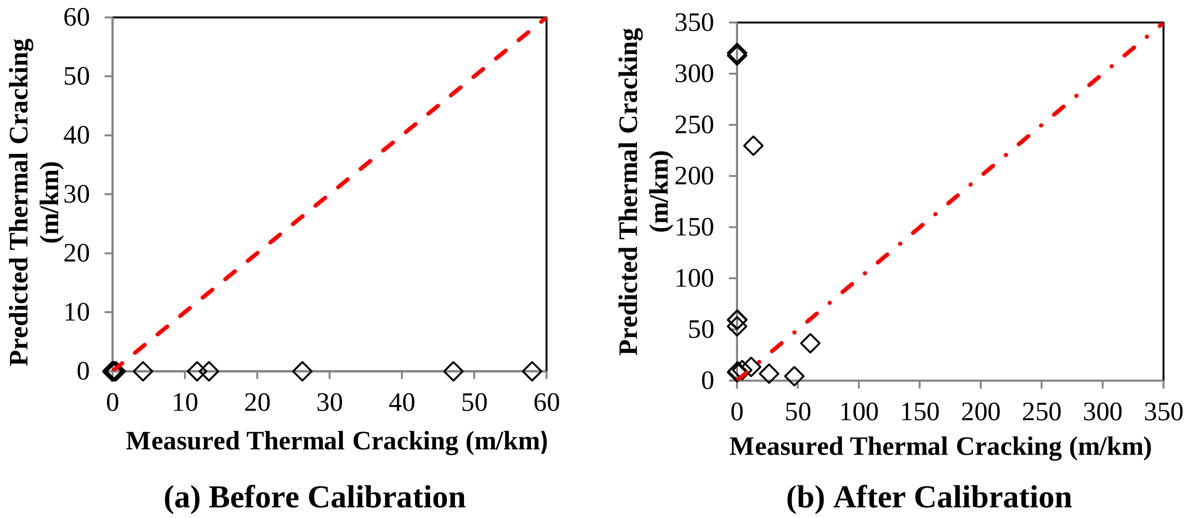

Figure 5-8 Comparison of predicted and measured thermal cracking (a) before calibration and (b) after calibration

Figure 5-8 shows a comparison of the predicted and measured thermal cracking before and after calibration (for k=10). The locally calibrated model (SEE=142 m/km) did not improve the prediction as compared to the nationally calibrated model (SEE=23 m/km). No consistent trend in the predictions could be identified to reduce the bias and standard error, and improve the accuracy of this prediction model. It is believed that there is a significant lack-of-fit modeling error for the occurrence of thermal cracks.

Validation

Calibrated models are needed to be validated to confirm that the locally calibrated performance prediction models can produce robust and accurate predictions for cases other than those used for model calibration. The calibrated models were validated by running the Darwin M-E on the remaining projects that were not included in the calibration process to compare predicted and measured performance. Figure 5-9 shows the comparison of the predicted and measured performance. It was observed that local calibration significantly reduced the difference between predicted and measured distresses. However, it is recommended that additional sites be established in the future calibration effort to further reduce this difference.

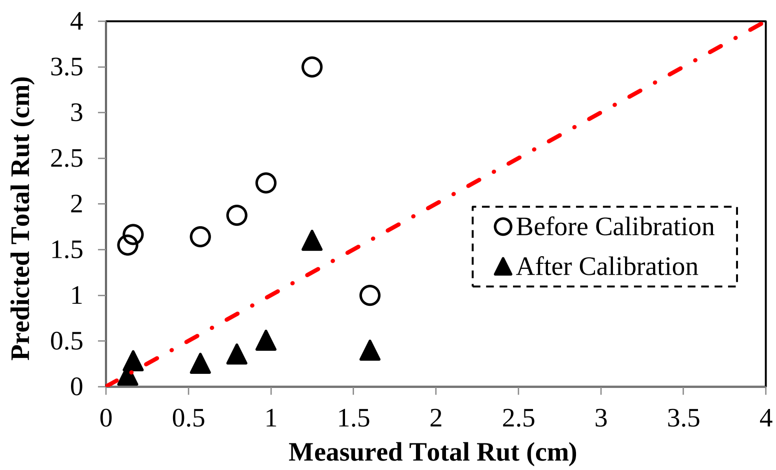

(a)

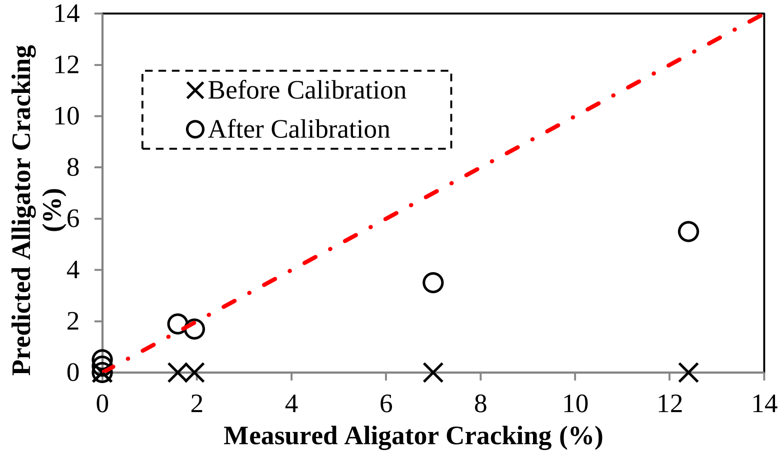

(b)

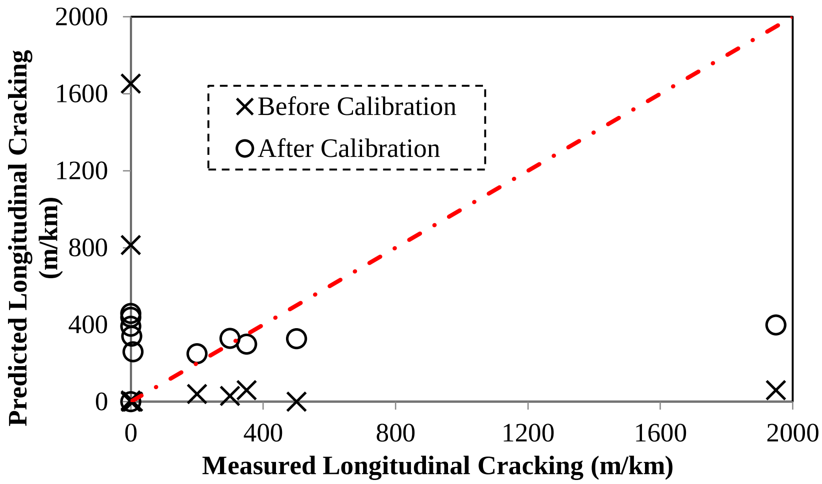

(c)

Figure 5-9 Comparison of national (before calibration) and calibrated performance models for (a) rutting, (b) alligator cracking, and longitudinal cracking

Conclusions and Recommendations

This paper presents the findings for calibration of the Darwin M-E performance prediction models of AC rehabilitation of the existing pavements for Oregon. The following conclusions and recommendations are made from this study:

- Predicted distresses using the Darwin M-E default calibration coefficients did not match well with actual distresses observed during the condition surveys, suggesting extensive local calibration is required for Oregon conditions. Further, it was observed that most of the rutting predicted by Darwin M-E occurred in the subgrade.
- The locally calibrated models of rutting, alligator cracking, and longitudinal cracking provided better predictions with lower bias and standard error than the nationally (default) calibrated models. However, there was a high degree of variability between the predicted and measured distresses, especially for longitudinal cracking, even after the calibration. The locally calibrated thermal cracking model did not improve the predictions as compared to the nationally (default) calibrated model. It is believed that there is a significant lack-of-fit modeling error for the occurrence of thermal cracks.
- From the validation results, both rutting and alligator cracking models provided reasonable predictions. Though the locally calibrated longitudinal cracking provided better predictions than the nationally calibrated model, a high degree of variability between the predicted and observed longitudinal cracking was found.
- It always remains a challenge to delineate between alligator (bottom-up) cracking and longitudinal (top-down) cracking as it is not practical to take cores or trenches at each single crack to distinguish between alligator cracking and longitudinal cracking. Therefore, there could be measurement error, which may affect the calibration effort.
- The availability and quality of data (materials, construction, and performance data) required for Darwin M-E are critical for local calibration. It is recommended that more detailed inputs (Level 1 mostly) be established for future calibration efforts, which will help reduce a significant amount of input error and, thus, may improve the accuracy of prediction models.

- There remains a question regarding the usability of longitudinal cracking and thermal cracking models, as was supported by previous research. Currently, improved thermal cracking models are being developed through FHWA pooled-fund studies. And, a NCHRP project 01-52 is underway to improve the longitudinal cracking model (http://apps.trb.org/cmsfeed/TRBNetProjectDisplay.asp?ProjectID=3152). Therefore, it is recommended that longitudinal cracking and thermal cracking models be recalibrated once these models are improved in Darwin M-E.
- Although the Oregon DOT has an extensive PMS database, most of the PMS data, especially pavement distress data, do not directly support the MEPDG. The difference between the distress measurement techniques of the ODOT and the MEPDG poses direct challenges to the implementation and local calibration efforts for the MEPDG. It is recommended that ODOT adopts the MEPDG (LTPP) standard procedure, at least for the sections to be used in the future calibration effort. By doing so, a significant amount of measurement error and input error can be reduced. And, the accuracy of performance prediction models can be improved.

Acknowledgments

This study was sponsored by the Oregon Department of Transportation (ODOT) and the Federal Highway Administration (FHWA) under project, “Mechanistic Design Guide Calibration for Pavement Rehabilitation”. The authors gratefully acknowledge Oregon State University and ODOT engineers for all the technical assistance and data provided. The contents of this paper reflect the views of the authors, who are responsible for the accuracy of the facts and data presented herein, and do not necessarily reflect the official policies of the ODOT and Iowa State University. This paper does not constitute a standard, specification, or regulation.

References

AASHTO. (1993). *AASHTO guide for design of pavement structures*, Washington,

ARA, Inc., ERES Consultants Division. (2004). “Guide for Mechanistic–Empirical Design of New and Rehabilitated Pavement Structures”. *Final report, NCHRP Project 1-37A*. Transportation Research Board of the National Academies, Washington, D.C. http://www.trb.org/ mepdg/guide.htm.

Banerjee, A., Prozzi, J. A., and Aguiar-Moya, J. P. (2010). “Calibrating the MEPDG permanent deformation performance model for different maintenance and rehabilitation strategies”, DVD. *Presented at the 89th Annual Meeting of the Transportation Research Board*. Washington, DC: Transportation Research Board.

Li, J., Pierce, L. M., and Uhlmeyer, J. S. (2009). “Calibration of flexible pavement in mechanistic-empirical pavement design guide for Washington State”. *Transportation Research Record* 2095: 73-83. Washington DC: Transportation Research Board, National Research Council.

Galal, K. A., and Chehab, G. R. (2005). “Implementing the mechanistic-empirical design guide procedure for a Hot-Mix Asphalt-rehabilitated pavement in Indiana”. In *Transportation Research Record: Journal of the Transportation Research Board, No. 1919*, TRB, National Research Council, Washington, D.C., pp. 121-133.

Hall, K.D., Xiao, D. X., and Wang, K.C.P. (2011). “Calibration of the MEPDG for flexible pavement design in Arkansas”. In *Transportation Research Record: Journal of the Transportation Research Board, No. 2226*, TRB, National Research Council, Washington, D.C., pp. 135-141.

Hoegh, K., Khazanovich, L., and Jensen, M. R. (2010). “Local calibration of MEPDG rutting model for MnROAD test sections”, DVD. *Presented at the 89th Annual Meeting of the Transportation Research Board*. Washington, DC: Transportation Research Board.

Kim, S., Ceylan, H., Gopalakrishnan, K., Smadi, O., Brakke, C., and Behnami, F. (2010). “Verification of MEPDG performance predictions using pavement management information system (PMIS)”, DVD. *Presented at the 89th Annual Meeting of the Transportation Research Board*. Washington, DC: Transportation Research Board.

Miller, J. S., and W. Y. Bellinger. (2003). “Distress Identification Manual for the Long-Term Pavement Performance Program”. *FHWA-RD-03-031*. FHWA, U.S. Department of Transportation.

Muthadi, N. R. (2007). *Local Calibration of the MEPDG for Flexible Pavement Design*. M.S thesis. North Carolina State University.

Muthadi, N. R., and Kim, R. (2008). "Local calibration of mechanistic-empirical pavement design guide for flexible pavement design". *In Transportation Research Record: Journal of the Transportation Research Board, No. 2087*, TRB, National Research Council, Washington, D.C., pp. 131-141.

National Cooperative Highway Research Program (NCHRP). (2004). "Guide for Mechanistic-Empirical Design of New and Rehabilitated Pavement Structures". *Draft Final Report NCHRP Project 1-37A*, Transportation Research Board, National Research Council, Washington, D.C.

Souliman, M. I., Mamlouk, M. S., El-Basyouny, M. M., and Zapata, C. E. (2010). "Calibration of the AASHTO MEPDG for flexible pavement for Arizona conditions", DVD. *Presented at the 89th Annual Meeting of the Transportation Research Board*. Washington, DC: Transportation Research Board.

Von Quintus, H. L. and Moulthrop, J. S. (2007). "Mechanistic-Empirical Pavement Design Guide Flexible Pavement Performance Prediction Models: Volume I- Executive Research Summary". *FHWA/MT-07-008/8158-1*. Texas: Fugro Consultants, Inc.

Von Quintus, H. L. (2008a). "MEPDG Overview & National Perspective". *Presented at North-Central MEPDG User Group*, Ames, IA.

Von Quintus, H. L. (2008b). "Local calibration of MEPDG—an overview of selected studies". *Presented at 2008 AAPT Symposium Session: Implementation of the New MEPDG*, Philadelphia, PA.

Von Quintus, H. L., Darter, M. I., and Mallela, J. (2009a). "Recommended Practice for Local Calibration of the M-E Pavement Design Guide". *National Cooperative Highway Research Program Project 1- 40B Manual of Practice*, Washington, DC: Transportation Research Board, National Research Council.

Von Quintus, H. L., Darter, M. I., and Mallela, J. (2009b). "Examples Using the Recommended Practice for Local Calibration of the MEPDG Software". *National Cooperative Highway Research Program Project 1- 40B Manual of Practice (under review)*, Washington, DC: Transportation Research Board, National Research Council.

CHAPTER 6 - A STUDY OF TOP-DOWN CRACKING IN THE STATE OF OREGOEN

Md. S. Rahman[1 2] and R. Christopher Williams[3]

A paper to be submitted to the *Transportation Engineering Journal*, published by the American Society of Civil Engineers (ASCE)

Abstract

Recently, the Oregon Department of Transportation (ODOT) has identified hot mix asphalt concrete (HMAC) pavements that have displayed top-down cracking within three years of construction. The objective of the study was to evaluate the top-down cracked pavement sections and compare the results with the non-cracked pavement sections. Research involved evaluating six surface cracked pavements and four non-cracked pavement sections. The research included extensive field and laboratory investigations of the 10 pavement sections by conducting distress surveys, falling weight deflectometer (FWD) testing, dynamic cone penetrometer (DCP) testing, and coring from the cracked and non-cracked pavement sections. Cores were then subjected to a full laboratory-testing program to evaluate the HMAC mixtures and binder rheology. The laboratory investigation included dynamic modulus, indirect tensile (IDT) strength, and specific

---

[1] Ph.D. Candidate, Department of Civil, Construction & Environmental Engineering, Ames, IA 50011. PH: 515 817 3774, E-mail: msrahman@iastate.edu

[2] Primary researcher and author

[3] Professor, Department of Civil, Construction & Environmental Engineering, Ames, IA 50011. PH: 515 294 4419, Fax: 515 294 8216, E-mail: rwilliam@iastate.edu

gravity testing on the HMAC cores, binder rheological tests on asphalt binder and aggregate gradation analysis. The FWD and DCP tests indicated that top-down cracked pavement sections were structurally sound, even some of the sections with top-down cracking showed better structural capacity compared to non-cracked sections. The study also found that top-down cracking initiation and propagation were independent of pavement cross-section or the HMAC thickness. The dynamic modulus testing indicated that cores from all the top-down cracked pavement sections except one section (OR 140) possessed stiffer mixtures than that of non-cracked pavement sections. All four non-cracked pavement areas were found to be exhibiting fairly high IDT strength, and low variability in IDT strength and HMAC density when compared to top-down cracked sections as indicated by the IDT strength tests and air void analysis. Asphalt binder rheological test result indicated that asphalt binders from all the top-down cracked sections except OR140 showed higher complex shear modulus (stiffer binder) compared to non-cracked pavement sections. The study concluded that top-down cracking could be caused by a number of contributors such as stiffer HMAC mixtures, mixture segregation, binder aging, low HMAC tensile strength, and high variability in tensile strength or by combination of any.

Key Words: Top-down cracking, Hot mix asphalt pavement, Falling weight deflectometer, Backcalculation, Dynamic modulus, Dynamic shear rheometer, Bending beam rheometer.

Introduction

For over a century, highways have been paved using asphalt concrete mixes in State of Oregon as well as across the United States. However, a major problem still exists involving premature pavement failures caused by cracking, rutting, potholes etc. Recently, Oregon Department of Transportation (ODOT) has constructed hot mix asphalt (HMA) pavements that have displayed premature cracking within three years of construction. Early cracking allows moisture to penetrate the pavement structure reducing the pavement section's design life and significantly increasing the life cycle cost. Also within the last several years, design and material changes occurred that may or may not have contributed to the early cracking. The changes include an increase in the quantity of recycled asphalt pavement (RAP) allowed in the wearing surface; the use of binder modifications including acid and polymers; and a shift in mix gyration levels. Construction factors like properties of the produced mix (volumetrics) and placement also play a part of the pavement performance.

It has been well recognized that cracking of hot-mix asphalt (HMA) pavements is a major mode of premature failure. Currently, four major mode of failure associated with HMAC cracking are identified: (Birgisson et al.,2002, Von Quintus and Moulthrop, 2007) 1) fatigue cracking, also known as bottom-up cracking, which starts at the bottom of the HMA pavement and propagates upward to the surface of the pavement, 2) top-down cracking, also known as longitudinal cracking, initiating at the top of the asphalt pavement layer in a direction along the wheel path and propagating down-ward, 3) thermal cracking, and 4) reflective cracking, in which existing cracks or joints cause stress concentrations that result in crack propagation through an HMA overlay.

Notional investigations into cracking have identified areas where the cracking is top-down versus bottom-up. While both are serious, bottom-up cracking typically indicates the pavement structure was underdesigned indicating a need to change structural design practices. Top-down cracking, however, may indicate that material selection process can be fine-tuned. The only means to differentiate between top-down versus bottom-up cracking is through coring. Traditionally, most flexible pavement design methods consider fatigue cracking initiating at the bottom of the HMA layer and propagating upward as the most critical criteria for the fatigue failure of HMA pavements. However, recent research has suggested that premature pavement fatigue failure initiates at the surface of HMA pavement and propagates downward, which is known as top-down cracking. A study by Myers et al.(1998) in Florida reported that fatigue failure of HMA pavement in Florida was mainly caused by top-down cracking A more recent study by Wang et al. (2007) revealed that 90% cracking encountered in Florida HMA pavements were recognized as top-down cracking. This scenario is not unique to Florida. Similar results have been reported in other states and countries, including Colorado, Indiana, Washington, India, Japan, Kenya, South Africa, France, Netherlands, and United Kingdom (Kim and Underwood, 2003). Figure 6-1 shows the pattern of top-down cracking developed within early years of construction, which was confirmed by taking cores.

The objectives of the research are to determine the causes of early cracking on the State of Oregon highways system. The results of the study will be used to modify the pavement design process including modifications to the Pavement Design Guide and Mix Design Guidelines. By doing so, the ODOT will be able to design pavements that are long lasting, resulting in significant benefits to the department by reducing the life cycle cost needed to maintain the state highway system.

Figure 6-1 Photos showing the development of top-down cracking

Background

It is important that the causes and mechanisms associated with top-down cracking should be better understood to improve the cracking resistance of mixtures. This will prevent premature pavement failure, reduce significant costs incurred on highway state agencies and eventually, provide a cost-effective, long lasting pavement. There are various opinions related to mechanisms that causes top-down cracking, but there are no conclusive data to suggest that one is more applicable than the other one.

For years pavement engineers within the Washington State Department of Transportation (WSDOT) have observed that HMA pavements in State of Washington have displayed top-down cracking that appear to crack from the top of the pavement and propagate downward. Often, the cracks stop at the interface between the wearing course and the underlying bituminous layers (a depth of about 50 mm).The top-down cracking was observed in thicker sections with thinner sections cracking full depth. Top-down cracking generally started within three to eight years of paving for pavement sections that were structurally adequate and were designed for adequate ESALs (Uhlmeyer et al., 2000).

Svasdisant et al. (2002) conducted field and laboratory investigations on HMA and rubblized pavements exhibiting top-down cracking. Detailed mechanistic analyses were conducted using the engineering characteristics obtained from field and laboratory test results to determine the potential for top-down cracking. The study concluded that surface radial tensile stress induced by wheel load and enhanced by differential stiffness due to construction (poor compaction and segregation), temperature, and aging could cause top-down cracking.

Baladi et al. (2002) studied the effects of segregation on the initiation and propagation of top-down cracking in HMA pavements. Both field and forensic investigation were conducted and it was confirmed that top-down cracking initiated in segregated areas. The results from the mechanistic analysis revealed that segregated areas were susceptible to fatigue cracking manifested as top-down cracking.

Myers et al. (1998) observed that top-down cracking predominated in Florida five to ten years after construction. Based on the computer modeling, they found out that tensile stresses under the treads of the tire-not the tire edges-were the primary cause of the cracks. Further, they stated that wide based tires caused the highest tensile stresses, which confirmed the results conducted by Nunn (1998). They concluded that top-down cracking is not a structural design issue but more related to mixture composition. They suggested that more fracture resistant mixtures be used to improve the top-down cracking performance of the pavement.

Gerritsen et al. (1987) observed that pavements in Netherlands were experiencing premature cracking in the wearing course, both inside and outside the wheelpath areas, soon after the construction. They reported that the surface cracking outside of the wheelpaths had low mix strength characteristics at low temperature and the surface cracks in the wheelpaths areas were largely due to radial shear forces under truck tires near the tire edges. They concluded that both load and thermal related effects could be attributed to the observed surface cracking. Their recommendation was to increase the binder film thickness to reduce early age hardening of the mixtures.

Dauzats et al. (1987) reported that top-down cracks, either longitudinal or transverse, were observed in France, typically three to five years after paving. They found that these types of surface cracks were initially caused by thermal stresses and then further propagated by traffic loads. They noted that a rapid hardening of the mix binder likely contributed to this type of pavement distress.

Studies based on measured tire/pavement contact pressures by De Beer et al. (1997) and Himeno et al. (1997) and instrumented pavements by Dai et al. (1997) in MnRoad supported the view that truck tires were a primary cause of top-down cracking in asphalt concrete wearing courses.

In a study by Harmelink et al. (2008), 28 projects were evaluated from a wide geographical area of Colorado and 18 sites out of 28 sites were found exhibiting top-down cracking. Of these 18 sites, 12 had visual evidence of segregation observed at the bottom of the upper pavement lift that was not visible on the surface. Other factors included percentage of air voids, volume of effective asphalt binder, and physical properties of the asphalt binder.

A study conducted by the Illinois Department of Transportation (IDOT) in 1993 detailed the history and investigation of top-down cracks in HMA pavements. The study indicated that there was a high degree of correlation between the outside edges of the conveyors on the paver and the top-down cracking in the pavement. Two pavers were identified in the study that demonstrated the correlation between the longitudinal cracking in the pavement and the outside edges of the conveyor slats.

A micromechanics study on top-down cracking based on the material's microstructure by Wang et al. (2003) concluded that both tensile-type and shear-type cracking could initiate top-down cracking. They also concluded that when the mastic was weaker or the pavement surface temperature was higher, top-down cracking most likely initiated. Therefore, a mix sensitive to rutting may also be sensitive to top-down cracking.

Myers et al. (2001) concluded that top-down cracking could be initiated by traffic induced stresses, temperature changes, or due to their combined effect. Temperature and modulus gradients were assumed to be critical to the top-down cracking initiation and propagation.

Baladi et al. (2003) concluded that a segregated area in pavement due to poor construction was more prone to top-down cracking along with raveling. They also mentioned that differential stiffness between HMA courses caused a significant increase in load-induced surface tensile stresses. Nighttime temperatures produced the highest magnitude of surface tensile stress.

A study by Freitas et al. (2005) concluded that air voids, segregation and binder content had a significant effect on the top-down cracking for all temperatures. They also found that higher temperature and rutted surface contributed significantly to top-down cracking initiation. El-Basyouny and Witczak (2005) stated that top-down cracking was caused by extremely large contact pressures at the tire edge-pavement interface in combination with highly aged thin surface layer that had become oxidized.

A study by Sridhar et al. (2008) on the Indian Highways indicated that temperature, especially in combination with heavy axle loading, was a critical parameter influencing the top-down cracking susceptibility of the HMA layer. H. Wang and I.L. Al-Qadi (2010) concluded that at high temperatures, shear-induced top-down cracking could initiate from some distance below the pavement surface in conjunction with the distortional deformation. They also indicated that negative temperature gradient in the HMA layer and debonding under the surface layer could lead to premature top-down cracking. Ozer et al. (2011) stated that several factors contribute to the top-down cracking such as, heavy traffic and thermal loads, stiffness gradients due to binder aging, variation in bituminous characteristics between lifts, and bituminous material segregation.

Development of Experimental Plan and Site Selection

The proposed experimental plan summarized in Table 6-1 below represents sampling 10 pavements, 6 with top-down cracking and 4 without top-down cracking. ODOT pavement management databases have been explored to identify top performers and early failures.

Database investigation also included reviewing pavement designs, mix designs and construction history. This represents a factorial plan based upon the main effects- with and without top-down cracking, and ESAL level (low vs. high trafficking levels). Each of the pavements with top-down cracking would need 10 cores of 152-mm diameter, 5 next to a crack and 5 away from the crack. Prior to removing the 10 cores, the top-down cracking would need to be verified by coring on a crack. Overall, this would allow for determination of what led to the crack initiation and propagation at a particular location and thus identify potential differences within the same pavement section. Sampling pavements that have not undergone top-down cracking, 5 152-mm diameter cores, will allow for comparison of good performing pavements as compared to ones that are experiencing inadequate performance. These comparisons will allow for determining the mechanisms leading to good performing pavements and those experiencing top-down cracking. Table 6-2 illustrates the designation of the pavement sections that will be used in this study.

Table 6-1 Proposed experimental plan

Pavement Performance	Location	ESAL Level							
		Low Volume Traffic				High Volume Traffic			
		Proposed Candidates				Proposed Candidates			
		Name	Highway Number	Begin MP	End MP	Name	Highway Number	Begin MP	End MP
Pavements with Top-Down Cracking	Next To Crack	OR221	150	17.3	20.15	OR99EB	072	0.47	3.41
		OR238	272	38.09	38.75	OR99W	091	21.8	23.76
		OR140	270	53.6	53.79	OR99	091	108.82	109.65
	Away From Crack	OR221	150	17.3	20.15	OR99EB	072	0.47	3.41
		OR238	272	38.09	38.75	OR99W	091	21.8	23.76
		OR140	270	53.6	53.79	OR99*	091	108.82	109.65
Pavements without Top-Down Cracking	N/A	OR22	162	12.11	13.8	US20	007	1.11	2.29
						US97	004	114.25	115.2
						OR99	091	108.82	109.65

* Denotes top-down cracking section of OR99

Table 6-2 Designation of the test sections in the study

Test Section	Route	Cracking	Designation Used in this Study
OR22:Sublimity Intchg Sect (RW2-WB)	OR22	NO	OR22-U
OR238: Beg. Div Hwy-Jct Hwy 063	OR238	YES	OR238-C
OR 99W:Brutscher St-Jct Hwy 151	OR99W	YES	OR99W-C
OR 221: N. Salem-Orchard Heights Rd	OR221	YES	OR221-C
OR 99EB: Jct Hwy 001-Comm. St.	OR99EB	YES	OR99EB-C
US97: NW Wimp Way-Terrebonne	US97	NO	US97-U
US20: NE 11th St-Purcell Blvd	US20	NO	US20-U
OR 140: Aspen Lake Rd-Boat Landing	OR140	YES	OR140-C
OR99: Junction City 1 (Cracked)	OR99	YES	OR99*-C
OR99: Junction City 1 (Uncracked)	OR99	NO	OR99-U

Field Work Plan

This phase included field work including identification of pavements with and without top-down cracking, and field sampling. It is difficult to identify pavements with top-down cracking through examining pavement performance records and only through forensic field study that includes coring, can identify top-down cracking. Thus candidate pavements for top-down cracking evaluation would likely need to be identified through a combination of paper records review, discussion with ODOT personnel, as well as utilizing information gathered from the recently completed M-E Pavement Design Guide calibration project. Once pavements that have been identified as top-down cracking candidates, field sampling via coring will be done for subsequent assessment. It is important to verify top-down cracking via sampling on top of cracks as well as sampling next to the crack and well away for the cracks. Before coring is done, field condition survey and falling weight deflectometer (FWD) testing will be conducted. Also, dynamic cone penetrometer (DCP) testing on base/subbase as well as geoprobe samples up to 122 cm deep at core locations after coring. This field testing information will subsequently be used to assess the adequacy of the pavement structure. Visible assessment of drainage conditions will also done on site. In this phase the following tasks are to be completed:

- Field condition survey compatible with MEPDG
- FWD testing to assess the adequancy of the pavement structure
- Field sampling-10 cores from each pavement with top-down cracking and 5 cores from each pavement without top-down cracking
- DCP testing and geoprobe samples at core locations after coring

Laboratory Testing Plan

Laboratory testing on the extracted asphalt mixture cores will include dynamic modulus and indirect tensile strength testing in a diametrical test configuration over a range of temperatures and at multiple frequencies. The binder will then be extracted and recovered from the cores for subsequent rheological testing for binder grade determination. The binder grading will include dynamic shear rheometer and bending beam rheometer testing for grade determination. Further, the recovered aggregate will be tested for gradation, and coarse and fine aggregate angularity. Table 6-3 lists all the tests that will be performed on the asphalt cores, and extracted asphalt binder and aggregate.

Table 6-3 Tests on asphalt mix cores and asphalt binder

Test Name	Standard Be Used
Bulk Specific Gravity & Density of Asphalt Mix Cores	AASHTO T 166-93
Dynamic Modulus (E^*)	AASHTO T342-11
Indirect Tensile Strength (ITS)	AASHTO T322-07
Theoretical Maximum Specific gravity of Asphalt Mix	AASHTO T 209-94
Binder Recover & Extraction	AASHTO T319-08
Dynamic Shear Rheometer (DSR)	AASHTO T315
Bending Beam Rheometer (BBR)	AASHTO T313
Aggregate Gradation	AASHTO T 27-93

Upon completion of the tests on asphalt mix cores and asphalt binder, gradation analysis on removed unbound base materials will be performed for subsequent comparison to construction records and material design specifications in place at the time of construction. This will allow for determination whether or not fines have migrated into the unbound base materials and adversely affecting their performance.

Discussion of Field and Laboratory Investigation

Field Investigation

Six pavement sections with top-down cracking and four sections without top-down cracking were selected for field and laboratory investigations. Field investigation included conducting a distress survey, taking cores, conducting falling weight deflectometer (FWD), and dynamic cone penetrometer (DCP) testing. Figure 6-2 shows the top-down cracking displayed some of the test sections included in this study.

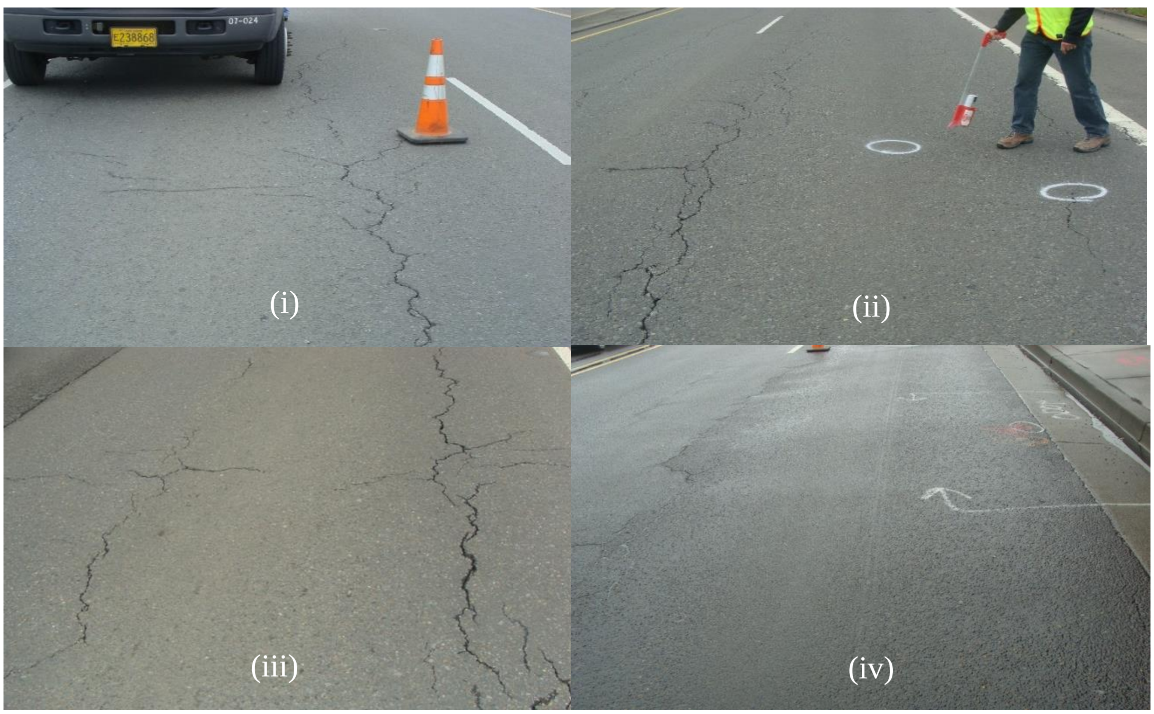

Figure 6-2 Top-Down Cracking on (i) OR238-C, (ii) OR221-C, (iii) OR99EB-C, and (iv) OR99-C*

Falling Weight Deflectometer Testing

Falling weight deflectometer (FWD) testing has been widely adopted to obtain surface deflection data in order to evaluate existing pavement conditions since the 1980s. The Oregon Department of Transportation (ODOT) has been using FWD testing as a non-destructive evaluation method of pavement structure. The FWD test imparts an impulse load on the road surface and the resulting surface deflections are recorded at different locations using deflection measuring sensors known as geophones. Then the stiffness moduli of the pavement layers are estimated by measuring the deflection basin under the applied load.

The stiffness moduli of the pavement layers were determined from the FWD deflection data using backcalculation software Elmod 6.0 (Evaluation of Layer Moduli and Overlay Design) and BAKFAA (FAA backcalculation analysis). Both software, Elmod 6.0 and BAKFAA, require information on pavement layers (layer thickness and type of materials), pavement condition (pavement temperature and time of the day) at FWD test site, and the FWD measured deflection data to obtain backcalculated layer moduli (shown in Table 6-4). As HMA mixture stiffness varies with the temperature, all backcalculated HMA stiffness (modulus) were corrected to a standard reference temperature of 20℃ following procedures developed by Chen et al. (2000). Before correction of the backcalculated HMA moduli to a standard reference temperature, mid-depth HMA pavement temperatures at which FWD deflections were obtained were estimated by BELLS3 equation developed by Lukanen et al. (2000).

Table 6-4 Input used in the backcalculation process

Test Section	Surface Temp. (℃)	Air Temp. (℃)	Pavement Temp. (℃)	Thickness (mm)	
				AC	Base
OR22-U	41.9	24.9	37.6	243	279
US97-U	20.0	15.2	17.1	212	356
US20-U	18.4	14.0	15.9	251	229
OR99-U	33.4	29.2	30.6	254	203
OR238-C	33.3	26.4	32.9	216	254
OR99W-C	28.0	25.7	26.7	324	203
OR221-C	25.2	21.1	23.6	219	279
OR99EB-C	25.6	21.8	24.0	208	279
OR140-C	22.8	11.4	16.2	241	203
OR99*-C	28.0	25.7	26.5	227	203

Figure 6-3 illustrates comparisons of the normalized (temperature corrected to℃) backcalculated layer moduli of the projects included in this study while Table 6-5 shows the coefficient of variation of the backcalculated layer moduli. As can be seen, OR22-U and OR99-U exhibited higher AC moduli (E1) values compared to US97-U and US20-U, among non-cracked sections. Among pavements with top-down cracking, OR238-C, OR99W-C, OR99EB-C, and OR99*-C display higher AC moduli (E1) values compared to values of OR221-C and OR140-C. For base moduli (E2), higher moduli values are observed with US20-U, OR99-U, OR238-C, and OR99*-C than the remaining sections included in this study. For subgrade moduli (E3), similar moduli values are displayed by most of the sections included in this study except OR238-C.

Table 6-5 Coefficients of variation of the backcalculated layer moduli

Test Section	Coefficient of Variation of Backcalculated Moduli (%)					
	Elmod			BAKFAA		
	E1	E2	E3	E1	E2	E3
OR22-U	17	39	17	18	86	25
US97-U	22	30	22	35	115	34
US20-U	21	51	26	39	77	40
OR99-U	28	27	15	29	63	13
OR238-C	34	32	26	39	66	25
OR99W-C	36	53	24	45	98	94
OR221-C	16	30	26	19	85	19
OR99EB-C	27	52	9	38	148	21
OR140-C	16	27	16	30	93	54
OR99*-C				31	39	22

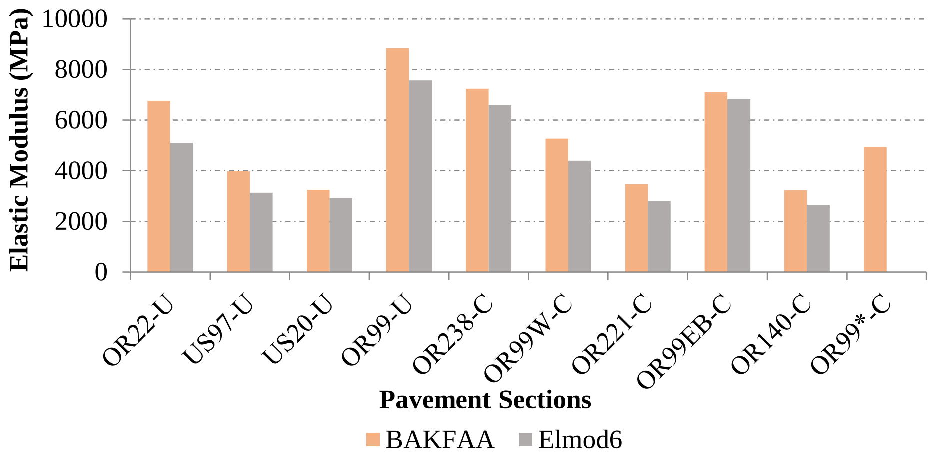
Elastic Modulus (MPa)
10000
8000
6000
4000
2000
0
OR22-U
US97-U
US20-U
OR99-U
OR238-C
OR99W-C
OR221-C
OR99EB-C
OR140-C
OR99*-C
Pavement Sections
BAKFAA
Elmod6

(i)

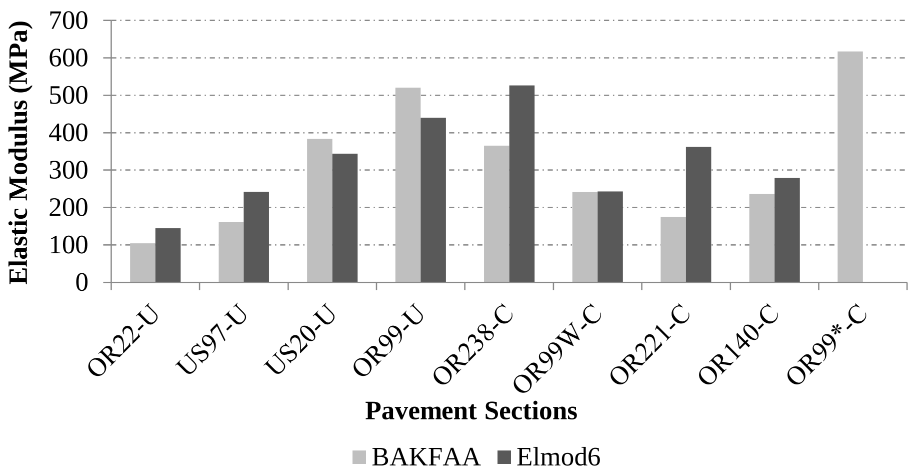
Elastic Modulus (MPa)
700
600
500
400
300
200
100
0
OR22-U
US97-U
US20-U
OR99-U
OR238-C
OR99W-C
OR221-C
OR140-C
OR99*-C
Pavement Sections
BAKFAA
Elmod6

(ii)

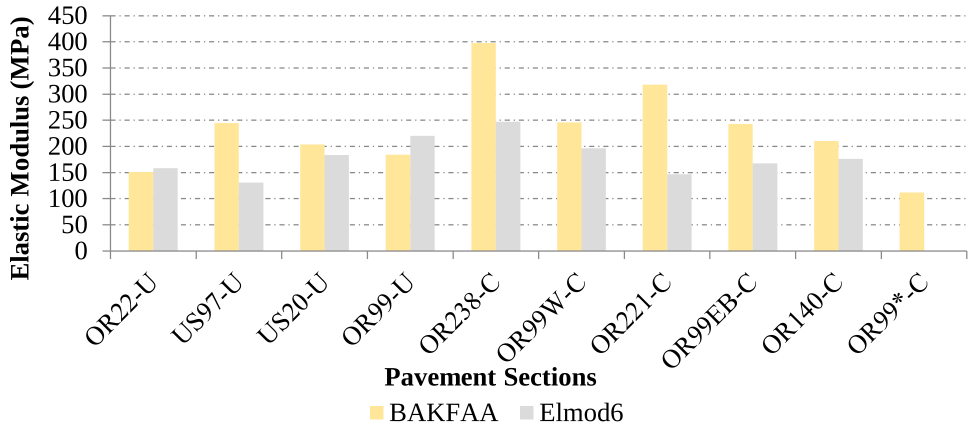

(iii)

Figure 6-3 Average backcalculated moduli (i) AC moduli, (ii) base Moduli, and (iii) subgrade moduli

FWD testing is currently the most widely used method for non-destructive evaluation of the structural capacity of a pavement. Many different approaches have been proposed to estimate the structural number (SN) of an existing pavement directly from FWD deflections. AASHTO (1993) has developed equations to calculate SN from non-destructive deflection test results. The equation used to estimate subgrade resilient modulus (M_r) is expressed in Equation 6-1. Equation 6-2 provides the distance requirement be determined based on the radius of the stress bulb at the subgrade-pavement interface. The average values of the M_r back calculated from deflections at 914 and 1219 mm were used as the determined subgrade resilient moduli.

$$M_R = \frac{0.24P}{d_r r} \tag{6-1}$$

where:

M_r = Backcalculated subgrade resilient modulus (psi);

P = Applied load (lb);

r = Radial distance (in); and

d_r = Deflection at a distance r (in) from the center of the load (in).

$$r \geq 0.7\sqrt{[a^2 + (D\sqrt[3]{\frac{E_p}{M_R}})^2]} \tag{6-2}$$

where:

a = FWD loading plate radius (in);

D = Total thickness of pavement layers above the subgrade (in); and

E_p = Effective modulus of all pavement layers above the subgrade (psi).

When the subgrade resilient modulus and total thickness of all layers above the subgrade are known, the effective modulus (Ep) of the entire pavement structure above the subgrade is determined from the deflection measured at the center of the load through Equation 6-3. And, Equation 6-4 is used to compute the effective structural number (SN_{eff}).

$$d_0 = 1.5pa\{\frac{1}{M_R\sqrt{1+(\frac{D}{a}\sqrt[3]{\frac{E_p}{M_R}})^2}} + \frac{1+\frac{1}{\sqrt{a+(\frac{D}{a})^2}}}{E_p}\} \tag{6-3}$$

where:

E_p = Effective modulus of all pavement layers above the subgrade (psi);

d_0 = Deflection measured at the center of the load plate (adjusted to a standard reference temperature of 20 ^{0}C) (in);

p = FWD loading plate pressure (psi);

a = FWD loading plate radius (in);

M_r = Subgrade resilient modulus (psi); and

D = Total thickness of pavement layers above the subgrade (in).

$$SN_{eff} = 0.0045D\sqrt[3]{E_p} \tag{6-4}$$

where:

SN_{eff} = Effective structural number;

D = Total thickness of pavement layers above the subgrade (in); and

E_p = Effective modulus of all pavement layers above the subgrade (psi).

Table 6-6 summarizes the average subgrade resilient modulus, effective pavement elastic modulus, and effective structural number of each test section included in this study. Among non-cracked sections, the highest SNeff value of 7.1 was estimated with OR99-U while US97-U had the lowest SNeff value of 4.8. The highest SNeff value of 7.9 and the lowest SNeff value of 4.9 were estimated for OR99EB-C and OR221-C, respectively, among top-down cracked pavement sections.

Table 6-6 Subgrade resilient modulus, effective modulus and effective structural number backcalculated from FWD test results

Section	Mr (MPa)	Ep (MPa)	SNeff
OR22-U	127	2297	6.4
US97-U	197	749	4.8
US20-U	173	1758	5.4
OR99-U	176	4571	7.1
OR238-C	421	2677	6.1
OR99W-C	176	2009	6.8
OR221-C	333	1190	4.9
OR99EB-C	293	5229	7.9
OR140-C	180	1905	5.1
OR99*-C	166	4386	6.6

Dynamic Cone Penetrometer Testing

The Oregon Department of Transportation has been using dynamic cone penetrometer (DCP) test to verify the quality of unbound base materials during construction because variations in density can have relatively large effects on the properties that determine pavement performance. DCP consists of two vertical shafts connected to each other at the anvil. The upper shaft has a handle and hammer. Along with providing a way to easily hold the DCP vertical, the handle is used to provide a standard drop height of 575 mm. The hammer is 8 kg and provides a constant impact force. The lower shaft contains an anvil at the top and a pointed cone on the bottom. The anvil is fixed and stops the hammer from falling any farther than the standard drop height. When the hammer is dropped and hits the anvil, the cone is driven into the base materials.

The DCP penetration distance per drop is known as the DCP penetration index (DCPI) or penetration resistance (PR).

Dynamic cone penetrometer (DCP) tests were conducted on each of the pavement sections except OR99W-C and OR140-C to evaluate the variations in density. Figure 6-4 illustrates average penetration resistance (PR) of the test sections included in this study. Both sections OR238-C and OR221-C had three locations along the longitudinal direction where DCP tests were conducted. Only one location on OR99-U while the remaining sections had two locations for DCP tests. As can be seen, OR99EB-C exhibited the highest variability in PR while sections US20-U, OR238-C, and OR99*-C showed consistent PR values at different locations. Similar variability in PR values at different locations was observed on the sections OR22-U and US97-U. For section OR221-C, two locations had identical PR (around 3 mm/blow) values but the third location had a PR value of over 5 mm/blow.

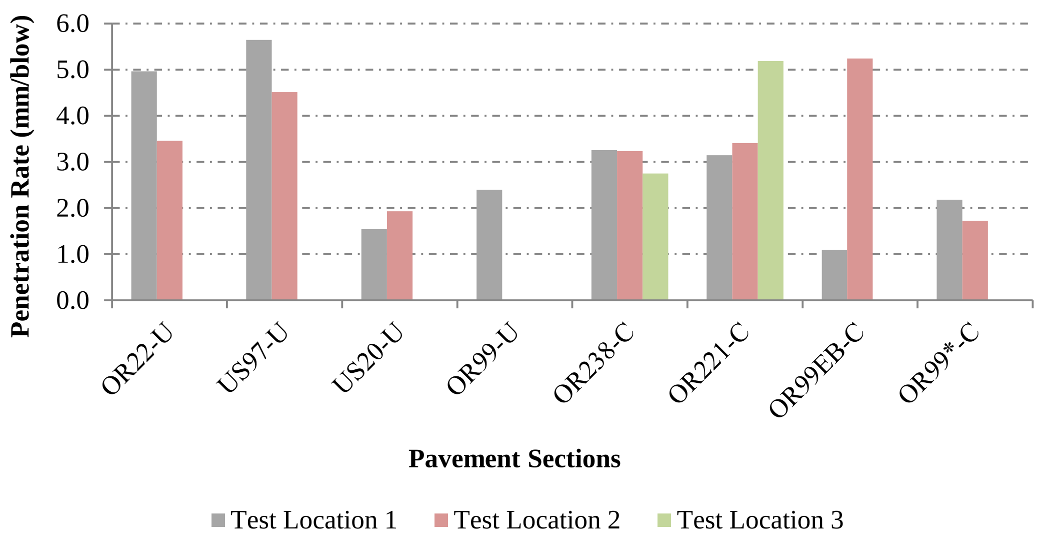

Figure 6-4 Average penetration resistance (PR) of the test sections

Core Thickness Data

After all non-destructive tests were completed, cores were extracted at the designated locations using a power rotary drill. Ten cores were extracted from each of the pavement section with top-down cracking and five cores from each of the non-cracked pavement sections. Figures 6-5 illustrates the comparison of core thicknesses with standard deviations among the pavement sections. Among non-cracked sections, an average core thickness of 213-mm was found with US97-U whereas the remaining sections had identical average core thicknesses of around 254 mm. Section OR99-U exhibited largest variability (standard deviation of 44.30 mm) in core thicknesses followed by US97-U with standard deviation of 25.4 mm. OR99W-C had the largest core thickness of 325-mm while the remaining sections showed an average core thickness in the range between 208 and 241-mm, among top-down cracked sections.

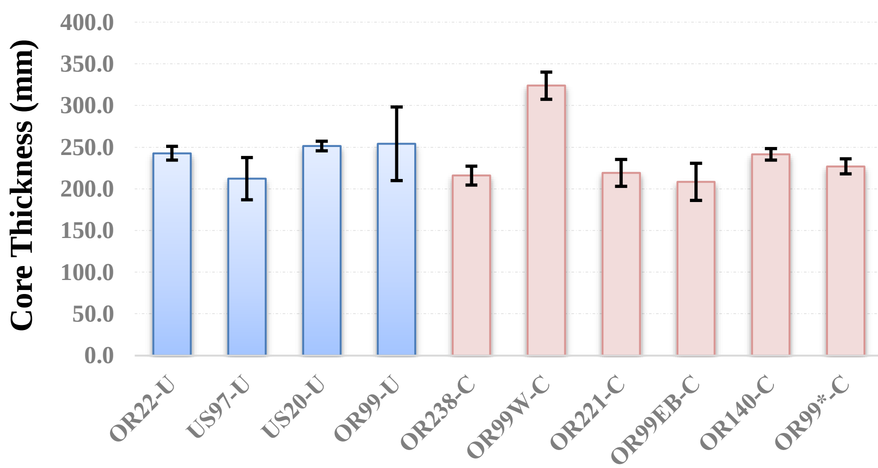

Figure 6-5 Average core thickness of the test sections

Laboratory Investigation

After all non-destructive tests had been completed, cores were extracted at the designated locations using a power rotary drill. Five cores from each of non-cracked pavement sections and 10 cores from each of top-down cracked sections were brought to the laboratory for testing and evaluation. For top-down cracked sections, approximately five cores were taken near the cracked areas while the remaining cores were taken away from the cracks.

Dynamic Modulus Test

Dynamic modulus testing is generally conducted in axial compression mode on laboratory fabricated asphalt concrete specimens of 100-mm diameter and 150-mm tall. It is sometimes impossible to obtain this size of specimen (e.g., height) from actual pavements. Thus, the indirect tension (IDT) testing of cores becomes more appropriate for the evaluation of existing pavements. Kim et al. (2004) developed the linear viscoelastic solution for the dynamic modulus of HMA under the IDT mode and the results were verified by conducting both axial compression and IDT test methods on 12 asphalt mixtures commonly used in North Carolina. Unlike axial compression test, both vertical and horizontal linear variable differential transformers (LVDTs) are needed in the IDT dynamic modulus testing as shown in Figure 6-6. Dynamic modulus tests were conducted on all the extracted cores (specimen size of 150-mm diameter and 62-mm height) under IDT mode. Each sample was tested at three different temperatures (4, 21, and 37℃) and six different frequencies (25, 10, 5, 1, 0.5, and 0.1 Hz). Testing was done with a closed-loop servo-hydraulic testing machine to apply the sinusoidal loading. A temperature chamber was used to control the test temperature. A dummy specimen with a thermocouple embedded in the middle of the specimen was used to control the temperature of the testing specimens.

Figure 6-7 shows the dynamic modulus ($|E^*|$) master curves of all the projects at a reference temperature of 21℃. In general, it can be observed that all the top-down cracked sections except OR140-C displayed higher dynamic modulus values compared to the non-cracked sections. At low and intermediate frequencies, the difference in dynamic modulus between top-down cracked sections and non-cracked sections was more pronounced while identical modulus values were observed for the all sections at high frequencies.

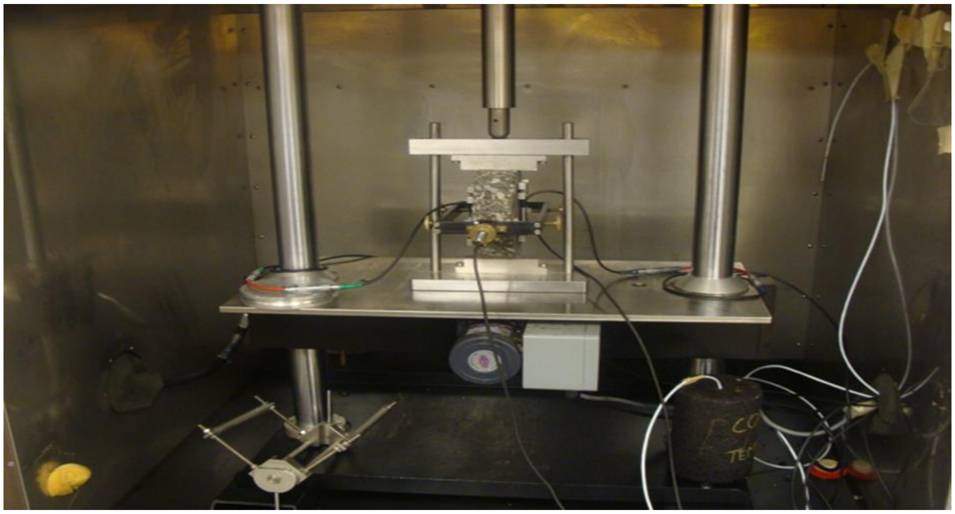

Figure 6-6 Specimen set-up for dynamic modulus testing in IDT mode

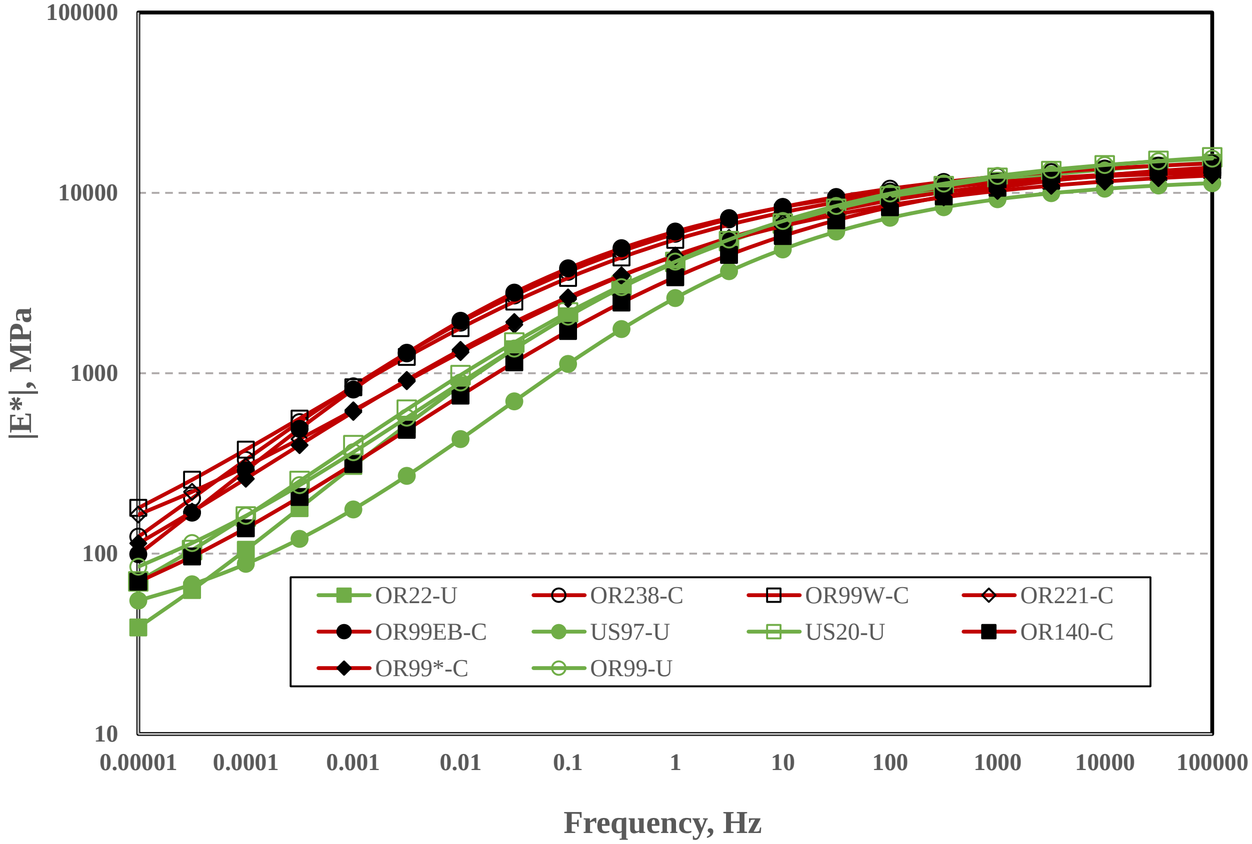

Figure 6-7 Dynamic modulus master curves

Indirect Tensile Strength Test

Indirect tensile (IDT) strength tests were conducted on specimens obtained from pavement cores to evaluate the tensile strength of the asphalt mix. Tensile strength is also an indicator of fatigue performance of the mixture. The IDT test was performed following ASTM D6931-12 "*Standard Test Method for Indirect Tensile (IDT) Strength of Bituminous Mixtures*". The test was performed at 21℃. Table 6-7 summarizes the average IDT strength along with standard deviation and coefficient of variation. Figure 6-8 illustrates the comparison of the IDT strength of the all projects investigated in this study.

Table 6-7 Indirect tensile (IDT) strength test results

Test Section	IDT Strength Results (kPa)				
	Average	Max	Min	Std Dev	CV (%)
OR22-U	1561	1675	1455	96	6
US97-U	1317	1393	1220	86	7
US20-U	1271	1310	1089	123	10
OR99-U	1456	1551	1358	97	7
OR238-C	1526	1793	931	316	21
OR99W-C	1438	1648	1000	248	17
OR221-C	1150	1620	779	299	26
OR99EB-C	1705	1834	1662	54	3
OR140-C	1170	1462	1000	235	20
OR99*-C	1309	1910	772	364	28

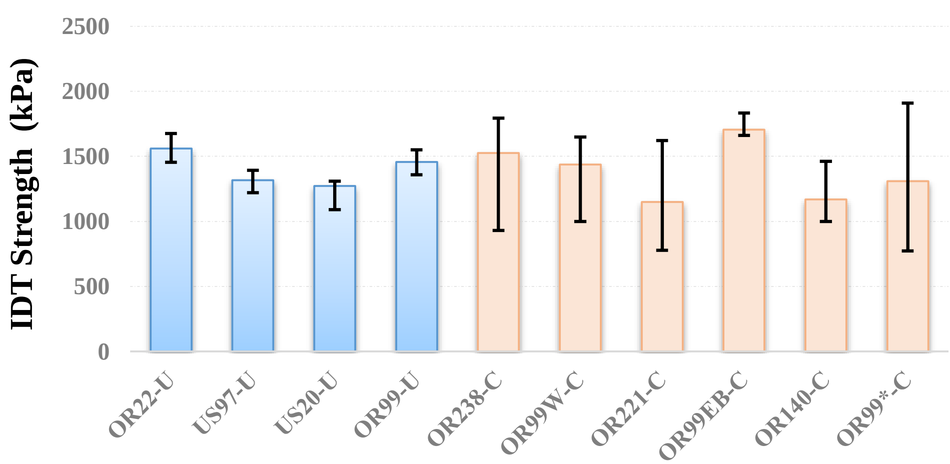

Figure 6-8 Comparison of IDT Strength Test Results

Among pavement sections with top-down cracking, sections OR221-C, OR140-C, and OR99*-C displayed substantially lower IDT strength values than the values obtained from OR238-C, OR99W-C, and OR99EB-C. All the top-down cracked sections except OR99EB-C exhibited very high variability in IDT strength with standard deviation ranging from 235 kPa for OR140-C to 364 kPa for OR99*-C. All the non-cracked sections showed fairly low variability (standard deviation ranges from 86 to 123 psi) in IDT strength compared to the top-down cracked sections. Among non-cracked sections, the highest IDT strength value of 1561 kPa was obtained with OR22-U while section US20-U displayed the lowest IDT strength value of 1271 kPa.

Air Void Analysis Results

Bulk specific gravity (Gmb) tests and theoretical maximum specific gravity (Gmm) tests were conducted on the extracted cores following appropriate standard test procedures. The air voids (%) were then computed by the following equation:

$$Air\ Voids\ (\%) = \frac{(G_{mm} - G_{mb})}{G_{mm}} \times 100 \tag{6-5}$$

where:

G_{mm} = Theoretical maximum specific gravity of the mixture; and

G_{mb} = Bulk specific gravity of the mixture.

Figure 6-9 shows the comparison of the air voids of the all projects investigated in this study. Among non-cracked sections, an average air voids of 7.3% was observed with section US97-U followed by 6.0%, 5.3%, and 4.1% with OR99-U, OR22-U, and US20-U, respectively. Section OR99*-C displayed the highest average air voids of 8.3% while the lowest average air voids of 5.4% was observed on the section OR238-C, among top-down cracked pavement sections. It is important to point out that top-down cracked sections exhibited higher variability in air voids than the non-cracked sections.

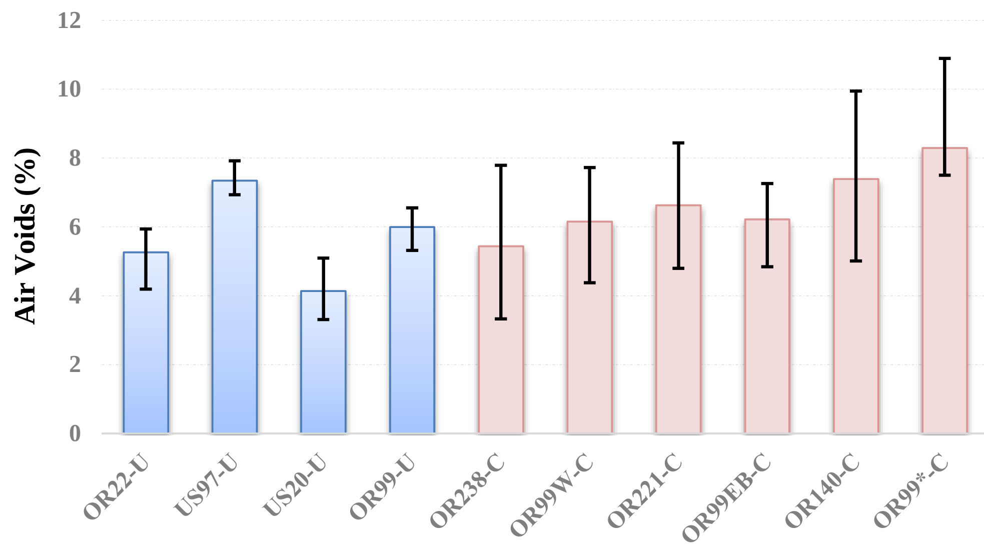

Figure 6-9 Comparison of air voids (%) test results

Binder Rheological Test Results

Asphalt binders were subjected to rheological tests once the binders were extracted and recovered from field cores following AASHTO TP2-94, "*Standard Test Method for the Quantitative Extraction and Recovery of Asphalt Binder from Hot Mix Asphalt (HMA)".* Dynamic shear rheometer (DSR) testing was employed to test three replicate samples for each pavement section according to ASTM D7175, "*Standard Test Method for Determining the Rheological Properties of Asphalt Binder using a Dynamic Shear Rheometer*" to characterize the binder rheological properties at high and intermediate temperatures. The complex shear modulus (G*) and phase angle (δ) determined from the DSR tests were used to evaluate the high and intermediate critical temperatures and PG ranges. Moreover, DSR frequency sweep tests were performed to construct master curves for the asphalt binder complex shear modulus (G^*) and phase angle (δ). The master curves characterizes binder rheological properties over a wide range of temperature or frequency. The frequency sweep procedure was performed at different temperatures ranging from 20 to 82°C at frequencies ranging between 0.1 to 100 Hz.

Bending beam rheometer (BBR) tests were also conducted to evaluate the binder rheological properties at low temperatures. The standard method for BBR testing is AASHTO T 313, "*Determining the Flexural Creep Stiffness of Asphalt Binder Using the Bending Beam Rheometer (BBR)*" and was followed to test the asphalt binders at low temperatures. Two key properties, stiffness (S) and change in stiffness (m-slope) were recorded from the computer-generated output of the BBR test. The BBR test was employed to evaluate the low critical temperatures.

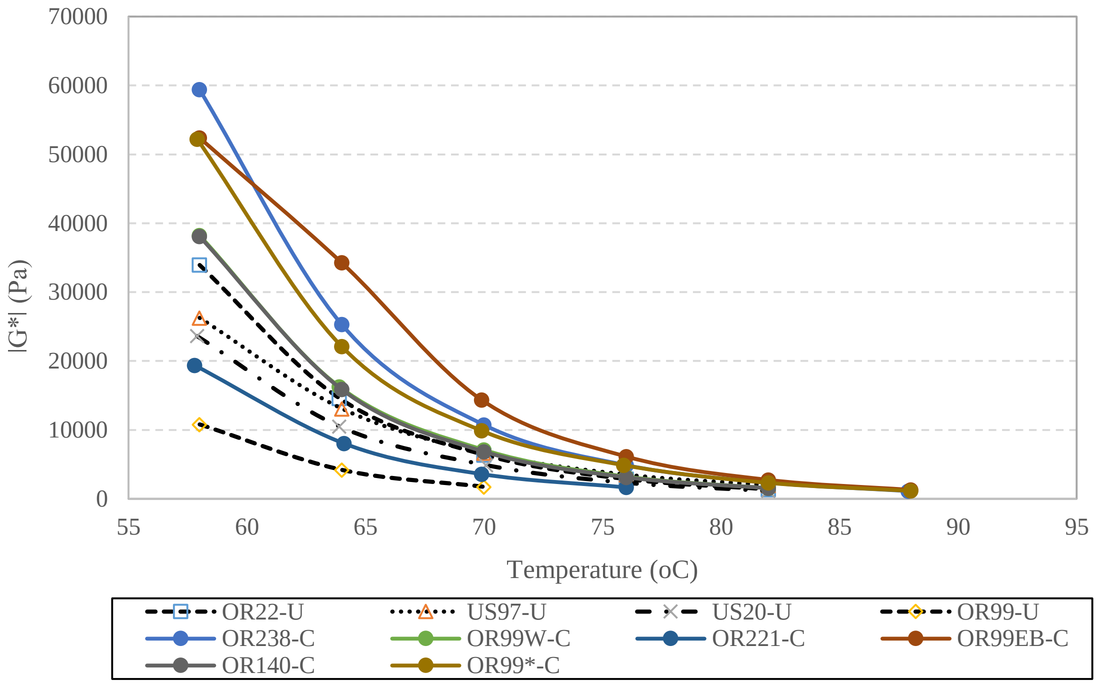

Figure 6-10 Variation of binder complex shear modulus at high temperatures

Figure 6-10 shows the variation of binder complex shear modulus with the corresponding DSR high test temperatures. As can be seen from Figure 6-10, all top-down cracked sections except OR221-C exhibited higher complex shear modulus than the non-cracked sections across all test temperatures. Among sections with top-down cracking, OR99EB-C, OR238-C, and OR99*-C displayed higher complex shear modulus values than the other sections. OR99-U showed the lowest complex shear modulus while sections US20-U and US-97 exhibited identical behavior, among non-cracked sections. It was mentioned earlier that OR99 the Junction City section, had two sections, one OR99-U (non-cracked section) and the other one OR99*-C with top-down cracking. Rut on OR99-U (rut of 0.48 in) was found to be higher than that of OR99*-C (rut value of 0.25 in) during the distress surveys. Section OR99*-C is more rut resistant than section OR99-U but more susceptible to fatigue cracking as evident from Figure 6-10. Table 6-8 lists the high temperature performance grade for all the sections investigated in this study, determined from the DSR tests.

Table 6-8 High temperature Performance Grade (PG)

OR22-U	US97-U	US20-U	OR99-U	OR238-C	OR99W-C	OR221-C	OR99EB-C	OR140-C	OR99*-C
76	76	76	64	82	76	70	82	76	82

DSR tests at intermediate temperatures were conducted to evaluate the fatigue cracking susceptibility in asphalt binders. The temperatures at which a maximum value of 5000 kPa for |G*|Sin(δ) is recorded determines the limiting temperature related to fatigue cracking. Figure 6-11 illustrates the variation of |G*|Sin(δ) with respect to test temperatures. As can be seen, the DSR test results at intermediate temperatures are almost identical to the DSR test results at high temperatures discussed in the previous section. Most of the top-down cracked sections except OR221-C were more susceptible to fatigue cracking compared to non-cracked sections. Table 6-9 lists the temperatures at which the asphalt binders investigated in this study met the criteria for fatigue cracking in binders.

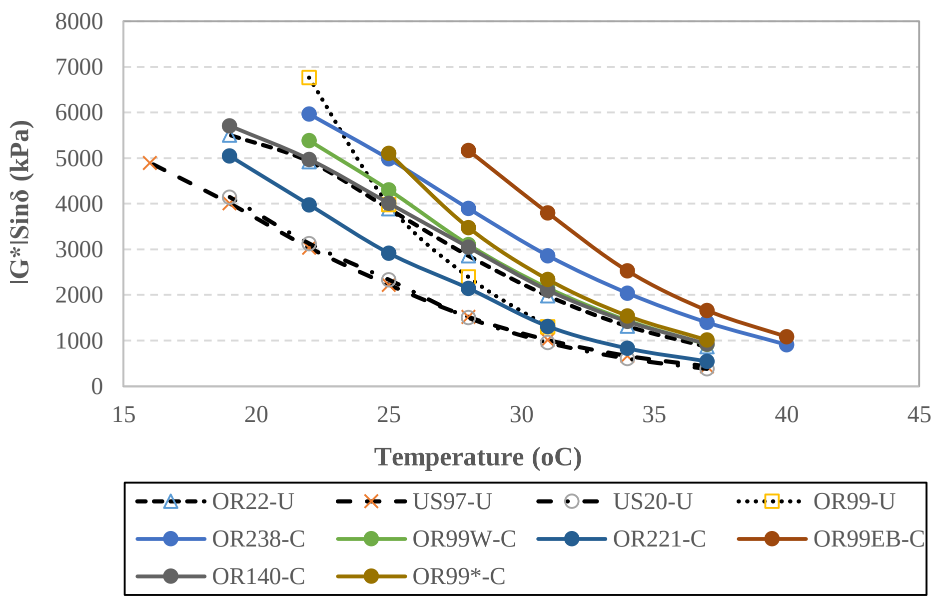

Figure 6-11 Variation of |G|Sin(δ) at intermediate temperatures*

Table 6-9 Minimum temperature for fatigue cracking in asphalt binder

OR22-U	US97-U	US20-U	OR99-U	OR238-C	OR99W-C	OR221-C	OR99EB-C	OR140-C	OR99*-C
21.58	17.14	16.78	23.74	24.87	23.43	20.13	28.6	21.87	25.26

Frequency sweep tests were conducted at different temperatures ranging from 20 to 82℃ at frequencies ranging between 0.1 to 100 Hz to develop master curves for asphalt binders. Figure 6-12 illustrates complex shear modulus (|G*|) master curves of all the sections at 20℃ while phase angle master curves are shown in Figure 6-13. As can be seen, all the sections with top-down cracking except OR221-C exhibited higher shear modulus than the non-cracked pavement sections.

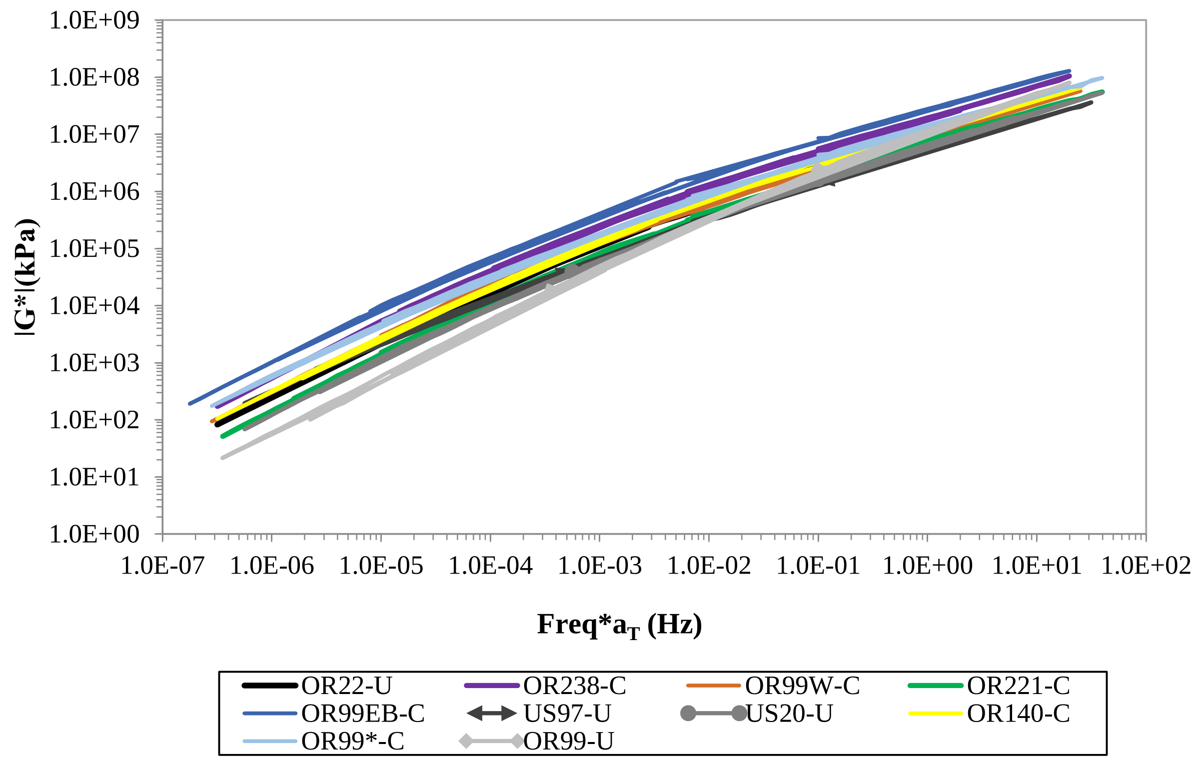

Figure 6-12 Complex shear modulus master curves

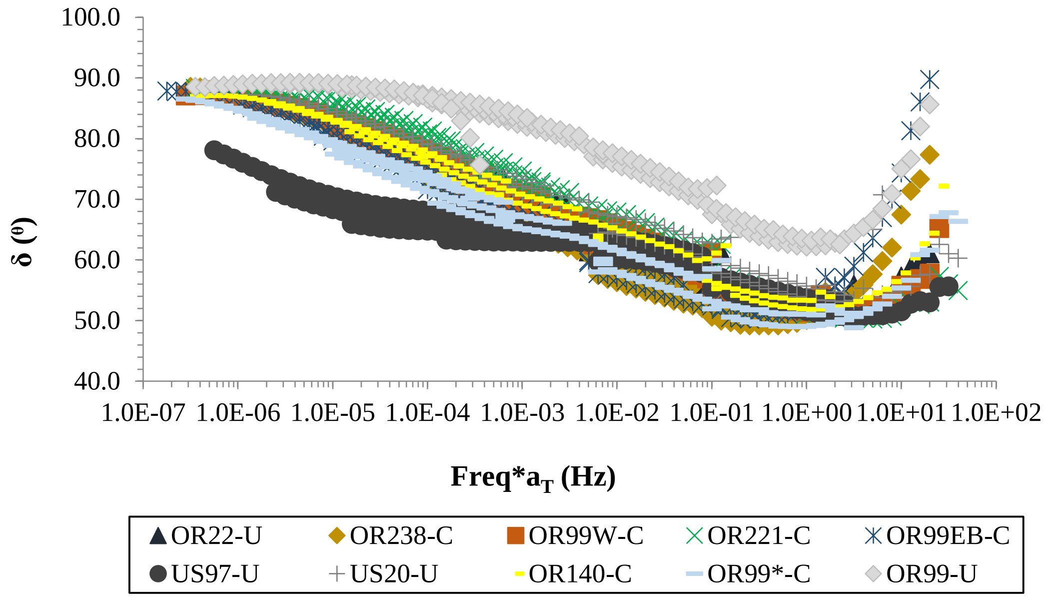

Figure 6-13 Phase angle master curves

Table 6-10 BBR test results

<table>
<tr><td rowspan="4">OR22-U</td><td colspan="4">Temp. (℃)</td><td colspan="4">Temp. (℃)</td><td rowspan="4">US97-U</td></tr>
<tr><td colspan="2">-12</td><td colspan="2">-18</td><td colspan="2">-12</td><td colspan="2">-18</td></tr>
<tr><td>m-value</td><td>S (MPa)</td><td>m-value</td><td>S (MPa)</td><td>m-value</td><td>S (MPa)</td><td>m-value</td><td>S (MPa)</td></tr>
<tr><td>0.35</td><td>226</td><td>0.25</td><td>378</td><td>0.37</td><td>120</td><td>0.28</td><td>250</td></tr>
<tr><td rowspan="4">US20-U</td><td colspan="4">Temp. (℃)</td><td colspan="4">Temp. (℃)</td><td rowspan="4">OR99-U</td></tr>
<tr><td colspan="2">-12</td><td colspan="2">-18</td><td colspan="2">-12</td><td colspan="2">-18</td></tr>
<tr><td>m-value</td><td>S (MPa)</td><td>m-value</td><td>S (MPa)</td><td>m-value</td><td>S (MPa)</td><td>m-value</td><td>S (MPa)</td></tr>
<tr><td>0.38</td><td>165</td><td>0.28</td><td>326</td><td>0.32</td><td>344</td><td>0.23</td><td>564</td></tr>
<tr><td rowspan="4">OR238-C</td><td colspan="4">Temp. (℃)</td><td colspan="4">Temp. (℃)</td><td rowspan="4">OR99W-C</td></tr>
<tr><td colspan="2">-6</td><td colspan="2">-12</td><td colspan="2">-12</td><td colspan="2">-18</td></tr>
<tr><td>m-value</td><td>S (MPa)</td><td>m-value</td><td>S (MPa)</td><td>m-value</td><td>S (MPa)</td><td>m-value</td><td>S (MPa)</td></tr>
<tr><td>0.34</td><td>124</td><td>0.29</td><td>250</td><td>0.32</td><td>244</td><td>0.25</td><td>421</td></tr>
<tr><td rowspan="4">OR221-C</td><td colspan="4">Temp. (℃)</td><td colspan="4">Temp. (℃)</td><td rowspan="4">OR99EB-C</td></tr>
<tr><td colspan="2">-12</td><td colspan="2">-18</td><td colspan="2">-6</td><td colspan="2">-12</td></tr>
<tr><td>m-value</td><td>S (MPa)</td><td>m-value</td><td>S (MPa)</td><td>m-value</td><td>S (MPa)</td><td>m-value</td><td>S (MPa)</td></tr>
<tr><td>0.33</td><td>184</td><td>0.29</td><td>295</td><td>0.32</td><td>206</td><td>0.27</td><td>370</td></tr>
<tr><td rowspan="4">OR140-C</td><td colspan="4">Temp. (℃)</td><td colspan="4">Temp. (℃)</td><td rowspan="4">OR99*-C</td></tr>
<tr><td colspan="2">-12</td><td colspan="2">-18</td><td colspan="2">-6</td><td colspan="2">-12</td></tr>
<tr><td>m-value</td><td>S (MPa)</td><td>m-value</td><td>S (MPa)</td><td>m-value</td><td>S (MPa)</td><td>m-value</td><td>S (MPa)</td></tr>
<tr><td>0.32</td><td>176</td><td>0.25</td><td>408</td><td>0.35</td><td>167</td><td>0.30</td><td>224</td></tr>
</table>

BBR tests were conducted to evaluate binder low temperatures properties. For each temperature three replicate samples from each project were tested to determine two key properties: the stiffness (S) and the change in stiffness (m-value). Table 6-10 shows the average m-value and the average stiffness parameter S. The low critical temperatures of all the projects were determined from the m-value and stiffness (S) obtained from the two temperatures. Table 6-11 lists the low temperature performance grade for all the sections investigated in this study, determined from BBR tests. It could be observed that all the non-cracked sections except OR99-U exhibited better performance in resisting low temperature cracking than most of the top-down cracked sections. (Except OR221-C).

Table 6-11 Low temperatures Performance Grade (PG)

OR22-U	US97-U	US20-U	OR99-U	OR238-C	OR99W-C	OR221-C	OR99EB-C	OR140-C	OR99*-C
BBR Failure Temp. (℃)									
-15	-17	-17	-11	-11	-14	-17	-8	-14	-8
Continuous Low Temp. Performance Grade (PG)									
-25	-27	-27	-21	-21	-24	-27	-18	-24	-18

Gradation Analysis and Binder Content

Gradation analysis on the recovered aggregate was conducted in accordance with the standard procedure AASHTO T 27-93. Figure 6-14 shows the gradation curves of the all the projects. It could be observed that gradation curves of all the projects are identical except one non-cracked section, US20-U. No significant difference could be observed among the projects with respect to aggregate gradation that would impact cracking.

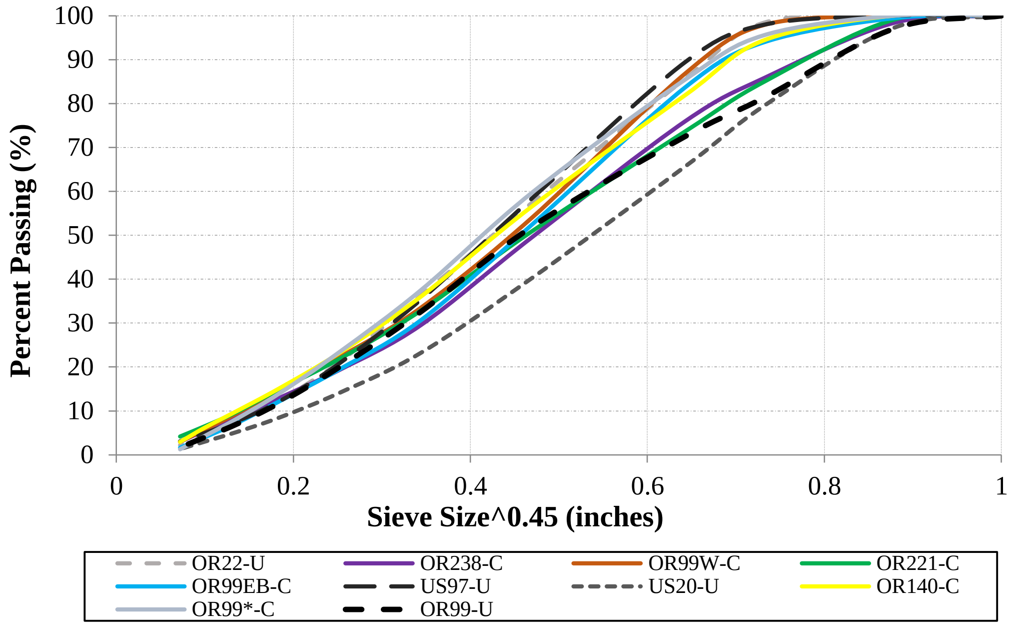

Figure 6-14 Gradation analysis

Percent binder content by weight of the sections investigated in this study are illustrated in Figure 6-15 and were determined without a fines correction. Among top-down cracked sections, a maximum binder content of 6.6% was found with section OR140-C followed by 5.7% with OR221-C and the lowest value of 4.6% with OR238-C. A binder content of just over 5% was found with the remaining top-down cracked sections. Among non-cracked sections, section US97-U showed highest binder content of 5.4% whereas a lowest value of 4.1% was found with US20-U. On average, top-down cracked sections exhibited slightly higher binder content compared to non-cracked sections. It is important to point out that loss of fines during the ignition oven process may have contributed some errors in the data.

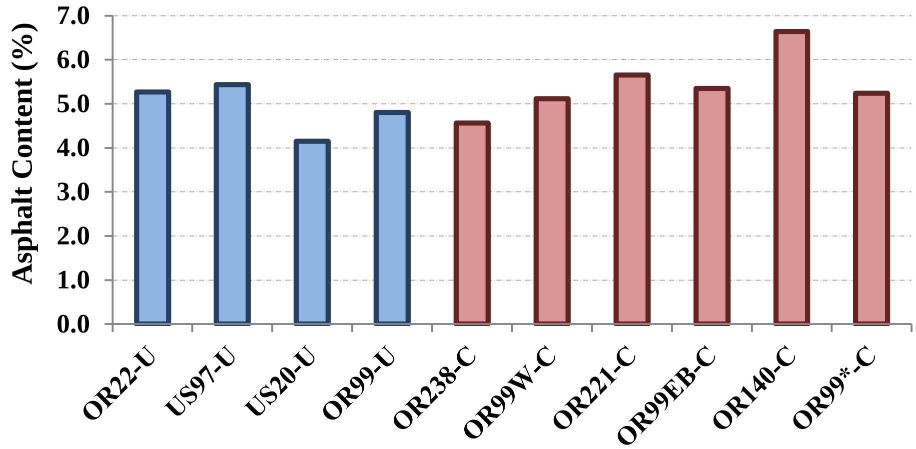

Figure 6-15 Binder content of the test sections

Conclusions and Recommendations

Recently the Oregon Department of Transportation (ODOT) has identified hot mix asphalt concrete (HMAC) pavements that have displayed top-down cracking within three years of construction. The objective of the study was to evaluate the top-down cracked pavement sections and compare the results with the non-cracked pavement sections.

Summary and Conclusions

Based on the literature review, and the field and laboratory investigations, the following conclusions are drawn:

- Visual distress survey indicated that all the six sites exhibiting longitudinal wheel path cracking and transverse cracking were identified as top-down cracked pavements which was confirmed by examining cores. The only means to differentiate top-down cracking form bottom-up cracking is taking cores on the cracked areas.
- FWD tests were conducted to evaluate the structural capacity of top-down cracked pavements and pavement sections without top-down cracking. FWD tests indicated that

top-down cracked pavements were structurally sound, even some of the sections with top-down cracking showed better structural capacity compared to non-cracked sections.

- DCP tests were carried out on the aggregate base materials to evaluate the variations in density (strength) of both top-down cracked pavements and non-cracked pavements. Like FWD test results, no significant difference in density variations of aggregate base were observed between top-down cracked pavements and non-cracked pavements. Only one section (OR99EB-C) from six top-down cracked pavement sections was found to be displaying high variability in density.
- Top-down cracking initiation and propagation were found to be independent of pavement cross-section or the AC thickness.
- Dynamic modulus testing was conducted on the extracted cores to evaluate the mixture stiffness of both top-down cracked and non-cracked areas. Cores from all the top-down cracked pavement sections except OR140-C exhibited higher dynamic modulus (stiffer) values than that of non-cracked pavement sections.
- Indirect tensile (IDT) strength test results indicated that AC mixtures from all four non-cracked pavement areas exhibited fairly high IDT strength and low variability in IDT strength. Three top-down cracked pavement sections displayed low IDT strength and very high variability in IDT strength. All top-down cracked pavement sections except OR99EB-C showed much higher variability in IDT strength compared to non-cracked pavement areas.
- Air voids analysis results indicated that all six top-down cracked sections showed much higher variability in AC density compared to the four non-cracked pavement areas, like the IDT strength test results.
- Asphalt binder rheological test results indicated that asphalt binders from all the top-down cracked sections except OR140-C showed higher complex shear modulus (stiffer binder) compared to non-cracked pavement sections.
- The literature review indicated that there was no conclusive evidence based on the structural capacity that would lead to top-down cracking. Top-down cracking can be caused by a number of contributors such as stiffer AC mixtures, mixture segregation, binder aging, low AC tensile strength, and stiffness differentials between pavement layers or by combination of any.

Recommendations

Currently, no pavement design method is capable of predicting or analyzing top-down cracking phenomenon which could explain the universally conclusive reasoning for top-down cracking occurrence and progression. The following recommendations could be made based on the literature review, and the field and laboratory investigations to prevent top-down cracking in terms of material selection, material properties, and construction practices:

- It is recommended that a tighter density specification be established to ensure uniformity for in-situ air voids. Based on the study, the in-situ air voids should be kept below or equal to 6%. It is recommended that this be considered in a shadow specification prior to placing in actual construction specifications.
- Asphalt mixtures with higher tensile strength and low variability in tensile strength should be used. Tensile strength testing or another performance test could be developed as part of the mixture design and selection process and integrated into quality control and quality assurance testing. This would facilitate the need for developing criteria and would be best implemented on a shadow project basis.
- Top-down cracked sections found to be possessing relatively stiffer binder and mixtures compared to non-cracked sections. However, the careful selection of binder grade is recommended to ensure a delicate balance between rutting and fatigue cracking. It is important to point out that OR99 the Junction City section, had two sections, one OR99-U (non-cracked section) and the other one OR99*-C with top-down cracking. Section OR99*-C was found to displaying stiffer binder than section OR99-U. Section OR99*-C was found to better rut resistant than section OR99-C but was more susceptible to top-down cracking.
- It is recommended that non-uniformities in the material properties be prevented along with prevention of segregation during construction. Segregation could be caused by areas within the pavers as indicated in the literature review. The Colorado Department of Transportation established a segregation specification in 2003 which led paving

equipment manufacturers taking initiative to develop an anti-segregation kit so that existing paving equipment could be retrofitted.

- In this study, IDT strength tests were conducted at only one temperature due to the nature of the tests (destructive tests) and limitation on the number of cores. It is recommended that cores be tested at different temperatures to evaluate the tensile strength as well as moisture susceptibility.

Acknowledgments

This study was sponsored by the Oregon Department of Transportation (ODOT) and the Federal Highway Administration (FHWA) under project, “Premature Asphalt Concrete Pavement Cracking”. The authors gratefully acknowledge ODOT engineers for all the technical assistance and data provided. The contents of this paper reflect the views of the authors, who are responsible for the accuracy of the facts and data presented herein, and do not necessarily reflect the official policies of the ODOT and Iowa State University. This paper does not constitute a standard, specification, or regulation.

References

AASHTO. (1993). *AASHTO guide for design of pavement structures*, Washington, D.C.

Baladi. G. Y., M. Schorsch, and T. Svasdisnat. “*Determination of Top-Down Cracks in Bituminous Pavements”*. Publication MDOT-PRCE-MSU-2003-110. MDOT, Michigan Department of Transportation, US, 2002.

Baladi. G. Y., M. Schorsch, and C. Chang. “*Effects of Segregation on the Initiation and Propagation of Top-Down Cracks”*. . 82st Transportation Research Board Annual Meeting. Proceedings CD-Room. Washington D.C., 2003.

Birgisson, B., B. Sangpetngam, and R.Roque. “*Predicting Viscoelastic Response and Crack Growth in Asphalt Mixtures with the Boundary Element Method”*. In Transportation Research

Record No. 1789, Transportation Research Board of theNational Academies, Washington D.C., 2002, pp129–135.

Dai, S.T., Van Deusen, D., Beer, M., Rettner, D., and Cochran, G., "*Investigation of Flexible Pavement Response To Truck Speed and FWD Load Through Instrumented Pavements*," Proceedings, 8th International Conference on Asphalt Pavements, University of Washington, Seattle, Washington, August 1997, p. 141-160.

Dauzats, M. and Rampal, A., "*Mechanism of Surface Cracking in Wearing Courses*," Proceedings, 6th International Conference Structural Design of Asphalt Pavements, The University of Michigan, Ann Arbor, Michigan, July 1987, p. 232-247.

De Beer, M., Fisher, C., and Jootse, F.J., "*Determination of Pneumatic Tyre/Pavement Interface Contact Stresses Under Moving Loads and Some Effects on Pavements With Thin Asphalt Surfacing Layers*," Proceedings, 8th International Conference on Asphalt Pavements, University of Washington, Seattle, Washington, August 1997, p. 179-227.

Freitas, E.F., P. Pereira, L. Picado-Santos, and T. Papagiannakis. "*Construction Quality, Temperature and Rutting Effect on Top-Down Cracking Initiation".* In Transportation Research Record No. 1929, Transportation Research Board of theNational Academies, Washington D.C., 2005, pp174-182.

Gerritsen, A.H., van Gurp, C.A.P.M., van der Heide, J.P.J., Molenaar, A.A.A., and Pronk, A.C., "*Prediction and Prevention of Surface Cracking in Asphaltic Pavements*," 6th International Conference Structural Design of Asphalt Pavements, The University of Michigan, Ann Arbor, Michigan, July 1987, p. 378-391.

Harmelink, D., Aschenbrener, T., and Shuler, S. "*Top-Down Cracking in Asphalt Pavements: Causes, Effects, and Cures"*. Journal of Transportation Engineering, Vol. 134, No. 1, January 1, 2008.

Illinois Department of Transportation. "*A review of cracking on full depth bituminous pavement (longitudinal cracking).*" III. 1993.

Kim, Y. R. and Underwood, B. S. "*Determination of Depth of Surface Cracks in Asphalt Pavements".* In Transportation Research Record No. 1853, Transportation Research Board of theNational Academies, Washington D.C., 2003, pp143-149.

Myers, L.A., R. Roque, and B. Ruth*. "Mechanisms of Surface-Initiated Longitudinal Wheel Path Cracks in High-Type Bituminous Pavements".* Journal of the Asphalt Paving Technologists, vol. 67 (1998), pp. 401-432.

Myers, L. A., R. Roque and B. Birgisson. "*Propagation Mechanisms for Surface-Initiated LongitudinalWheel Path Cracks".* In Transportation Research Record No. 1778, Transportation Research Board of theNational Academies, Washington D.C., 2001, pp113-122.

Nunn, M., "*Design of Long-Life Roads for Heavy Traffic*," Proceedings, Industry Conference, Australian Asphalt Pavement Association, Surfers Paradise, Queensland, Australia, 1998.

Ozer, H., I.L. Al-Qadi, and C.A. Duarte. "*Effects of Non-Uniform and Three Dimensional Contact Stresses on the Near-Surface Cracking Problem*.". 90th Transportation Research Board Annual Meeting. Proceedings CD-Room. Washington D.C., 2011.

Svasdisant, T., M. Achorsch, G.Y. Baladi, and S. Pinyosunun. "*Mechanistic Analysis of Top-Down Cracking in Asphalt Pavements"*. 81st Transportation Research Board Annual *Meeting*. Proceedings CD-Room. Washington D.C., 2002.

Uhlmeyer, J.S., K. Willoughby, L. M. Pierce, and J. P. Mahoney. "*Top-Down Cracking in Washington State Asphalt Concrete Wearing Courses".* In Transportation Research Record No. 1730, Transportation Research Board of the National Academies, Washington, D.C., 2000, pp 110-116.

Von Quintus, H.L. and Moulthrop, J.S. "*Mechanistic-Empirical Pavement Design Guide Flexible Pavement Performance Prediction Models:Volume II-Reference Manual".* No. FHWA/MT-07-008/8158-2. Montana Department of Transportation. Research Programs. Helena, MT, 2007.

Wang, L. B., L. A. Myers, L. N. Mohammad, and Y. R. Fu. *"A Micromechanics Study on Top-Down Cracking".* In Transportation Research Record No. 1853, Transportation Research Board of theNational Academies, Washington D.C., 2003, pp121-133.

Wang, J., B. Birgisson and R. Roque. *"Windows-Based Top-Down Cracking Design Tool for Florida: Using Energy Ratio Concept".* In Transportation Research Record No. 2037, Transportation Research Board of the National Academies, Washington, D.C., 2007, pp 86-96.

Wang, H. and Al-Qadi,I.L. "*Near-Surface Pavement Failure under Multiaxial Stress State in Thick Asphalt Pavement"*. In Transportation Research Record No. 2154, Transportation Research Board of the National Academies, Washington D.C., 2010, pp 91-99.

Witczak, M. and El-Basyouny, M. "*Development of the Fatigue Cracking Models for the 2002 Design Guide".* 84th Transportation Research Board Annual Meeting. Proceedings CD-Room. Washington D.C., 2005.

CHAPTER 7 - CONCLUSIONS AND RECOMMENDATIONS

Local Calibration of the MEPDG Prediction Models

Summary and Conclusions

This section presents the findings for calibration of the Darwin M-E performance prediction models for AC rehabilitation of existing pavements for Oregon. The following conclusions are made from this study:

- From the verification results, it was found that predicted distresses using the Darwin M-E default calibration coefficients did not match well with actual distresses observed during the condition surveys, suggesting extensive local calibration was required for Oregon conditions.
- Darwin M-E over predicted total rutting compared to the measured total rutting, as was evident from the verification runs using the Darwin M-E default calibration coefficients. Further, it was observed that most of the rutting predicted by Darwin M-E occurred in the subgrade.
- For alligator (bottom-up) cracking and thermal (transverse) cracking, the Darwin M-E underestimated the amount of cracking considerably as compared to the actual amount measured in the field. A high amount of variability between predicted and measured values was observed for longitudinal (top-down) cracking.
- From the verification runs on the four CRCP pavement sections, the Darwin M-E under predicted the number of punchouts per mile on the three CRCP sections while the remaining CRCP section's punchouts per mile were over predicted as compared to what was actually measured in the field. It is difficult to comment on the accuracy of the nationally calibrated punchout model based on only four pavement sections, however the initial assessment shows the nationally calibrated Darwin M-E model provided a reasonable estimate of the punchouts.
- From the calibration results, the locally calibrated models of rutting, alligator cracking, and longitudinal cracking provided better predictions with lower bias and standard error

than the nationally (default) calibrated models. However, there was a high degree of variability between the predicted and measured distresses, especially for longitudinal cracking and thermal cracking, even after the calibration.

- From the validation results, both rutting and alligator cracking models provided reasonable predictions. Though the locally calibrated longitudinal cracking provided better predictions than the nationally calibrated model, a high degree of variability between the predicted and observed longitudinal cracking was found.
- It always remains a challenge to delineate between alligator (bottom-up) cracking and longitudinal (top-down) cracking as it is not practical to take cores or trenches at each single crack to distinguish between alligator cracking and longitudinal cracking. Therefore, there could be measurement error, which may affect the calibration effort related to these distresses.

Recommendations

The following recommendations are drawn from this study:

- The calibrated models of the MEPDG contained in Darwin M-E and summarized in Chapter 5 can be implemented. Continued assessment of the calibrated Darwin M-E should be done to ensure reasonable designs are being developed.
- Updates to the Darwin M-E will be needed in the future as new materials and newer pavement design strategies are being employed. One such set of materials and pavement design method are the use of interlayer mixes to mitigate reflective cracking as these mixes are high asphalt/low air void mixes using a highly polymerized asphalt binder.
- It is recommended that additional sites be established to include in future calibration efforts and thus, to further improve the accuracy of the rutting and alligator cracking models.
- The availability and quality of data (materials, construction, and performance data) required for Darwin M-E are critical for local calibration. It is recommended that more detailed inputs (Level 1 mostly) be established for future calibration efforts, which will

help reduce a significant amount of input error and, thus, may improve the accuracy of prediction models.

- There remains a question regarding the usability of longitudinal cracking and thermal cracking models, as was supported by previous research. Currently, improved thermal cracking models are being developed through FHWA pooled-fund studies. And, a NCHRP project 01-52 is underway to improve the longitudinal cracking model (http://apps.trb.org/cmsfeed/TRBNetProjectDisplay.asp?ProjectID=3152). Therefore, it is recommended that longitudinal cracking and thermal cracking models be recalibrated once these models are improved by MEPDG.
- Only four CRCP pavement sections were included in the verification study. Therefore, it is recommended that additional CRCP pavement sections be established for future verification and subsequent calibration, if needed, to improve the accuracy of the punchout model.
- Although the Oregon DOT has an extensive PMS database, most of the PMS data, especially pavement distress data, do not directly support the MEPDG. The difference between the distress measurement techniques of the ODOT and the MEPDG poses direct challenges to the implementation and local calibration efforts for the MEPDG. It is recommended that ODOT adopts the MEPDG (LTPP) standard procedure, at least for the sections to be used in the future calibration effort. By doing so, a significant amount of measurement error and input error can be reduced. And, the accuracy of performance prediction models can be improved

Top-Down Cracking Investigation Study

Recently the Oregon Department of Transportation (ODOT) has identified hot mix asphalt concrete (HMAC) pavements that have displayed top-down cracking within three years of construction. The objective of the study was to evaluate the top-down cracked pavement sections and compare the results with the non-cracked pavement sections. Research involved evaluating six surface cracked pavements and four non-cracked pavement sections. The research included extensive field and laboratory investigations of the 10 pavement sections by conducting distress surveys, falling weight deflectometer (FWD) testing, dynamic cone penetrometer (DCP) testing, and coring from the cracked and non-cracked pavement sections. Cores were then subjected to a full laboratory-testing program to evaluate the HMAC mixtures and binder rheology. The laboratory investigation included dynamic modulus, indirect tensile (IDT) strength, and specific gravity testing on the HMAC cores, binder rheological tests on asphalt binder and aggregate gradation analysis.

Summary and Conclusions

Based on the literature review, and the field and laboratory investigations, the following conclusions are drawn:

- Visual distress survey indicated that all the six sites exhibiting longitudinal wheel path cracking and transverse cracking were identified as top-down cracked pavements which was confirmed by examining cores. The only means to differentiate top-down cracking form bottom-up cracking is taking cores on the cracked areas.
- FWD tests were conducted to evaluate the structural capacity of top-down cracked pavements and pavement sections without top-down cracking. FWD tests indicated that top-down cracked pavements were structurally sound, even some of the sections with top-down cracking showed better structural capacity compared to non-cracked sections.
- Two backcalculation software programs were employed in the study to estimate backcalculated layer moduli. The study found a good correlation for AC moduli between Elmod and BAKFAA while no consistent correlation for base and subgrade moduli were observed between the two software packages.
- DCP tests were carried out on the aggregate base materials to evaluate the variations in density (strength) of both top-down cracked pavements and non-cracked pavements. Like FWD test results, no significant difference in density variations of aggregate base were observed between top-down cracked pavements and non-cracked pavements. Only one section (OR99EB-C) from six top-down cracked pavement sections was found to be displaying high variability in density.

- Top-down cracking initiation and propagation were found to be independent of pavement cross-section or the AC thickness.
- Dynamic modulus testing was conducted on the extracted cores to evaluate the mixture stiffness of both top-down cracked and non-cracked areas. Cores from all the top-down cracked pavement sections except OR140-C exhibited higher dynamic modulus (stiffer) values than that of non-cracked pavement sections.
- Indirect tensile (IDT) strength test results indicated that AC mixtures from all four non-cracked pavement areas exhibited fairly high IDT strength and low variability in IDT strength. Three top-down cracked pavement sections displayed low IDT strength and very high variability in IDT strength. All top-down cracked pavement sections except OR99EB-C showed much higher variability in IDT strength compared to non-cracked pavement areas.
- Air voids analysis results indicated that all six top-down cracked sections showed much higher variability in AC density compared to the four non-cracked pavement areas, like the IDT strength test results.
- Asphalt binder rheological test results indicated that asphalt binders from all the top-down cracked sections except OR140-C showed higher complex shear modulus (stiffer binder) compared to non-cracked pavement sections.
- The literature review indicated that there was no conclusive evidence based on the structural capacity that would lead to top-down cracking. Top-down cracking can be caused by a number of contributors such as stiffer AC mixtures, mixture segregation, binder aging, low AC tensile strength, and stiffness differentials between pavement layers or by combination of any.

Recommendations

Currently, no pavement design method is capable of predicting or analyzing top-down cracking phenomenon which could explain the universally conclusive reasoning for top-down cracking occurrence and progression. The literature review indicated a number of factors that could contribute to the top-down cracking initiation and propagation such as high tensile contact stresses generated on the road surface close to the tire edges, climatic conditions, aging, construction quality, low AC tensile strength, and differential stiffness between pavement layers. This study found that top-down cracked sections displayed higher variability in density and tensile strength, low tensile strength, and stiffer binder of mixtures when compared to non-cracked sections. While the structural capacity (thickness) of pavements was found to be a non-contributing factor to top-down cracking, the material properties and construction practices could be fine-tuned to reduce the occurrence of top-down cracking. The following recommendations could be made based on the literature review, and the field and laboratory investigations to prevent top-down cracking in terms of material selection, material properties, and construction practices:

- It is recommended that a tighter density specification be established to ensure uniformity for in-situ air voids. Based on the study, the in-situ air voids should be kept below or equal to 6%. It is recommended that this be considered in a shadow specification prior to placing in actual construction specifications
- Asphalt mixtures with higher tensile strength and low variability in tensile strength should be used. Tensile strength testing or another performance test could be developed as part of the mixture design and selection process and integrated into quality control and quality assurance testing. This would facilitate the need for developing criteria and would be best implemented on a shadow project basis.
- Top-down cracked sections found to be possessing relatively stiffer binder and mixtures compared to non-cracked sections. However, the careful selection of binder grade is recommended to ensure a delicate balance between rutting and fatigue cracking. It is important to point out that OR99 the Junction City section, had two sections, one OR99-U (non-cracked section) and the other one OR99*-C with top-down cracking. Section OR99*-C was found to displaying stiffer binder than section OR99-U. Section OR99*-C was found to better rut resistant than section OR99-C but was more susceptible to top-down cracking.
- It is recommended that non-uniformities in the material properties be prevented along with prevention of segregation during construction. Segregation could be caused by areas within the pavers as indicated in the literature review. The Colorado Department of

Transportation established a segregation specification in 2003 which led paving equipment manufacturers taking initiative to develop an anti-segregation kit so that existing paving equipment could be retrofitted.

Recommendations for Future Study

Based on the results and conclusions of this study, the following recommendations can be made:

- It is important to differentiate between top-down cracking and classical bottom-up cracks because preventive and rehabilitation actions for top-down cracked pavements are much different than those of bottom-up cracked sections. Thus, it is recommended top-down cracking identification criteria be implemented in the Pavement Management System (PMS) database.
- In this study, IDT strength tests were conducted at only one temperature due to the nature of the tests (destructive tests) and limitation on the number of cores. It is recommended that cores be tested at different temperatures to evaluate the tensile strength as well as moisture susceptibility.
- A more in-depth study could be done to evaluate the effects and aging on the properties of the asphalt mixes.

RERERENCES

ARA, Inc., ERES Consultants Division. 2004. *Guide for Mechanistic–Empirical Design of New and Rehabilitated Pavement Structures.* Final report, NCHRP Project 1-37A. Transportation. Research Board of the National Academies, Washington, D.C., 2004. http://www.trb.org/ mepdg/guide.htm.

Baladi. G. Y., M. Schorsch, and T. Svasdisnat. "*Determination of Top-Down Cracks in Bituminous Pavements"*. Publication MDOT-PRCE-MSU-2003-110. MDOT, Michigan Department of Transportation, US, 2002.

Baladi. G. Y., M. Schorsch, and C. Chang. "*Effects of Segregation on the Initiation and Propagation of Top-Down Cracks"*. . 82st Transportation Research Board Annual Meeting. Proceedings CD-Room. Washington D.C., 2003.

Banerjee, A., Prozzi, J. A., and Aguiar-Moya, J. P. 2010. Calibrating the MEPDG permanent deformation performance model for different maintenance and rehabilitation strategies, DVD. *Presented at the 89th Annual Meeting of the Transportation Research Board*. Washington, DC: Transportation Research Board.

Banaerjee, A., Prozzi, J. A., and Aguiar-Moya, J. P. 2009. Calibration of mechanistic-empirical pavement design guide permanent deformation models: Texas experience with long-term pavement performance. *Transportation Research Record* 2094: 12-20. Washington DC: Transportation Research Board, National Research Council.

Birgisson, B., B. Sangpetngam, and R.Roque. "*Predicting Viscoelastic Response and Crack Growth in Asphalt Mixtures with the Boundary Element Method"*. In Transportation Research Record No. 1789, Transportation Research Board of theNational Academies, Washington D.C., 2002, pp129–135.

Bustos, M. G., Cordo, C., Girardi, P., and Pereyra, M. 2009. Developing a methodology to calibrate Mechanistic-Empirical Pavement Design Guide procedures for rigid pavement design in Argentina, DVD. *Presented at the 88th Annual Meeting of the Transportation Research Board*. Washington, DC: Transportation Research Board.

Corley-Lay, J. B., Jadoun, F., Mastin, J., and Kim, R. 2010. Comparison of NCDOT and LTPP monitored flexible pavement distresses, DVD. *Presented at the 89th Annual Meeting of the Transportation Research Board*. Washington, DC: Transportation Research Board.

Dai, S.T., Van Deusen, D., Beer, M., Rettner, D., and Cochran, G., "*Investigation of Flexible Pavement Response To Truck Speed and FWD Load Through Instrumented Pavements*," Proceedings, 8th International Conference on Asphalt Pavements, University of Washington, Seattle, Washington, August 1997, p. 141-160.

Dauzats, M. and Rampal, A., "*Mechanism of Surface Cracking in Wearing Courses*," Proceedings, 6th International Conference Structural Design of Asphalt Pavements, The University of Michigan, Ann Arbor, Michigan, July 1987, p. 232-247.

De Beer, M., Fisher, C., and Jootse, F.J., "*Determination of Pneumatic Tyre/Pavement Interface Contact Stresses Under Moving Loads and Some Effects on Pavements With Thin Asphalt Surfacing Layers*," Proceedings, 8th International Conference on Asphalt Pavements, University of Washington, Seattle, Washington, August 1997, p. 179-227.

Deepika, C., and Chakravarthi, V.K. *"Evaluation of Properties of Soil Subgrade Using Dynamic Cone Penetration Index-A Case Study,"* International Journal of Engineering Research and Development, Volume 4, Issue 4, PP. 07-15, 2012.

Emery, J. J**. "***Evaluation and Mitigation of Asphalt Pavement Top-Down Cracking".* Annual Conference of the Transportation Association of Canada Charlottetown, Prince Edward Island, 2006.

Ese, D., Myre, J., Noss, P., and Vaernes, E. *"The Use of Dynamic Cone Penetrometer (DCP) for Road Strengthening Design in Norway,"* Proceedings. The Fourth International Conference on the Bearing Capacity of Roads and Airfields, 1994.

Freitas, E.F., P. Pereira, L. Picado-Santos, and T. Papagiannakis. "*Construction Quality, Temperature and Rutting Effect on Top-Down Cracking Initiation".* In Transportation Research Record No. 1929, Transportation Research Board of theNational Academies, Washington D.C., 2005, pp174-182.

Galal, K. A., and Chehab, G. R. 2005. Implementing the mechanistic-empirical design guide procedure for a Hot-Mix Asphalt-rehabilitated pavement in Indiana. *Transportation Research Record* 1919: 121-133. Washington DC: Transportation Research Board, National Research Council.

Gerritsen, A.H., van Gurp, C.A.P.M., van der Heide, J.P.J., Molenaar, A.A.A., and Pronk, A.C., "*Prediction and Prevention of Surface Cracking in Asphaltic Pavements*," 6th International Conference Structural Design of Asphalt Pavements, The University of Michigan, Ann Arbor, Michigan, July 1987, p. 378-391.

Hall K.D., Xiao, D. X., and Wang, K.C.P. Calibration of the MEPDG for flexible pavement design in Arkansas. In *Transportation Research Record: Journal of the Transportation Research Board, No. 2226,* TRB, National Research Council, Washington, D.C., 2011, pp. 135-141.

Harmelink, D., Aschenbrener, T., and Shuler, S. "*Top-Down Cracking in Asphalt Pavements: Causes, Effects, and Cures*". Journal of Transportation Engineering, Vol. 134, No. 1, January 1, 2008.

Hoegh, K., Khazanovich, L., Jensen, M. R. 2010. Local calibration of MEPDG rutting model for MnROAD test sections, DVD. *Presented at the 89th Annual Meeting of the Transportation Research Board*. Washington, DC: Transportation Research Board.

Illinois Department of Transportation. "*A review of cracking on full depth bituminous pavement (longitudinal cracking).*" III. 1993.

Kang, M., Adams, T. M., and Bahia, H. 2007. *Development of a Regional Pavement Performance Database of the AASHTO Mechanistic-Empirical Pavement Design Guide: Part 2: Validations and Local Calibration*. MRUTC 07-01. Wisconsin: Midwest Regional University Transportation Center, University of Wisconsin-Madison.

Khazanovich, L., Yut, L., Husein, S., Turgeon, C., and Burnham, T. 2008. Adaptation of Mechanistic–Empirical Pavement Design Guide for design of Minnesota low-volume Portland Cement Concrete Pavements. *Transportation Research Record* 2087: 57-67. Washington DC: Transportation Research Board, National Research Council.

Kim,J., R. Roque and T. Byron. "*Viscoelastic Analysis of Flexible Pavements and Its Effects on Top-Down Cracking*". Journal of Materials in Civil Engineering, Vol. 21, No. 7, July 1, 2009.

Kim, S., Ceylan, H., Gopalakrishnan, K., Smadi, O., Brakke, C., and Behnami, F. 2010. Verification of MEPDG performance predictions using pavement management information system (PMIS), DVD. *Presented at the 89th Annual Meeting of the Transportation Research Board*. Washington, DC: Transportation Research Board.

Kim, Y. R. and Underwood, B. S. "*Determination of Depth of Surface Cracks in Asphalt Pavements".* In Transportation Research Record No. 1853, Transportation Research Board of theNational Academies, Washington D.C., 2003, pp143-149.

Li, J., Muench, S. T., Mahoney, J. P., Sivaneswaran, N., and Pierce, L. M. 2006. Calibration of NCHRP 1-37A software for the Washington State Department of Transportation: rigid Pavement portion. *Transportation Research Record* 1949: 43-53. Washington DC: Transportation Research Board, National Research Council.

Li, J., Pierce, L. M., and Uhlmeyer, J. S. 2009. Calibration of flexible pavement in mechanistic-empirical pavement design guide for Washington State. *Transportation Research Record* 2095: 73-83. Washington DC: Transportation Research Board, National Research Council.

Li, J., Luhr, D. R., and Uhlmeyer, J. S. 2010. Pavement performance modeling using piecewise approximation, DVD. *Presented at the 89th Annual Meeting of the Transportation Research Board*. Washington, DC: Transportation Research Board.

Mamlouk, M. S., and Zapata, C. E. 2010. The Need to carefully assess use of State PMS data for MEPDG calibration process, DVD. *Presented at the 89th Annual Meeting of the Transportation Research Board*. Washington, DC: Transportation Research Board.

McGennis, R.B, Shuler, S., and Bahia, H. U. *"Background of SUPERPAVE Asphalt Binder Test Methods,"* U.S. Department of Transportation, Federal Highway Administration, Report No. FHWA-SA-94-069, 1994.

Miller, J. S. and Bellinger, W. Y. 2003. *Distress Identification Manual for the Long-Term Pavement Performance (LTPP) Project*. FHWA-RD-03-031 (4th edition). Federal Highway Administration. Mclean, Virginia.

Muthadi, N. R. 2007. Local Calibration of the MEPDG for Flexible Pavement Design. M.S thesis. North Carolina State University.

Muthadi, N. R., and Kim, R. 2008. Local calibration of mechanistic-empirical pavement design guide for flexible pavement design. *Transportation Research Record* 2087: 131-141. Washington DC: Transportation Research Board, National Research Council.

Myers, L.A., R. Roque, and B. Ruth. *"Mechanisms of Surface-Initiated Longitudinal Wheel Path Cracks in High-Type Bituminous Pavements".* Journal of the Asphalt Paving Technologists, vol. 67 (1998), pp. 401-432.

Myers, L. A., R. Roque and B. Birgisson. "*Propagation Mechanisms for Surface-Initiated LongitudinalWheel Path Cracks".* In Transportation Research Record No. 1778, Transportation Research Board of theNational Academies, Washington D.C., 2001, pp113-122.

NCHRP. 2003a. *Jackknife Testing—An Experimental Approach to Refine Model Calibration and Validation*. Research Results Digest 283. National Cooperative Highway Research Program 9-30. Washington, DC: Transportation Research Board, National Research Council.

NCHRP. 2003b. *Refining the Calibration and Validation of Hot Mix Asphalt Performance Models: An Experimental Plan and Database*. Research Results Digest 284. National

Cooperative Highway Research Program 9-30. Washington, DC: Transportation Research Board, National Research Council.

NCHRP. 2004. *Guide for Mechanistic-Empirical Design of New and Rehabilitated Pavement Structures*. www.trb.org/mepdg., National Cooperative Highway Research Program 1-37 A. Washington, DC: Transportation Research Board, National Research Council.

NCHRP. 2006a. *Independent Review of the Mechanistic-Empirical Pavement Design Guide and Software*. Research Results Digest 307. National Cooperative Highway Research Program 1-40 A. Washington, DC: Transportation Research Board, National Research Council.

NCHRP. 2006b. *Changes to The Mechanistic-Empirical Pavement Design Guide Software Through Version 0.900-July, 2006*. Research Results Digest 308. National Cooperative Highway Research Program 1-40 D. Washington, DC: Transportation Research Board, National Research Council.

NCHRP. 2007. *Recommended Practice for Local Calibration of the ME Pavement Design Guide*. National Cooperative Highway Research Program 1-40B Draft. Texas: ARA, Inc.

NCHRP. 2009. *Standard Practice for Conducting Local or Regional Calibration Parameters for the MEPDG*. National Cooperative Highway Research Program Project 1- 40B Report (publication under review), Washington, DC: Transportation Research Board, National Research Council.

Nunn, M., "*Design of Long-Life Roads for Heavy Traffic*," Proceedings, Industry Conference, Australian Asphalt Pavement Association, Surfers Paradise, Queensland, Australia, 1998.

Ozer, H., I.L. Al-Qadi, and C.A. Duarte. "*Effects of Non-Uniform and Three Dimensional Contact Stresses on the Near-Surface Cracking Problem*.". 90th Transportation Research Board Annual Meeting. Proceedings CD-Room. Washington D.C., 2011.

Schram, S., and Abdelrahman, M. 2006. Improving prediction accuracy in mechanistic-empirical pavement design guide. *Transportation Research Record* 1947: 59-68. Washington DC: Transportation Research Board, National Research Council.

Souliman, M. I., Mamlouk, M. S., El-Basyouny, M. M., and Zapata, C. E. 2010. Calibration of the AASHTO MEPDG for flexible pavement for Arizona conditions, DVD. *Presented at the 89th Annual Meeting of the Transportation Research Board*. Washington, DC: Transportation Research Board.

TRB. 2009. *NCHRP Projects*, http://www.trb.org/CRP/NCHRP/NCHRPProjects.asp, assessed by February, 2009.

TRB. 2010. *NCHRP 01-40B [Completed] User Manual and Local Calibration Guide for the Mechanistic-Empirical Pavement Design Guide and Software*, http://144.171.11.40/cmsfeed/TRBNetProjectDisplay.asp?ProjectID=223, assessed by April, 2010.

Pellinen, T. K., G. Rowe, and K. Biswas. "*Evaluation of Surface (Top Down) Longitudinal Wheel Path Cracking"*. Publication FHWA/IN/JTRP-2004/06. Joint Transportation Research Program, Indiana Department of Transportation and Purdue University, West Lafayette, Indiana, 2004. doi: 10.5703/1288284313216

Reddy, K. S., S. S. Kumar, S. Bose, and B. B. Pandey. *"Analysis of Top-Down Cracking Behavior of Asphalt Pavements"*. 87th Transportation Research Board Annual Meeting. Proceedings CD-Room. Washington D.C., 2008.

Roque, R., Birgisson, B., Drakos, C., and Dietrich, B. "*Development and field evaluation of energy-based criteria for top-down cracking performance of hot mix asphalt*." Asph. Paving Technol., 73, 229–260, 2004.

Roque, R., et al. "*Evaluation of surface-initiated longitudinal wheel path cracking."* Final Rep. for FDOT No. C5978 Contract, Univ. of Florida, Gainesville, Fla, 2006.

Svasdisant, T., M. Achorsch, G.Y. Baladi, and S. Pinyosunun. "*Mechanistic Analysis of Top-Down Cracking in Asphalt Pavements"*. 81st Transportation Research Board Annual Meeting. Proceedings CD-Room. Washington D.C., 2002.

Uhlmeyer, J.S., K. Willoughby, L. M. Pierce, and J. P. Mahoney. "*Top-Down Cracking in Washington State Asphalt Concrete Wearing Courses".* In Transportation Research Record No. 1730, Transportation Research Board of the National Academies, Washington, D.C., 2000, pp 110-116.

Von Quintus, H.L. and Moulthrop, J.S. "*Mechanistic-Empirical Pavement Design Guide Flexible Pavement Performance Prediction Models:Volume II-Reference Manual".* No. FHWA/MT-07-008/8158-2. Montana Department of Transportation. Research Programs. Helena, MT, 2007.

Von Quintus, H. L., Darter, M. I., and Mallela, J. 2005. *Phase I – Local Calibration Adjustments for the HMA Distress Prediction Models in the M-E Pavement Design Guide Software*. Interim Report. National Cooperative Highway Research Program 1-40 B. Washington, DC: Transportation Research Board, National Research Council.

Von Quintus, H. L. and Moulthrop, J. S. 2007. *Mechanistic-Empirical Pavement Design Guide Flexible Pavement Performance Prediction Models: Volume I- Executive Research Summar*y. FHWA/MT-07-008/8158-1. Texas: Fugro Consultants, Inc.

Von Quintus, H. L. 2008a. MEPDG Overview & National Perspective. *Presented at North-Central MEPDG User Group,* Ames, IA: February 19, 2008.

Von Quintus, H. L. 2008b. Local calibration of MEPDG—an overview of selected studies. *Presented at 2008 AAPT Symposium Session: Implementation of the New MEPDG*, Philadelphia, PA: April 29 2008.

Von Quintus, H. L., Darter, M. I., and Mallela, J. 2009a. *Recommended Practice for Local Calibration of the M-E Pavement Design Guide*. National Cooperative Highway Research Program Project 1- 40B Manual of Practice (under review), Washington, DC: Transportation Research Board, National Research Council.

Von Quintus, H. L., Darter, M. I., and Mallela, J. 2009a. *Examples Using the Recommended Practice for Local Calibration of the MEPDG Software*. National Cooperative Highway Research Program Project 1- 40B Manual of Practice (under review), Washington, DC: Transportation Research Board, National Research Council.

Wang, L. B., L. A. Myers, L. N. Mohammad, and Y. R. Fu. *"A Micromechanics Study on Top-Down Cracking".* In Transportation Research Record No. 1853, Transportation Research Board of theNational Academies, Washington D.C., 2003, pp121-133.

Wang, J., B. Birgisson and R. Roque. *"Windows-Based Top-Down Cracking Design Tool for Florida: Using Energy Ratio Concept".* In Transportation Research Record No. 2037, Transportation Research Board of the National Academies, Washington, D.C., 2007, pp 86-96.

Wang, H. and Al-Qadi,I.L. "*Near-Surface Pavement Failure under Multiaxial Stress State in Thick Asphalt Pavement"*. In Transportation Research Record No. 2154, Transportation Research Board of the National Academies, Washington D.C., 2010, pp 91-99.

Webster, S. L., Grau, R. H., and Williams, T. P. *"Description and Application of Dual Mass Dynamic Cone Penetrometer"*. Instruction Rep. GL-92-3, U.S. Army Engineer Research and Development Center, Waterways Experiment Station, Vicksburg, Miss., 1992.

Witczak, M. and El-Basyouny, M. "*Development of the Fatigue Cracking Models for the 2002 Design Guide".* 84th Transportation Research Board Annual Meeting. Proceedings CD-Room. Washington D.C., 2005.

Wu, S. *"DCP Field Application".* Internally circulated report, North Carolina Department of Transportation, 1987.

.

APPENDIX A-SCREEN SHOOTS OF DARWIN M-E

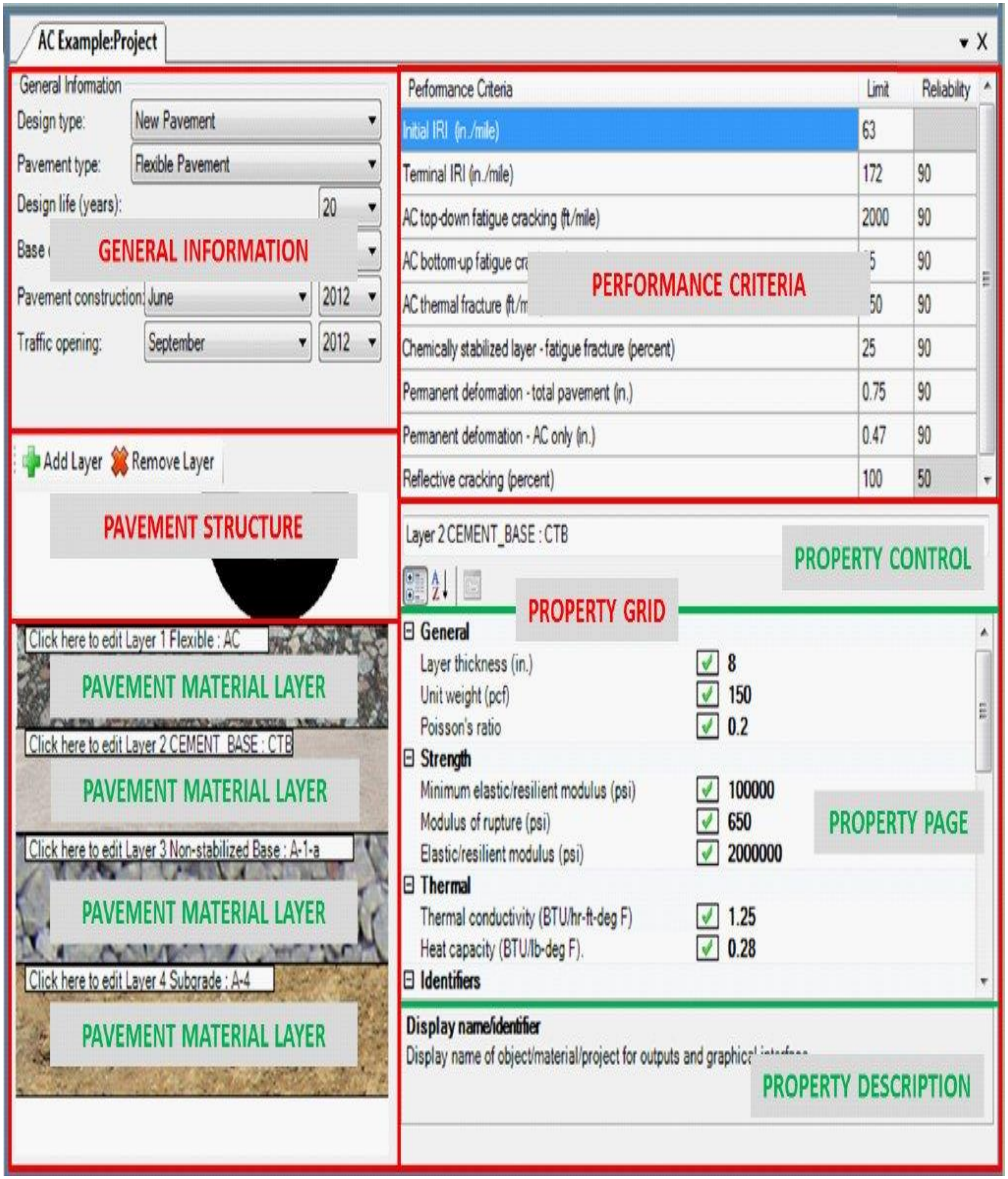

Figure A-1 Project Tab Showing General Information and Performance Criteria

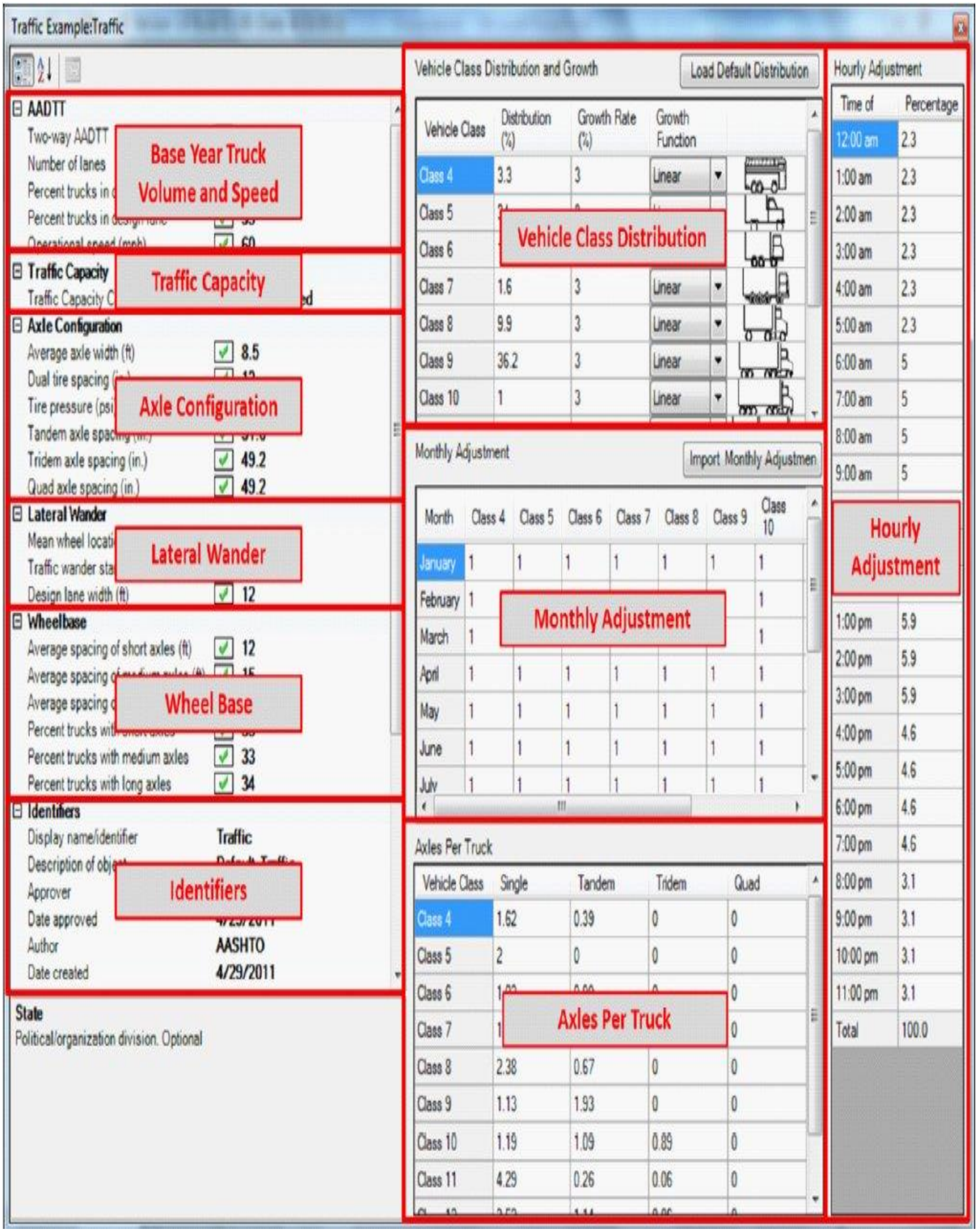

Figure A-2 Traffic Inputs Consisting of Traffic Tab

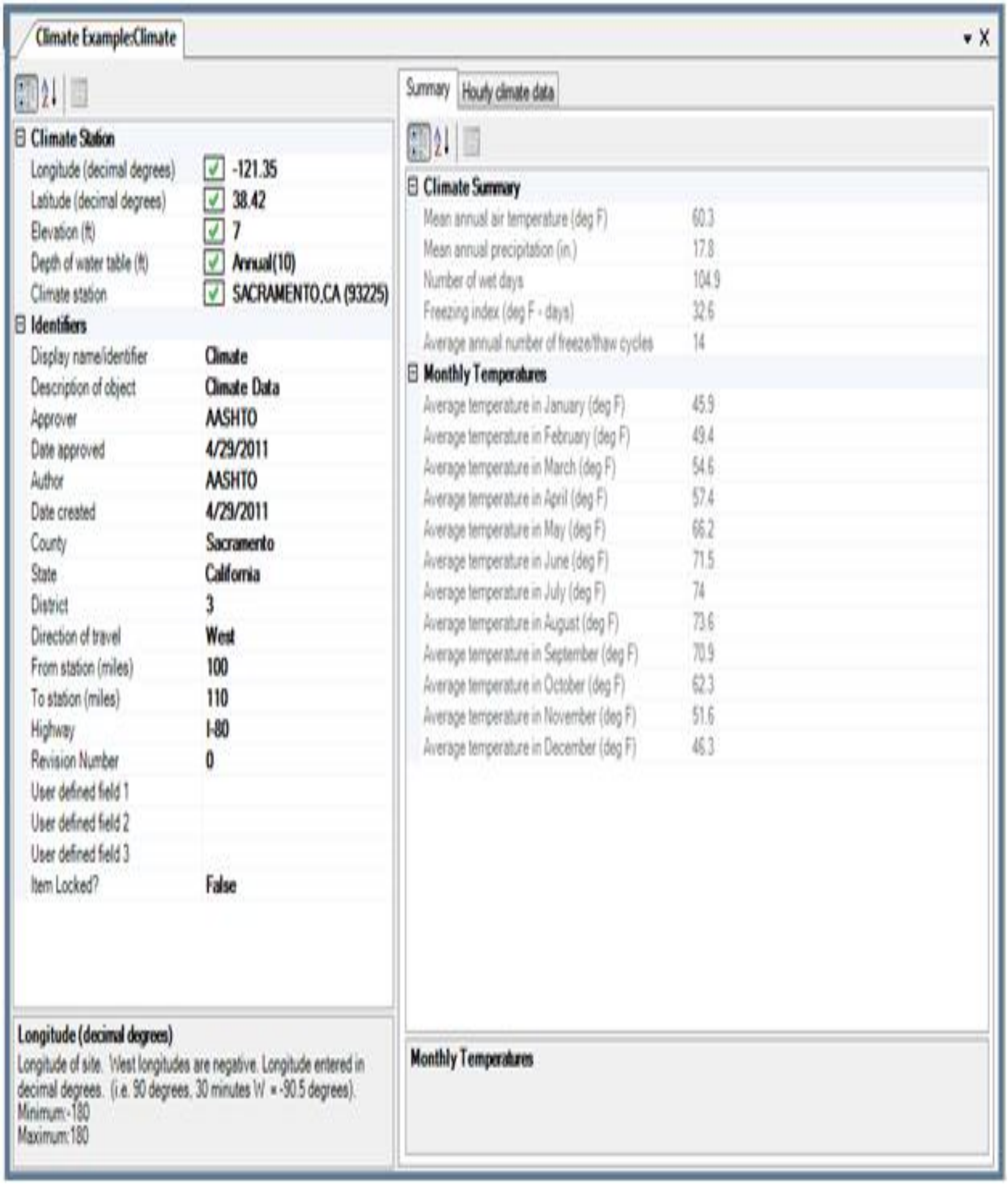

Figure A-3 Climate Tab

Rehabilitation input level	3
Milled thickness (in.)	0
Fatigue cracking (%)	
Pavement rating	Fair (3)
Total rut depth (in.)	0

Figure A-4 AC Rehabilitation (Level 3)

Asphalt Layer	
Thickness (in.)	10
Mixture Volumetrics	
Unit weight (pcf)	150
Effective binder content (%)	11.6
Air voids (%)	7
Poisson's ratio	0.35
Mechanical Properties	
Dynamic modulus	Input level:3
Select HMA Estar predictive model	Use Viscosity based model (nationally calibrated).
Reference temperature (deg F)	70
Asphalt binder	Select Binder
Indirect tensile strength at 14 deg F (psi)	388.87
Creep compliance (1/psi)	Input level:3
Thermal	
Thermal conductivity (BTU/hr-ft-deg F)	0.67
Heat capacity (BTU/lb-deg F)	0.23
Thermal contraction	1.301E-05 (calculated)
Is thermal contraction calculated?	True
Mix coefficient of thermal contraction (in./in./deg F)	
Aggregate coefficient of thermal contraction (in./in./deg	5E-06
Voids in Mineral Aggregate (%)	18.6
Identifiers	
Display name/identifier	New Asphalt Concrete Layer

Figure A-5 HMA Layer Properties

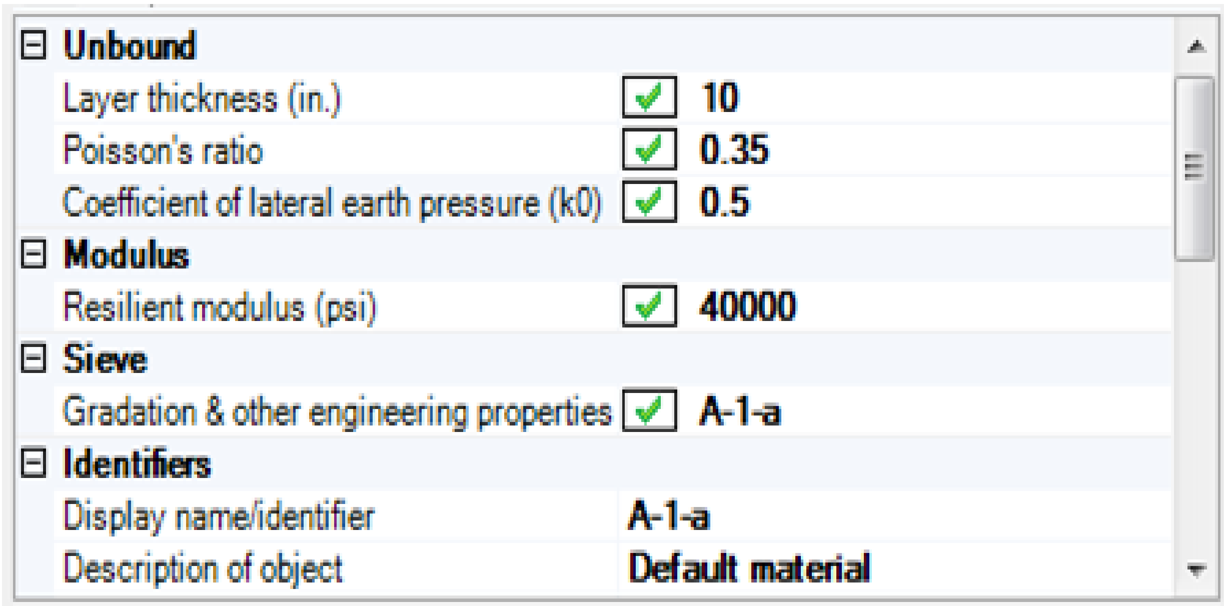

(a)

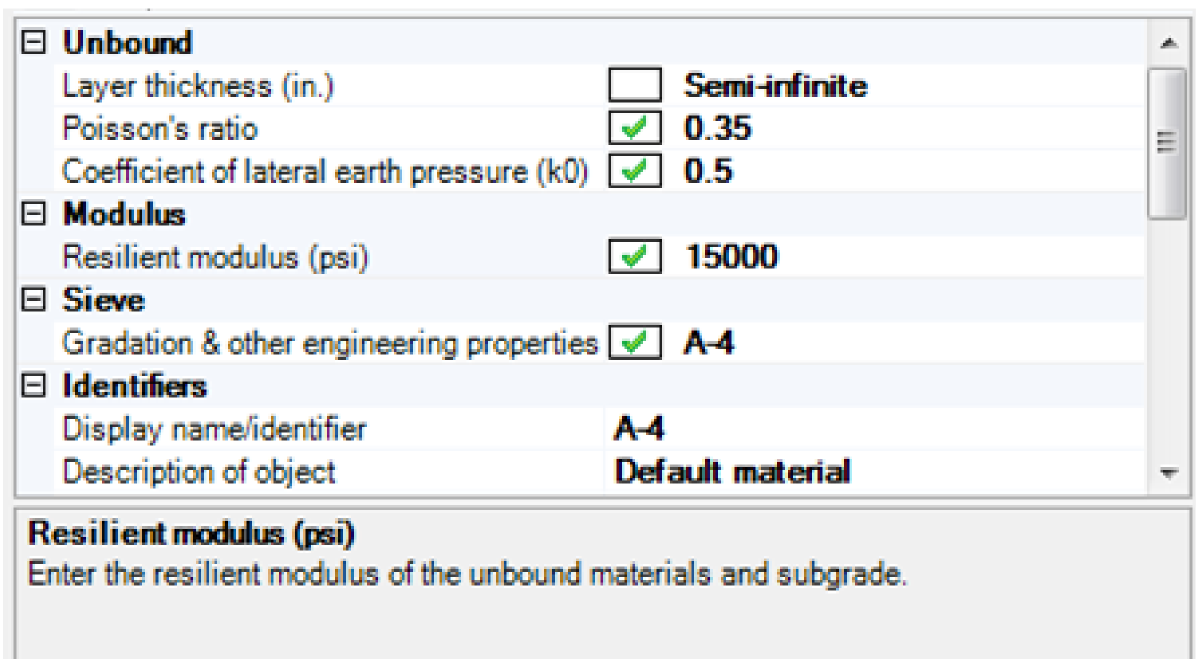

(b)

Figure A- 6 Layer Properties of (a) Non-stabilized Base and (b) Subgrade

APPENDIX B-INPUTS FOR PAVEMENT SECTIONS UNDER STUDY

US 101: NEPTUNE DR-CAMP RILEA

Traffic Info		Climatic Info	
Initial Two-way AADTT	2300	Latitude	46.159198
No of Lanes in Design Direction	1	Longitude	-123.90206
Growth Rate (%)	0	Elevation	22.586
Lane Distribution Factor	1	Depth to Water Table (ft)	1.02
Speed Limit (MPH)	45		

HMA Layer Properties				
Aggregate Gradation (% passing)		Asphalt Binder Grade	Volumetric Properties (In place)	
3/4 in. Sieve	100	PG 64-22	Effective Binder Content, Pbe (%)	11.93
3/8 in. Sieve	81		Air Voids (%)	5
#4 Sieve	56		Unit Weight (lb/ft^3)	151.64
#200 Sieve	5.5		Pbe (%) by Wt	5.1

Other Layer Properties					
Subgrade		Aggregate Base		Chemically-Stabilized Base	
Type	A-4	Type	A-1-a	Type	-
Resilient Modulus (psi)	5500	Resilient Modulus (psi)	25000	Other Values	-

US 101: Tillamook Couplet

Traffic Info		Climatic Info	
Initial Two-way AADTT	1220	Latitude	45.45552
No of Lanes in Design Direction	1	Longitude	-123.843062
Growth Rate (%)	0	Elevation	25.094
Lane Distribution Factor	1	Depth to Water Table (ft)	10
Speed Limit (MPH)	25		

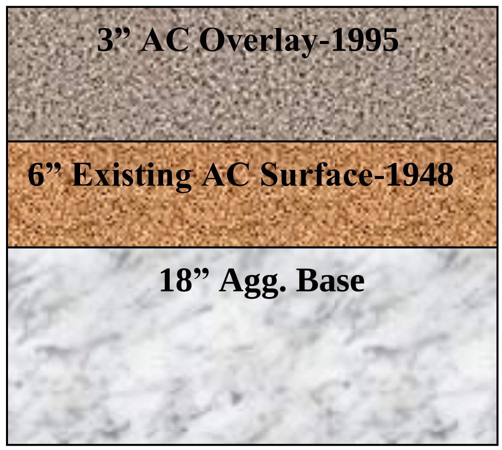

HMA Layer Properties				
Aggregate Gradation (% passing)		Asphalt Binder Grade	Volumetric Properties (In place)	
3/4 in. Sieve	96	PG 64-22	Effective Binder Content, Pbe (%)	9.9
3/8 in. Sieve	68		Air Voids (%)	4.4
#4 Sieve	46		Unit Weight (lb/ft^3)	163.92
#200 Sieve	4.1		Pbe (%) by Wt	3.9

Other Layer Properties					
Subgrade		Aggregate Base		Chemically-Stabilized Base	
Type	A-4	Type	A-1-a	Type	-
Resilient Modulus (psi)	5500	Resilient Modulus (psi)	25000	Other Values	-

US 101: DOOLEY BR-JCT HWY 047

Traffic Info		Climatic Info	
Initial Two-way AADTT	1852	Latitude	45.94336
No of Lanes in Design Direction	1	Longitude	-123.920167
Growth Rate (%)	0	Elevation	35.128
Lane Distribution Factor	1	Depth to Water Table (ft)	4
Speed Limit (MPH)	50		

HMA Layer Properties				
Aggregate Gradation (% passing)		Asphalt Binder Grade	Volumetric Properties (In place)	
3/4 in. Sieve	100	PG 64-22	Effective Binder Content, Pbe (%)	11.01
3/8 in. Sieve	88		Air Voids (%)	5.49
#4 Sieve	57		Unit Weight (lb/ft^3)	148.01
#200 Sieve	6.5		Pbe (%) by Wt	4.7

Other Layer Properties					
Subgrade		Aggregate Base		Chemically-Stabilized Base	
Type	A-4	Type	A-1-a	Type	-
Resilient Modulus (psi)	5500	Resilient Modulus (psi)	25000	Other Values	-

US 101: NCL BANDON-JUNE AVE

Traffic Info		Climatic Info	
Initial Two-way AADTT	1680	Latitude	43.11893
No of Lanes in Design Direction	2	Longitude	-124.403407
Growth Rate (%)	0	Elevation	65.799
Lane Distribution Factor	0.90	Depth to Water Table (ft)	4
Speed Limit (MPH)	30		

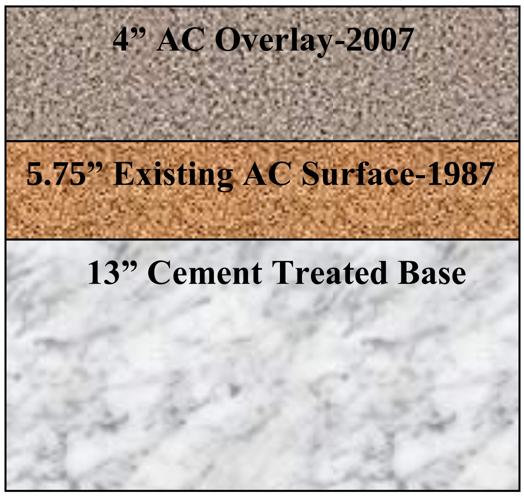

HMA Layer Properties				
Aggregate Gradation (% passing)		Asphalt Binder Grade	Volumetric Properties (In place)	
3/4 in. Sieve	100	PG 64-22	Effective Binder Content, Pbe (%)	11.19
3/8 in. Sieve	87		Air Voids (%)	4
#4 Sieve	57		Unit Weight (lb/ft^3)	149.34
#200 Sieve	5.9		Pbe (%) by Wt	4.86

Other Layer Properties					
Subgrade		Aggregate Base		Chemically-Stabilized Base	
Type	A-7-5	Type	-	Type	Cement Stabilized
Resilient Modulus (psi)	4000	Resilient Modulus (psi)	-	Other Values	Default

US 101: WILSON R.-TILLAMOOK COUPLET

Traffic Info		Climatic Info	
Initial Two-way AADTT	3090	Latitude	45.472916
No of Lanes in Design Direction	2	Longitude	-123.844162
Growth Rate (%)	0	Elevation	13.494
Lane Distribution Factor	0.90	Depth to Water Table (ft)	10
Speed Limit (MPH)	45		

HMA Layer Properties				
Aggregate Gradation (% passing)		Asphalt Binder Grade	Volumetric Properties (In place)	
3/4 in. Sieve	95	PG 64-22	Effective Binder Content, Pbe (%)	10.94
3/8 in. Sieve	69		Air Voids (%)	4.2
#4 Sieve	45		Unit Weight (lb/ft^3)	150.95
#200 Sieve	4.7		Pbe (%) by Wt	4.7

Other Layer Properties					
Subgrade		Aggregate Base		Chemically-Stabilized Subgrade	
Type	A-4	Type	A-1-a	Type	-
Resilient Modulus (psi)	5500	Resilient Modulus (psi)	Default	Other Values	-

US 101: FLORIDA AVE-WASHINGTON AVE

Traffic Info		Climatic Info	
Initial Two-way AADTT	1410	Latitude	43.410704
No of Lanes in Design Direction	3	Longitude	-124.223529
Growth Rate (%)	0	Elevation	44.496
Lane Distribution Factor	0.50	Depth to Water Table (ft)	10
Speed Limit (MPH)	45		

HMA Layer Properties				
Aggregate Gradation (% passing)		Asphalt Binder Grade	Volumetric Properties (In place)	
3/4 in. Sieve	100	PG 64-22	Effective Binder Content, Pbe (%)	11.93
3/8 in. Sieve	81		Air Voids (%)	5
#4 Sieve	56		Unit Weight (lb/ft^3)	151.64
#200 Sieve	5.5		Pbe (%) by Wt	5.1

Other Layer Properties					
Subgrade		Aggregate Base		Chemically-Stabilized Base	
Type	A-7-5	Type	A-1-a	Type	-
Resilient Modulus (psi)	4000	Resilient Modulus (psi)	Default	Other Values	-

US 101: SUTTON CREEK-MUNSEL LAKE RD

Traffic Info		Climatic Info	
Initial Two-way AADTT	1170	Latitude	43.970103
No of Lanes in Design Direction	1	Longitude	-124.096968
Growth Rate (%)	0	Elevation	17.136
Lane Distribution Factor	1	Depth to Water Table (ft)	10
Speed Limit (MPH)	55		

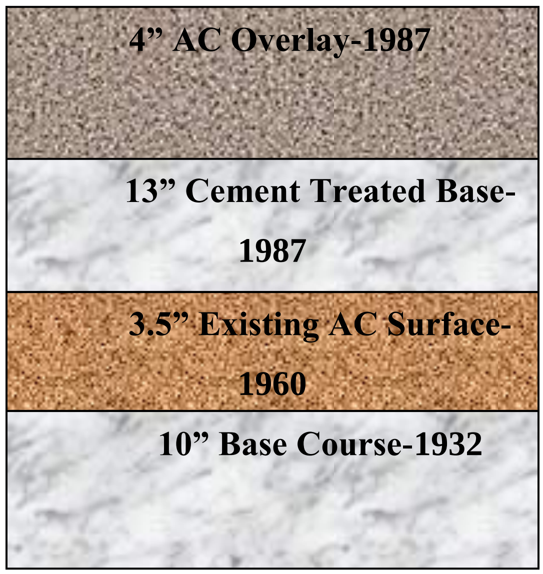

HMA Layer Properties (AC Wearing Course)				
Aggregate Gradation (% passing)		Asphalt Binder Grade	Volumetric Properties (In place)	
3/4 in. Sieve	100	PG 64-22	Effective Binder Content, Pbe (%)	11.23
3/8 in. Sieve	86		Air Voids (%)	4
#4 Sieve	44		Unit Weight (lb/ft^3)	148.64
#200 Sieve	5.5		Pbe (%) by Wt	4.9
HMA Layer Properties (AC Base Course)				
Aggregate Gradation (% passing)		Asphalt Binder Grade	Volumetric Properties (In place)	
3/4 in. Sieve	99	PG 64-22	Effective Binder Content, Pbe (%)	13.43
3/8 in. Sieve	47		Air Voids (%)	4
#4 Sieve	17		Unit Weight (lb/ft^3)	150.18
#200 Sieve	3.4		Pbe (%) by Wt	5.8

Other Layer Properties					
Subgrade		Aggregate Base		Chemically-Stabilized Base	
Type	A-7-5	Type	A-1-a	Type	Cement
Resilient Modulus (psi)	4000	Resilient Modulus (psi)	Default	Other Values	Default

US 20: SWEET HOME-18 TH AVE

Traffic Info		Climatic Info	
Initial Two-way AADTT	1172	Latitude	44.398201
No of Lanes in Design Direction	2	Longitude	-122.726715
Growth Rate (%)	0	Elevation	544.404
Lane Distribution Factor	0.90	Depth to Water Table (ft)	2
Speed Limit (MPH)	35		

HMA Layer Properties				
Aggregate Gradation (% passing)		Asphalt Binder Grade	Volumetric Properties (In place)	
3/4 in. Sieve	100	PG 64-22	Effective Binder Content, Pbe (%)	10.53
3/8 in. Sieve	87		Air Voids (%)	5.1
#4 Sieve	54		Unit Weight (lb/ft^3)	151.69
#200 Sieve	6		Pbe (%) by Wt	4.5

Other Layer Properties					
Subgrade		Aggregate Base		Chemically-Stabilized Base	
Type	A-6	Type	A-1-a	Type	-
Resilient Modulus (psi)	4500	Resilient Modulus (psi)	Default	Other Values	-

OR 99E: ALBANY AVE-CALAPOOIA ST

Traffic Info		Climatic Info	
Initial Two-way AADTT	2366	Latitude	44.624824
No of Lanes in Design Direction	2	Longitude	-123.108543
Growth Rate (%)	2	Elevation	220.115
Lane Distribution Factor	0.90	Depth to Water Table (ft)	1
Speed Limit (MPH)	35		

HMA Layer Properties				
Aggregate Gradation (% passing)		Asphalt Binder Grade	Volumetric Properties (In place)	
3/4 in. Sieve	100	PG 64-22	Effective Binder Content, Pbe (%)	10.77
3/8 in. Sieve	79		Air Voids (%)	2.4
#4 Sieve	51		Unit Weight (lb/ft^3)	148.54
#200 Sieve	5		Pbe (%) by Wt	4.7

Other Layer Properties					
Subgrade		Aggregate Base		Chemically-Stabilized Base	
Type	A-4	Type	A-1-a	Type	-
Resilient Modulus (psi)	5500	Resilient Modulus (psi)	Default	Other Values	-

OR 34: WCL LEBANON-RXR X-ING

Traffic Info		Climatic Info	
Initial Two-way AADTT	1580	Latitude	44.545045
No of Lanes in Design Direction	2	Longitude	-122.910956
Growth Rate (%)	0	Elevation	345.532
Lane Distribution Factor	0.90	Depth to Water Table (ft)	2
Speed Limit (MPH)	35		

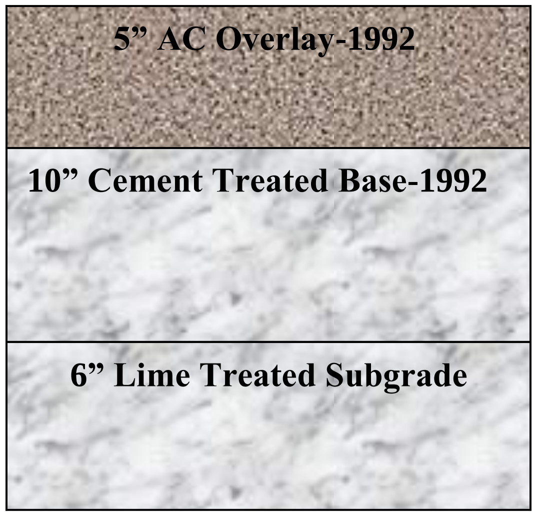

HMA Layer Properties				
Aggregate Gradation (% passing)		Asphalt Binder Grade	Volumetric Properties (In place)	
3/4 in. Sieve	100	PG 64-22	Effective Binder Content, Pbe (%)	10.44
3/8 in. Sieve	87		Air Voids (%)	4.4
#4 Sieve	54		Unit Weight (lb/ft^3)	144.1
#200 Sieve	4.6		Pbe (%) by Wt	4.7

Other Layer Properties					
Subgrade		Aggregate Base		Chemically-Stabilized Base	
Type	A-6	Type	-	Type	Cement
Resilient Modulus (psi)	4000	Resilient Modulus (psi)	-	Other Values	Default

OR 221: N. SALEM-ORCHARD HEIGHTS RD

Traffic Info		Climatic Info	
Initial Two-way AADTT	1850	Latitude	44.953147
No of Lanes in Design Direction	2	Longitude	-123.052461
Growth Rate (%)	2.5	Elevation	178.247
Lane Distribution Factor	0.90	Depth to Water Table (ft)	3.5
Speed Limit (MPH)	35		

HMA Layer Properties				
Aggregate Gradation (% passing)		Asphalt Binder Grade	Volumetric Properties (In place)	
3/4 in. Sieve	96	PG 64-22	Effective Binder Content, Pbe (%)	10.84
3/8 in. Sieve	72		Air Voids (%)	4.5
#4 Sieve	49		Unit Weight (lb/ft^3)	146.5
#200 Sieve	5.7		Pbe (%) by Wt	4.8

Other Layer Properties					
Subgrade		Aggregate Base		Chemically-Stabilized Base	
Type	A-4	Type	A-1-a	Type	-
Resilient Modulus (psi)	5500	Resilient Modulus (psi)	Default	Other Values	-

OR 22: END HWY 072-I-5 NB RAMPS

Traffic Info		Climatic Info	
Initial Two-way AADTT	7042	Latitude	44.913469
No of Lanes in Design Direction	2	Longitude	-122.982268
Growth Rate (%)	1	Elevation	214.157
Lane Distribution Factor	0.90	Depth to Water Table (ft)	2
Speed Limit (MPH)	55		

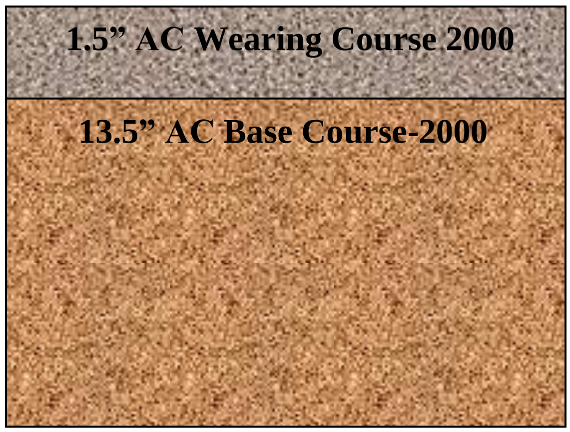

HMA Layer Properties				
Aggregate Gradation (% passing)		Asphalt Binder Grade	Volumetric Properties (In place)	
3/4 in. Sieve	96	PG 64-28	Effective Binder Content, Pbe (%)	9.81
3/8 in. Sieve	76		Air Voids (%)	4
#4 Sieve	49		Unit Weight (lb/ft^3)	147.9
#200 Sieve	4.6		Pbe (%) by Wt	4.3

Other Layer Properties					
Subgrade		Aggregate Base		Chemically-Stabilized Base	
Type	A-4	Type	-	Type	-
Resilient Modulus (psi)	5500	Resilient Modulus (psi)	-	Other Values	-

I-5: AZALEA-CANYONVILLE

Traffic Info		Climatic Info	
Initial Two-way AADTT	13286	Latitude	42.8838
No of Lanes in Design Direction	2	Longitude	-123.24059
Growth Rate (%)	1.5	Elevation	1030.166
Lane Distribution Factor	0.90	Depth to Water Table (ft)	10
Speed Limit (MPH)	65		

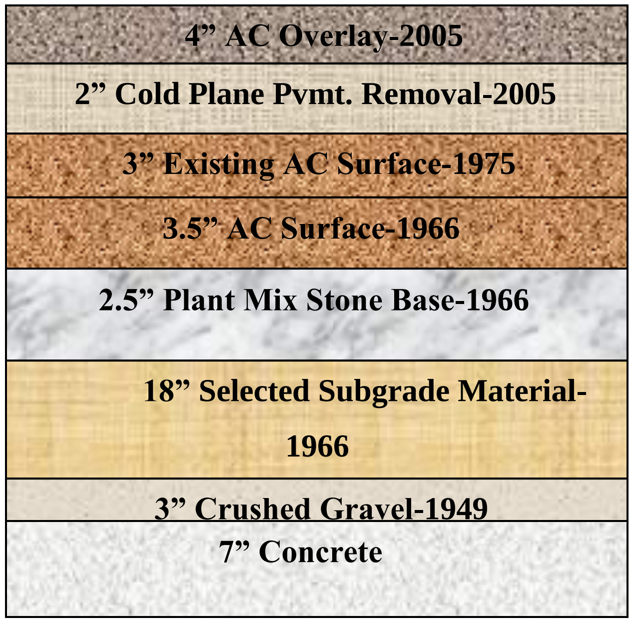

HMA Layer Properties				
Aggregate Gradation (% passing)		Asphalt Binder Grade	Volumetric Properties (In place)	
3/4 in. Sieve	100	PG 76-22	Effective Binder Content, Pbe (%)	10.62
3/8 in. Sieve	80		Air Voids (%)	4
#4 Sieve	50		Unit Weight (lb/ft^3)	160.7
#200 Sieve	6.1		Pbe (%) by Wt	4.3

Other Layer Properties					
Subgrade		Aggregate Base		Chemically-Stabilized Base	
Type	A-4	Type	A-1-a	Type	-
Resilient Modulus (psi)	5500	Resilient Modulus (psi)	Default	Other Values	-

I-5: I-5 Haysville Intch to Woodburn

Traffic Info		Climatic Info	
Initial Two-way AADTT	29270	Latitude	45.013501
No of Lanes in Design Direction	2	Longitude	-122.991968
Growth Rate (%)	0.5	Elevation	143.410
Lane Distribution Factor	0.90	Depth to Water Table (ft)	2
Speed Limit (MPH)	65		

HMA Layer Properties (2007 AC Overlay)				
Aggregate Gradation (% passing)		Asphalt Binder Grade	Volumetric Properties (In place)	
3/4 in. Sieve	93	PG 70-28	Effective Binder Content, Pbe (%)	9.68
3/8 in. Sieve	47		Air Voids (%)	14.4
#4 Sieve	23		Unit Weight (lb/ft^3)	130.1
#200 Sieve	2.3		Pbe (%) by Wt	4.818
HMA Layer Properties (1998 Existing AC Overlay)				
Aggregate Gradation (% passing)		Asphalt Binder Grade	Volumetric Properties (In place)	
3/4 in. Sieve	100	PG 64-22	Effective Binder Content, Pbe (%)	10.45
3/8 in. Sieve	86		Air Voids (%)	4.2
#4 Sieve	52		Unit Weight (lb/ft^3)	147.3
#200 Sieve	6		Pbe (%) by Wt	4.6

Other Layer Properties					
Subgrade		Aggregate Base		Chemically-Stabilized Base/Subgrade	
Type	A-4	Type	A-1-a	Type	-
Resilient Modulus (psi)	5500	Resilient Modulus (psi)	Default	Other Values	-

I-5: Corvallis/Lebanon Interchange

Traffic Info		Climatic Info	
Initial Two-way AADTT	21730	Latitude	44.560965
No of Lanes in Design Direction	2	Longitude	-123.062016
Growth Rate (%)	0	Elevation	261.947
Lane Distribution Factor	0.90	Depth to Water Table (ft)	2
Speed Limit (MPH)	65		

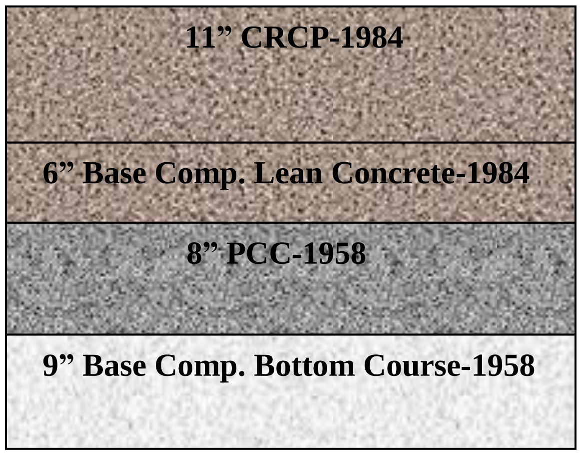

CRCP		
Steel Reinforcement	Steel (%)	0.60
	Steel Diameter (in.)	0.63
	Steel Depth (in.)	4.0
Other Properties	Default	
Other Layer Properties		Default

Unbound Layer Properties					
Subgrade		Aggregate Base		Chemically-Stabilized Base	
Type	A-4	Type	A-1-a	Type	-
Resilient Modulus (psi)	5500	Resilient Modulus (psi)	Default	Other Values	-

I-5: I-5 Wilsonville Intch - Tualatin R

Traffic Info		Climatic Info	
Initial Two-way AADTT	35560	Latitude	45.314104
No of Lanes in Design Direction	4	Longitude	-122.769525
Growth Rate (%)	0.7	Elevation	218.278
Lane Distribution Factor	0.12	Depth to Water Table (ft)	2
Speed Limit (MPH)	65		

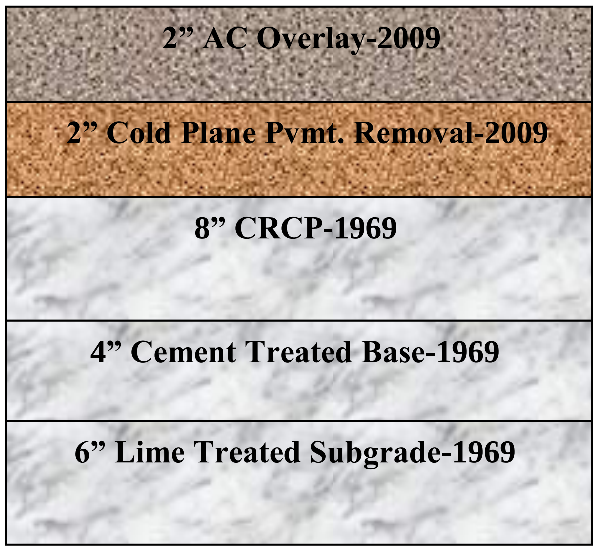

HMA Layer Properties				
Aggregate Gradation (% passing)		Asphalt Binder Grade	Volumetric Properties (In place)	
3/4 in. Sieve	93	PG 70-28	Effective Binder Content, Pbe (%)	9.68
3/8 in. Sieve	47		Air Voids (%)	14.4
#4 Sieve	23		Unit Weight (lb/ft^3)	130.1
#200 Sieve	2.3		Pbe (%) by Wt	4.818

Other Layer Properties					
Subgrade		Aggregate Base		Chemically-Stabilized Base/Subgrade	
Type	A-4	Type	-	Type/Type	Cement/Lime
Resilient Modulus (psi)	6000	Resilient Modulus (psi)	-	Other Values	Default

I-84: N. Powder-Baldock Slough

Traffic Info		Climatic Info	
Initial Two-way AADTT	8000	Latitude	44.953623
No of Lanes in Design Direction	2	Longitude	-117.857208
Growth Rate (%)	0	Elevation	3451.530
Lane Distribution Factor	0.90	Depth to Water Table (ft)	10
Speed Limit (MPH)	55		

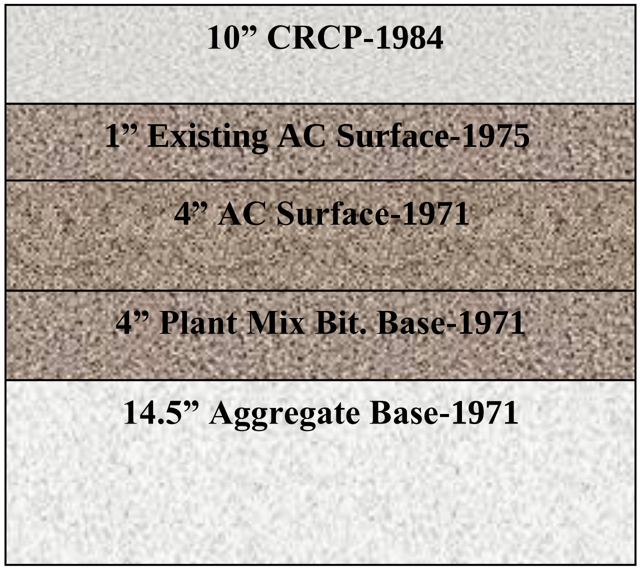

CRCP		
Steel Reinforcement	Steel (%)	0.60
	Steel Diameter (in.)	0.63
	Steel Depth (in.)	4.0
Other Properties	Default	

HMA Layer Properties				
Aggregate Gradation (% passing)		Asphalt Binder Grade	Volumetric Properties (In place)	
3/4 in. Sieve	100	PG 70-22	Effective Binder Content, Pbe (%)	11.96
3/8 in. Sieve	84		Air Voids (%)	4.1
#4 Sieve	58		Unit Weight (lb/ft^3)	146.14
#200 Sieve	5.7		Pbe (%) by Wt	5.3

Unbound Layer Properties					
Subgrade		Aggregate Base		Chemically-Stabilized Base	
Type	A-6	Type	A-1-a	Type	-
Resilient Modulus (psi)	6000	Resilient Modulus (psi)	Default	Other Values	-

I-84: I-84 NE Union Ave - S. Banfield Intch

Traffic Info		Climatic Info	
Initial Two-way AADTT	18820	Latitude	45.531068
No of Lanes in Design Direction	3	Longitude	-122.597988
Growth Rate (%)	1.5	Elevation	205.778
Lane Distribution Factor	0.50	Depth to Water Table (ft)	10
Speed Limit (MPH)	55		

HMA Layer Properties				
Aggregate Gradation (% passing)		Asphalt Binder Grade	Volumetric Properties (In place)	
3/4 in. Sieve	100	PG 70-22	Effective Binder Content, Pbe (%)	11.96
3/8 in. Sieve	84		Air Voids (%)	4.1
#4 Sieve	58		Unit Weight (lb/ft^3)	146.14
#200 Sieve	5.7		Pbe (%) by Wt	5.3

Other Layer Properties					
Subgrade		Aggregate Base		Chemically-Stabilized Base	
Type	A-4	Type	-	Type	Default
Resilient Modulus (psi)	5500	Resilient Modulus (psi)	-	Other Values	Default

US 730: I-84-Canal Rd

Traffic Info		Climatic Info	
Initial Two-way AADTT	1500	Latitude	45.867421
No of Lanes in Design Direction	1	Longitude	-119.559059
Growth Rate (%)	0	Elevation	331.366
Lane Distribution Factor	1	Depth to Water Table (ft)	10
Speed Limit (MPH)	55		

HMA Layer Properties				
Aggregate Gradation (% passing)		Asphalt Binder Grade	Volumetric Properties (In place)	
3/4 in. Sieve	100	PG 70-28	Effective Binder Content, Pbe (%)	11.08
3/8 in. Sieve	86		Air Voids (%)	4
#4 Sieve	64		Unit Weight (lb/ft^3)	149.5
#200 Sieve	5.8		Pbe (%) by Wt	4.8

Other Layer Properties					
Subgrade		Aggregate Base		Chemically-Stabilized Base	
Type	A-1-a	Type	A-1-a	Type	-
Resilient Modulus (psi)	8000	Resilient Modulus (psi)	Default	Other Values	-

I-84: Stanfield Int-Pendleton

Traffic Info		Climatic Info	
Initial Two-way AADTT	9380	Latitude	45.747881
No of Lanes in Design Direction	2	Longitude	-119.110336
Growth Rate (%)	1	Elevation	877.991
Lane Distribution Factor	0.90	Depth to Water Table (ft)	10
Speed Limit (MPH)	65		

CRCP		
Steel Reinforcement	Steel (%)	0.60
	Steel Diameter (in.)	0.63
	Steel Depth (in.)	4.0
Other Properties	Default	

Unbound Layer Properties					
Subgrade		Aggregate Base		Chemically-Stabilized Base	
Type	A-4	Type	A-1-a	Type	-
Resilient Modulus (psi)	5500	Resilient Modulus (psi)	Default	Other Values	-

US 730: Canal Rd-Umatilla Bridge

Traffic Info		Climatic Info	
Initial Two-way AADTT	2766	Latitude	45.915751
No of Lanes in Design Direction	1	Longitude	-119.352722
Growth Rate (%)	0	Elevation	269.120
Lane Distribution Factor	1	Depth to Water Table (ft)	10
Speed Limit (MPH)	45		

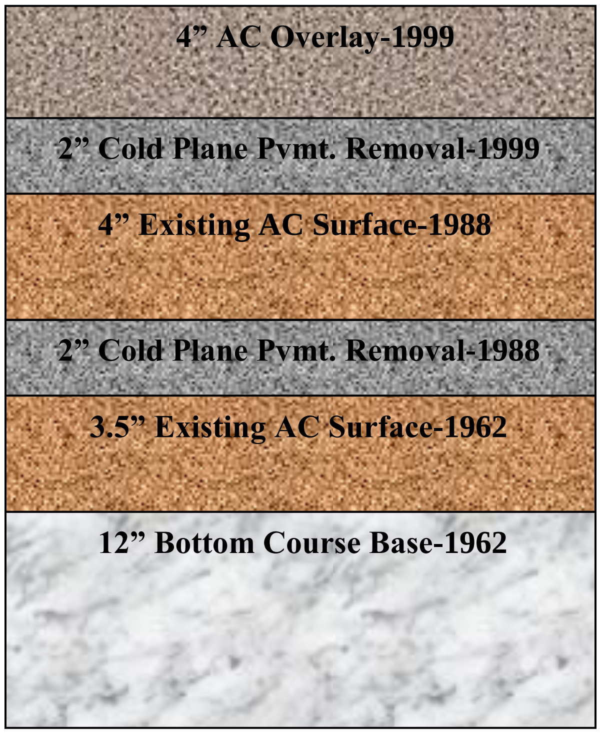

HMA Layer Properties				
Aggregate Gradation (% passing)		Asphalt Binder Grade	Volumetric Properties (In place)	
3/4 in. Sieve	100	PG 70-28	Effective Binder Content, Pbe (%)	11.08
3/8 in. Sieve	86		Air Voids (%)	4
#4 Sieve	64		Unit Weight (lb/ft^3)	149.5
#200 Sieve	5.8		Pbe (%) by Wt	4.8

Other Layer Properties					
Subgrade		Aggregate Base		Chemically-Stabilized Base	
Type	A-2-4	Type	A-1-a	Type	-
Resilient Modulus (psi)	7500	Resilient Modulus (psi)	Default	Other Values	-

US 97: Madras Couplet-Hwy360

Traffic Info		Climatic Info	
Initial Two-way AADTT	4510	Latitude	44.619463
No of Lanes in Design Direction	1	Longitude	-121.132722
Growth Rate (%)	0	Elevation	2323.570
Lane Distribution Factor	1	Depth to Water Table (ft)	10
Speed Limit (MPH)	35		

HMA Layer Properties				
Aggregate Gradation (% passing)		Asphalt Binder Grade	Volumetric Properties (In place)	
3/4 in. Sieve	97	PG 64-28	Effective Binder Content, Pbe (%)	11.12
3/8 in. Sieve	74		Air Voids (%)	4.2
#4 Sieve	49		Unit Weight (lb/ft^3)	153.5
#200 Sieve	6.4		Pbe (%) by Wt	4.7

Other Layer Properties					
Subgrade		Aggregate Base		Chemically-Stabilized Base	
Type	A-2-4	Type	-	Type	Cement
Resilient Modulus (psi)	5800	Resilient Modulus (psi)	-	Other Values	Default

US 97: S. Century Drive-MP 161

Traffic Info		Climatic Info	
Initial Two-way AADTT	3044	Latitude	43.837622
No of Lanes in Design Direction	2	Longitude	-121.422272
Growth Rate (%)	2.5	Elevation	4210.241
Lane Distribution Factor	0.9	Depth to Water Table (ft)	4
Speed Limit (MPH)	55		

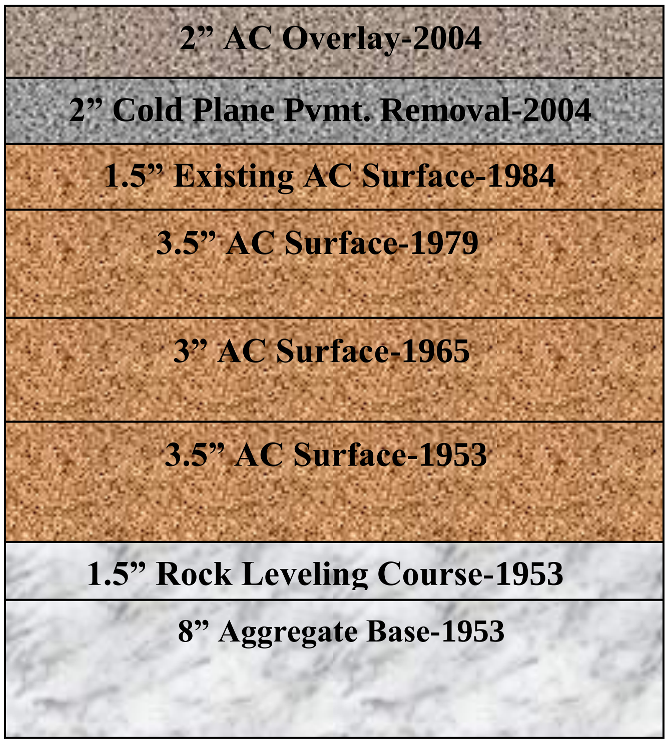

HMA Layer Properties				
Aggregate Gradation (% passing)		Asphalt Binder Grade	Volumetric Properties (In place)	
3/4 in. Sieve	100	PG 70-28	Effective Binder Content, Pbe (%)	10.89
3/8 in. Sieve	85		Air Voids (%)	4
#4 Sieve	57		Unit Weight (lb/ft^3)	146.9
#200 Sieve	7		Pbe (%) by Wt	4.8

Other Layer Properties					
Subgrade		Aggregate Base		Chemically-Stabilized Base	
Type	A-7-5	Type	A-1-a	Type	-
Resilient Modulus (psi)	4000	Resilient Modulus (psi)	Default	Other Values	-

US 97: Weighb Station-Crawford Road

Traffic Info		Climatic Info	
Initial Two-way AADTT	3282	Latitude	43.917124
No of Lanes in Design Direction	2	Longitude	-121.349401
Growth Rate (%)	0	Elevation	4522.131
Lane Distribution Factor	0.90	Depth to Water Table (ft)	4
Speed Limit (MPH)	55		

SB

NB

HMA Layer Properties				
Aggregate Gradation (% passing)		Asphalt Binder Grade	Volumetric Properties (In place)	
3/4 in. Sieve	98	PG 64-28	Effective Binder Content, Pbe (%)	10.34
3/8 in. Sieve	80		Air Voids (%)	4
#4 Sieve	53		Unit Weight (lb/ft^3)	152.2
#200 Sieve	5.8		Pbe (%) by Wt	4.4

Other Layer Properties					
Subgrade		Aggregate Base		Chemically-Stabilized Base	
Type	A-4	Type	A-1-a	Type	Cement
Resilient Modulus (psi)	7000	Resilient Modulus (psi)	Default	Other Values	Default

US 26: Prairie City-Dixie Summit

Traffic Info		Climatic Info	
Initial Two-way AADTT	762	Latitude	44.460924
No of Lanes in Design Direction	2	Longitude	-118.672342
Growth Rate (%)	2.5	Elevation	3608.283
Lane Distribution Factor	0.90	Depth to Water Table (ft)	4
Speed Limit (MPH)	55		

HMA Layer Properties				
Aggregate Gradation (% passing)		Asphalt Binder Grade	Volumetric Properties (In place)	
3/4 in. Sieve	96	PG 64-28	Effective Binder Content, Pbe (%)	10.85
3/8 in. Sieve	71		Air Voids (%)	5.3
#4 Sieve	47		Unit Weight (lb/ft^3)	143.5
#200 Sieve	4.4		Pbe (%) by Wt	4.9

Other Layer Properties					
Subgrade		Aggregate Base		Chemically-Stabilized Base	
Type	A-4	Type	A-1-a	Type	-
Resilient Modulus (psi)	5500	Resilient Modulus (psi)	Default	Other Values	-

US 26: Prairie City Section

Traffic Info		Climatic Info	
Initial Two-way AADTT	792	Latitude	44.462563
No of Lanes in Design Direction	1	Longitude	-118.710752
Growth Rate (%)	3	Elevation	3540.107
Lane Distribution Factor	1	Depth to Water Table (ft)	4
Speed Limit (MPH)	25		

HMA Layer Properties				
Aggregate Gradation (% passing)		Asphalt Binder Grade	Volumetric Properties (In place)	
3/4 in. Sieve	96	PG 64-28	Effective Binder Content, Pbe (%)	10.85
3/8 in. Sieve	71		Air Voids (%)	5.3
#4 Sieve	47		Unit Weight (lb/ft^3)	143.5
#200 Sieve	4.4		Pbe (%) by Wt	4.9

Other Layer Properties					
Subgrade		Aggregate Base		Chemically-Stabilized Base	
Type	A-4	Type	A-1-a	Type	-
Resilient Modulus (psi)	5500	Resilient Modulus (psi)	Default	Other Values	-

I-84: N. FK Jocobsen Gulch-Malheur River (EB)

Traffic Info		Climatic Info	
Initial Two-way AADTT	9648	Latitude	44.072540
No of Lanes in Design Direction	2	Longitude	-117.001648
Growth Rate (%)	1.5	Elevation	2293.092
Lane Distribution Factor	0.90	Depth to Water Table (ft)	10
Speed Limit (MPH)	55		

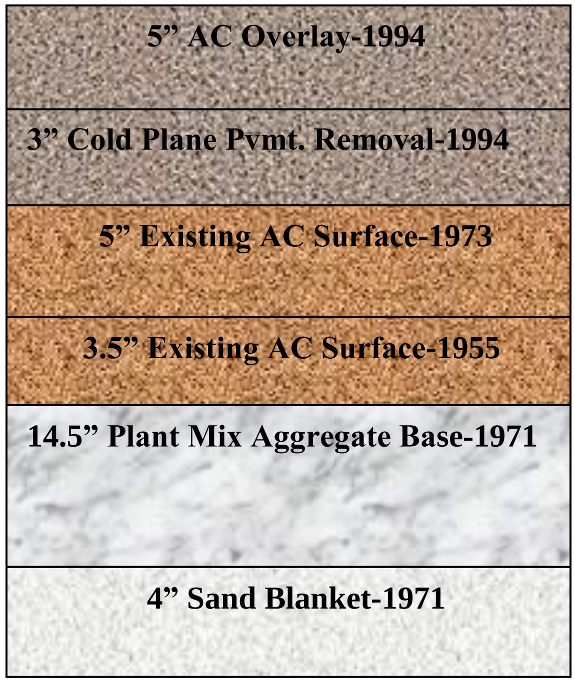

HMA Layer Properties				
Aggregate Gradation (% passing)		Asphalt Binder Grade	Volumetric Properties (In place)	
3/4 in. Sieve	89	PG 70-28	Effective Binder Content, Pbe (%)	9.70
3/8 in. Sieve	44		Air Voids (%)	14.2
#4 Sieve	27		Unit Weight (lb/ft^3)	130.5
#200 Sieve	3		Pbe (%) by Wt	4.818

Other Layer Properties					
Subgrade		Aggregate Base		Chemically-Stabilized Base	
Type	A-4	Type	A-1-a	Type	-
Resilient Modulus (psi)	7000	Resilient Modulus (psi)	Default	Other Values	-

I-84: N. FK Jocobsen Gulch-Malheur River (WB)

Traffic Info		Climatic Info	
Initial Two-way AADTT	8200	Latitude	44.072540
No of Lanes in Design Direction	2	Longitude	-117.001648
Growth Rate (%)	1.5	Elevation	2293.092
Lane Distribution Factor	0.90	Depth to Water Table (ft)	10
Speed Limit (MPH)	55		

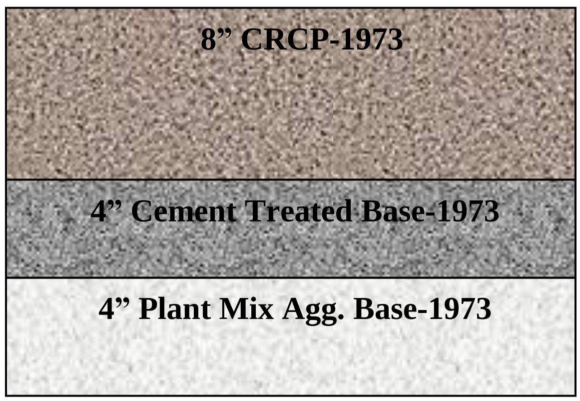

CRCP		
Steel Reinforcement	Steel (%)	0.60
	Steel Diameter (in.)	0.63
	Steel Depth (in.)	3.5

Unbound Layer Properties					
Subgrade		Aggregate Base		Chemically-Stabilized Base	
Type	A-4	Type	A-1-a	Type	-
Resilient Modulus (psi)	5500	Resilient Modulus (psi)	Default	Other Values	-

US 20: MP 10.3-MP 12.5

Traffic Info		Climatic Info	
Initial Two-way AADTT	1706	Latitude	44.181096
No of Lanes in Design Direction	2	Longitude	-121.379871
Growth Rate (%)	2	Elevation	3334.959
Lane Distribution Factor	0.90	Depth to Water Table (ft)	10
Speed Limit (MPH)	55		

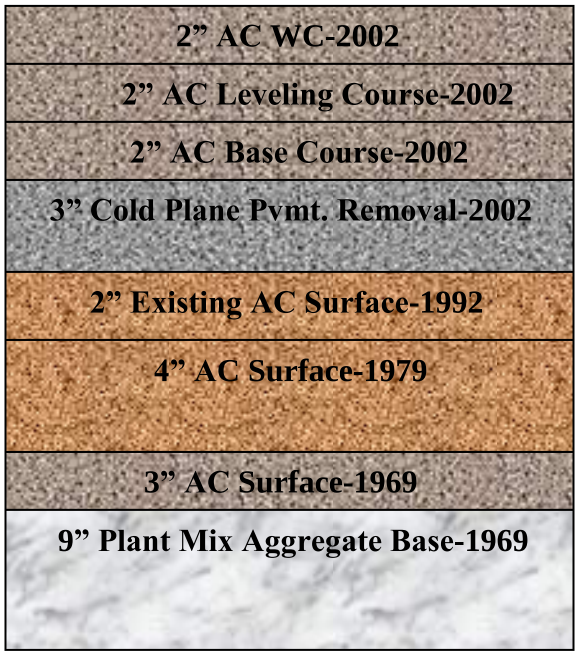

HMA Layer Properties (2002 AC Wearing Course)				
Aggregate Gradation (% passing)		Asphalt Binder Grade	Volumetric Properties (In place)	
3/4 in. Sieve	98	PG 64-28	Effective Binder Content, Pbe (%)	10.29
3/8 in. Sieve	80		Air Voids (%)	4.1
#4 Sieve	53		Unit Weight (lb/ft^3)	151.7
#200 Sieve	6.4		Pbe (%) by Wt	4.4
HMA Layer Properties (2002 AC Base Course)				
Aggregate Gradation (% passing)		Asphalt Binder Grade	Volumetric Properties (In place)	
3/4 in. Sieve	92	PG 70-28	Effective Binder Content, Pbe (%)	9.28
3/8 in. Sieve	41		Air Voids (%)	14.1
#4 Sieve	15		Unit Weight (lb/ft^3)	136.7
#200 Sieve	3.1		Pbe (%) by Wt	4.4

Other Layer Properties					
Subgrade		Aggregate Base		Chemically-Stabilized Base	
Type	A-2-5	Type	A-1-a	Type	-
Resilient Modulus (psi)	7000	Resilient Modulus (psi)	Default	Other Values	-

US 395: Jct Hwy2-Hwy33 (Elm Ave)

Traffic Info		Climatic Info	
Initial Two-way AADTT	2186	Latitude	45.914736
No of Lanes in Design Direction	2	Longitude	-119.305172
Growth Rate (%)	0	Elevation	463.668
Lane Distribution Factor	0.90	Depth to Water Table (ft)	2.5
Speed Limit (MPH)	55		

HMA Layer Properties				
Aggregate Gradation (% passing)		Asphalt Binder Grade	Volumetric Properties (In place)	
3/4 in. Sieve	100	PG 58-28	Effective Binder Content, Pbe (%)	9.97
3/8 in. Sieve	82		Air Voids (%)	5.1
#4 Sieve	55		Unit Weight (lb/ft^3)	153.6
#200 Sieve	4.9		Pbe (%) by Wt	4.2

Other Layer Properties					
Subgrade		Aggregate Base		Chemically-Stabilized Base	
Type	A-4	Type	A-1-a	Type	-
Resilient Modulus (psi)	5500	Resilient Modulus (psi)	Default	Other Values	-

OR 569: Hwy 091 Williamette R E/B

Traffic Info		Climatic Info	
Initial Two-way AADTT	11650	Latitude	44.097542
No of Lanes in Design Direction	2	Longitude	-123.114935
Growth Rate (%)	1	Elevation	-393.701
Lane Distribution Factor	0.90	Depth to Water Table (ft)	10
Speed Limit (MPH)	55		

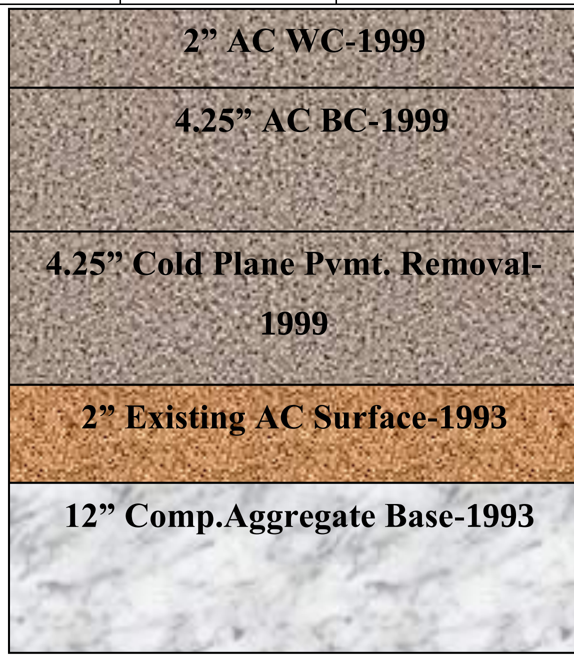

HMA Layer Properties (1999 AC Wearing Course)				
Aggregate Gradation (% passing)		Asphalt Binder Grade	Volumetric Properties (In place)	
3/4 in. Sieve	92	PG 70-28	Effective Binder Content, Pbe (%)	9.743
3/8 in. Sieve	40		Air Voids (%)	14
#4 Sieve	20		Unit Weight (lb/ft^3)	131.5
#200 Sieve	3.1		Pbe (%) by Wt	4.8
HMA Layer Properties (1999 AC Base Course)				
Aggregate Gradation (% passing)		Asphalt Binder Grade	Volumetric Properties (In place)	
3/4 in. Sieve	95	PG 64-22	Effective Binder Content, Pbe (%)	10.02
3/8 in. Sieve	65		Air Voids (%)	4.4
#4 Sieve	40		Unit Weight (lb/ft^3)	147.6
#200 Sieve	5.2		Pbe (%) by Wt	4.4
HMA Layer Properties (1993 AC Surface)				
Aggregate Gradation (% passing)		Asphalt Binder Grade	Volumetric Properties (In place)	
3/4 in. Sieve	92	PG 64-22	Effective Binder Content, Pbe (%)	9.743
3/8 in. Sieve	48		Air Voids (%)	14.5
#4 Sieve	17		Unit Weight (lb/ft^3)	132.9
#200 Sieve	3.3		Pbe (%) by Wt	4.8

Other Layer Properties					
Subgrade		Aggregate Base		Chemically-Stabilized Base	
Type	A-4	Type	A-1-a	Type	-
Resilient Modulus (psi)	5500	Resilient Modulus (psi)	Default	Other Values	-

<u>OR 99W: Marys R-Kiger Island Dr</u>

Traffic Info		Climatic Info	
Initial Two-way AADTT	2450	Latitude	44.519931
No of Lanes in Design Direction	2	Longitude	-123.276689
Growth Rate (%)	0	Elevation	239.624
Lane Distribution Factor	0.90	Depth to Water Table (ft)	2
Speed Limit (MPH)	35		

HMA Layer Properties (AC Wearing Course)				
Aggregate Gradation (% passing)		Asphalt Binder Grade	Volumetric Properties (In place)	
3/4 in. Sieve	100	PG 70-22	Effective Binder Content, Pbe (%)	10.90
3/8 in. Sieve	83		Air Voids (%)	5.6
#4 Sieve	50		Unit Weight (lb/ft^3)	147.20
#200 Sieve	5		Pbe (%) by Wt	4.8
HMA Layer Properties (AC Base Course)				
Aggregate Gradation (% passing)		Asphalt Binder Grade	Volumetric Properties (In place)	
3/4 in. Sieve	95	PG 64-22	Effective Binder Content, Pbe (%)	10.723
3/8 in. Sieve	71		Air Voids (%)	4.6
#4 Sieve	45		Unit Weight (lb/ft^3)	144.83
#200 Sieve	5		Pbe (%) by Wt	4.8

Other Layer Properties					
Subgrade		Aggregate Base		Chemically-Stabilized Base	
Type	A-4	Type	-	Type	-
Resilient Modulus (psi)	5500	Resilient Modulus (psi)	-	Other Values	-

OR 99W: Brutschr St. Jct. Hwy. 151

Traffic Info		Climatic Info	
Initial Two-way AADTT	4522	Latitude	45.303512
No of Lanes in Design Direction	2	Longitude	-122.940909
Growth Rate (%)	0	Elevation	199.047
Lane Distribution Factor	0.90	Depth to Water Table (ft)	1.5
Speed Limit (MPH)	40		

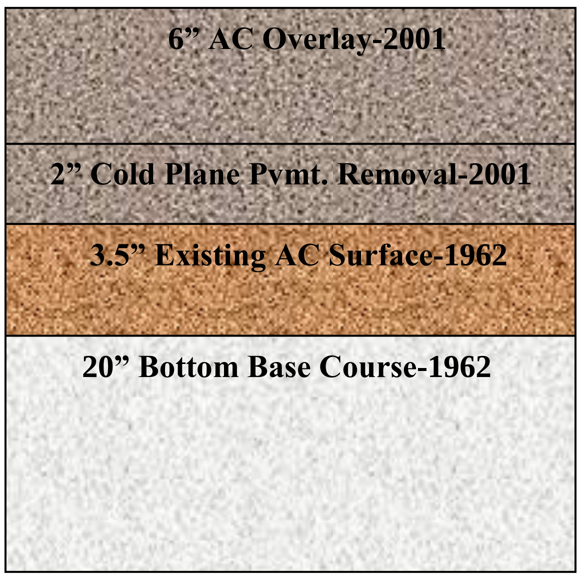

HMA Layer Properties				
Aggregate Gradation (% passing)		Asphalt Binder Grade	Volumetric Properties (In place)	
3/4 in. Sieve	100	PG 70-22	Effective Binder Content, Pbe (%)	9.93
3/8 in. Sieve	85		Air Voids (%)	4
#4 Sieve	54		Unit Weight (lb/ft^3)	146.3
#200 Sieve	5.4		Pbe (%) by Wt	4.4

Other Layer Properties					
Subgrade		Aggregate Base		Chemically-Stabilized Base	
Type	A-4	Type	A-1-a	Type	-
Resilient Modulus (psi)	5500	Resilient Modulus (psi)	Default	Other Values	-

OR 99W: N Sherwood to SW 12th Street

Traffic Info		Climatic Info	
Initial Two-way AADTT	4750	Latitude	45.369778
No of Lanes in Design Direction	3	Longitude	-122.843731
Growth Rate (%)	1.5	Elevation	205.145
Lane Distribution Factor	0.50	Depth to Water Table (ft)	10
Speed Limit (MPH)	45		

HMA Layer Properties (AC WC)				
Aggregate Gradation (% passing)		Asphalt Binder Grade	Volumetric Properties (In place)	
3/4 in. Sieve	93	PG 64-22	Effective Binder Content, Pbe (%)	10.91
3/8 in. Sieve	46		Air Voids (%)	15.2
#4 Sieve	15		Unit Weight (lb/ft^3)	133.54
#200 Sieve	3.2		Pbe (%) by Wt	5.3
HMA Layer Properties (AC Base Course)				
Aggregate Gradation (% passing)		Asphalt Binder Grade	Volumetric Properties (In place)	
3/4 in. Sieve	95	PG 64-22	Effective Binder Content, Pbe (%)	12.53
3/8 in. Sieve	68		Air Voids (%)	4.6
#4 Sieve	45		Unit Weight (lb/ft^3)	147.70
#200 Sieve	4.8		Pbe (%) by Wt	5.5

Other Layer Properties					
Subgrade		Aggregate Base		Chemically-Stabilized Base	
Type	A-4	Type	A-1-a	Type	-
Resilient Modulus (psi)	5500	Resilient Modulus (psi)	Default	Other Values	-

<u>US 30: Cornelius Pass Rd</u>

Traffic Info		Climatic Info	
Initial Two-way AADTT	5540	Latitude	44.560937
No of Lanes in Design Direction	2	Longitude	-123.25716
Growth Rate (%)	0	Elevation	208.118
Lane Distribution Factor	0.90	Depth to Water Table (ft)	10
Speed Limit (MPH)	55		

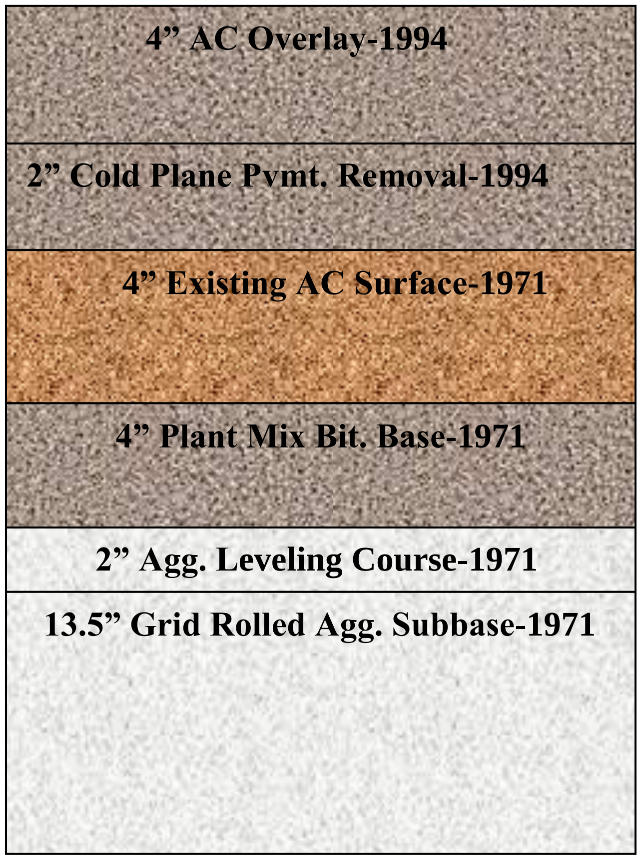

HMA Layer Properties				
Aggregate Gradation (% passing)		Asphalt Binder Grade	Volumetric Properties (In place)	
3/4 in. Sieve	96	PG 58-28	Effective Binder Content, Pbe (%)	10.03
3/8 in. Sieve	71		Air Voids (%)	4.4
#4 Sieve	49		Unit Weight (lb/ft^3)	147.6
#200 Sieve	6.4		Pbe (%) by Wt	4.4

Other Layer Properties					
Subgrade		Aggregate Base		Chemically-Stabilized Base	
Type	A-4	Type	A-1-a	Type	-
Resilient Modulus (psi)	5500	Resilient Modulus (psi)	Default	Other Values	-

OR 120: End Jcp-Beg Hwy 081

Traffic Info		Climatic Info	
Initial Two-way AADTT	7010	Latitude	45.607822
No of Lanes in Design Direction	2	Longitude	-122.687225
Growth Rate (%)	0	Elevation	22.391
Lane Distribution Factor	0.90	Depth to Water Table (ft)	10
Speed Limit (MPH)	45		

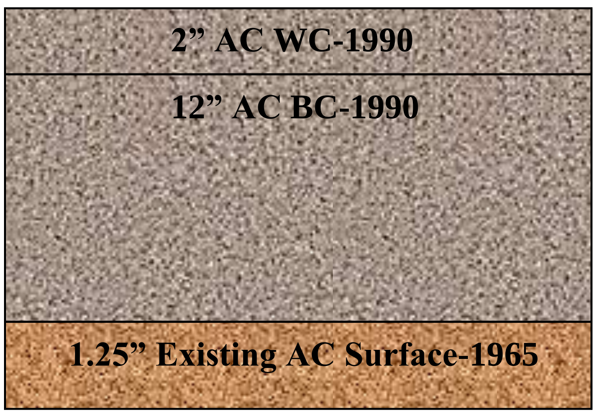

HMA Layer Properties				
Aggregate Gradation (% passing)		Asphalt Binder Grade	Volumetric Properties (In place)	
3/4 in. Sieve	99	PG 64-28	Effective Binder Content, Pbe (%)	11.53
3/8 in. Sieve	69		Air Voids (%)	4
#4 Sieve	48		Unit Weight (lb/ft^3)	143.8
#200 Sieve	4.9		Pbe (%) by Wt	5.2

Other Layer Properties					
Subgrade		Aggregate Base		Chemically-Stabilized Base	
Type	A-4	Type	-	Type	-
Resilient Modulus (psi)	5500	Resilient Modulus (psi)	-	Other Values	-

OR 201: Washington Ave-Airport Way

Traffic Info		Climatic Info	
Initial Two-way AADTT	620	Latitude	44.032197
No of Lanes in Design Direction	1	Longitude	-117.002935
Growth Rate (%)	5	Elevation	2151.704
Lane Distribution Factor	1	Depth to Water Table (ft)	10
Speed Limit (MPH)	55		

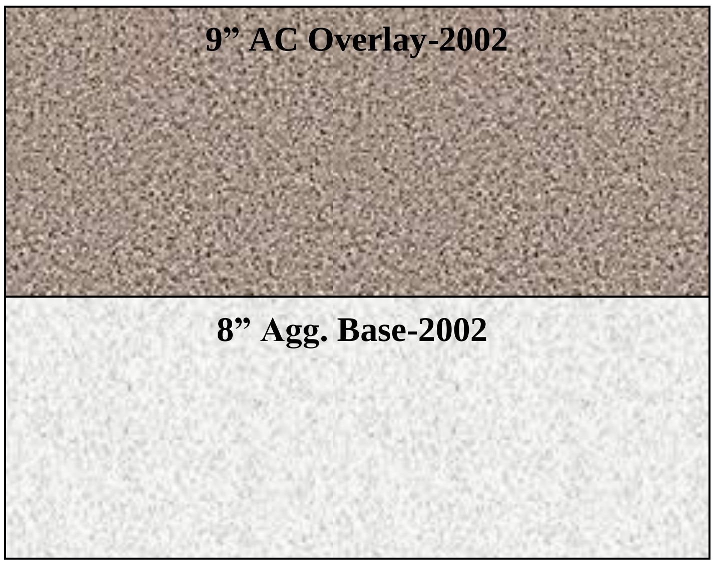

HMA Layer Properties				
Aggregate Gradation (% passing)		Asphalt Binder Grade	Volumetric Properties (In place)	
3/4 in. Sieve	99	PG 64-28	Effective Binder Content, Pbe (%)	11.53
3/8 in. Sieve	69		Air Voids (%)	4
#4 Sieve	48		Unit Weight (lb/ft^3)	143.8
#200 Sieve	4.9		Pbe (%) by Wt	5.2

Other Layer Properties					
Subgrade		Aggregate Base		Chemically-Stabilized Base	
Type	A-4	Type	A-1-a	Type	-
Resilient Modulus (psi)	5500	Resilient Modulus (psi)	-	Other Values	-

OR 140: Jct Hwy 019-Bowers Bridges Creek

Traffic Info		Climatic Info	
Initial Two-way AADTT	160	Latitude	42.188772
No of Lanes in Design Direction	1	Longitude	-120.345792
Growth Rate (%)	0	Elevation	4794.002
Lane Distribution Factor	1	Depth to Water Table (ft)	10
Speed Limit (MPH)	40		

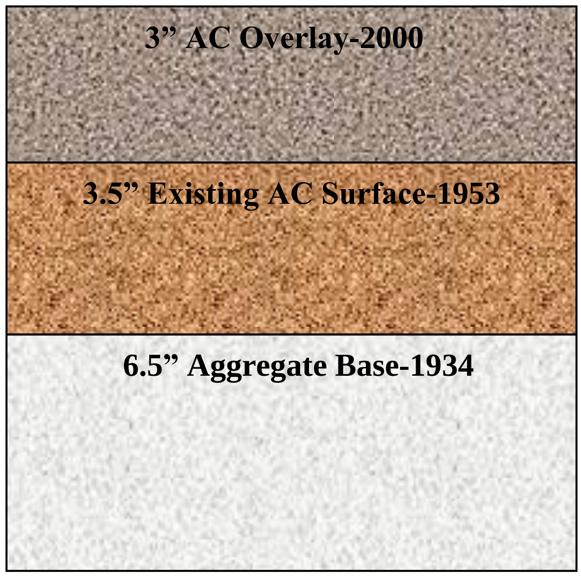

HMA Layer Properties				
Aggregate Gradation (% passing)		Asphalt Binder Grade	Volumetric Properties (In place)	
3/4 in. Sieve	100	PG 64-28	Effective Binder Content, Pbe (%)	13.95
3/8 in. Sieve	81.5		Air Voids (%)	3.84
#4 Sieve	50.5		Unit Weight (lb/ft^3)	153.32
#200 Sieve	6		Pbe (%) by Wt	5.9

Other Layer Properties					
Subgrade		Aggregate Base		Chemically-Stabilized Base	
Type	A-4	Type	A-1-a	Type	-
Resilient Modulus (psi)	5500	Resilient Modulus (psi)	Default	Other Values	-

US 97: N. Chiloquin Intch-Williamson Dr

Traffic Info		Climatic Info	
Initial Two-way AADTT	3570	Latitude	42.577636
No of Lanes in Design Direction	1	Longitude	-121.866126
Growth Rate (%)	0	Elevation	4179.410
Lane Distribution Factor	1	Depth to Water Table (ft)	5
Speed Limit (MPH)	40		

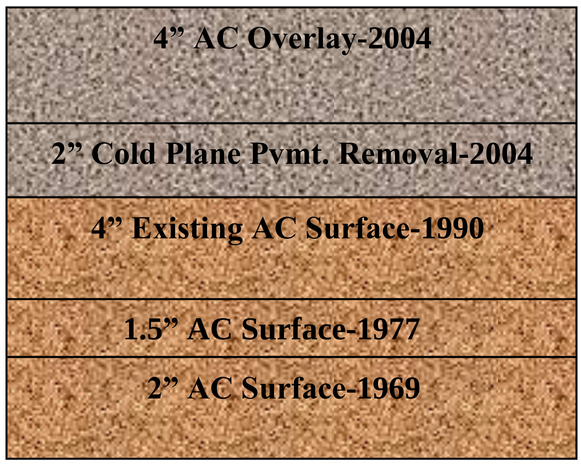

HMA Layer Properties				
Aggregate Gradation (% passing)		Asphalt Binder Grade	Volumetric Properties (In place)	
3/4 in. Sieve	100	PG 70-28	Effective Binder Content, Pbe (%)	12.42
3/8 in. Sieve	75		Air Voids (%)	3.93
#4 Sieve	40		Unit Weight (lb/ft^3)	146.27
#200 Sieve	6.7		Pbe (%) by Wt	5.5

Other Layer Properties					
Subgrade		Aggregate Base		Chemically-Stabilized Base	
Type	A-4	Type	-	Type	-
Resilient Modulus (psi)	5500	Resilient Modulus (psi)	-	Other Values	-

APPENDIX C-FWD DEFLECTION DATA

<u>OR22-U</u>

FWD Station	Force (lb)	Deflection (mils)						
		D1	D2	D3	D4	D5	D6	D7
1	9132	14.04	10.74	9.81	7.79	6.27	3.84	1.75
2	9188	12.49	9.61	8.90	7.25	6.03	3.86	1.67
3	9286	13.28	10.03	9.28	7.49	6.05	3.74	1.61
4	9283	13.49	10.64	9.80	7.78	6.24	3.69	1.54
5	9246	12.53	9.88	9.14	7.44	6.17	3.87	1.61
6	9246	12.56	9.81	9.10	7.33	5.98	3.74	1.57
7	9191	12.48	9.58	8.90	7.14	5.76	3.47	1.50
8	9199	11.90	9.30	8.74	6.96	5.57	3.27	1.47
9	9267	11.32	8.75	8.18	6.67	5.51	3.51	1.61
10	9275	11.41	8.91	8.33	6.78	5.59	3.58	1.66
11	9362	11.09	9.23	8.58	7.18	6.06	4.09	2.03
12	9191	13.42	10.22	9.46	7.69	6.29	4.07	2.04
13	9183	12.93	9.88	9.13	7.31	5.98	3.82	1.88
14	9188	14.56	11.36	10.63	8.65	7.13	4.74	2.46
15	9119	14.54	11.66	10.82	8.89	7.40	5.04	2.71
16	9219	14.15	11.56	10.89	8.97	7.46	5.00	2.55
17	9111	11.96	9.66	9.14	7.78	6.72	4.82	2.52
18	9172	13.43	10.92	10.26	8.67	7.41	5.32	2.78
19	9156	13.67	10.81	10.14	8.48	7.17	4.99	2.57
20	9156	13.31	10.13	9.63	8.13	6.91	4.96	2.59
21	9040	13.29	10.27	9.69	8.09	6.96	4.91	2.63
22	9148	12.96	10.17	9.57	7.92	6.67	4.59	2.41
23	9135	12.57	9.61	8.97	7.41	6.18	4.14	1.89

US97-U

FWD Station	Force (lb)	Deflection (mils)						
		D1	D2	D3	D4	D5	D6	D7
2	9640	10.83	8.87	8.21	6.71	5.63	3.70	1.47
3	9577	9.80	8.16	7.61	6.35	5.40	3.64	1.45
4	9680	9.63	8.06	7.54	6.23	5.28	3.48	1.25
5	9609	11.39	9.30	8.67	7.03	5.84	3.81	1.33
6	9601	11.68	9.40	8.65	7.01	5.82	3.71	1.31
7	9664	11.97	9.83	9.03	7.35	6.15	4.11	1.64
8	9572	13.26	10.73	9.89	7.99	6.67	4.45	1.91
9	9644	11.05	9.24	8.58	7.09	6.04	4.18	1.91
10	9799	9.04	7.18	6.58	5.19	4.27	2.63	0.82
11	9810	8.26	6.41	5.87	4.61	3.79	2.31	0.69
12	9810	7.76	6.04	5.57	4.40	3.61	2.19	0.63
13	9842	8.69	6.94	6.34	5.09	4.13	2.52	0.76
14	9664	10.06	7.81	7.08	5.63	4.56	2.79	0.89

US20-U

FWD Station	Force (lb)	Deflection (mils)						
		D1	D2	D3	D4	D5	D6	D7
2	9493	6.96	5.12	4.62	3.61	2.91	1.79	0.69
3	9572	6.86	5.02	4.59	3.81	3.26	2.35	1.28
4	9421	11.19	8.74	8.12	6.75	5.82	4.05	1.92
5	9545	9.61	7.41	6.92	5.82	5.02	3.54	1.75
6	10049	6.61	5.39	5.07	4.30	3.78	2.81	1.43
7	9998	6.61	5.72	5.36	4.70	4.00	3.03	1.56
8	9969	7.25	5.96	5.60	4.82	4.09	2.93	1.29
9	9919	7.62	6.20	5.85	4.99	4.41	3.26	1.61
10	9898	8.58	7.19	6.93	5.89	5.34	3.99	1.57
11	9675	10.15	8.49	8.20	7.14	6.32	4.74	2.48
12	9752	9.26	7.77	7.37	6.33	5.53	4.04	2.02
13	9723	8.43	6.92	6.48	5.57	4.77	3.41	1.52

<u>OR99-U</u>

FWD Station	Force (lb)	Deflection (mils)						
		D1	D2	D3	D4	D5	D6	D7
2	9469	6.07	5.13	4.81	4.09	3.57	2.62	1.41
3	9413	7.49	5.61	5.11	4.17	3.56	2.46	1.25
4	9445	7.73	6.39	5.98	4.98	4.23	2.99	1.55
5	9342	8.80	7.48	6.96	5.76	4.90	3.45	2.13
6	9302	8.02	6.67	6.23	5.05	4.32	3.06	1.87
7	9331	5.30	4.46	4.19	3.57	3.11	2.32	1.53
8	9339	6.38	5.17	4.76	3.97	3.43	2.55	1.65
9	9302	6.56	5.29	4.91	4.02	3.42	2.51	1.68
10	9382	6.28	5.31	4.96	4.19	3.61	2.67	1.73
11	9434	7.74	6.42	5.95	4.98	4.23	3.00	1.78
12	9294	7.40	6.17	5.75	4.78	4.07	2.91	1.70
13	9270	8.57	6.56	6.08	5.03	4.28	3.09	1.83
14	9291	7.06	6.00	5.68	4.89	4.26	3.19	1.87
15	9315	6.63	5.80	5.53	4.86	4.33	3.32	1.98
16	9283	7.61	6.34	6.02	5.28	4.67	3.50	1.97
17	9442	7.67	6.38	6.05	5.31	4.71	3.58	2.04
18	9474	6.28	5.51	5.27	4.69	4.18	3.19	1.77
19	9350	8.89	7.17	6.56	5.58	4.74	3.39	1.77

OR238-C

FWD Station	Force (lb)	Deflection (mils)						
		D1	D2	D3	D4	D5	D6	D7
2	9429	5.97	4.29	3.80	2.68	1.98	1.01	0.37
3	9421	6.93	4.76	4.12	2.81	2.00	1.02	0.36
4	9397	6.42	4.86	4.33	3.31	2.57	1.58	0.68
5	9386	6.83	5.00	4.30	3.01	2.15	1.10	0.55
6	9382	7.98	4.92	4.09	2.71	2.02	1.17	0.55
7	9450	6.32	4.67	4.09	2.94	2.26	1.35	0.64
8	9382	6.61	4.86	4.24	3.07	2.34	1.38	0.69
9	9323	7.63	5.25	4.58	3.26	2.49	1.44	0.63
10	9434	6.47	4.92	4.38	3.28	2.56	1.50	0.61
11	9402	6.54	5.28	4.79	3.74	2.98	1.76	0.69
12	9537	6.40	4.44	3.92	3.03	2.39	1.48	0.65
13	9525	7.46	5.14	4.38	3.17	2.46	1.50	0.72
14	9501	6.63	4.97	4.35	3.21	2.51	1.51	0.70
15	9493	6.83	4.63	3.98	2.83	2.19	1.35	0.65
16	9382	8.47	5.48	4.66	3.26	2.41	1.38	0.72
17	9461	7.14	4.77	4.12	2.97	2.28	1.39	0.66
18	9466	5.80	4.42	3.99	3.06	2.44	1.50	0.65
19	9370	6.92	5.22	4.58	3.27	2.49	1.40	0.64
20	9501	5.77	4.38	3.93	3.02	2.39	1.44	0.68
21	9374	5.97	4.74	4.22	3.17	2.47	1.47	0.66

OR99W-C

FWD Station	Force (lb)	Deflection (mils)						
		D1	D2	D3	D4	D5	D6	D7
2	9664	8.94	7.02	6.52	5.29	4.41	3.01	1.55
3	9532	8.71	6.72	6.26	5.18	4.38	3.03	1.55
4	9505	8.21	6.69	6.24	5.16	4.38	3.02	1.56
5	9334	7.50	6.26	5.89	4.99	4.33	3.08	1.65
6	9609	8.54	6.89	6.41	5.40	4.67	3.27	1.72
7	9763	8.66	7.18	6.69	5.57	4.76	3.31	1.61
8	9556	8.35	6.80	6.34	5.23	4.46	3.13	1.56
9	9474	8.30	6.71	6.21	5.15	4.38	3.09	1.61
10	9561	9.38	6.46	6.08	5.11	4.34	3.14	1.70
11	9763	7.91	6.56	6.11	5.07	4.35	3.20	1.70
12	9633	7.31	6.10	5.70	4.85	4.23	3.11	1.71
13	9358	8.24	6.67	6.26	5.33	4.63	3.37	1.85
14	9683	7.88	6.59	6.19	5.30	4.64	3.41	1.83
15	9803	7.82	6.34	5.98	5.13	4.50	3.35	1.81
16	9699	7.48	6.15	5.82	5.05	4.46	3.31	1.83
17	9656	6.96	6.09	5.79	4.96	4.38	3.20	1.77
18	9934	7.08	5.65	5.31	4.53	3.95	2.94	1.58
19	9529	7.32	5.74	5.41	4.63	4.09	2.99	1.63
20	9704	7.43	6.06	5.63	4.83	4.20	3.07	1.62
21	10120	7.72	5.95	5.57	4.76	4.13	3.06	1.66
22	9776	7.79	6.22	5.84	5.08	4.48	3.36	1.81
23	9834	5.88	4.43	4.14	3.56	3.05	2.36	1.38
24	10104	5.59	4.22	3.93	3.39	3.02	2.30	1.34
25	9953	5.48	4.33	4.04	3.51	3.09	2.35	1.37
26	9890	6.45	4.85	4.55	3.91	3.45	2.56	1.50
27	9553	5.47	4.49	4.20	3.68	3.27	2.51	1.45
28	9548	6.66	5.19	4.91	4.30	3.85	3.00	1.65
29	9537	7.17	6.06	5.80	4.89	4.29	3.26	1.38
30	9747	8.61	6.68	6.22	5.31	4.61	3.43	1.76

<u>OR221-C</u>

FWD Station	Force (lb)	Deflection (mils)						
		D1	D2	D3	D4	D5	D6	D7
2	9720	7.51	5.49	4.93	3.78	3.01	1.78	0.75
3	9421	9.20	6.74	6.08	4.61	3.83	2.38	0.96
4	9577	7.69	5.72	5.10	3.93	3.15	1.85	0.73
5	9529	8.08	6.10	5.48	4.19	3.32	1.91	0.72
6	9358	8.52	6.01	5.28	3.91	3.01	1.58	0.68
7	9490	8.22	5.82	5.10	3.80	2.96	1.61	0.67
8	9517	7.33	5.23	4.67	3.52	2.74	1.61	0.70
9	9410	8.41	5.71	5.14	3.81	2.96	1.63	0.68
10	9477	7.99	5.54	4.69	3.41	2.65	1.39	0.62
11	9513	7.45	5.07	4.44	3.30	2.50	1.36	0.62
12	9501	8.94	5.96	5.07	3.54	2.63	1.39	0.64
13	9501	9.78	6.92	6.04	4.36	3.37	1.86	0.67
14	9532	9.17	6.43	5.51	3.82	2.81	1.51	0.66
15	9426	11.29	8.11	6.94	4.88	3.70	1.98	0.73
16	9389	10.78	8.07	7.03	4.89	3.67	1.91	0.71
17	9485	9.11	6.80	5.98	4.50	3.55	2.04	0.70
18	9723	9.07	7.06	6.42	5.00	4.06	2.43	0.86
19	9532	9.76	7.39	6.59	5.03	3.98	2.27	0.80
20	9307	11.14	8.13	7.36	5.45	4.35	2.46	0.75
21	9291	13.07	9.79	8.43	6.10	4.52	2.20	0.69
22	9442	13.21	9.50	8.20	5.86	4.49	2.37	0.76
23	9469	12.24	9.23	8.29	6.31	4.92	2.74	0.89
24	9358	12.45	9.28	8.24	6.11	4.85	2.69	0.83
25	9382	11.02	8.12	7.24	5.45	4.31	2.49	0.80
26	9593	11.52	8.33	7.28	5.51	4.29	2.40	0.80

OR99EB-C

FWD Station	Force (lb)	Deflection (mils)						
		D1	D2	D3	D4	D5	D6	D7
2	9842	2.04	1.51	1.57	1.48	1.37	1.28	1.03
3	9879	2.35	1.82	1.80	1.70	1.61	1.43	1.06
4	10033	2.53	1.93	1.85	1.69	1.54	1.37	1.06
5	9911	2.09	1.80	1.70	1.63	1.46	1.37	1.06
6	9863	2.07	1.51	1.48	1.43	1.37	1.27	1.00
7	9914	3.06	2.23	2.11	1.86	1.71	1.45	1.04
8	9922	2.81	2.07	1.96	1.76	1.56	1.39	1.03
9	9898	2.91	2.24	2.18	2.02	1.88	1.65	1.13
10	9866	3.00	2.43	2.29	2.06	1.88	1.61	1.16
11	9799	3.22	2.54	2.43	2.20	2.02	1.72	1.18
12	10006	3.02	2.51	2.44	2.29	2.15	1.89	1.20
13	10252	3.48	2.49	2.39	2.23	2.06	1.78	1.30
14	10065	2.80	1.93	1.85	1.74	1.65	1.49	1.20
15	9942	5.16	2.88	2.57	2.17	1.94	1.69	1.28
16	10041	2.75	2.05	2.01	1.89	1.81	1.62	1.28
17	10128	2.60	1.96	1.89	1.79	1.71	1.56	1.20
18	10001	3.11	2.32	2.25	2.12	2.01	1.84	1.33
19	9998	3.60	2.46	2.33	2.13	1.99	1.74	1.29
20	10057	3.28	2.28	2.20	1.99	1.83	1.61	1.20
21	10030	2.94	2.13	2.09	1.96	1.85	1.65	1.24
22	10033	3.34	2.39	2.20	2.09	1.94	1.68	1.22
23	9858	3.38	2.21	2.17	2.04	1.92	1.66	1.19
24	9823	4.54	3.20	3.02	2.57	2.16	1.86	1.18
25	9961	3.49	2.16	2.09	1.96	1.83	1.63	1.23
26	9858	2.85	1.98	1.93	1.84	1.74	1.55	1.16
27	9942	3.33	1.99	1.92	1.79	1.68	1.48	1.12

OR140-C

FWD Station	Force (lb)	Deflection (mils)						
		D1	D2	D3	D4	D5	D6	D7
2	10200	9.33	7.11	6.61	5.44	4.61	3.15	1.37
3	10081	7.42	6.02	5.61	4.54	3.77	2.38	0.79
4	9966	6.35	4.97	4.60	3.64	2.96	1.81	0.63
5	9990	6.17	4.87	4.44	3.54	2.87	1.80	0.62
6	9906	8.71	7.12	6.72	5.70	4.94	3.56	1.80
7	9942	10.15	8.62	8.13	7.06	6.20	4.57	2.43
8	9990	9.00	7.45	6.96	5.87	5.08	3.56	1.69
9	10014	9.13	7.55	7.11	6.08	5.22	3.69	1.74
10	9966	9.97	8.30	7.79	6.50	5.59	3.85	1.85
11	9882	10.15	8.34	7.86	6.60	5.60	3.83	1.78
12	9911	9.80	8.07	7.54	6.30	5.36	3.68	1.76
13	9934	8.22	6.70	6.18	5.02	4.17	2.71	1.18
14	9823	9.36	7.41	6.97	5.75	4.80	3.21	1.33
15	9930	9.75	7.52	6.95	5.58	4.65	3.08	1.43
16	9930	10.38	8.33	7.75	6.33	5.33	3.54	1.63
17	9961	9.33	7.53	7.02	5.78	4.82	3.19	1.49
18	9895	12.26	10.35	9.73	8.20	7.07	5.00	2.39

OR99*-C

FWD Station	Force (lb)	Deflection (mils)						
		D1	D2	D3	D4	D5	D6	D7
2	9664	8.94	7.02	6.52	5.29	4.41	3.01	1.55
3	9532	8.71	6.72	6.26	5.18	4.38	3.03	1.55
4	9505	8.21	6.69	6.24	5.16	4.38	3.02	1.56
5	9334	7.50	6.26	5.89	4.99	4.33	3.08	1.65
6	9609	8.54	6.89	6.41	5.40	4.67	3.27	1.72
7	9763	8.66	7.18	6.69	5.57	4.76	3.31	1.61
8	9556	8.35	6.80	6.34	5.23	4.46	3.13	1.56
9	9474	8.30	6.71	6.21	5.15	4.38	3.09	1.61
10	9561	9.38	6.46	6.08	5.11	4.34	3.14	1.70
11	9763	7.91	6.56	6.11	5.07	4.35	3.20	1.70
12	9633	7.31	6.10	5.70	4.85	4.23	3.11	1.71
13	9358	8.24	6.67	6.26	5.33	4.63	3.37	1.85
14	9683	7.88	6.59	6.19	5.30	4.64	3.41	1.83
15	9803	7.82	6.34	5.98	5.13	4.50	3.35	1.81
16	9699	7.48	6.15	5.82	5.05	4.46	3.31	1.83
17	9656	6.96	6.09	5.79	4.96	4.38	3.20	1.77
18	9934	7.08	5.65	5.31	4.53	3.95	2.94	1.58
19	9529	7.32	5.74	5.41	4.63	4.09	2.99	1.63
20	9704	7.43	6.06	5.63	4.83	4.20	3.07	1.62
21	10120	7.72	5.95	5.57	4.76	4.13	3.06	1.66
22	9776	7.79	6.22	5.84	5.08	4.48	3.36	1.81
23	9834	5.88	4.43	4.14	3.56	3.05	2.36	1.38
24	10104	5.59	4.22	3.93	3.39	3.02	2.30	1.34
25	9953	5.48	4.33	4.04	3.51	3.09	2.35	1.37
26	9890	6.45	4.85	4.55	3.91	3.45	2.56	1.50
27	9553	5.47	4.49	4.20	3.68	3.27	2.51	1.45
28	9548	6.66	5.19	4.91	4.30	3.85	3.00	1.65
29	9537	7.17	6.06	5.80	4.89	4.29	3.26	1.38
30	9747	8.61	6.68	6.22	5.31	4.61	3.43	1.76

APPENDIX D- BACKCALCULATED STIFFNESS MODULUS

OR22-U

FWD Station	Backcalculated Modulus (ksi)					
	Elmod			BAKFAA		
	AC	Base	Subgrade	AC	Base	Subgrade
1	567	23	23	880	9	24
2	619	17	25	874	8	26
3	620	13	26	865	6	28
4	796	12	27	1098	6	28
5	761	13	27	1052	6	29
6	721	14	29	965	8	28
7	829	11	31	1084	6	31
8	800	22	26	1135	10	26
9	876	18	27	1240	8	27
10	627	25	24	1376	8	23
11	649	20	23	856	12	20
12	688	26	23	839	13	22
13	592	17	19	798	10	18
14	738	14	19	649	33	14
15	764	15	19	1054	7	18
16	830	30	19	743	57	15
17	759	26	18	1091	14	16
18	788	21	19	1054	14	17
19	719	36	19	951	28	16
20	622	42	18	747	39	15
21	781	28	20	1087	16	18
22	1157	16	25	1127	13	21

US97-U

FWD Station	Backcalculated Modulus (ksi)					
	Elmod			BAKFAA		
	AC	Base	Subgrade	AC	Base	Subgrade
1	438	39	19	651	15	28
2	398	35	14	573	9	32
3	486	29	19	314	63	20
4	532	35	15	791	6	49
5	365	35	13	559	7	36
6	330	29	17	503	9	35
7	359	18	28	509	10	28
8	309	20	24	438	12	23
9	407	25	25	625	13	24
10	503	35	19	703	9	55
11	464	55	19	293	74	31
12	545	50	21	317	80	33
13	652	45	17	981	9	59
14	570	40	17	819	12	43

US20-U

FWD Station	Backcalculated Modulus (ksi)					
	Elmod			BAKFAA		
	AC	Base	Subgrade	AC	Base	Subgrade
1	402	65	28	505	15	59
2	469	36	14	639	3	46
3	331	110	43	388	99	36
4	265	34	24	316	67	22
5	344	49	23	405	15	22
6	387	92	27	319	146	28
7	615	33	34	879	12	32
8	495	51	23	468	59	25
9	410	53	31	263	77	32
10	417	39	25	406	72	20
11	400	28	25	341	80	19
12	520	25	21	775	7	21
13	442	34	30	423	71	23

OR99-U

FWD Station	Backcalculated Modulus (ksi)					
	Elmod			BAKFAA		
	AC	Base	Subgrade	AC	Base	Subgrade
1	793	45	32	1034	142	28
2	1426	45	37	1165	147	28
3	636	75	38	635	77	32
4	933	45	32	1399	13	31
5	919	32	27	1227	17	24
6	918	40	31	935	68	24
7	1601	76	41	1460	177	32
8	1070	85	36	1251	94	30
9	1477	51	36	1165	79	31
10	1236	80	35	1619	60	30
11	662	74	27	1235	33	27
12	1089	41	32	1419	26	28
13	670	68	30	810	61	25
14	1187	69	28	1737	34	25
15	1506	69	27	2246	27	24
16	1085	81	26	1215	101	21
17	1074	74	26	1346	74	22
18	1590	82	28	1672	139	23
19	988	81	37	801	65	23

OR238-C

FWD Station	Backcalculated Modulus (ksi)					
	Elmod			BAKFAA		
	AC	Base	Subgrade	AC	Base	Subgrade
Station	E1(EM)	E2(EM)	E3(EM)	E1(BF)	E2(BF)	E3(BF)
1	860	70	30	1207	13	105
2	1147	94	28	819	111	53
3	799	88	27	1040	22	84
4	1247	36	61	1686	21	58
5	1026	72	26	1289	22	69
6	531	91	38	519	65	57
7	1131	68	37	1407	28	62
8	981	64	38	1219	29	59
9	628	80	32	779	36	53
10	1186	71	28	956	100	40
11	1490	19	61	2043	10	66
12	651	137	32	648	99	47
13	593	91	34	725	43	52
14	749	86	32	985	32	55
15	630	104	38	766	50	58
16	486	80	32	588	36	54
17	692	97	38	688	75	50
18	1388	58	41	1783	25	60
19	988	58	31	730	76	44
20	1436	78	37	1130	113	44
21	1433	61	33	1038	104	41

OR99W-C

FWD Station	Backcalculated Modulus (ksi)					
	Elmod			BAKFAA		
	AC	Base	Subgrade	AC	Base	Subgrade
1	527	35	21	619	11	33
2	429	28	18	513	7	34
3	465	29	19	554	7	35
4	491	24	21	400	61	22
5	211	57	31	199	92	24
6	540	28	17	647	6	35
7	523	26	16	630	4	38
8	491	26	19	576	7	33
9	500	29	19	589	7	33
10	278	53	26	295	47	25
11	543	19	30	482	67	21
12	573	23	31	526	66	22
13	512	16	29	697	5	34
14	553	17	30	730	7	30
15	573	19	30	757	7	30
16	715	18	30	603	68	21
17	643	23	29	1043	4	42
18	733	27	33	693	70	24
19	727	36	31	975	14	29
20	821	22	31	1127	6	34
21	729	29	32	941	15	29
22	746	31	29	740	63	22
23	835	68	39	986	55	33
24	996	60	40	1164	54	34
25	1001	54	39	1239	38	33
26	713	70	35	802	68	29
27	1233	39	36	1631	16	33
28	881	48	30	1105	35	26
29	912	13	35	1420	2	210
30	252	87	28	235	139	22

OR221-C

FWD Station	Backcalculated Modulus (ksi)					
	Elmod			BAKFAA		
	AC	Base	Subgrade	AC	Base	Subgrade
1	312	64	30	400	28	51
2	466	68	28	645	23	50
3	360	64	21	320	64	29
4	476	71	22	407	79	33
5	441	53	24	612	16	47
6	375	56	22	485	18	54
7	403	58	24	407	79	33
8	446	68	31	587	28	51
9	355	67	25	494	22	51
10	368	72	27	463	28	57
11	437	80	32	551	36	56
12	365	59	27	441	24	59
13	374	53	21	501	17	49
14	383	53	22	473	18	61
15	341	41	16	431	12	48
16	413	29	19	491	10	54
17	462	72	16	671	14	48
18	625	48	17	418	65	28
19	486	52	16	690	11	46
20	416	39	16	561	10	42
21	333	31	13	426	8	45
22	323	31	15	417	10	42
23	416	34	14	589	7	43
24	405	30	15	548	8	41
25	428	35	20	590	11	41
26	365	37	20	484	13	41

<u>OR99EB-C</u>

FWD Station	Backcalculated Modulus (ksi)					
	Elmod			BAKFAA		
	AC	Base	Subgrade	AC	Base	Subgrade
1	1304	1541	25	1886	831	41
2	1251	3879	23	1589	2373	40
3	686	2254	24	762	1644	40
4	1134	2197	25	828	1149	43
5	1143	3593	25	1485	1262	42
6	747	1710	26	808	20461	24
7	450	1093	25	487	743	42
8	844	1229	26	1093	696	44
9	972	1112	23	1227	681	37
10	1040	592	27	1151	455	40
11	1074	748	25	434	8740	19
12	1247	629	30	624	8972	18
13	1145	963	25	1298	751	33
14	831	2702	23	898	2148	38
15	301	847	29	319	644	41
16	1210	2183	21	1409	1443	35
17	1120	1470	23	975	2241	36
18	943	2801	22	759	8089	21
19	890	1099	26	956	886	35
20	1050	1663	22	758	7717	23
21	1682	1560	22	1890	1100	35
22	1035	1276	22	1135	888	37
23	1103	1440	22	1182	1076	37
24	959	398	27	1144	283	37
25	850	1749	23	907	1366	38
26	899	2402	22	961	2022	37
27	803	2051	24	851	1641	40

<u>OR140-C</u>

FWD Station	Backcalculated Modulus (ksi)					
	Elmod			BAKFAA		
	AC	Base	Subgrade	AC	Base	Subgrade
1	347	59	21	336	54	26
2	491	38	20	351	68	31
3	425	47	31	604	7	87
4	495	53	26	495	16	26
5	313	51	28	527	9	21
6	360	35	22	338	67	22
7	337	39	28	337	79	21
8	363	40	26	532	6	28
9	377	35	25	308	78	20
10	363	27	26	331	72	20
11	352	41	26	652	7	43
12	517	62	17	609	7	34
13	362	29	31	280	60	25
14	311	38	31	534	7	29
15	350	33	27	648	7	33
16	399	37	29	636	4	23

OR99*-C

FWD Station	Backcalculated Modulus (ksi)		
	BAKFAA		
	AC	Base	Subgrade
1	394	53	20
2	471	71	17
3	534	64	14
4	584	149	14
5	661	107	15
6	793	81	15
7	737	97	15
8	663	118	15
9	402	98	15
10	546	64	15
11	674	14	18
12	626	82	15
13	395	51	15
14	844	100	15
15	722	106	15
16	871	94	14
17	475	134	15
18	845	80	15
19	889	89	15
20	728	150	15
21	876	111	16
22	941	97	16
23	915	76	16
24	1357	116	16
25	962	123	18

APPENDIX E- DYNAMIC MODULUS TEST RESUTLS DATA

OR22-U

Temp, °C	Freq, Hz	Dynamic Modulus (Mpa)			
		Sample1	Sample 2	Sample 3	Sample 4
4	25	12076	12994	13942	12318
4	10	12063	12140	12716	14146
4	5	11902	12504	12605	10768
4	1	10185	11601	10753	10944
4	0.5	9288	11011	9518	9755
4	0.1	7966	8716	8013	7769
21	25	6913	7589	7540	7991
21	10	7640	7974	8159	8747
21	5	5542	6208	6540	6634
21	1	3580	4197	4030	4287
21	0.5	2820	3462	3220	3460
21	0.1	1677	2125	1936	2126
37	25	1587	2157	2004	2184
37	10	1480	2302	2125	1862
37	5	1458	1844	1555	1329
37	1	636	986	713	644
37	0.5	555	792	574	484
37	0.1	180	313	259	229

US97-U

Temp, °C	Freq, Hz	Dynamic Modulus (Mpa)			
		Sample 1	Sample 2	Sample 3	Sample 4
4	25	10332	3808	12257	10813
4	10	9932	10722	10798	10766
4	5	8972	8640	10543	9588
4	1	7728	7959	8555	7898
4	0.5	6978	8136	7616	7195
4	0.1	5122	6353	5728	5744
21	25	5898	5777	4842	4989
21	10	5749	6367	5819	4949
21	5	4773	4677	4205	3703
21	1	2917	2653	2312	2102
21	0.5	2359	2035	1755	1586
21	0.1	1459	1135	1072	882
37	25	1761	1488	1188	1454
37	10	1510	1337	1264	1192
37	5	1183	964	839	856
37	1	601	512	378	440
37	0.5	440	362	280	316
37	0.1	232	198	121	185

US20-U

Temp, °C	Freq, Hz	Dynamic Modulus (Mpa)			
		Sample1	Sample 2	Sample 3	Sample 4
4	25	11785	12943	15603	13025
4	10	14238	13752	15423	13316
4	5	13574	12555	11557	10693
4	1	11017	10714	10677	10312
4	0.5	9863	9938	10465	9610
4	0.1	8699	8122	8417	7797
21	25	8295	6719	7868	6881
21	10	7722	7268	7904	7342
21	5	6844	6202	5989	5873
21	1	4569	4271	3956	3442
21	0.5	3857	3479	3219	2839
21	0.1	2494	2148	2124	1702
37	25	2749	2171	2103	2065
37	10	2514	2317	2104	1949
37	5	2112	1833	1660	1388
37	1	1124	907	804	762
37	0.5	870	724	634	649
37	0.1	477	385	284	302

OR99-U

Temp, °C	Freq, Hz	Dynamic Modulus (Mpa)			
		Sample1	Sample 2	Sample 3	Sample 4
4	25	14980	12949	11518	13864
4	10	17436	12036	12011	13198
4	5	15787	11420	11055	13259
4	1	12850	11797	10370	12332
4	0.5	12580	10744	9608	10714
4	0.1	8735	8669	7975	10196
21	25	7591	7885	6817	3848
21	10	10653	10018	5835	7959
21	5	8706	7507	6956	7421
21	1	4269	5000	4341	4121
21	0.5	2913	3975	3063	3180
21	0.1	1570	2694	1026	1669
37	25	1049	1900	848	895
37	10	669	1463	1047	645
37	5	751	1370	619	511
37	1	340	985	267	595
37	0.5	222	748	164	390
37	0.1	61	357	49	137

OR238-C

Temp, °C	Freq, Hz	Dynamic Modulus (Mpa)				
		Sample1	Sample 2	Sample 3	Sample 4	Sample 5
4	25	13500	13094	12619	11688	14754
4	10	15732	16209	11766	14350	12267
4	5	13443	13919	12143	13056	12540
4	1	11818	12620	10446	13127	11875
4	0.5	11499	11807	9926	12132	11175
4	0.1	10474	10394	8217	11950	9821
21	25	9412	8842	6605	10063	8868
21	10	10220	9569	7809	10522	8099
21	5	8396	7906	6035	8853	7817
21	1	6926	5191	4391	7688	5311
21	0.5	6231	4209	3657	7163	4335
21	0.1	4595	2632	2454	5210	2840
37	25	4884	2301	2558	4956	3209
37	10	4773	2375	2657	5583	3561
37	5	3463	1798	2055	4808	2605
37	1	2243	876	986	3036	1299
37	0.5	2071	744	845	2516	1056
37	0.1	1254	384	473	1082	519

OR99W-C

Temp, °C	Freq, Hz	Dynamic Modulus (Mpa)					
		Sample1	Sample 2	Sample 3	Sample 4	Sample 5	Sample 6
4	25	8432	8726	10089	10719	12845	13171
4	10	13008	16274	16422	10776	12351	11764
4	5	14493	14435	14512	10360	14572	12981
4	1	12690	12458	12799	9045	12947	10350
4	0.5	12475	11480	11839	7770	10203	9575
4	0.1	10398	9419	10561	7260	9972	8106
21	25	10148	8092	8652	6967	9156	7255
21	10	9368	7872	8793	7562	10157	7763
21	5	8577	6423	7163	6145	8567	6343
21	1	7098	4271	5291	3910	7287	4687
21	0.5	6284	3491	4486	3187	6664	4010
21	0.1	4762	2104	2942	1900	5533	2670
37	25	4426	1701	3753	1961	5084	2366
37	10	5278	1839	4344	2176	3950	2147
37	5	4103	1345	3067	1674	4208	1435
37	1	2476	686	1480	825	2797	960
37	0.5	2204	521	1065	683	2572	733
37	0.1	1201	246	525	334	1531	368

OR221-C

Temp, °C	Freq, Hz	Dynamic Modulus (Mpa)					
		Sample1	Sample 2	Sample 3	Sample 4	Sample 5	Sample 6
4	25	11978	12290	11173	13358	11655	10421
4	10	11726	14362	11587	14288	11250	13572
4	5	10451	12483	10495	12201	10722	12965
4	1	9270	11333	9880	13116	9749	10518
4	0.5	8358	10727	9331	12507	8803	10247
4	0.1	6908	8585	7973	11716	7335	8731
21	25	6267	6509	7114	9607	6689	7974
21	10	6787	7241	6965	9134	7137	8312
21	5	5369	5558	6018	9089	5441	6742
21	1	3429	3454	4305	7446	3485	4425
21	0.5	2756	2798	3539	6565	2816	3600
21	0.1	1715	1877	2346	5381	1650	2279
37	25	1554	1738	3281	5765	1797	1903
37	10	1198	1931	3502	5414	2128	2235
37	5	1180	1344	2595	4506	1430	1611
37	1	712	637	1676	2682	753	849
37	0.5	610	466	1511	2550	630	653
37	0.1	314	213	873	1433	281	327

OR99EB-C

Temp, °C	Freq, Hz	Dynamic Modulus (Mpa)							
		Sample 1	Sample 2	Sample 3	Sample 4	Sample 5	Sample 6	Sample 7	Sample 8
4	25	10455	10241	6517	12539	13608	2585	14743	14710
4	10	11221	17786	12665	13534	14653	14331	17098	15777
4	5	11948	15221	11645	10747	13869	10207	16191	11581
4	1	10545	14827	10586	11968	12842	9928	16475	12834
4	0.5	9791	14263	10321	12452	12339	10442	11701	11905
4	0.1	7762	12488	9100	10797	11139	9599	11061	10434
21	25	7552	10287	8468	8899	9722	9200	6783	8678
21	10	8054	10895	7589	8478	9548	8657	9366	8813
21	5	6357	8931	7465	7775	8389	7859	10003	7092
21	1	4534	6419	5570	5493	6604	6026	8638	5077
21	0.5	3850	5445	4982	4699	5854	5304	7812	4344
21	0.1	2815	3747	3377	3078	4169	3925	6042	2841
37	25	2682	4363	3606	4298	4221	4479	5954	2822
37	10	2736	4226	3528	4349	4510	4751	4619	2585
37	5	2014	2973	2741	3458	3846	3519	3931	2107
37	1	1049	1673	1532	2129	2315	2155	3053	1170
37	0.5	804	1014	1254	1779	1891	1722	2480	787
37	0.1	389	147	676	968	1017	925	1494	370

OR140-C

Temp, °C	Freq, Hz	Dynamic Modulus (Mpa)					
		Sample1	Sample 2	Sample 3	Sample 4	Sample 5	Sample 6
4	25	6890	10252	12845	12304	12911	11796
4	10	8941	10831	13289	10721	14461	10415
4	5	5712	8943	11898	10812	12021	9072
4	1	4610	8114	10619	8759	11957	8140
4	0.5	3781	7240	9557	7565	11364	7364
4	0.1	2645	6081	7572	5235	9864	5684
21	25	5141	4945	8016	5357	7558	4848
21	10	6787	6847	7576	6149	6926	5601
21	5	5226	5103	5728	5155	6020	4292
21	1	2847	3051	4450	2539	4064	2293
21	0.5	2588	2389	3573	1871	3421	1740
21	0.1	1561	1392	2249	930	2399	1031
37	25	629	1102	2755	942	3639	1098
37	10	541	1328	2771	1055	3651	843
37	5	578	1139	2107	704	2596	642
37	1	424	533	1127	354	1425	385
37	0.5	258	387	934	243	1079	266
37	0.1	143	214	433	111	593	146

OR99*-C

Temp, °C	Freq, Hz	Dynamic Modulus (Mpa)						
		Sample1	Sample 2	Sample 3	Sample 4	Sample 5	Sample 6	Sample 7
4	25	11038	11385	9137	9617	11086	12657	11441
4	10	11292	11810	11036	9655	14951	12491	10802
4	5	10976	11498	10457	9196	14176	11374	10437
4	1	9680	10007	10064	8364	12070	10280	9229
4	0.5	9575	9546	9948	7853	10873	9828	8518
4	0.1	7848	8414	8535	6921	8630	7994	7070
21	25	7736	7601	8284	6322	6123	6843	6489
21	10	7285	7434	8408	6209	6525	6931	6823
21	5	6674	6419	7154	5493	5044	5799	5201
21	1	5261	4572	5994	4197	3272	4116	3512
21	0.5	4739	3884	5447	3614	2647	3498	2964
21	0.1	3524	2483	4147	2490	1537	2097	1781
37	25	3499	3367	3998	2713	2113	2443	2210
37	10	3235	3265	4186	2644	2157	2460	2093
37	5	2674	2385	3632	1959	1462	1639	1422
37	1	1456	1312	2622	1185	795	918	841
37	0.5	1294	1084	2414	973	665	723	698
37	0.1	658	578	1321	574	304	350	332

APPENDIX F- DSR FREQUENCY TEST RESULTS DATA

OR22-U

Freq (Hz)	20°C		30°C		46°C		58°C		70°C		82°C		Freq @ 1.6 Hz	
	δ	|G*|, Pa	δ	|G*|, Pa	δ	|G*|, Pa	δ	|G*|, Pa	δ	|G*|, Pa	δ	|G*|, Pa		
0.1	53.7	3.36E+06	61.38	5.09E+05	74.23	24380	81.89	2787	86.19	419.2	87.3	82.7	40°C	
0.1	55.4	3.42E+06	61.62	5.57E+05	73.55	29340	81.17	3614	85.94	511.6	87.3	103.8	δ	|G*|, Pa
0.2	52.7	4.12E+06	61.13	6.50E+05	72.93	35080	80.71	4283	85.59	648.1	87.4	129.8	62.54	5.80E+05
0.2	52.2	4.71E+06	60.56	7.60E+05	72.26	42510	80.11	5286	85.21	804.1	87.4	160.6	63.67	5.26E+05
0.3	51.8	5.37E+06	59.97	8.86E+05	71.63	50970	79.45	6547	84.87	971.7	87.3	199.3	52°C	
0.3	51.5	6.11E+06	59.37	1.03E+06	71.04	60790	78.85	7968	84.48	1204	87.2	247.8	δ	|G*|, Pa
0.4	51.2	6.96E+06	58.78	1.20E+06	70.5	72010	78.27	9609	83.99	1530	87	311.3	70.73	82670
0.5	50.9	7.92E+06	58.19	1.38E+06	70	84950	77.67	11780	83.49	1915	86.8	390.4	71	80900
0.6	50.7	8.99E+06	57.6	1.60E+06	69.5	1.00E+05	77	14500	82.97	2405	86.6	472.7	64°C	
0.8	50.6	1.02E+07	57.03	1.85E+06	69.05	1.18E+05	76.37	17770	82.46	2964	86.3	599.9	δ	|G*|, Pa
1.0	50.5	1.15E+07	56.5	2.13E+06	68.62	1.40E+05	75.75	21610	81.98	3609	85.9	773.6	77.94	12960
1.3	50.6	1.30E+07	55.96	2.47E+06	68.16	1.67E+05	75.18	26060	81.53	4337	85.5	973.2	77.94	12970
1.6	50.8	1.47E+07	55.43	2.85E+06	67.8	1.97E+05	74.63	31260	80.99	5337	85.1	1201	76°C	
2.0	51.0	1.66E+07	54.93	3.29E+06	67.44	2.32E+05	74.13	37160	80.44	6582	84.7	1480	δ	|G*|, Pa
2.5	51.3	1.87E+07	54.45	3.80E+06	67.13	2.71E+05	73.67	43810	79.83	8241	84.3	1870	83.29	2494
3.2	51.7	2.11E+07	54.05	4.37E+06	66.84	3.15E+05	73.12	53110	79.24	10210	83.8	2338	83.23	2548
4.0	52.4	2.39E+07	53.65	5.02E+06	66.63	3.59E+05	72.56	64620	78.63	12670	83.3	2891		
5.0	52.8	2.69E+07	53.24	5.75E+06	66.34	4.13E+05	72.02	78460	78.12	15260	82.9	3523		
6.3	53.3	3.07E+07	52.91	6.60E+06	65.74	4.89E+05	71.54	94020	77.57	18550	82.4	4347		
7.9	54.5	3.52E+07	52.75	7.57E+06	65.13	5.79E+05	71.12	1.11E+05	77.1	22020	82	5313		
10.0	57.3	4.08E+07	52.88	8.66E+06	64.48	6.90E+05	70.78	1.28E+05	76.59	26470	81.5	6434		
12.6	58.9	4.64E+07	52.47	9.85E+06	63.83	8.22E+05	70.42	1.49E+05	76.07	31980	81	7895		
15.9	59.7	5.22E+07	52.36	1.12E+07	63.14	9.77E+05	69.97	1.78E+05	75.53	38770	80.5	9610		
20.0	61.1	5.89E+07	52.22	1.27E+07	62.46	1.16E+06	69.61	2.07E+05	74.98	47030	80	11700		
25.1	67.1	5.97E+07	53.37	1.42E+07	61.91	1.37E+06	69.24	2.40E+05	74.45	56840	79.4	14380		
31.6	67.9	7.56E+07	52.77	1.65E+07	61.22	1.61E+06	68.88	2.72E+05	73.99	66960	78.8	17520		
39.8	67.1	8.39E+07	52.08	1.86E+07	60.51	1.88E+06	68.54	2.88E+05	73.48	79450	78.1	21620		
50.1	60.4	6.63E+07	50.78	1.93E+07	59.68	2.18E+06	68.14	2.84E+05	72.89	94580	77.4	26600		
63.1	82.5	8.49E+07	55.91	2.33E+07	59.73	2.55E+06	67.78	2.66E+05	72.31	1.11E+05	76.3	32220		
79.4	93.5	4.07E+07	66.2	2.03E+07	60.7	2.89E+06	67.27	2.46E+05	71.51	1.19E+05	74.8	39080		
100.0	131.5	5.49E+07	79.11	3.03E+07	61.34	3.46E+06	66.51	2.24E+05	70.54	1.13E+05	72.8	46850		

US97-U

Freq (Hz)	20℃		30℃		46℃		58℃		70℃		82℃		Freq @ 1.6 Hz	
	δ	|G*|, Pa	δ	|G*|, Pa	δ	|G*|, Pa	δ	|G*|, Pa	δ	|G*|, Pa	δ	|G*|, Pa		
0.1	55.4	1.46E+06	59.73	2.42E+05	63.36	17960	65.93	3638	71.24	784.2	78.1	196	40℃	
0.1	56.35	1.55E+06	60.11	2.70E+05	63.26	20950	65.73	4169	70.66	937.7	77.4	240.2	δ	|G*|, Pa
0.2	54.77	1.84E+06	60.06	3.14E+05	63.2	24710	65.52	4955	70.11	1123	76.7	292	61.04	3.02E+05
0.2	54.29	2.11E+06	60.11	3.45E+05	63.14	29030	65.32	5894	69.61	1337	76	351.7	61.77	2.85E+05
0.3	53.82	2.42E+06	60.05	3.93E+05	63.09	34020	65.16	6913	69.16	1590	75.3	425.4	52℃	
0.3	53.37	2.78E+06	59.82	4.59E+05	63.06	39880	65.04	8069	68.77	1890	74.6	518	δ	|G*|, Pa
0.4	52.98	3.18E+06	59.56	5.39E+05	63.03	46730	64.93	9485	68.38	2252	74	627.7	63.76	55250
0.5	52.6	3.62E+06	59.24	6.30E+05	63.01	54750	64.86	11180	68.05	2674	73.3	758.2	63.88	54380
0.6	52.26	4.13E+06	58.88	7.38E+05	63	64060	64.81	13210	67.76	3181	72.7	914.3	64℃	
0.8	51.89	4.70E+06	58.52	8.59E+05	63	74950	64.76	15580	67.49	3789	72.2	1096	δ	|G*|, Pa
1.0	51.58	5.35E+06	58.16	9.99E+05	63	87790	64.73	18370	67.27	4499	71.7	1313	65.63	12380
1.3	51.25	6.10E+06	57.79	1.16E+06	62.99	1.03E+05	64.72	21640	67.08	5337	71.2	1572	65.63	12430
1.6	51.05	6.94E+06	57.43	1.34E+06	62.99	1.20E+05	64.71	25400	66.93	6300	70.7	1875	76℃	
2.0	50.89	7.90E+06	57.05	1.55E+06	62.99	1.40E+05	64.72	29840	66.8	7447	70.3	2238	δ	|G*|, Pa
2.5	50.73	8.98E+06	56.67	1.79E+06	63	1.64E+05	64.73	35110	66.69	8804	70	2676	68.58	3376
3.2	50.76	1.02E+07	56.29	2.06E+06	63	1.90E+05	64.75	41200	66.6	10430	69.6	3200	68.54	3422
4.0	50.79	1.16E+07	55.9	2.38E+06	63.02	2.23E+05	64.78	48600	66.53	12390	69.3	3837		
5.0	50.87	1.31E+07	55.51	2.74E+06	63	2.66E+05	64.8	57300	66.48	14690	69.1	4579		
6.3	50.91	1.48E+07	55.15	3.17E+06	62.98	3.13E+05	64.82	67650	66.44	17400	68.9	5429		
7.9	51.14	1.69E+07	54.82	3.64E+06	63.01	3.58E+05	64.85	79590	66.42	20560	68.7	6436		
10.0	51.52	1.91E+07	54.43	4.21E+06	63.08	4.01E+05	64.88	93250	66.41	24260	68.5	7640		
12.6	52.79	2.18E+07	54.08	4.85E+06	62.89	4.62E+05	64.91	1.09E+05	66.4	28560	68.3	9081		
15.9	53.24	2.45E+07	53.75	5.57E+06	62.62	5.44E+05	64.92	1.27E+05	66.4	33660	68.2	10790		
20.0	52.98	2.79E+07	53.45	6.36E+06	62.29	6.42E+05	64.93	1.49E+05	66.39	39870	68	12840		
25.1	55.54	3.01E+07	53.59	7.24E+06	61.99	7.57E+05	64.92	1.75E+05	66.37	47370	67.9	15400		
31.6	55.63	3.61E+07	53.14	8.39E+06	61.59	8.98E+05	64.9	2.04E+05	66.34	56340	67.8	18270		
39.8	54.98	4.04E+07	52.64	9.56E+06	61.16	1.06E+06	64.85	2.40E+05	66.31	66510	67.6	21690		
50.1	50.74	3.87E+07	51.31	1.05E+07	60.56	1.25E+06	64.69	2.86E+05	66.24	78090	67.3	25790		
63.1	67.84	4.88E+07	54.77	1.24E+07	60.62	1.47E+06	64.74	3.31E+05	66.07	90620	66.7	30610		
79.4	78.94	3.11E+07	59.21	1.21E+07	60.9	1.69E+06	64.77	3.71E+05	65.8	1.06E+05	65.6	36560		
100.0	107.5	4.98E+07	65.89	1.64E+07	61.39	2.01E+06	64.92	4.07E+05	65.43	1.24E+05	63.9	43390		

US20-U

Freq (Hz)	20°C		30°C		46°C		58°C		70°C		82°C		Freq @ 1.6 Hz	
	δ	$\lvert G^*\rvert$, Pa	δ	$\lvert G^*\rvert$, Pa	δ	$\lvert G^*\rvert$, Pa	δ	$\lvert G^*\rvert$, Pa	δ	$\lvert G^*\rvert$, Pa	δ	$\lvert G^*\rvert$, Pa		
0.1	58.07	1.66E+06	64.35	2.46E+05	75.2	13840	82.11	1874	86.2	306.3	87.1	68.87	40°C	
0.1	57.74	1.81E+06	64.58	2.72E+05	74.58	16700	81.65	2227	85.84	393.7	87.3	85.91	δ	$\lvert G^*\rvert$, Pa
0.2	57.18	2.10E+06	64.28	3.17E+05	73.91	20380	80.96	2846	85.52	488.6	87.3	108	65.22	3.25E+05
0.2	56.73	2.44E+06	64.06	3.66E+05	73.25	24770	80.36	3501	85.2	596.9	87.3	137	66.03	2.96E+05
0.3	56.26	2.82E+06	63.73	4.26E+05	72.69	29440	79.83	4188	84.82	741.8	87.2	171.2	52°C	
0.3	55.75	3.27E+06	63.33	5.01E+05	72.18	34770	79.27	5092	84.38	921.6	87.1	215.8	δ	$\lvert G^*\rvert$, Pa
0.4	55.27	3.77E+06	62.87	5.89E+05	71.63	41720	78.66	6234	83.91	1144	87	267.9	71.86	48660
0.5	54.8	4.35E+06	62.4	6.94E+05	71.07	50440	78.04	7661	83.41	1420	86.8	330.2	72.03	47670
0.6	54.36	5.02E+06	61.93	8.14E+05	70.56	60560	77.45	9382	82.9	1759	86.5	407.4	64°C	
0.8	53.97	5.76E+06	61.43	9.56E+05	70.09	72400	76.84	11480	82.36	2182	86.2	506.1	δ	$\lvert G^*\rvert$, Pa
1.0	53.65	6.59E+06	61	1.12E+06	69.71	85200	76.24	13980	81.81	2696	85.8	638.9	78.04	8879
1.3	53.44	7.55E+06	60.5	1.31E+06	69.28	1.01E+05	75.67	16950	81.31	3262	85.4	807.3	78.02	8919
1.6	53.33	8.61E+06	60.03	1.53E+06	68.89	1.20E+05	75.13	20430	80.8	3968	84.9	1018	76°C	
2.0	53.24	9.83E+06	59.57	1.77E+06	68.56	1.41E+05	74.62	24480	80.19	4963	84.5	1265	δ	$\lvert G^*\rvert$, Pa
2.5	53.08	1.12E+07	59.1	2.07E+06	68.23	1.66E+05	74.13	29310	79.55	6262	84	1545	82.95	1977
3.2	53.32	1.28E+07	58.64	2.41E+06	67.91	1.96E+05	73.58	35620	79.02	7595	83.5	1919	82.96	1982
4.0	53.58	1.46E+07	58.19	2.80E+06	67.63	2.32E+05	73.1	42890	78.47	9264	83	2383		
5.0	53.78	1.66E+07	57.77	3.26E+06	67.37	2.72E+05	72.59	52170	77.95	11200	82.5	2904		
6.3	54.26	1.90E+07	57.44	3.79E+06	67.15	3.16E+05	72.13	62520	77.49	13290	82	3567		
7.9	54.72	2.16E+07	56.94	4.38E+06	66.95	3.64E+05	71.77	73160	76.96	16050	81.5	4339		
10.0	54.96	2.46E+07	56.49	5.03E+06	66.69	4.22E+05	71.39	85520	76.43	19500	80.9	5363		
12.6	55.65	2.82E+07	56.11	5.81E+06	66.2	5.00E+05	71.01	1.01E+05	75.88	23810	80.3	6655		
15.9	57.51	3.22E+07	55.71	6.68E+06	65.73	5.92E+05	70.6	1.22E+05	75.3	29380	79.8	8120		
20.0	57.64	3.64E+07	55.27	7.70E+06	65.22	7.02E+05	70.21	1.46E+05	74.78	35470	79.2	10070		
25.1	62.56	4.06E+07	55.82	8.80E+06	64.8	8.33E+05	69.87	1.71E+05	74.25	42890	78.6	12170		
31.6	61.03	4.80E+07	54.77	1.02E+07	64.22	9.91E+05	69.54	1.99E+05	73.81	50360	78	14710		
39.8	60.31	5.36E+07	54.22	1.16E+07	63.65	1.17E+06	69.23	2.22E+05	73.3	60240	77.3	17920		
50.1	59.46	4.69E+07	53.34	1.25E+07	62.98	1.37E+06	68.83	2.41E+05	72.77	71220	76.5	21490		
63.1	68.78	6.17E+07	55.34	1.50E+07	62.79	1.63E+06	68.52	2.59E+05	72.2	85440	75.2	25910		
79.4	93.46	3.85E+07	65.06	1.50E+07	63.45	1.89E+06	68.2	2.67E+05	71.43	1.02E+05	73.5	32080		
100.0	117.9	5.30E+07	70.72	1.99E+07	63.7	2.26E+06	67.85	2.64E+05	70.65	1.20E+05	71.1	38840		

OR99-U

Freq (Hz)	20°C		30°C		46°C		58°C		70°C		82°C		Freq @ 1.6 Hz	
	δ	$\lvert G^* \rvert$, Pa	δ	$\lvert G^* \rvert$, Pa	δ	$\lvert G^* \rvert$, Pa	δ	$\lvert G^* \rvert$, Pa	δ	$\lvert G^* \rvert$, Pa	δ	$\lvert G^* \rvert$, Pa		
0.1	67.54	2.46E+06	77.02	2.20E+05	85.93	6404	88.3	671.8	88.97	100.5	88.5	21.58	40°C	
0.1	67.69	2.68E+06	76.55	2.60E+05	85.63	7753	88.19	843.7	88.96	133.9	88.5	27.25	δ	$\lvert G^* \rvert$, Pa
0.2	65.84	3.33E+06	75.95	3.17E+05	85.29	9810	88.03	1055	88.97	164.2	88.7	33.89	77.35	2.70E+05
0.2	65.13	3.94E+06	75.38	3.81E+05	84.91	12250	87.85	1330	88.99	195.2	88.7	42.34	77.52	2.62E+05
0.3	64.47	4.65E+06	74.8	4.58E+05	84.52	15250	87.68	1673	89.02	247.5	88.9	53.52	52°C	
0.3	63.87	5.47E+06	74.17	5.53E+05	84.14	18700	87.47	2085	89.01	316.6	89	66.38	δ	$\lvert G^* \rvert$, Pa
0.4	63.37	6.41E+06	73.51	6.67E+05	83.76	22930	87.25	2583	88.92	406.5	89	82.75	83.75	27100
0.5	62.91	7.48E+06	72.81	8.05E+05	83.34	28490	87.03	3233	88.85	514	89.1	104.2	83.79	26650
0.6	62.59	8.74E+06	72.1	9.72E+05	82.89	35470	86.79	4017	88.74	644.8	89.1	133	64°C	
0.8	62.33	1.02E+07	71.37	1.17E+06	82.41	44340	86.54	4983	88.63	798.5	89.2	167.4	δ	$\lvert G^* \rvert$, Pa
1.0	62.19	1.19E+07	70.64	1.41E+06	81.95	54800	86.28	6271	88.49	1004	89.2	208.2	87.13	3786
1.3	62.22	1.38E+07	69.92	1.69E+06	81.49	67110	85.96	8041	88.32	1257	89.2	257.2	87.13	3796
1.6	62.41	1.60E+07	69.17	2.02E+06	81.1	79830	85.66	10060	88.14	1577	89.2	319.1	76°C	
2.0	62.82	1.86E+07	68.44	2.41E+06	80.62	97940	85.34	12540	87.94	1968	89.2	399.4	δ	$\lvert G^* \rvert$, Pa
2.5	63.42	2.15E+07	67.73	2.87E+06	80.1	1.21E+05	85.05	15220	87.75	2417	89.1	514.5	88.81	703.3
3.2	64.36	2.49E+07	67.04	3.41E+06	79.57	1.51E+05	84.74	18590	87.56	2979	89	651.6	88.81	706.7
4.0	65.4	2.87E+07	66.41	4.05E+06	79.04	1.86E+05	84.4	22820	87.31	3766	88.9	819.8		
5.0	66.62	3.32E+07	65.81	4.80E+06	78.55	2.24E+05	84.01	28480	87.05	4803	88.8	1038		
6.3	68.4	3.87E+07	65.17	5.61E+06	78.07	2.69E+05	83.58	35910	86.79	6063	88.6	1312		
7.9	70.92	4.51E+07	64.96	6.66E+06	77.58	3.24E+05	83.15	44670	86.53	7544	88.4	1663		
10.0	75.03	5.26E+07	64.18	7.75E+06	77.08	3.85E+05	82.71	55240	86.23	9436	88.2	2076		
12.6	76.59	5.94E+07	63.86	9.11E+06	76.5	4.61E+05	82.28	67460	85.94	11620	88.1	2578		
15.9	81.98	6.84E+07	63.53	1.07E+07	75.86	5.57E+05	81.84	81570	85.64	14350	87.9	3231		
20.0	85.62	8.10E+07	63.19	1.25E+07	75.17	6.74E+05	81.4	98440	85.3	17690	87.5	4070		
25.1	91.84	7.61E+07	63.71	1.42E+07	74.5	8.17E+05	80.89	1.21E+05	84.93	21780	87.1	5032		
31.6	97.97	9.73E+07	63.4	1.69E+07	73.77	9.91E+05	80.38	1.47E+05	84.51	26960	86.6	6302		
39.8	98.94	1.12E+08	62.58	1.96E+07	72.97	1.20E+06	79.75	1.77E+05	84	33560	85.9	7782		
50.1	78.33	9.08E+07	59.68	2.09E+07	71.93	1.44E+06	79.11	1.90E+05	83.43	41970	84.9	9746		
63.1	114.7	9.60E+07	66.58	2.56E+07	71.7	1.75E+06	78.5	1.75E+05	82.65	53160	82.9	12130		
79.4	110.8	4.28E+07	75.89	2.19E+07	71.85	2.05E+06	77.54	1.39E+05	81.69	65530	80.1	15150		
100.0	145.7	4.89E+07	91.58	3.14E+07	72.26	2.50E+06	75.99	1.07E+05	80.57	79160	75.7	18520		

OR238-C

Freq (Hz)	20°C		30°C		46°C		58°C		70°C		82°C		Freq @ 1.6 Hz	
	δ	|G*|, Pa	δ	|G*|, Pa	δ	|G*|, Pa	δ	|G*|, Pa	δ	|G*|, Pa	δ	|G*|, Pa		
0.1	50.61	5.56E+06	57.47	9.83E+05							88.5	171.5	40°C	
0.1	49.99	6.35E+06	56.85	1.14E+06							88.4	214.9	δ	|G*|, Pa
0.2	49.74	7.21E+06	56.35	1.31E+06							88.1	267.6	58.77	1.05E+06
0.2	49.33	8.16E+06	55.71	1.50E+06							87.8	337.7	58.77	1.05E+06
0.3	49.2	9.27E+06	55.29	1.72E+06							87.5	428.8	52°C	
0.3	49.23	1.05E+07	54.73	1.98E+06							87.1	537.4	δ	|G*|, Pa
0.4	49.21	1.19E+07	54.23	2.27E+06							86.8	675.5	67.26	1.64E+05
0.5	49.21	1.34E+07	53.78	2.60E+06							86.3	846	67.27	1.64E+05
0.6	49.42	1.52E+07	53.27	2.98E+06							85.8	1052	64°C	
0.8	49.64	1.71E+07	52.82	3.42E+06							85.4	1304	δ	|G*|, Pa
1.0	50.11	1.94E+07	52.47	3.91E+06	64.33	2.92E+05	72.69	45050	79.9	7932	85.1	1616	75.07	27730
1.3	50.51	2.19E+07	52.06	4.47E+06	63.75	3.44E+05	72.01	54480	79.22	9833	84.4	1996	75.07	27690
1.6	51.16	2.47E+07	51.71	5.11E+06	63.2	4.05E+05	71.34	65710	78.52	12030	83.9	2470	76°C	
2.0	52.11	2.79E+07	51.34	5.82E+06	62.64	4.77E+05	70.7	79110	77.85	14670	83.3	3070	δ	|G*|, Pa
2.5	53.12	3.15E+07	51.14	6.62E+06	62.1	5.60E+05	70.08	94960	77.19	17960	82.8	3764	81.41	5408
3.2	54.42	3.57E+07	50.94	7.52E+06	61.56	6.56E+05	69.5	1.13E+05	76.54	21930	82.2	4610	81.42	5390
4.0	55.92	4.05E+07	50.8	8.52E+06	61.04	7.68E+05	68.95	1.35E+05	75.91	26660	81.7	5719		
5.0	57.67	4.59E+07	50.69	9.66E+06	60.51	8.97E+05	68.37	1.60E+05	75.25	32050	81.1	7145		
6.3	59.82	5.23E+07	50.66	1.10E+07	60.02	1.05E+06	67.84	1.89E+05	74.36	38660	80.6	8729		
7.9	62.02	5.98E+07	50.68	1.24E+07	59.52	1.22E+06	67.3	2.25E+05	73.76	46590	80	10710		
10.0	67.49	6.95E+07	51.16	1.42E+07	59.06	1.41E+06	66.77	2.67E+05	73.27	55960	79.1	13170		
12.6	71.37	7.77E+07	50.08	1.60E+07	58.4	1.64E+06	66.21	3.16E+05	72.64	67390	78.3	16290		
15.9	73.35	8.80E+07	51.77	1.80E+07	58.08	1.90E+06	65.67	3.74E+05	72.22	80710	78	19700		
20.0	77.32	1.05E+08	51.71	2.04E+07	57.76	2.20E+06	65.18	4.43E+05	71.66	97570	77.2	23850		
25.1	83.14	9.57E+07	54.75	2.31E+07	57.13	2.55E+06	64.7	5.25E+05	71.04	1.17E+05	76.9	29470		
31.6	88.05	1.31E+08	52.92	2.66E+07	56.65	2.95E+06	64.12	6.19E+05	70.49	1.41E+05	76.8	36090		
39.8	86.8	1.44E+08	52.51	2.95E+07	56.2	3.39E+06	63.55	7.30E+05	69.98	1.70E+05	75.9	43620		
50.1	63.05	1.11E+08	49.82	3.02E+07	55.28	3.87E+06	62.99	8.57E+05	69.41	2.04E+05	75.4	52650		
63.1	107.2	1.18E+08	60.23	3.69E+07							74.6	63580		
79.4	102.9	4.62E+07	73.34	2.73E+07							74.6	78410		
100.0	145.9	6.68E+07	87.35	4.32E+07							74.7	92280		

OR99W-C

Freq (Hz)	20°C		30°C		46°C		58°C		70°C		82°C		Freq @ 1.6 Hz	
	δ	|G*|, Pa	δ	|G*|, Pa	δ	|G*|, Pa	δ	|G*|, Pa	δ	|G*|, Pa	δ	|G*|, Pa		
0.1	54.95	2.77E+06	62.57	4.15E+05	74.47	23350	82.11	3026	86.04	466.7	87.1	94.42	40°C	
0.1	54.61	3.07E+06	62.89	4.56E+05	73.75	28300	81.6	3695	85.81	575.3	87.2	117.4	δ	|G*|, Pa
0.2	54.14	3.51E+06	62.52	5.28E+05	73.08	34280	80.99	4536	85.43	720.8	87.2	146.1	63.49	5.15E+05
0.2	53.7	4.02E+06	62.05	6.14E+05	72.46	40990	80.36	5567	85.1	879.8	87.2	183.8	64.66	4.66E+05
0.3	53.25	4.59E+06	61.55	7.17E+05	71.87	48950	79.72	6950	84.77	1067	87.1	230.8	52°C	
0.3	52.88	5.26E+06	61	8.38E+05	71.32	58280	79.07	8482	84.43	1323	87	285.9	δ	|G*|, Pa
0.4	52.52	5.99E+06	60.44	9.79E+05	70.73	69910	78.45	10350	83.9	1712	86.8	357.3	70.97	80130
0.5	52.17	6.82E+06	59.86	1.14E+06	70.21	83610	77.82	12610	83.37	2194	86.7	448.1	71.33	76890
0.6	51.9	7.77E+06	59.26	1.34E+06	69.73	99320	77.2	15230	82.82	2776	86.4	562.8	64°C	
0.8	51.64	8.84E+06	58.7	1.56E+06	69.28	1.18E+05	76.6	18430	82.35	3361	86.1	699.4	δ	|G*|, Pa
1.0	51.44	1.01E+07	58.16	1.81E+06	68.92	1.38E+05	76.02	22130	81.86	4105	85.8	862.5	78.04	13840
1.3	51.33	1.14E+07	57.56	2.11E+06	68.57	1.61E+05	75.44	26740	81.39	4953	85.4	1077	78.02	13870
1.6	51.3	1.30E+07	56.99	2.45E+06	68.24	1.88E+05	74.83	32460	80.87	6034	85	1346	76°C	
2.0	51.36	1.47E+07	56.46	2.84E+06	67.93	2.18E+05	74.26	39320	80.36	7305	84.6	1660	δ	|G*|, Pa
2.5	51.52	1.66E+07	55.95	3.28E+06	67.64	2.52E+05	73.71	47480	79.78	9021	84.2	2061	83.12	2834
3.2	51.72	1.88E+07	55.48	3.78E+06	67.37	2.89E+05	73.21	56910	79.2	11110	83.7	2550	83.13	2821
4.0	51.81	2.11E+07	55.06	4.35E+06	67.13	3.22E+05	72.72	68040	78.58	13770	83.2	3177		
5.0	52.05	2.39E+07	54.66	5.02E+06	66.89	3.58E+05	72.21	82110	77.97	16940	82.8	3925		
6.3	52.42	2.71E+07	54.19	5.75E+06	66.57	4.09E+05	71.81	96840	77.45	20360	82.2	4905		
7.9	53.39	3.14E+07	53.76	6.61E+06	66.06	4.63E+05	71.4	1.15E+05	77	23980	81.7	6036		
10.0	55.74	3.61E+07	53.5	7.58E+06	65.44	5.44E+05	70.99	1.36E+05	76.46	28920	81.2	7323		
12.6	55.58	4.06E+07	53.68	8.75E+06	64.79	6.31E+05	70.68	1.57E+05	75.9	35320	80.7	8928		
15.9	56.86	4.60E+07	53.24	1.00E+07	64.16	7.34E+05	70.35	1.81E+05	75.35	42970	80.1	11000		
20.0	57.75	5.19E+07	53.01	1.15E+07	63.5	8.58E+05	69.97	2.10E+05	74.8	52190	79.6	13380		
25.1	65.23	5.72E+07	54.23	1.31E+07	62.9	1.01E+06	69.58	2.33E+05	74.25	63600	79	16390		
31.6	62.49	6.75E+07	53.12	1.50E+07	62.15	1.19E+06	69.16	2.51E+05	73.74	75520	78.3	20180		
39.8	61.34	7.44E+07	52.54	1.71E+07	61.47	1.40E+06	68.83	2.60E+05	73.31	86370	77.7	24460		
50.1	58.67	5.97E+07	51.89	1.78E+07	60.68	1.63E+06	68.35	2.63E+05	72.76	97750	76.9	29670		
63.1	72.8	8.35E+07	54.81	2.17E+07	60.28	1.89E+06	67.91	2.61E+05	72.19	1.06E+05	75.8	35640		
79.4	93.94	4.48E+07	66.67	2.04E+07	60.98	2.16E+06	67.22	2.56E+05	71.43	1.07E+05	74.4	42870		
100.0	125.8	5.65E+07	77.14	2.80E+07	61.08	2.57E+06	66.52	2.34E+05	70.21	1.02E+05	72.7	51700		

OR221-C

Freq (Hz)	20℃		30℃		46℃		58℃		70℃		82℃		Freq @ 1.6 Hz	
	δ	|G*|, Pa	δ	|G*|, Pa	δ	|G*|, Pa	δ	|G*|, Pa	δ	|G*|, Pa	δ	|G*|, Pa		
0.1	56.07	2.13E+06	64.57	3.12E+05	78.49	12910	84.8	1496	88.02	233.9	88.3	51.58	40℃	
0.1	65.07	1.36E+06	64.9	3.44E+05	77.58	16620	84.32	1875	87.87	293.7	88.3	65.16	δ	|G*|, Pa
0.2	61.85	2.01E+06	64.66	3.90E+05	77.13	18920	83.9	2290	87.7	359.7	88.4	82.53	65.61	3.61E+05
0.2	55.38	2.90E+06	64.17	4.52E+05	76.17	24560	83.43	2844	87.43	453.8	88.5	102.4	66.86	3.25E+05
0.3	53.83	3.48E+06	63.55	5.34E+05	75.41	29860	82.88	3602	87.14	588.6	88.5	127.2	52℃	
0.3	53.23	4.02E+06	62.88	6.29E+05	74.82	35080	82.31	4471	86.84	725.3	88.4	161.8	δ	|G*|, Pa
0.4	52.72	4.61E+06	62.19	7.42E+05	74.21	41640	81.76	5477	86.48	910.6	88.4	200	74.37	46620
0.5	52.25	5.26E+06	61.51	8.73E+05	73.6	49760	81.23	6656	86.14	1121	88.3	250.4	74.53	45760
0.6	51.86	6.00E+06	60.82	1.03E+06	72.96	59940	80.67	8085	85.74	1404	88.2	316.2	64℃	
0.8	51.47	6.82E+06	60.13	1.20E+06	72.3	72750	80.07	9920	85.31	1751	88	396.4	δ	|G*|, Pa
1.0	51.14	7.73E+06	59.46	1.41E+06	71.71	87480	79.45	12170	84.86	2183	87.8	491.1	81.38	7715
1.3	50.88	8.77E+06	58.81	1.64E+06	71.1	1.06E+05	78.8	15030	84.4	2701	87.5	614.5	81.39	7685
1.6	50.66	9.95E+06	58.18	1.90E+06	70.62	1.25E+05	78.14	18540	83.94	3324	87.2	770.2	76℃	
2.0	50.51	1.13E+07	57.56	2.21E+06	70.2	1.45E+05	77.52	22600	83.46	4072	86.9	953.9	δ	|G*|, Pa
2.5	50.44	1.28E+07	56.96	2.55E+06	69.81	1.68E+05	76.91	27380	82.93	5067	86.5	1201	85.81	1544
3.2	50.34	1.45E+07	56.39	2.94E+06	69.37	1.98E+05	76.31	33180	82.35	6366	86.1	1509	85.82	1540
4.0	50.44	1.64E+07	55.83	3.39E+06	68.9	2.37E+05	75.75	39620	81.8	7875	85.7	1874		
5.0	50.28	1.84E+07	55.29	3.90E+06	68.46	2.82E+05	75.16	47510	81.27	9602	85.3	2324		
6.3	50.37	2.09E+07	54.75	4.50E+06	68.11	3.26E+05	74.6	57130	80.77	11480	84.9	2878		
7.9	50.71	2.37E+07	54.21	5.18E+06	67.87	3.69E+05	74.03	68750	80.17	14150	84.4	3554		
10.0	52.31	2.73E+07	53.77	5.96E+06	67.47	4.27E+05	73.44	83400	79.57	17390	84	4394		
12.6	52.98	3.08E+07	53.57	6.88E+06	66.8	5.07E+05	72.9	1.00E+05	78.95	21440	83.5	5442		
15.9	52.68	3.46E+07	53.16	7.89E+06	66.13	6.04E+05	72.43	1.17E+05	78.33	26340	83	6717		
20.0	53.07	3.89E+07	52.75	9.02E+06	65.41	7.17E+05	71.99	1.36E+05	77.7	32150	82.5	8211		
25.1	57.26	4.17E+07	53.33	1.02E+07	64.74	8.50E+05	71.58	1.56E+05	77.15	38620	81.9	10040		
31.6	56.08	5.00E+07	52.45	1.18E+07	64	1.01E+06	71.13	1.80E+05	76.61	45670	81.2	12440		
39.8	54.95	5.54E+07	51.75	1.34E+07	63.21	1.20E+06	70.66	1.96E+05	76.01	54970	80.4	15380		
50.1	50.42	4.90E+07	50.04	1.43E+07	62.29	1.41E+06	70.17	1.91E+05	75.33	67270	79.6	18560		
63.1	67.59	6.43E+07	54.2	1.70E+07	62.12	1.67E+06	69.82	1.71E+05	74.64	81730	78.3	22670		
79.4	83.89	3.68E+07	61.79	1.58E+07	62.32	1.93E+06	69.04	1.46E+05	73.73	98540	76.3	27840		
100.0	114.5	5.61E+07	69.57	2.21E+07	62.57	2.31E+06	67.96	1.26E+05	72.85	1.16E+05	73.6	33890		

OR99EB-C

Freq (Hz)	20°C		30°C		46°C		58°C		70°C		82°C		Freq @ 1.6 Hz	
	δ	|G*|, Pa	δ	|G*|, Pa	δ	|G*|, Pa	δ	|G*|, Pa	δ	|G*|, Pa	δ	|G*|, Pa		
0.1	53.04	8.64E+06	57.77	1.63E+06	71.6	68370	80.38	7987	85.51	1120	87.8	191	40°C	
0.1	51.82	8.77E+06	57.55	1.75E+06	71.1	81600	79.63	10170	85.08	1414	87.8	235.3	δ	|G*|, Pa
0.2	50.54	1.03E+07	57.09	1.94E+06	70.39	99240	78.91	12450	84.66	1742	87.7	299.2	59.53	1.49E+06
0.2	50.41	1.18E+07	56.62	2.17E+06	69.95	1.14E+05	78.28	14950	84.21	2155	87.5	380.3	59.88	1.43E+06
0.3	50.27	1.34E+07	56.09	2.47E+06	69.38	1.35E+05	77.64	18050	83.74	2649	87.3	472.6	52°C	
0.3	50.35	1.52E+07	55.53	2.83E+06	68.76	1.62E+05	76.96	21980	83.26	3243	87	584.7	δ	|G*|, Pa
0.4	50.47	1.71E+07	55	3.25E+06	68.2	1.92E+05	76.26	26830	82.78	3985	86.8	725.2	68.37	2.13E+05
0.5	50.71	1.94E+07	54.46	3.74E+06	67.71	2.27E+05	75.56	32880	82.23	4933	86.5	903.9	69.04	1.99E+05
0.6	51.11	2.19E+07	53.98	4.31E+06	67.18	2.70E+05	74.89	40010	81.64	6163	86.1	1126	64°C	
0.8	51.56	2.47E+07	53.52	4.95E+06	66.73	3.20E+05	74.24	48340	81	7715	85.7	1417	δ	|G*|, Pa
1.0	52.2	2.78E+07	53.1	5.68E+06	66.37	3.76E+05	73.65	57910	80.35	9644	85.3	1776	75.82	34420
1.3	53.09	3.14E+07	52.75	6.49E+06	65.89	4.39E+05	73.09	68860	79.74	11840	84.8	2213	75.87	34260
1.6	54.2	3.54E+07	52.44	7.38E+06	65.33	5.15E+05	72.55	81580	79.19	14290	84.4	2742	76°C	
2.0	55.47	4.00E+07	52.17	8.38E+06	64.75	6.02E+05	72	97530	78.66	17040	83.9	3407	δ	|G*|, Pa
2.5	57.07	4.50E+07	51.97	9.47E+06	64.21	6.98E+05	71.47	1.17E+05	78.11	20550	83.4	4228	82.06	6122
3.2	58.98	5.09E+07	51.77	1.06E+07	63.66	8.10E+05	70.93	1.40E+05	77.49	25070	82.9	5212	82.03	6183
4.0	61.26	5.77E+07	51.69	1.20E+07	63.08	9.44E+05	70.42	1.68E+05	76.85	30880	82.4	6385		
5.0	63.64	6.49E+07	51.53	1.35E+07	62.47	1.11E+06	69.99	1.97E+05	76.2	37980	81.8	7802		
6.3	67.01	7.38E+07	51.55	1.52E+07	61.84	1.30E+06	69.55	2.32E+05	75.59	46340	81.3	9528		
7.9	70.02	8.37E+07	51.77	1.74E+07	61.22	1.53E+06	69.08	2.77E+05	75.06	55070	80.8	11690		
10.0	74.35	9.50E+07	52.34	1.96E+07	60.6	1.81E+06	68.64	3.28E+05	74.57	64740	80.2	14400		
12.6	81.3	1.06E+08	53.36	2.27E+07	59.93	2.13E+06	68.3	3.75E+05	74.07	77210	79.6	17790		
15.9	86.07	1.18E+08	53.08	2.57E+07	59.29	2.51E+06	67.92	4.27E+05	73.53	92120	78.9	21890		
20.0	89.73	1.29E+08	53.37	2.92E+07	58.67	2.94E+06	67.29	5.00E+05	72.97	1.11E+05	78.4	26400		
25.1	99.44	1.11E+08	57.1	3.21E+07	58.45	3.40E+06	66.73	5.87E+05	72.42	1.34E+05	77.8	31930		
31.6	104.1	1.52E+08	55.75	3.80E+07	57.67	3.97E+06	66.08	6.89E+05	71.87	1.58E+05	77.2	38660		
39.8	102.8	1.70E+08	55.1	4.25E+07	57	4.57E+06	65.39	8.13E+05	71.42	1.75E+05	76.5	46930		
50.1	73.42	1.23E+08	51.09	4.05E+07	55.89	5.16E+06	64.51	9.67E+05	70.94	1.83E+05	75.9	56760		
63.1	117.1	1.23E+08	65.04	5.09E+07	57	6.00E+06	64.15	1.15E+06	70.38	1.88E+05	75.2	67610		
79.4	108.8	4.59E+07	79.27	3.29E+07	59.9	6.43E+06	64.16	1.35E+06	69.52	1.84E+05	74.2	80150		
100.0	147.7	5.06E+07	108.3	4.82E+07	62.47	8.02E+06	64.24	1.62E+06	68.45	1.70E+05	73.2	94170		

OR140-C

Freq (Hz)	20°C		30°C		46°C		58°C		70°C		82°C		Freq @ 1.6 Hz	
	δ	|G*|, Pa	δ	|G*|, Pa	δ	|G*|, Pa	δ	|G*|, Pa	δ	|G*|, Pa	δ	|G*|, Pa		
0.1	55.25	3.15E+06	62.61	4.92E+05	74.03	25930	81.12	3471	85.82	528.9	87	103.9	40°C	
0.1	55.5	3.42E+06	62.5	5.49E+05	73.24	32280	80.46	4450	85.4	666.8	87.1	129.5	δ	|G*|, Pa
0.2	54.17	4.04E+06	61.98	6.47E+05	72.67	38050	79.83	5424	85.05	819.5	87.1	161.7	63.34	6.01E+05
0.2	53.69	4.65E+06	61.47	7.57E+05	72.09	45390	79.33	6424	84.65	1020	87.1	201.8	63.95	5.64E+05
0.3	53.27	5.33E+06	60.92	8.82E+05	71.46	54910	78.69	7945	84.17	1268	87	255.5	52°C	
0.3	52.9	6.10E+06	60.4	1.02E+06	70.89	65610	78.02	9841	83.71	1561	86.9	321.6	δ	|G*|, Pa
0.4	52.6	6.97E+06	59.87	1.18E+06	70.36	77960	77.36	12090	83.22	1918	86.6	403.1	70.51	90390
0.5	52.31	7.94E+06	59.3	1.37E+06	69.86	92620	76.74	14680	82.74	2358	86.4	500.1	70.72	88470
0.6	52.13	9.03E+06	58.79	1.59E+06	69.36	1.10E+05	76.15	17720	82.21	2906	86.1	618.7	64°C	
0.8	51.95	1.02E+07	58.27	1.83E+06	68.89	1.31E+05	75.56	21390	81.65	3625	85.7	765.8	δ	|G*|, Pa
1.0	51.87	1.15E+07	57.73	2.12E+06	68.45	1.55E+05	74.97	25880	81.04	4524	85.4	955.2	77.05	15670
1.3	51.89	1.31E+07	57.13	2.47E+06	68.02	1.84E+05	74.38	31490	80.47	5600	84.9	1193	76.99	15950
1.6	52.02	1.47E+07	56.63	2.87E+06	67.63	2.17E+05	73.81	38120	79.89	6885	84.5	1484	76°C	
2.0	52.25	1.67E+07	56.14	3.32E+06	67.28	2.57E+05	73.31	45330	79.36	8346	84	1851	δ	|G*|, Pa
2.5	52.63	1.89E+07	55.67	3.84E+06	66.87	3.08E+05	72.87	53110	78.84	10070	83.5	2299	82.33	3162
3.2	53.14	2.15E+07	55.23	4.44E+06	66.55	3.63E+05	72.38	63400	78.3	12210	83	2839	82.33	3168
4.0	53.78	2.43E+07	54.84	5.11E+06	66.23	4.20E+05	71.87	76490	77.74	14870	82.5	3485		
5.0	54.58	2.77E+07	54.52	5.90E+06	65.75	4.91E+05	71.35	92610	77.17	18160	82	4277		
6.3	55.17	3.17E+07	54.12	6.73E+06	65.28	5.73E+05	70.86	1.12E+05	76.6	22220	81.5	5271		
7.9	56.44	3.64E+07	53.86	7.71E+06	64.8	6.67E+05	70.42	1.34E+05	76.03	27120	80.9	6498		
10.0	57.86	4.10E+07	53.74	8.83E+06	64.28	7.81E+05	70.07	1.56E+05	75.51	32730	80.3	8005		
12.6	60.35	4.79E+07	53.39	1.01E+07	63.76	9.18E+05	69.74	1.80E+05	74.97	39620	79.8	9816		
15.9	62.66	5.38E+07	53.4	1.16E+07	63.21	1.08E+06	69.36	2.13E+05	74.47	47620	79.2	11920		
20.0	64.42	6.07E+07	53.34	1.32E+07	62.63	1.28E+06	68.78	2.66E+05	73.98	56930	78.7	14540		
25.1	72.17	6.51E+07	54.71	1.48E+07	62.17	1.51E+06	68.41	3.11E+05	73.5	67350	78.1	17700		
31.6	71.03	7.96E+07	53.94	1.73E+07	61.51	1.79E+06	68.12	3.44E+05	73.01	80660	77.5	21560		
39.8	70.28	8.86E+07	53.41	1.96E+07	60.83	2.10E+06	67.88	3.63E+05	72.5	96760	76.8	26400		
50.1	60.99	7.16E+07	51.42	2.05E+07	59.92	2.45E+06	67.51	3.81E+05	71.94	1.15E+05	76.1	32260		
63.1	87.28	8.94E+07	57.85	2.49E+07	60.19	2.88E+06	67.34	3.98E+05	71.42	1.30E+05	75.1	38860		
79.4	96.94	4.29E+07	68.1	2.17E+07	61.14	3.25E+06	67.24	4.03E+05	70.75	1.39E+05	73.9	46810		
100.0	133.6	5.20E+07	84.02	3.13E+07	62.35	3.92E+06	67.06	3.75E+05	69.88	1.36E+05	72.3	56200		

OR99*-C

Freq (Hz)	20°C		30°C		46°C		58°C		70°C		82°C		Freq @ 1.6 Hz	
	δ	|G*|, Pa	δ	|G*|, Pa	δ	|G*|, Pa	δ	|G*|, Pa	δ	|G*|, Pa	δ	|G*|, Pa		
0.1	51.94	4.43E+06	58.04	7.28E+05	69.37	40670	77.43	5399	83.38	821.7	86.5	174.8	40°C	
0.1	52.51	4.57E+06	58.41	7.96E+05	68.85	48480	76.8	6545	82.85	994.5	86.3	221.1	δ	|G*|, Pa
0.2	50.58	5.41E+06	57.95	9.23E+05	68.3	57190	76.07	8040	82.31	1257	86.1	275.6	59.4	8.30E+05
0.2	50.13	6.17E+06	57.45	1.07E+06	67.81	67290	75.5	9571	81.76	1549	85.7	347.8	60.14	7.64E+05
0.3	49.79	7.00E+06	56.97	1.23E+06	67.31	79600	74.86	11500	81.24	1877	85.4	436.7	52°C	
0.3	49.49	7.94E+06	56.45	1.42E+06	66.84	93940	74.21	13970	80.68	2299	85	544.5	δ	|G*|, Pa
0.4	49.29	8.98E+06	55.96	1.64E+06	66.35	1.11E+05	73.57	16930	80.13	2799	84.5	679.5	66.58	1.27E+05
0.5	49.11	1.02E+07	55.46	1.89E+06	65.92	1.31E+05	72.95	20470	79.53	3469	84.1	831.4	67.01	1.22E+05
0.6	49.05	1.15E+07	54.99	2.17E+06	65.5	1.55E+05	72.35	24640	78.85	4329	83.6	1016	64°C	
0.8	48.99	1.29E+07	54.52	2.49E+06	65.16	1.82E+05	71.8	29350	78.19	5387	83.1	1244	δ	|G*|, Pa
1.0	49.03	1.45E+07	54.03	2.86E+06	64.91	2.10E+05	71.28	34940	77.59	6553	82.6	1539	73.39	21280
1.3	49.19	1.63E+07	53.55	3.29E+06	64.65	2.42E+05	70.76	41620	77.01	7926	82.1	1909	73.4	21180
1.6	49.44	1.83E+07	53.14	3.78E+06	64.39	2.82E+05	70.24	49850	76.45	9531	81.5	2363	76°C	
2.0	49.72	2.06E+07	52.76	4.33E+06	64.12	3.29E+05	69.73	59970	75.98	11200	80.9	2914	δ	|G*|, Pa
2.5	50.17	2.31E+07	52.41	4.96E+06	63.91	3.82E+05	69.28	71300	75.39	13660	80.4	3563	79.35	4389
3.2	50.7	2.60E+07	52.1	5.67E+06	63.56	4.43E+05	68.91	83260	74.78	16780	79.8	4326	79.36	4371
4.0	51.22	2.91E+07	51.8	6.47E+06	63.05	5.21E+05	68.55	96940	74.18	20570	79.2	5320		
5.0	51.94	3.28E+07	51.81	7.38E+06	62.57	6.09E+05	68.17	1.14E+05	73.62	24940	78.7	6481		
6.3	52.74	3.70E+07	51.29	8.39E+06	62.07	7.13E+05	67.79	1.36E+05	73.1	29880	78.2	7769		
7.9	54.03	4.16E+07	51.13	9.54E+06	61.59	8.35E+05	67.44	1.61E+05	72.61	35720	77.7	9338		
10.0	55.4	4.83E+07	51.14	1.09E+07	61.04	9.80E+05	67.13	1.88E+05	72.14	42320	77.1	11330		
12.6	56.66	5.27E+07	51.04	1.23E+07	60.58	1.15E+06	66.85	2.18E+05	71.76	49260	76.5	13840		
15.9	60.89	6.09E+07	51.06	1.40E+07	60.02	1.34E+06	66.55	2.55E+05	71.31	58940	76	16600		
20.0	61.63	6.77E+07	50.96	1.58E+07	59.45	1.58E+06	66.25	2.96E+05	70.81	71030	75.5	19680		
25.1	67.14	6.89E+07	52.43	1.75E+07	59.06	1.85E+06	66.04	3.36E+05	70.34	85550	75	23620		
31.6	67.8	8.83E+07	51.73	2.03E+07	58.41	2.17E+06	65.82	3.64E+05	69.89	1.01E+05	74.4	28650		
39.8	66.38	9.72E+07	51.19	2.29E+07	57.79	2.54E+06	65.58	3.95E+05	69.53	1.17E+05	73.8	34480		
50.1	54.78	7.71E+07	48.83	2.36E+07	56.95	2.92E+06	65.08	4.50E+05	69.09	1.33E+05	73.2	41630		
63.1	88.86	9.24E+07	57.57	2.85E+07	57.3	3.42E+06	64.65	5.27E+05	68.75	1.44E+05	72.5	48900		
79.4	91.27	4.34E+07	65.39	2.35E+07	58.54	3.81E+06	64.39	6.13E+05	68.23	1.52E+05	71.5	58380		
100.0	131.7	5.65E+07	83.42	3.51E+07	59.91	4.57E+06	64.25	7.21E+05	67.64	1.49E+05	70.2	69240		

APPENDIX G-EXPERIMENTAL SET-UP FOR IDT TEST